

PHOTOCATALYTIC ACTIVITY IN NANO SIZED
TITANIUM DIOXIDE STRUCTURES

A THESIS SUBMITTED TO
THE GRADUATE SCHOOL OF NATURAL AND APPLIED SCIENCES
OF
MIDDLE EAST TECHNICAL UNIVERSITY

BY

MERT MEHMET OYMAK

IN PARTIAL FULFILLMENT OF THE REQUIREMENTS
FOR
THE DEGREE OF DOCTOR OF PHILOSOPHY
IN
CHEMICAL ENGINEERING

SEPTEMBER 2012

Approval of the Thesis

**“PHOTOCATALYTIC ACTIVITY IN NANO SIZED
TITANIUM DIOXIDE STRUCTURES”**

submitted by **MERT MEHMET OYMAK** in partial fulfillment of the requirements for the degree of **Doctor of Philosophy in Chemical Engineering Department, Middle East Technical University** by,

Prof. Dr. Canan Özgen
Dean, Graduate School of **Natural and Applied Sciences** _____

Prof. Dr. Deniz Üner
Head of Department, **Chemical Engineering** _____

Prof. Dr. Deniz Üner
Supervisor, **Chemical Engineering Dept., METU** _____

Dr. İstem Özen
Co-supervisor, **Istituto Officina dei Materiali – CNR
and International Centre for Theoretical Physics,
Trieste, Italy** _____

Examining Committee Members:

Prof. Dr. Gürkan Karakaş
Chemical Engineering Dept., METU _____

Prof. Dr. Deniz Üner
Chemical Engineering Dept., METU _____

Prof. Dr. Güngör Gündüz
Chemical Engineering Dept., METU _____

Prof. Dr. Şinasi Ellialtıoğlu
Basic Sciences Dept., TED University _____

Y. Doç. Dr. Levent Hoşgün
Chemical Engineering Dept., Osmangazi University _____

Date: _____

I hereby declare that all information in this document has been obtained and presented in accordance with academic rules and ethical conduct. I also declare that, as required by these rules and conduct, I have fully cited and referenced all material and results that are not original to this work.

Name, Last name:

Signature:

ABSTRACT

PHOTOCATALYTIC ACTIVITY IN NANO SIZED TITANIUM DIOXIDE STRUCTURES

Oymak, Mert Mehmet

Ph.D., Department of Chemical Engineering

Supervisor : Prof. Dr. Deniz Üner

Co-supervisor : Dr. İstem Özen

September 2012, 222 Pages

The objective of this thesis is to investigate the photocatalytic activity in nanosized TiO₂ structures. Two different structures were used for two different reaction systems. In the first part of the study, TiO₂ coated on glass beads by a sol-gel procedure were used to test the photocatalytic CO₂ reduction reaction with H₂O and H₂ in the gas phase. The results of photocatalytic CO₂ reduction reaction revealed that CO₂ reduction step of the overall reaction proceeds in dark; while illumination is required for water splitting reaction.

In the second part of the study, Photocatalytic oxidation activity of the commercial TiO₂ powders mixed with grout and plaster were studied for a potential commercial self cleaning material.

A method based on gas phase benzene oxidation was developed for testing TiO₂ added cement based self cleaning surfaces. This method was used to screen 15 commercial TiO₂ samples with and without cement. Based on this method a commercial TiO₂ sample (S9) was selected for further use. Surface of

15 commercial TiO₂ samples were characterized by using NO and CO₂ as probe molecules.

Photocatalytic benzene oxidation experiments showed that using TiO₂ on the surface lead to more effective surfaces in terms of photocatalytic activity. TiO₂ was bound to surface by inorganic materials without much activity loss. This kind of amount optimization is of commercial importance.

Keywords: Photocatalysis, Plaster, Grout, Cement, TiO₂, Gas phase CO₂ reduction, Methane, Artificial photosynthesis.

ÖZ

NANO BOYUTLU TİTANYUM DİOKSİT YAPILARINDA FOTOKATALİTİK AKTİVİTE

Oymak, Mert Mehmet

Doktora, Kimya Mühendisliği Bölümü

Tez Yöneticisi : Prof. Dr. Deniz Üner

Ortak Tez Yöneticisi : Dr. İstem Özen

Eylül 2012, 222 Sayfa

Bu tezin amacı nanoboyutlu TiO_2 yapılarında fotokatalitik aktiviteyi incelemektir. 2 farklı reaksiyon sistemi için 2 farklı yapı kullanılmıştır. Çalışmanın ilk bölümünde, cam boncukların üzerine sol-gel prosedürü ile kaplanmış TiO_2 , gaz fazında su ve hidrojen ile fotokatalitik CO_2 indirgenmesinde kullanılmıştır. Fotokatalitik CO_2 indirgeme reaksiyonu sonuçları, su parçalanma reaksiyonları için aydınlatma gerektiğini, toplam reaksiyonun CO_2 indirgenme basamağının karanlıkta gerçekleştiğini ortaya koymuştur.

Çalışmanın ikinci bölümünde, ticari potansiyele sahip kendi kendini temizleyen yüzey oluşturmak için, derz ve sıva ile karıştırılmış ticari TiO_2 tozlarının fotokatalitik oksidasyon aktiviteleri belirlenmiştir.

Kendi kendini temizleyen TiO_2 eklentili çimento bazlı yüzeylerin testi için gaz fazında benzen oksidasyonuna dayanan bir metot geliştirilmiştir. Bu metot, çimentolu ve çimentosuz 15 ticari TiO_2 örneğini elemek için kullanılmıştır. Bu metoda dayanarak ticari bir TiO_2 örneği (S9) seçilmiştir. 15

ticari TiO₂ örnek yüzeyi, NO ve CO₂ prob molekülleri kullanılarak karakterize edilmiştir.

Fotokatalitik benzen oksidasyonu deneyleri, titanyum dioksitin yüzeyde kullanımının fotokatalitik aktivite açısından daha etkili olduğunu göstermiştir. İnorganik malzeme kullanımı ile TiO₂ yüzeye fazla aktivite kaybı olmadan bağlanmıştır. Bu tarz miktara dayalı bir optimizasyon ticari açıdan önemlidir.

Anahtar kelimeler: Fotokataliz, Sıva, Derz Dolgusu, Çimento, TiO₂, Gaz Fazında CO₂ İndirgenmesi, Metan, Yapay fotosentez.

For hard-working people who cares for this world and dream on a better future for humanity,

For my family who brought me up and my family, my love and my friends who gave without expecting,

ACKNOWLEDGMENTS

I owe my deepest gratitude to my supervisor Prof. Dr. Deniz Üner for her support as an advisor, sometimes as a mother and as a friend. It would be hard to finish this thesis without her intellectual guidance, concreteness. She showed me amazing patience for correcting my mistakes. I also want to thank Dr. İstem Özen as my co-supervisor for her enthusiasm. Besides these valuable contributions, she started the collaboration project with Kalekim, which has formed the main part of this thesis.

The members of the thesis supervision committee, Prof. Dr. Gürkan Karakaş and Prof. Dr. Şinasi Ellialtıođlu are gratefully acknowledged for their invaluable comments and support.

The Scientific and Research Council of Turkey (TUBİTAK) is kindly acknowledged for the Project No: 106Y075, since I worked in the first years of my PhD studies. The author is also thankful to the Ministry of Science, Industry and Technology through Project No: 00336.STZ.2008-2 for financial support of his late PhD work.

I also want to give my thanks to Elsevier Publishing Group, for their permission to use the article “On the Mechanism of Photocatalytic CO₂ Reduction in the Gas Phase” into my thesis. I also want to thank Inderscience Publishing Group for their permission to use the review article partly “CO₂ Utilization by Photocatalytic Conversion to Methane and Methanol”, which I make use of in visible light photocatalysis part.

The author is thankful to Prof. Dr. Hans Joachim Kleebe, Margaret Schlossel and Mathis M. Müller for their workshop on TEM and providing the TEM images of the catalysts.

The author is grateful to the Prof. Dr. Saim Özkar in Chemistry Department for his good lecture “Coordination and Catalysis” and also his

group especially Serdar Akbayrak for his assistance to UV Vis measurements with integrating sphere (diffuse reflectance mode).

The technical assistance of Dr. Volkan Değirmenci for assistance in GC measurements and chemisorption setup is well appreciated.

The parallel project to this thesis work with the collaboration between Kalekim and ODTÜ, the author prepared the samples in Kalekim, which he finds the chance to work with Beyhan Gözoğul, Gülden Tombaş, Dr. Funda İnceoğlu, Dilber Memiş besides Dr. İstem Özen. The author thanks for the warm atmosphere of the firm. İstem Özen and Funda İnceoğlu are greatly acknowledged for SEM Images.

The special gratitude goes to electric technician Nevzat Bekçi for his invaluable support during my studies in METU, we lost him during my PhD studies from cancer. We shared too much with him. Also glass technician İsa Çağlar patiently made hundreds of the single use reactors. The technical assistance by Gülten Orakçı in BET and GC measurements was important in my thesis. The author wishes to thank Gürsel Ulutuncel and Sibel Erkal for technical assistance to DRIFTS measurements and Sacit Ersen is also appreciated for his invaluable help in technical support to GC.

The memories in the laboratory could not be forgotten. Sometimes I studied alone in lab but mostly I have some people around, from the legendary Cactus Group, which we created common memories, happy and exciting moments. The thanks goes to a long list: Volkan Değirmenci, Ebru Erünel, Hilal Demir Kıvrak, Mukaddes Can, Orçun Ergün, Osman Karslıoğlu, Başar Çağlar, Arzu Kanca, Bahar İpek, Mehmet Kaptan, Saygın Aras, Hale Ay, Mustafa Yasin Arslan, Atalay Çalışan, İbrahim Bayar, Güvenç Oğulgöner and Necip Üner.

I also want to thank my family, my father and mother for their endless supports and encouragements, and my sister for understanding and commenting on me by observing in an objective way. They all wanted me to finish PhD study and they did everything necessary for this purpose. I want to

express my gratitude and love to Sevgi Alver for her supports and sharing her love with me. I also want to thank my flatmates and friends for their participation and contribution in my life during PhD years.

TABLE OF CONTENTS

ABSTRACT	iv
ÖZ	vi
ACKNOWLEDGMENTS	ix
TABLE OF CONTENTS	xii
LIST OF TABLES	xvii
LIST OF FIGURES	xx
LIST OF SYMBOLS	xxiii
CHAPTERS	1
1. INTRODUCTION AND SCOPE OF THESIS	1
1.1 DEFINITION OF TiO ₂ PHOTOCATALYSIS	1
1.2 UTILIZATION of TiO ₂ PHOTOCATALYSIS in SELF-AIR CLEANING	4
1.3 PHOTOCATALYTIC TiO ₂ USAGE in CEMENTITIOUS PRODUCTS	6
1.4 SCOPE OF THESIS	10
2. LITERATURE SURVEY	12
2.1 SELF CLEANING SURFACES - CEMENT	12
2.1.1 Particle Size – Crystal Face - Phase Effects on Activity	12
2.1.2 Photocatalysis in Oxidation Reactions	15
2.1.2.1 Photocatalytic Benzene Oxidation as a Model Reaction	16
2.1.2.2 Benzene Decomposition Mechanism Studies	26
2.1.2.3 Regeneration Studies	30
2.1.2.4 Application of Photocatalytic Activity to Cement Based Materials	31
2.1.2.4.1 Cement Structure	31
2.1.2.4.2 Clay	36
2.1.2.4.3 Gypsum	36

2.1.2.4.4 Lime	36
2.1.2.4.5 Plastering.....	37
2.1.2.4.6 Grout	37
2.1.2.4.7 Other Components used in Mortars.....	38
2.1.2.4.8 Activity Studies with Cement Based Materials	41
2.1.3 Enhancing Self Cleaning Effect	46
2.1.3.1 Superhydrophilicity	46
2.1.3.2 Superhydrophobicity	49
2.1.3.3 Inorganic Resin Selection	50
2.2 VISIBLE LIGHT PHOTOCATALYSIS - METAL AND ANION DOPING	52
2.3 SURFACE CHARACTERISTICS OF A METAL OXIDE.....	56
2.3.1 What Are The Possible Probe Molecules to Measure The Acidity and Basicity? ...	58
2.3.1.1 Acidic Probe molecules	59
2.3.1.2 Basic Probe molecules	59
2.3.2 The Techniques Used to Measure Surface Acidity and Basicity	60
2.3.2.1 FTIR Spectroscopy	60
2.3.2.1.1 Theoretical Background for DRIFTS	61
2.3.2.1.2 CO ₂ Adsorption Using FTIR Spectroscopy.....	63
2.3.2.1.3 NO Adsorption Using FTIR Spectroscopy.....	65
2.3.2.1.4 Benzene Adsorption on TiO ₂	66
2.3.3 Surface Acidity Correlation with Photocatalytic Activity	70
2.4 PATENT SUMMARY	71
3. EXPERIMENTAL.....	83
3.1 SOL-GEL COATED SAMPLES	83
3.1.1 Preparation of the Samples	83
3.1.2 Characterization of the Samples	84
3.2 CEMENT BASED MATERIALS.....	85
3.2.1 TiO ₂ Powder Selection.....	85

3.2.2 Sample Preparation	85
3.2.2.1 Cement Based Sample Preparation.....	85
3.2.2.2 Sample Preparation for Visible Light Studies	87
3.2.2.3 Sample Preparation for Pure TiO ₂ Studies	87
3.2.2.4 Sample Preparation for Coating Studies	87
3.2.2.4.1 Direct Addition to Paint Formulation.....	87
3.2.2.4.2 Solution Deposition using Grout Maker.....	88
3.2.2.4.3 Binding using White Cement	88
3.2.2.4.4 Coating Study with a Commercial Binder.....	88
3.2.3 Photocatalytic Reactivity Experiments	88
3.2.4 Characterization of the Samples	89
4. RESULTS.....	91
4.1 CHARACTERIZATION	91
4.1.1 X-Ray Diffraction Measurements	91
4.1.2 BET Measurements.....	91
4.1.3 TGA Measurements	93
4.1.4 UV-Vis Measurements.....	94
4.1.5 Surface Characterization using CO ₂ and NO as Probe Molecules on TiO ₂ with DRIFTS.....	95
4.1.5.1 CO ₂ Adsorption Studies.....	95
4.1.5.2 NO Adsorption Studies.....	98
4.1.6 Search for Ti-O-Si bond: Raman Characterization of Degussa P25 on Glass	101
4.1.7 SEM Analysis	103
4.2 PHOTOCATALYTIC BENZENE OXIDATION EXPERIMENTS	105
4.2.1 Kinetic Screening Tests on Photocatalytic Benzene Oxidation	105
4.2.2 Photocatalytic Benzene Oxidation Studies	108
4.2.2.1 Pure TiO ₂ Coatings.....	111
4.2.2.2 Comparison of the Results on Glass and on Grout	113

4.2.2.2.1 The Particles in the Bulk are not Accessible	113
4.2.2.2.2 The Contents of Grout Interact with TiO ₂	113
4.2.2.3 Cured Cement Based Materials Studies.....	115
4.2.2.3.1 Bulk Addition Studies	115
4.2.2.3.2 Coating Studies on Grout	117
4.2.2.3.3 Experiments done with Plaster Samples	118
4.2.2.4 Visible Light Studies	119
4.2.2.4.1 Kinetic Screening Tests on Photocatalytic Benzene Oxidation	119
4.2.2.4.2 Fe Addition by Wet-Impregnation Method.....	121
4.2.2.5 Changes in Initial Adsorption with Sample and Water Amount	122
4.2.2.6 Experiments done in the Dark Conditions	123
4.2.2.6.1 Mass Transfer Limitations due to Thickness of the Coating and TiO ₂ Concentration	125
4.2.2.7 CO ₂ Measurement for Verification of Benzene Degradation	126
4.2.2.8 Stable Coating Project on Surface: Coating Formulation Studies	127
4.2.2.8.1 Addition to a Paint Formulation.....	127
4.2.2.8.2 Application using Commercial Grout Marker Manifold.....	129
4.2.2.8.3 Using White Cement as Inorganic Binder.....	129
4.2.2.9 Precipitation Study	130
4.2.2.10 Precision of the Experiments	131
4.3 SUMMARY OF THIS CHAPTER	132
5. DISCUSSION.....	135
5.1 COMMENTS ON SELECTION OF TiO ₂ POWDER and ACTIVITY MAXIMIZATION	135
5.2 COMMENTS ON OTHER PARTS OF THESIS	137
5.2.1 Visible Light Studies.....	137
5.2.2 Synergic Effect of TiO ₂ and Cement Medium for the NO _x Removal	138
5.2.3 Photocatalysis in Reduction Reactions	140
5.2.4 UV-VIS Diffuse Reflectance Studies.....	141

6. CONCLUSIONS.....	142
7. RECOMMENDATIONS	143
REFERENCES	144
APPENDICES.....	165
A. HYDRATION AND PRE-PRODUCTION REACTIONS FOR IMPORTANT BINDERS IN CONSTRUCTION INDUSTRY AND ADDITIVES USED.....	165
B. PICTURES FROM THE EXPERIMENTAL SET UP AND SAMPLES USED IN THIS THESIS	170
C. DRIFTS SPECTRA of GROUT, POWDER, and COATING APPLICATIONS of S8 in the REGION 4000-1200 cm⁻¹	172
D. PEAK ASSIGNMENTS OF NO ADSORPTION ON 15 TiO₂ POWDERS	173
E. UV-VIS DIFFUSE REFLECTANCE STUDIES.....	182
F. REPEATIBILITY EXPERIMENTS.....	185
G. EXPERIMENTS CONDUCTED IN DARK CONDITIONS.....	187
H. IR AND UV-VIS SPECTRA OF SOME MATERIALS USED IN THE STUDY.....	189
I. COATING APPLICATION USING COMMERCIAL SILICONE BASED RESIN ..	190
I.1 HYDROPHILIC-HYDROPHOBIC STUDIES	190
I.2 EFFECT OF POST TREATMENT TO THE ACTIVITY	190
J. ON THE MECHANISM OF PHOTOCATALYTIC CO₂ REDUCTION WITH WATER IN THE GAS PHASE.....	193
CURRICULUM VITAE	217

LIST OF TABLES

TABLES

Table 1.1 Classes of VOCs and their possible emission sources	6
Table 1.2 Applications of cement based materials.....	7
Table 2.1 History of benzene regulatory standards	17
Table 2.2 Literature survey for benzene and related compound oxidation	25
Table 2.3 Less active intermediates and surface products formed from benzene on TiO ₂ surfaces due to radical chemistry.....	29
Table 2.4 Typical composition of binders used in construction industry	34
Table 2.5 Types of plasters.....	39
Table 2.6 Literature survey for photocatalytic degradation of benzene and toluene using TiO ₂ added cement based materials.....	44
Table 2.7 Silicones in coatings and benefits according to usage ratio.....	51
Table 2.8 Peak assignment literature survey related with CO ₂ adsorption on TiO ₂	64
Table 2.9 Peak assignment literature survey related with NO adsorption on TiO ₂	67
Table 2.10. Patent survey on TiO ₂ mediated self cleaning cement based materials.....	74
Table 3.1 Structural properties of TiO ₂ samples used in this study.....	86
Table 4.1 BET results comparison for TiO ₂ powders (A = anatase, R = rutile)93	
Table 4.2 Pure TiO ₂ coating study on glass lamels.....	111
Table 4.3 Pure TiO ₂ coating activity results on 2 cm ² glass slides.....	112
Table 4.4 Comparison of activity change with coating amount for the same coated area (2 cm ²) for S13 sample.....	112
Table 4.5 Bulk addition of TiO ₂ samples in grout under UV source	116

Table 4.6 Comparison of bulk added TiO ₂ samples in grout results with Aiessa <i>et al.</i> study.	117
Table 4.7 Activity comparison of TiO ₂ in the bulk and on the surface.	117
Table 4.8 Activity results of coating studies on grout under UV light.	118
Table 4.9 Comparison of activity results done with plaster and grout.	119
Table 4.10 Visible light activity results of Degussa P25 coatings with different Fe loadings.	121
Table 4.11 Dark activity results for S13 with different thickness.	125
Table 4.12 Dark activity changes due to particle size and surface areas	125
Table 4.13 Activity comparison of pure S13 and S13 in the paint.	128
Table 4.14 Surface binding studies on grout media.	130
Table 4.15 Observation on precipitation speeds of TiO ₂ powders.	131
Table 4.16 Standard deviations and R ² test results for selected bulk addition experiments	132
Table A.1. Important inorganic binding agents used in construction industry	166
Table A.2 Examples of plaster admixtures	168
Table D.1. Peak assignments in 1750 – 1150 cm ⁻¹ region for NO Adsorption on 15 Commercial TiO ₂ Powders *.....	174
Table D.2. Peak Assignments in 4000 – 1800 cm ⁻¹ region for NO Adsorption on 15 Commercial TiO ₂ Powders *.....	177
Table D.3 Table abbreviations and literature assignments done for Table D.1 and Table D.2.	179
Table F.1 Repeatability experiment results for UV illuminated area increase experiments of TiO ₂ on glass	185
Table F.2 Repeatability experiment results for UV illuminated area increase experiments of TiO ₂ on grout.....	186
Table F.3 Repeatability experiment results for 10% TiO ₂ added grout experiments	186
Table F.4 Repeatability experiment results for TiO ₂ on grout experiments ..	186

Table G.1 Dark experiment results averaged and used for calculating 10%, 1%, TiO ₂ on grout samples.....	188
Table G.2 Dark experiment results averaged and used for calculating 2 cm ² pure TiO ₂ samples	188
Table I.1 Studies done for binding TiO ₂ to the surface.....	191
Table I.2 Results of photocatalytic benzene oxidation activity test	192

LIST OF FIGURES

FIGURES

Figure 1.1 Phase diagram of Ti-O system.....	3
Figure 1.2 Construction material sector export chart (The charts are redrawn and translated to the English).	9
Figure 1.3 Toto company sales chart.....	9
Figure 2.1 Possible surface interactions of NH ₃ and CO ₂ with metal oxide surfaces.....	58
Figure 3.1 a) Home made dipping apparatus b) Glass apparatus	84
Figure 3.2 a) Sample placed in a reactor. b) Experimental set up.....	89
Figure 4.1 X-Ray Diffraction Results of TiO ₂ powders.....	92
Figure 4.2 TGA results for cured sample S1.....	94
Figure 4.3 UV-Vis spectra for selected TiO ₂ powders.....	94
Figure 4.4 Comparison of carbonate region for 15 TiO ₂ powders	96
Figure 4.5 DRIFTS spectra comparison of pure powder, coating and grout applications using S8 on carbonate (1800-1200 cm ⁻¹) region.	97
Figure 4.6 Changes in the nitrite-nitrate region of 15 TiO ₂ powders.....	99
Figure 4.7 NO adsorption spectrum of nitrite and nitrate region for S1, S2, S6, S8, S14, S15 samples under 70 torr NO atmosphere at RT.	100
Figure 4.8 NO adsorption spectrum of nitrite and nitrate region for S3, S4, S5, S7, S9, S10, S11, S13 samples under 70 Torr NO atmosphere at RT.....	100
Figure 4.9 NO adsorption spectrum for S1, S8, S9, S13, S15 samples under 70 Torr NO atmosphere at RT.....	101
Figure 4.10 Raman spectra of S13 coatings on glass slide for different coating areas (deposited amount is 0.004 g for all coatings).	103
Figure 4.11. SEM images of (a) S12, (b) S8, (c) S1, (d) S15.....	104

Figure 4.12 SEM Images (a), (b), (c) and point (d) and regional (e) EDX analysis of 10 % S1-plaster	105
Figure 4.13 Comparison of the grout and plaster samples (S1) for the same TiO ₂ % under UV light.....	107
Figure 4.14 (a) Pure rutile (S15) coating, (b) Pure grout sample.....	107
Figure 4.15 Illustrative diagram that shows trend lines for UV irradiated and dark experiments of 10% TiO ₂ added grout samples. Full symbol represents UV experiments, whereas empty symbol represents experiments conducted in dark conditions.	110
Figure 4.16. Typical flow system diagram for photocatalytic benzene oxidation reaction.	110
Figure 4.17 Specific rate constant vs. UV illuminated area for Degussa P25 on glass (The experiments were repeated 3 times and the results are given in Appendix F-Table F.1).	114
Figure 4.18 Specific rate constant vs. UV illuminated area for Degussa P25 on grout (The experiments were repeated 3 times and the results are given in Appendix F -Table F.2).	115
Figure 4.19 Photo-oxidative benzene degradation for grout samples under a) UV light b) Visible light.....	120
Figure 4.20 Photo-oxidative benzene degradation for plaster samples under a) UV light b) Visible light.....	120
Figure 4.21 UV-Vis spectrum comparison of Degussa P25 coatings with different Fe loadings.....	121
Figure 4.22 Effect of grout amount increase and water content change on 10 % S13 sample activity under dark and UV conditions.	122
Figure 4.23 Comparison between dark experiments using 10% TiO ₂ added samples and grout sample without TiO ₂ .The results are given in table form in Appendix G-Table G.1.	123
Figure 4.24 Dark experiment results for pure TiO ₂ samples. The results are given in table form in Appendix G-Table G.2.	124

Figure 4.25 Benzene degradation justification by measuring CO ₂ with TCD detector 1 st experiment.	126
Figure 4.26 Benzene degradation justification by measuring CO ₂ with TCD detector. 2 nd and 3 rd experiment.	127
Figure 4.27 Finger testing of a) addition to commercial paint, b) S8 after deposition with water solution.	129
Figure 4.28 Finger testing of a) S9 sample a) without and b) with white cement binder.	130
Figure 5.1 Frost Diagram formed for N atom.	139
Figure 5.2 Frost Diagram formed for C atom.	139
Figure 5.3 Schematic diagram of the formation of methane from spilled over hydrogen and carbon containing species on the surface under UV and dark conditions.	141
Figure A.1 Phase Diagram of CaO-SiO ₂ System	167
Figure B.1 a) Cured grout sample b) Pure Coated Glass Slides used in the experiments.	170
Figure B.2 Experimental set up used in a) Photocatalytic Benzene Oxidation Experiments b) CO ₂ hydrogenation to methane experiments.	171
Figure C.1 DRIFTS Spectra Comparison of pure powder, coating and grout applications using S8 powder.	172
Figure E.1 Results of UV-Vis spectra for changing S9 wt%.	183
Figure E.2 a) Graphical representation of calculated area under UV absorption, b) the increase of the area intensity with TiO ₂ % content.	183
Figure E.3 Absorption area vs reaction rate correlation for S9 sample.	184
Figure H.1 UV-Vis Spectra of used materials in photocatalytic experiments.	189
Figure H.2 Typical IR spectrum of anatase sample in ambient conditions....	189
Figure I.1 Finger testing of S13-binder formulation prepared at 700°C.	192

LIST OF SYMBOLS

\AA	Angstrom, length unit
A	Absorbance
a	Absorptivity of the species
a_0	Radius of the hydrogenic wave function of the trapped carriers
at	Atomic
ATR	Attenuated Total Reflectance
b	Cell path length
BET	Brunauer-Emmett-Teller
C_2S	Dicalcium silicate
C_3S	Tricalcium silicate
C_3A	Tricalcium aluminate
C_4AF	Tetracalcium alumino-ferrite
C-S-H	Calcium-silicate-hydrate
C_{a0}	Initial benzene concentration
C_a	Concentration of benzene at time t
C	Molar concentration of the analyte
DRIFTS	Diffuse Reflectance Infrared Fourier Transform Spectroscopy
e^-	Electron
ϵ	Molar absorptivity
FID	Flame Ionization Detector
FTIR	Fourier Transform Infrared
GC	Gas Chromatography
h^+	Hole
k	rate constant of the reaction, s^{-1}
k_{recomb}	Recombination rate through tunneling between the trapped charge carriers
k	Molar absorption coefficient of the analyte
K	Proportionality constant based on absorption coefficient and the path

	length
M	Molarity, mol/liter
MCM	Mobil Composition of Matter
M_n	Molecular weight, g/mol
NOx	Generic term for NO-NO ₂ mixture
ppm	Parts per million
ppmv	Parts per million by volume
pts.wt.	Parts per weight
R	Universal gas constant
RH	Relative humidity
R_{∞}^t	Reflected intensity of the sample to that of a nonabsorbing standard
rxn	Reaction
s	Scattering coefficient
SBA-15	Santa Barbara Number 15
T	Temperature, K
τ	Residence time, s
TCD	Thermal Conductivity Detector
TEM	Transmission Electron Microscopy
TGA	Thermal Gravimetric Analyzer
θ_o	Macroscopic (apparent) contact angle
θ	Intrinsic (Young) contact angle
Vis	Visible
XPS	X-Ray Photoelectron Spectroscopy
XRD	X-ray Diffraction
VOC	Volatile Organic Compounds
wt.	Weight
w.r.t.	with respect to

CHAPTER 1

INTRODUCTION AND SCOPE OF THESIS

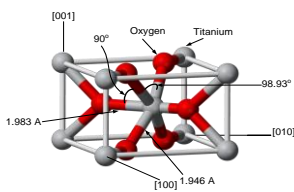
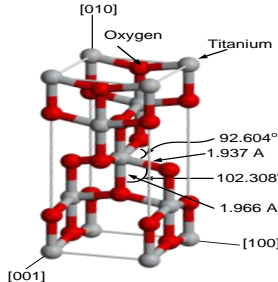
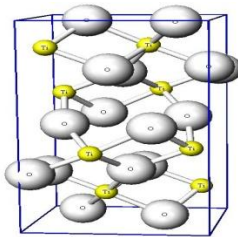
1.1 DEFINITION OF TiO₂ PHOTOCATALYSIS

Photocatalysis is the increase of the rate of photo induced reaction in the presence of a semiconductor catalyst, which can be manipulated by changing electron density in the conduction band. This manipulation can be done easily by the energy of light enough to create an electron excitation from valence band to conduction band. Under this condition, semiconductor creates electron - hole pairs, which leads to further oxidation and reduction reactions through radical chemistry. Photocatalysis is generally known with TiO₂ since TiO₂ is the classic semiconductor used in the area historically.

TiO₂ is a white pigmentary material, inexpensive and harmless semiconductor. There are three crystal phases of TiO₂. Anatase, rutile and brookite (Table 1.1). Other structures may exist such as cotunnite TiO₂ has been synthesized at high pressures and is one of the hardest polycrystalline materials known. Only rutile and anatase play role in TiO₂ applications. In both structures, the basic building of block consists of a titanium atom surrounded by six oxygen atoms in a more or less distorted octahedral configuration (Table 1.1). In all three TiO₂ structures, the stacking of octohedra results in threefold coordinated oxygen atoms. Rutile TiO₂ single crystals are widely available.

Experimental studies on anatase surfaces are lower than rutile single crystal studies, since anatase phase is a metastable phase and transformation to rutile is easy at low temperatures. The rutile (110) surface is the most stable crystal surface. The shapes of the crystallites vary with the preparation techniques and procedures. Typically, (101) and (100)/(010) surface planes are found, together with some (001). The (101) surface is thermodynamically most stable surface [1]. Refractive indices are given as 2.488, 2.583, and 2.690 for anatase, brookite and rutile respectively [2].

Table 1.1 Bulk structures of rutile, anatase and brookite [1].

	Unit Cell	Unit Cell Dimensions
Rutile		Tetragonal, $D_{4h}^{14} - P4_2/mnm$, $a=b=4.584$ Å, $c=2.953$ Å
Anatase		Tetragonal, $D_{4h}^{19} - I4_1/amd$, $a=b=3.782$ Å, $c=9.502$ Å
Brookite		Rhombohedral, $D_{2h}^{15} - Pbca$, $a=5.436$ Å, $b=9.166$ Å, $c=5.135$ Å

The phase diagram of Ti-O system is given in Figure 1.1. As seen in the Figure 1.1, Ti-O system has many stable phases, which is an indication of easy reducibility. The region $\text{Ti}_2\text{O}_3 + \text{TiO}_2$ also includes seven Magneli phases ($\text{Ti}_n\text{O}_{2n-1}$) [1].

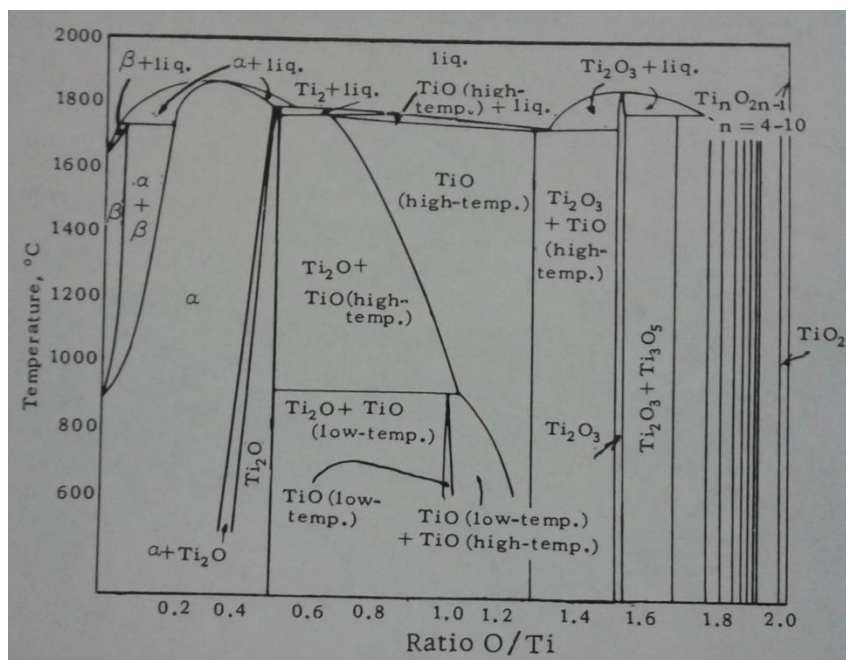


Figure 1.1 Phase diagram of Ti-O system [3].

When a TiO_2 photocatalyst absorbs a photon with energy equal to or greater than its band-gap, an electron hole pair is generated; subsequently, the pair is separated into a free electron and a free hole in femtosecond range. The electron and hole “walk randomly” to the surface of the photocatalyst and are trapped there. The trapping of electron and holes and their relaxation times are in picosecond range. The trapped electron e_{tr}^- and hole h_{tr}^+ react with acceptor

or donor molecules, respectively, or recombine at surface trapping sites. The electron and hole can also be trapped at bulk trapping sites and recombine there with the release of heat [4].

Charge carrier trapping is needed in the photocatalysis process to suppress recombination and increase the probability of interfacial charge transfer [5]. The recombination can be delayed, with a lifetime on the scale of μs in nanocrystalline TiO_2 films. This makes the slow charge transfer of electrons to molecular oxygen competitive with the recombination. O_2 reduction with electron is observed between 10-100 μs [6]. With Pt deposition, transfer of electron to Pt is observed in 2.3 ps [7]. Identified oxidizing species include holes, either free or trapped, $\bullet\text{OH}$ radicals, $\text{O}_2\bullet^-$ and $^1\text{O}_2$ [5,8,9]. H_2O_2 and O_2 are also involved in photocatalytic oxidation processes in various mechanisms. [10,5,8]. Photoproduced holes are trapped within picoseconds at the TiO_2 photocatalyst surface. This indicates that primary oxidation processes are caused by trapped holes [4]. Interfacial charge transfer is seen for 300 ps for methanol oxidation [11], 3 ns for 2-propanol oxidation [11] and around 2 microsecond for water oxidation [6]. The valence band holes are powerful oxidants (+1.0 to +3.5 V vs. NHE depending on the semiconductor and pH), whereas the conduction band electrons are good reductants (+0.5 to -1.5 V vs. NHE). Such redox potentials can easily achieve the complete degradation of many organic pollutants [12]. The photocatalytic activity increases in anatase phase mostly due to high OH radical generation rate [13].

1.2 UTILIZATION of TiO_2 PHOTOCATALYSIS in SELF-AIR CLEANING

One of the most important applications of TiO_2 photocatalysis is to decontaminate, deodorize, and disinfect indoor air. Low-concentration volatile organic compounds (VOCs), such as formaldehyde, and toluene, emitted from

interior furnishings and construction materials, may lead to the "sick building syndrome" and other diseases. Besides, the indoor air of public facilities, which is normally contaminated with bacteria, fungi, etc., threatens the health of users [4].

"Indoor air" is defined as the air in non-industrial areas of dwellings, offices, schools and hospitals. Indoor air pollutants mainly include nitrogen oxides, carbon oxides, volatile organic compounds (VOCs), and particulates. These pollutants are emitted from different sources such as cooking, combustion by-products, office equipment, construction materials, and consumer products. According to definition of World Health Organization (WHO), VOCs are referred as all organic compounds in the boiling range of 50-260°C, excluding pesticides (Table 1.1). The main concentration of each VOC is dependent on the environment. The mean concentration of each VOC in established buildings is generally below 50 $\mu\text{g}/\text{m}^3$, but higher than 5 $\mu\text{g}/\text{m}^3$. Building materials and coverings are major contributors to indoor VOCs with various emission rates. Many VOCs are known to be carcinogenic or mutagenic. These VOCs have a close relation with the sick building syndrome which is used to describe symptoms of reduced comfort and health [14].

Three methods are suggested to improve indoor air quality; source control, air cleaning and increasing ventilation. Source control is ungovernable in cities. Ventilation increase may bring more pollutants from outdoor. Air cleaning is the most feasible option. Activated carbon adsorption only transfers pollutants from gaseous phase to solid phase. Advanced thermal oxidation is not economic in low pollutant concentrations. Photodegradation occurs at room temperature (RT) and pressure and it seems like a cost-effective method [14].

Self cleaning term is used for surfaces, which have the ability of cleaning itself. The aim is maintain surface as clean as possible and decrease maintenance costs. A good self-cleaning surface should have photocatalytic properties. However, in some cases, only photocatalysis is not enough due to slow rates of decomposition reactions. When concentration of carbon

containing compounds is high on the surface, utilizing natural cleaning effects such as rain could be useful to minimize the carbon containing compounds on the surface. For efficient use of these natural effects, surface properties are modified such as hydrophilic or hydrophobic, both of them have advantages and disadvantages.

Table 1.1 Classes of VOCs and their possible emission sources [15]

VOC Class	Environment and sources
Aliphatic and cyclic hydrocarbons	1,2,4,5,7,9-11
Aromatic hydrocarbons	1-7,9,11,12
Aldehydes	1-12
Terpenes	1-4,7-10
Alcohols	1-9,11
Esters	1,2,4,7-9
Halocarbons	1,2,7,11
Glycols/glycoethers/glycolesters	1-4,7,9
Ketones	1-4,6-12
Siloxanes	11
Alkene	2,7
Organic acids	2,3,7-9,11
Ethers	9
Other VOCs	1,2,4,7,11

1:Established buildings, 2:new and renovated buildings, 3:school, 4:new car interiors, 5:carpets, 6:floor coverings, 7:wood-based panel and furniture, 8:solid woods, 9:paints, 10:cleaning products, 11:unflued gas heaters and electric ovens, 12:office equipment.

1.3 PHOTOCATALYTIC TiO₂ USAGE in CEMENTITIOUS PRODUCTS

With increasing urbanization, population of cities and therefore usage of cementitious materials is continuously rising. Cementitious materials are

ideal due to their large availability as outdoor and indoor surfaces. Convenient surfaces for photocatalytic activity such as roads, pavements, tunnels are cement based materials. Cementitious materials are also used in large amounts under sunlight, which is the most abundant source of energy with possible photocatalytic utilization. Unlike high organic resin containing paints, they contain lower amount of organics and due to high inorganic content, show resistance to degradation reactions caused by photocatalytic material. A broad list of applications of photocatalytic cement based materials is summarized in Table 1.2 [16].

Table 1.2 Applications of cement based materials [16].

Horizontal applications	Vertical Applications	Tunnels
-Concrete pavements	- Indoor and Outdoor paints	-Paints and renderings
-Paving blocks and paving plates	- Finishing coatings, plasters, and other final rendering cement-based materials	-Concrete panels
-Other coating systems for pavement and roads (white topping, self leveling mortars,...)	- Covering precast panels	-Concrete pavements
- Roofing tiles	- Permanent formworks	-Ultra-thin white topping
- Roofing panels	- Masonry blocks	
- Cement-based tiles	- Sound-absorbent elements for buildings and roads applications.	
	- Traffic divider elements	
	- Street furniture	
	- Retaining fair-faced elements	

Using photocatalytic properties in cementitious materials give self cleaning ability to the surfaces, which preserve the aesthetic view of the surface, decreases the cleaning and renewing costs. In recent years, some important buildings have been built using photocatalytically active cement on

top layers such as Dives in Misericordia church in Rome and ‘l’Ecole de Musique’ in Chambéry, France [17]. In Europe some collaborative projects with industry have taken place such as PICADA (Photocatalytic Innovative Coverings Applications for Depollution Assessment), which focuses on the air de-pollution and on self cleaning activity on cementitious products and coatings. In Japan, photoactive paint is used near the roads to reduce NO_x concentrations. Construction material sector export is increasing for Turkey where Turkey has reached 8th place in the world (Figure 1.2). When total sales of Toto (Japan) Company is inspected as the representative of a photocatalyst firm, it is seen that 90% of sales are of construction materials (Figure 1.3).

The economics of dry mix production are important, it is a competitive business and an uncompetitive producer will not survive. Certainly reliability and reputation are also important, but costs must be included. The main cost factors are; ability to design economical mixes, unit costs of materials, control margin (necessary difference between mean and specified strength), expenditure on equipment, staff, software and efficiency of operation. A producer must be able to make the correct choice of materials, taking into account the variability of those materials, which can increase costs by increasing concrete variability and therefore the necessary control margin. The ability to determine the relative proportions of available aggregates without extensive trial mixes is a substantial factor in making the correct decision [18].

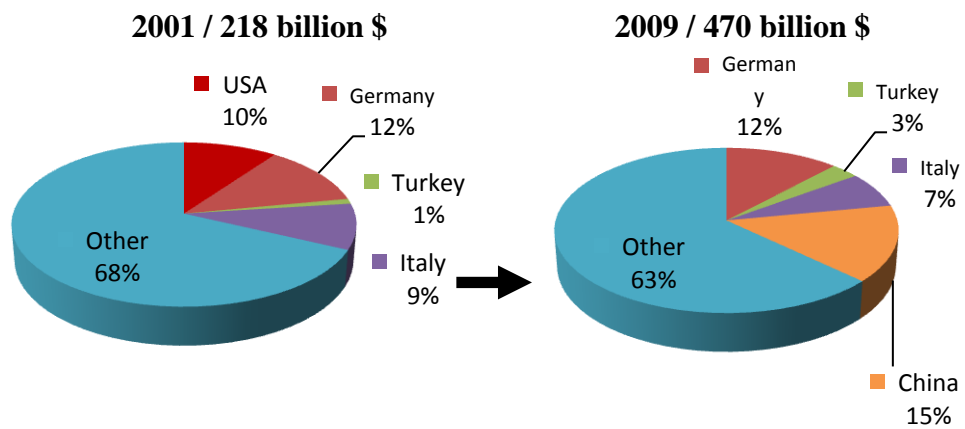


Figure 1.2 Construction material sector export chart (The charts are redrawn and translated to the English) [19].

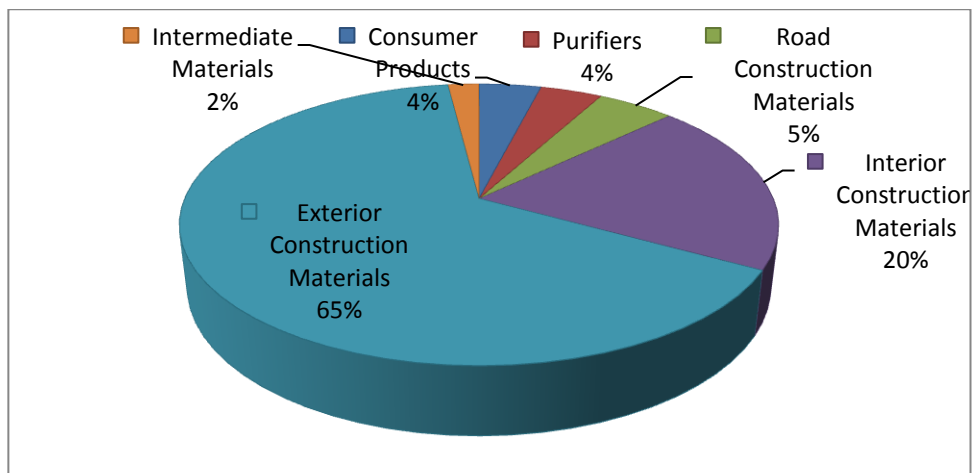


Figure 1.3 Toto company sales chart (The chart is redrawn from ref [20])

1.4 SCOPE OF THESIS

In this thesis, cement based materials were promoted and photocatalytic activity was brought into plaster and grout. The photocatalytic efficiency of the products was increased by using TiO_2 on the surface. A commercial TiO_2 powder was selected out of 15 commercial TiO_2 samples to be used in self cleaning applications. A method based on gas phase benzene oxidation was developed to evaluate the activity of TiO_2 powders, grout and plaster samples. 15 TiO_2 powders, grout and plaster samples were characterized using different techniques such as XRD, BET, DRIFTS, UV-Vis with diffuse reflectance, SEM and Raman Spectroscopy. The morphology of the materials were characterized and related with the activity. In addition, gaseous phase photocatalytic CO_2 reduction was also studied and given in this thesis study.

The scope of thesis is to promote the cementitious materials with TiO_2 and apply photocatalysis to grout and plaster, which will lead us to self cleaned surfaces and also elimination of VOC and PM. For this purpose, the distribution and mixing of TiO_2 in the media is important since the activity depends on the sites present on the surface and on the bulk. Commercial TiO_2 with different structural and chemical properties were used in order to understand the effect on activity. Determination of reactive volume in the media and optimum amount of TiO_2 usage are important in terms of efficiency.

In this thesis, a brief introduction and scope of thesis is given in chapter 1. In Chapter 2, a detailed literature summary is given on self cleaning surfaces, visible light photocatalysis, surface characteristics of a metal oxide and patents on TiO_2 mediated self cleaning cement based materials. The synthesis procedures for studied samples, the details on used equipment for activity measurements and characterization experiments are explained in experimental part in Chapter 3. In Chapter 4, characterization and photocatalytic benzene oxidation studies are given. By using photocatalytic benzene oxidation experiments, the activities of pure TiO_2 , Fe- TiO_2 , TiO_2

added grout and plaster samples are measured. In addition to that, XRD, BET, UV-VIS, Raman, SEM and DRIFT Spectroscopy techniques are used in characterization of samples. In Chapter 5, factors effecting the selection of TiO_2 powder and utilization of TiO_2 on the surface, visible light studies, synergic effect of TiO_2 and cement medium for the NO_x removal, photocatalysis in reduction reactions and UV-Vis diffuse reflectance studies are discussed in separate parts. In Chapter 6 and 7, conclusions and recommendations are given respectively.

CHAPTER 2

LITERATURE SURVEY

2.1 SELF CLEANING SURFACES - CEMENT

2.1.1 Particle Size – Crystal Face - Phase Effects on Activity

Decrease in particle size affects the volume and surface e^-/h^+ recombination rates. Reducing the particle size decreases the volume recombination and leads to a higher photonic efficiency from a higher interfacial charge carrier transfer rate. But when going to ultra small particles, surface recombination becomes important and photoactivity is balanced. Reduction in particle size also leads to difference in adsorption properties and increase in activity of surface sites which is due to formation of large amount of defects, corners, edges compared to planar surfaces [21]. Particle size effect is important since it is closely related with photocatalytic activity. According to Zhang *et al.*, the photoreactivity of pure TiO_2 increases when particle size is reduced from 21 to 11 nm, but decreases when it is further reduced to 6 nm. A particle size of about 10 nm might be the optimal value for pure TiO_2 photocatalyst in liquid-phase decomposition of $CHCl_3$. They also claim that an optimum dopant (in this case Fe^{+3}) concentration which depends on particle size exists for higher photocatalytic activity [22]. A model based on the mechanism of photocatalysis predicts higher quantum efficiency with an

increase in particle size from 3 to 21 nm [23]. Increase in activity with decreasing particle size were reported in gas phase photocatalytic oxidation studies for pure TiO₂ samples [24,25]. Lackhoff *et al.* observed decrease in photocatalytic activity using atreazine as a model compound with the increase of TiO₂ particle size when TiO₂ particles are used as cement additive (Degussa P25, Hombikat UV-100 (anatase), Jenapharm (anatase)) [26].

TiO₂ nanoparticles start to show different properties than bulk such as increase in conduction band and decrease in valence band when ultra small particles form. The increase in band gap is observed as blue shift in the absorption edge which is also called quantum-size effect [27]. Quantization effect is observed when crystallite dimension at least for one dimension is comparable with the exciton (Bohr) radius. The exciton radius of TiO₂ is small due to high effective mass of electrons in TiO₂ [28]. The effective mass of electron and hole or charge carriers influences the quantization threshold [29]. The quantum size effect is generally observed for particles smaller than 3 nm which particles are prepared by temperature controlled hydrolysis of TiCl₄ in different solutions [30], anodic oxidative hydrolysis of TiCl₃ [28] or using dendrimer templates [27]. There are studies which do not observe band gap energy change [31] or which relates observations other than quantization effects such as direct (Frank-Condon type) transitions in an otherwise indirect band gap semiconductor [29]. According to Anpo *et al.*, photocatalytic activity increases as particle size decreases due to quantum size effects at particle sizes smaller than 10 nm which is a bigger threshold than other studies mentioned above. They also relate the activity with surface area using BET measurements for anatase and rutile particles [25].

Phase effect is important in TiO₂ studies since there is an incredible difference in photocatalytic activity among its different crystalline phases. Anatase is the photocatalytically active phase while rutile activity is almost zero despite the fact that the photoactivity of rutile extends into the visible light range. When two phases are mixed, enhancements in the photocatalytic activity

are observed in most cases such as commercial Degussa P25. Degussa P25 is roughly composed of 75% anatase and 25% rutile phases. There are numerous articles which try to explain the mixed phase effect. According to a model, the increased activity is based on rutile e^- sink, which prevents anatase e^-/h^+ recombination and leads anatase originating hole to the surface [32]. In other study, it was confirmed by ESR (Electron Spin Resonance) that rutile also facilitates stable charge separation by e^- transfer from rutile to lower energy anatase lattice trapping sites. This creates holes on the rutile. e^- moves from anatase trapping sites to surface trapping sites separating e^-/h^+ pair [33]. Since the excitation of e^-h^+ pairs occurs on different phases, contribution to the activity is possible for both theories. The light energy changes the contribution ratio to the activity. Bickley *et al.*, examined Degussa P25 structure by diffuse reflectance UV spectroscopy, TEM and XRD. They concluded that anatase forms the core of the particle and rutile exists as a thin overlayer on anatase in most of the particles. They discussed the production process of TiO_2 (flame aerosol process) is convenient for such a formation and proposed the above model [32]. In a different study, a mixture of anatase and rutile were obtained from different commercial products and a synergy was observed as in Degussa P25 [34]. In other studies [22,35], anatase and rutile particles of Degussa P25 were observed distinct from each other.

Matsumura *et al.* studied the crystal-face-dependent photocatalytic reactivity of rutile and anatase particles [36]. The TiO_2 powder used in their study consisted of 1- μm size rutile and anatase particles with well-developed crystal faces. The rutile particles showed a tetragonal prism structure with four planes, which are assigned to the (110) faces. Each end of the prism is capped by four planes, which were assigned to the (011) faces. The anatase particle had a tetragonal bipyramid structure consisting of eight (011) faces. Both vertexes were removed and capped by (001) faces. After photocatalytic oxidation of water on the powder using hexachloroplatinate ions as the electron acceptors, Pt deposits were observed mostly on the rutile particles, especially

on the (110) face, indicating that the reduction sites of rutile particles were on the (110) face. When 2-propanol was added to the solution, Pt was deposited on both the anatase and rutile particles. Using the thus-prepared Pt-deposited TiO₂ powder, Pb²⁺ ions were photocatalytically oxidized to PbO₂, which were deposited on the TiO₂ particles. They observed the selective deposition of PbO₂ on the (011) face of rutile particles, and for anatase particles, PbO₂ was deposited in a larger amount on the (001) face than on the (011) face. This means that the (011) face provides the oxidation site for rutile particles, while for anatase particles the (001) face is more oxidative than the (011) face. In another study, Matsumura and co-workers etched the same anatase particles with HF solution [37]. By this process, the edge between two (011) faces was selectively etched and as a result, eight new faces were generated on each particle, which were assigned as (112) faces. The new anatase particles were photocatalytically deposited with Pt and PbO₂ in sequence. Interestingly, most of the Pt was deposited on the (011) faces, while PbO₂ was deposited on the newly generated (112) faces, indicating the reductive function of the (011) faces and the oxidative function of the (112) faces for the anatase particles. These results suggest that crystal faces could assist in the separation of electrons and holes, and thus, it may be possible to obtain high photocatalytic activity through control of the surface atomic arrangement of TiO₂ photocatalysts.

2.1.2 Photocatalysis in Oxidation Reactions

Previous product analyses on various photocatalytic reactions led to the postulate that •OH radicals, produced by oxidation of surface hydroxyl or adsorbed water, play an important role in initiating oxidation reactions, especially for substances that adsorb weakly on the TiO₂ surface [5,38]. Superoxide O₂•⁻ is less important in initiating oxidation reactions compared to

those concerning holes and $\bullet\text{OH}$ radicals. The role of $\text{O}_2^{\bullet-}$ in photocatalytic oxidation processes was discussed mainly within the framework of participation in the total mineralization of organic substances through reaction with organoperoxy radicals, the production of H_2O_2 by disproportionation reaction, and the anti-microbial activities [5,8,10]. Molecular oxygen plays an indispensable role in TiO_2 photocatalysis, especially in reactions related to environmental cleanup applications [5,8,10]. It assists the charge separation in TiO_2 by capturing TiO_2 electrons; it generates active species such as $\text{O}_2^{\bullet-}$, H_2O_2 ; $^1\text{O}_2$, etc. that participate in reactions; it participates in the reaction and accelerates the mineralization of organic substances; it also helps the TiO_2 photocatalyst to maintain stoichiometry during photocatalytic reactions.

Berger *et al.* found that molecular oxygen could not only capture the photogenerated electrons to suppress charge recombination, but also improve the photostimulated charge separation in TiO_2 nanoparticles, i.e., more holes could be trapped within the particles in the presence of molecular oxygen [39]. Superoxide ($\text{O}_2^{\bullet-}$) and hydrogen peroxide are two main products of O_2 reduction in TiO_2 photocatalysis and are involved in the production of other active oxygen species such as $\bullet\text{OH}$, $^1\text{O}_2$.

2.1.2.1 Photocatalytic Benzene Oxidation as a Model Reaction

Benzene is found naturally in crude oil and thus passes into refined products, including transportation fuels. The U.S. Environmental Protection Agency (EPA) classifies benzene as a Group A, known human carcinogen, which can have harmful effects on bone marrow and lower red blood cell count. Controlling benzene levels in gasoline is the most direct way to limit evaporative and exhaust emissions of benzene from vehicles [40].

During the past 60 years, concerns about the adverse effects of benzene in exposed workers have led to a series of increasingly stringent regulatory

standards in the United States for benzene in the workplace (Table 2.1), and in 1978, there was a voluntary withdrawal of benzene as an added ingredient to consumer products manufactured in the United States [41,42]. Over the past 25 years, concentrations of benzene in various consumer products have generally been between zero and less than 0.1% [43].

Table 2.1 History of benzene regulatory standards [41].

Time period	TLV (ppm)	PEL (ppm)
<1946	100	-
1947	100	-
1948	50	-
1949-1957	35	-
1964-1969	25 (ceiling)	-
1957-1976	25	-
1972-1986		10
1987-current		1
1977-1996	10	-
1997-current	0.5	-

TLV = threshold limit value, a recommended standard from the American Conference of Governmental Industrial Hygienists (ACGIH); PPM = parts per million; PEL = permissible exposure limit, an enforceable standard created by Occupational Safety and Health Administration (OSHA). All concentrations represent time-weighted averages (TWA) unless otherwise noted.

Benzene has been selected as model compound in photo oxidation reactions, because benzene is a hard molecule to decompose, since it is a stable aromatic ring with no side groups. Zuo *et al.* [44] studied gas-phase photolytic and photocatalytic reactions of several aromatics and chloro hydrocarbons and showed that chloro hydrocarbons and toluene may degrade with photolysis

reactions whereas for benzene the degradation was hard with photolysis reactions. Another reason to select benzene is to utilize the background of previous studies done in our laboratory [45,46].

Bouazza *et al.* studied benzene and propene at 100 ppmv in terms of humidity. The conversion of benzene increased noticeably when compared with zero humidity. It remained nearly constant further increasing relative humidity from 38%-93%. 35% benzene conversion was detected for 93% RH (Degussa P25). Propene activity showed different trend than benzene and decreased linearly with humidity [47].

Einaga *et al.* [48,49,50] studied the effect of humidity, benzene concentration and incident light intensity. The benzene conversion increased with increasing TiO₂ amount. Benzene conversion decreased with time from 100% to 80% with 125 ppmv benzene to 20% with 250 ppmv. Reaction rate decreased with benzene concentration, increased with incident light intensity, decreased with humidity. They changed weight of catalyst /flow ratio (W/F), water, initial benzene, and O₂ concentration and found that O₂ and H₂O are necessary for the reactions and these parameters increased the benzene conversion from 0% to 60-100%. W/F ratio increase enhanced benzene conversion. The increase in initial benzene concentration (80 ppm to 260 ppm) decreased the conversion from 90% to 15%. CO₂/CO selectivities remained constant for almost all experiments at 93/07% respectively. They also discussed a reaction mechanism. Same group studied diffuse reflectance FTIR measurements in order to investigate photo-oxidation of benzene and ethylene. In the absence of water vapor, oxygen containing by-product compounds were formed and they were decomposed in the presence of water vapor with a slight induction period. Pt deposition to TiO₂ slightly enhanced the rate. They proposed that the formation and decomposition behavior of by-product compounds is one of the important factors controlling the catalytic activity. DRIFTS spectra was taken at RT. They attributed the formation of phenol and brownish material to the polymeric products on catalyst surface.

Geng *et al.* [51] designed a circulated photocatalytic reactor to enhance the performance of photocatalytic degradation of benzene. The results indicated that the degradation conversion, apparent reaction rate constants and initial degradation rate were closely related with initial concentration of benzene. Kinetics of the photocatalytic degradation of benzene were analyzed using the Langmuir adsorption isotherm and Langmuir-Hinshelwood kinetic model. The reaction kinetics was described by a pseudo-first order kinetic equation of photocatalytic degradation of benzene. The kinetics is mostly governed by the mass transfer effect at low concentrations of reactant and adsorption characteristics of the catalyst, while they are controlled by the photon transfer effect at high concentrations of benzene. It was found that the decomposition reaction rates of benzene are significantly affected by mass transfer at higher flow rates, but at lower flow rates, surface reaction controls the progress of such reactions.

Doucet *et al.* [52] studied the influences of the concentration, light flux and temperature on the initial degradation rate. Apparent deactivation of the catalyst has been observed due to the formation of an intermediate which decomposes to CO and CO₂ with a slow photocatalytic reaction. The relative humidity is not important in the first attack of benzene but enhances the conversion due to the increase in the degradation of the intermediate.

Jo *et al.* [53] investigated the photocatalytic removal of five VOCs: benzene, ethyl benzene, o-, m-, p-xylenes. They changed the relative humidity, reactor diameter and flow rate in order to develop strategies for the control of in-vehicle VOCs. The degradation rate was dependent on hydraulic diameter of the reactor and flow rate. Some CO formation occurred. For different humidity levels, the conversion was 100% between 4-93 ppbv benzene initial concentrations.

Larson *et al.* [54] studied the initial steps in photocatalytic oxidation of benzene, toluene, p-xylene, mesitylene, benzyl alcohol, benzaldehyde, and m-cresol adsorbed on TiO₂ thin film. Adsorbed aromatics were oxidized by O₂

photocatalytically in the absence of gas-phase aromatics. The surface compounds were characterized by temperature programmed oxidation and desorption. Benzene and methyl benzenes oxidize rapidly at 273 and 300 K to form adsorbed intermediates that are more strongly adsorbed and less reactive than original aromatic, which is relatively weakly adsorbed on TiO₂. The rates of photocatalytic oxidation of benzene to CO₂ are slow relative to complete oxidation of alcohols or chlorinated hydrocarbons. The intermediates do not appear to be alcohols or aldehydes formed by oxidation of a methyl group, nor do they correspond to addition of a hydroxyl to the aromatic ring. m-cresol does not photocatalytically oxidize.

Lewandowski *et al.* [55], considered two variations of a simple kinetic model for photocatalytic oxidation of benzene, toluene and m-xylene. Kinetic model using a single adsorption site is unable to replicate the experimental results but using a two site adsorption was able to produce results consistent with experimental data. Two-site model incorporates hydrophobic type 1 site which is accessible to aromatic contaminants and reaction intermediates and hydrophilic type 2 sites which is only accessible by partially oxidized reaction intermediates. These sites allow to accumulate intermediates in the initial period of the UV exposure and give high initial reaction rates. As the quantity of intermediates become higher, type 1 sites become blocked by intermediates, aromatic adsorption rate decreases until a steady state removal rate is reached. Authors also extended model to consider the photocatalytic degradation behavior of toluene at various feed concentrations. The model reasonably fits for experimental data with no significant changes to model [56].

Ma *et al.* [57] studied the effects of UV, humidity, and benzene concentration on benzene decomposition kinetics with a optical-fiber reactor. The benzene decomposition and CO₂ production rates increased with UV intensity. The humidity influenced the degradation strongly giving a maximum at 20% RH. They proposed a competitive mechanism between water and reactive species at higher RH. Low relative humidity promotes formation of

free hydroxyl radicals. Purging with ozone containing air rapidly decomposed the organic residues on the surface within 30 minutes.

Tsoukleris *et al.* [58] tested the photocatalytic oxidation of VOCs (benzene, toluene, o-, m-, p-xylenes) using a photocatalytic packed bed reactor. The photocatalytic oxidation rate increased with light intensity. Reproducibility tests proved that photocatalytic activity of the photocatalyst remains intact even after thirty consecutive experiments.

Vorontsov *et al.* [59] studied the effect of gas phase H_2O_2 on photocatalytic oxidation of benzene vapors. The increase in the inlet H_2O_2 concentration from 0 to 1000 ppm led to one order of magnitude increase in the benzene complete oxidation rate. The results suggest that additions of hydrogen peroxide vapors can prevent the deactivation of the TiO_2 photocatalyst (Degussa P25).

Wang *et al.* [60,61] studied the effects of humidity, UV light intensity and benzene concentration on the photocatalytic conversion and mineralization of benzene. Experimental results can be described by Langmuir-Hinshelwood kinetics. Concentration distribution of benzene in annular flow reactors of various dimensions can be described by combining the reactor design equation with L-H kinetics. Deactivation of the catalyst was observed and attributed to the adsorption of reaction intermediates on TiO_2 surface. The deactivated catalyst could be photochemically regenerated by ozone-purging in the presence of humidity. The reaction products adhered to the surface were determined by FTIR spectrum. Phenol was identified as the major intermediate generated at early stages of benzene decomposition.

Wu *et al.* [62] studied the effects of temperature, humidity and benzene concentration on the photocatalytic oxidation of benzene vapor on TiO_2 (Degussa P25). The experiments were conducted with 250-450 ppmv benzene concentrations, water concentrations of 13500-27500 ppmv and reaction temperatures of 100-200°C. Benzene oxidation rates increased with temperature below 160–180°C, but decreased with temperature above 160–

180°C. Raising the reaction temperature increased the chemical reaction rates but reduced the reactant adsorption rate on TiO₂ surfaces. The overall reaction rate increased with temperature, indicating that the reduction of reactant adsorption rate did not affect the overall reaction, and thus the chemical reaction was the rate-limiting step. As the chemical reaction rate gradually exceeds the reactant adsorption rate with temperature, the rate-limiting step was shifted from the chemical reaction to the reactant adsorption. Additionally, the competitive adsorption between benzene and water for the active sites on TiO₂ resulted in the promotion and inhibition of reaction rate by humidity. A modified bimolecular Langmuir–Hinshelwood kinetic model was developed to simulate the temperature and humidity related promotion and inhibition of the photocatalysis of benzene.

Wu *et al.* [63] studied the adsorption, thermal reactions and photochemistry of benzene on powdered TiO₂ using FTIR. Benzene is adsorbed with its π electrons interacting with the surface Ti⁺⁴ ions, is stable even at 400°C. However, thermal decomposition occurs below 225°C to H₂O (g), CO(g) and CO₂(g). It is found that phenoxy groups formed on the surface with photooxidation of benzene. The amount increases with H₂O and O₂. Other surface products containing carboxylates or carbonyl groups are formed. The extracted surface products may not be true surface products. Phenoxy groups may form phenol especially in acidic extract solutions whereas in most of the studies, adsorbed phenol was shown as the surface species on TiO₂ (Degussa P25).

Zhong *et al.* [64] studied photocatalytic oxidation of benzene in air with pure TiO₂ and TiO₂/Sr₂CeO₄ catalysts. The kinetic data was modeled with Langmuir–Hinshelwood kinetic model with the limiting rate constant and adsorption constant were 0.0064 mg l⁻¹min⁻¹ and 9.2078 l mg⁻¹ respectively. No gas phase intermediates were detected by GC/FID analysis despite high benzene concentrations. Ethyl acetate and (3-methyl-oxiran-2-yl)-methanol were two major surface intermediates detected.

Hong *et al.* [65] studied superhydrophilic properties of metal-TiO₂ photocatalysts, including Bi³⁺, V⁵⁺, and Bi³⁺-V⁵⁺ ions and their benzene photodecompositions with or without H₂O addition. The benzene decomposition in batch system increased in the order of Bi(3.3)-V(6.7)-TiO₂>V-TiO₂>pure TiO₂>Bi-TiO₂, and the maximum benzene conversion was 35% after 60 min. The conversion remarkably increased in almost all catalysts with H₂O addition during the benzene photo-decomposition reaction, reached up to 80% after 180 min in Bi-V-TiO₂. In continuous system for Bi-V-TiO₂ with H₂O addition, the photodecomposition rate of 50% was maintained for 168 h, without catalytic deactivation.

Lin *et al.* [66] studied TiO₂ and TiO₂/Bi₁₂TiO₂₀ catalysts with decomposition of gaseous benzene in a batch reactor. They showed that TiO₂/Bi₁₂TiO₂₀ absorbed more UV light than TiO₂ and showed a red shift and the activity was enhanced. 2.0 % TiO₂/Bi₁₂TiO₂₀ system exhibited highest photoactivity.

Jacoby *et al.* [67] studied benzene oxidation on TiO₂ films (Degussa P25). The products formed in the gas and liquid phases and reaction conditions are given in Table 2.2-2.3. They observed CO additionally as gas phase product. This observation has been commented that the contact time was too low for a complete oxidation reaction between TiO₂ and organics [68]. They observed difference in the adsorption amount of benzene between the dark and UV irradiated conditions. They showed that co-adsorption of O₂ does not affect the benzene adsorption whereas water does. Since the steady and maximum rates for different benzene concentration do not change too much, it is indicative that adsorption is much faster than reaction steps. As the concentration of the pollutant decreases, the number of molecules adsorbing on the surface at a given flow rate also decreases, the difference between the rate of adsorption and rate of reaction becomes smaller. They also made an extrapolation of steady state curve to interpret that 5 ppm or less benzene would undergo complete conversion. This concentration is higher than typical

indoor pollutants [69]. The decrease from maximum rate to steady state rate occurs due to occupation of active sites by less reactive intermediates and leading to reactions which are much slower. This is also verified by regeneration of the catalyst by feeding air without benzene under UV irradiation. This is also a proof that it can be used as a self cleaning filter which has the capability of regeneration and can withstand purges of pollutant concentrations. Also by washing the catalyst surface with water, quick regeneration is possible.

D'hennezel *et al.* [68] studied benzene and toluene gas-phase photocatalytic degradation over H₂O and HCl pretreated TiO₂ catalysts. Their aim is to show the enhancement effect of Cl radicals. In their previous study [70], they showed the enhancement effect in rate for toluene and other branched aromatics such as ethyl benzene and m-xylene using trichloroethylene as co-reactant. Benzene rate enhancement was negligible. A combination of chlorine radical preferential attack on side chain vs. aromatic ring and low benzene vs. branched aromatic surface coverage are believed to contribute to the strong difference in reactivities. In this study, same increase was expected from HCl pretreated TiO₂ catalysts. They observed increase in rate for toluene whereas the effect is negligible for benzene similar to the case of trichloroethylene addition.

Mendez-Roman *et al.* [71] studied photocatalytic oxidation of toluene on TiO₂ (Degussa P25) using in-situ FTIR spectroscopy. They observed benzaldehyde, benzoic acid and small amount of benzyl alcohol. They used SiO₂-TiO₂ catalysts using pyridine adsorption technique, they observed increased amount of Bronsted acidity and correlated it with the increased activity. Literature data is summarized in Table 2.2.

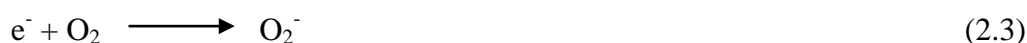
Table 2.2 Literature survey for benzene and related compound oxidation

Catalyst -coated amount mg – area cm ² -water	Volumetric flow rate (ml/min) – residence time (τ)	VOC	λ (nm) – light intensity (mW / cm ²)	Initial concentration (ppmv)	Conversion (%)	Referenc e
TiO ₂ (Degussa P25)-50-NA-NA	34	Benzene	365	200	15	[45]
TiO ₂ -19000-NA-NA	29	Benzene	350	500	60	[72]
TiO ₂ (P25)-40-107-1000ppm	265 – 4.9	Benzene	356 – 5	116	4	[67]
TiO ₂ (P25)-150-?-1342ppm- 5% RH	1 or 2 – NA	Benzene	365 – NA	15.5	~40	[68]
TiO ₂ (P25)-110-powder-93% RH	7.5,30,60-6.5,1.6,0.8	Benzene	260 - NA	100	100,35,4	[47]
TiO ₂ (P25)-110-powder-0% RH	7.5,30,60 – 6.5,1.6,0.8	Benzene	260 - NA	100	31,5,3	[47]
TiO ₂ (P25)-240 – 125-2.2 ml/min	100 - NA	Benzene	365	80	100(0m)-80(180 m)	[50]
TiO ₂ (P25)-240-NA-50% RH	100 - NA	Benzene	365	125	100(0m)-80(180 m)	[48]
TiO ₂ -20000-980-50% RH	Batch	Benzene	254 - NA	291	32(2 h cat.dc.)	[64]
TiO ₂ /Sr ₂ CeO ₄ -20000-980-50% RH	Batch	Benzene	254 - NA	291	65(4 h, cat.dc.)	[64]
TiO ₂ -500–4-10%RH	Batch	Benzene	365 - NA	200	40	[65]
TiO ₂ -V(10%)-500–4-10%RH	Batch	Benzene	365 - NA	200	60	[65]
TiO ₂ (2%)/Bi ₁₂ TiO ₂₀ -20000-980-NA	Batch	Benzene	365 - NA	291	47	[66]
TiO ₂ (Degussa P25)-40–80-54%RH	1000 – 2	Benzene	352 - 5	0.093	100	[53]
TiO ₂ (Degussa P25)-40-80-54%RH	1000 – 2	m-Xylene	352 – 5	0.078	100	[53]
TiO ₂ (Degussa P25)-40-80-54%RH	1000 – 2	p-Xylene	352 - 5	0.078	100	[53]
TiO ₂ (Degussa P25)-40-80-54%RH	1000 – 2	o-Xylene	352 – 5	0.045	100	[53]
TiO ₂ (Degussa P25)-40-80-54%RH	1000 – 2	Ethyl Benzene	352 – 5	0.021	100	[53]
TiO ₂ (Degussa P25)-63-63-50% RH	100 - NA	Benzene	355 – 1.4	0.088	5	[73]
TiO ₂ (Degussa P25)-63-63-50% RH	100 - NA	Toluene	355 – 1.4	0.080	24	[73]
TiO ₂ (Degussa P25)-63-63-50% RH	100 - NA	Ethyl Benzene	355 – 1.4	0.065	48	[73]

NA: Not available

2.1.2.2 Benzene Decomposition Mechanism Studies

It has been reported that highly reactive electron-hole pairs are generated on TiO₂ by the absorption of near UV light. The hole subsequently oxidizes the surface hydroxyl groups (denoted by –OH) and forms the OH radicals and e⁻ reduces O₂ to give superoxide anions (O₂⁻) (Equation 2.1-3) [48].



Photoholes have great potential to oxidize organic species directly or indirectly via the combination with OH• predominant in aqueous solution (Equation 2.4-6) [74].



The OH radical is highly reactive, and it can oxidize benzene to CO₂. In the course of benzene oxidation, many kinds of intermediate radicals are formed. The intermediate radicals are decomposed to CO₂ and CO, or

transformed to other intermediate species. The superoxide anion has a poor oxidizing ability toward benzene, and it cannot be responsible for benzene decomposition. However, it has been suggested that they facilitate the decomposition of intermediate radicals. After the OH groups are consumed, direct oxidation of hole (h^+) with benzene can occur to give benzene cation radical. This radical can react with benzene to form dimer species, which is one of the steps in the formation of carbonaceous materials. In the absence of water vapor, these reactions mainly proceed and the carbonaceous materials are accumulated [48].

D'hennezel *et al.* studied benzene gas-phase photocatalytic degradation and obtained products from surface of reacted catalysts and reaction conditions are given in Table 2.2-2.3. The extraction were done by diethyl ether + ultrasonification and water. For toluene both methods worked whereas only water extraction worked for benzene. The extracted liquid contained a clear solution and yellowish liquid at TiO_2 interface. The analysis has been done to the clear liquid. The yellowish portion was expected to be polymeric products formed during photocatalysis [68]. Zhong *et al.* [64] observed only CO_2 as gaseous products in their study. The main products detected on the surface are ethyl acetate and (3-methyl-oxiran-2yl)-methanol (Table 2.3). Wang *et al.* [61] observed phenol as the major intermediate and some secondary intermediates shown in Table 2.3. They observed the products in the gaseous phase which is not the case for other studies in the field. They used FTIR-ATR equipment and interpret the bonding vibrations. Wu *et al.* [63] studied the adsorption, thermal reactions and photochemistry of benzene on powdered TiO_2 using FTIR. Benzene is adsorbed with its π electrons interacting with the surface Ti^{+4} ions, which are stable even at $400^\circ C$. However, thermal decomposition occurs below $225^\circ C$ to H_2O (g), CO (g) and CO_2 (g). It is found that phenoxy groups formed on the surface with photooxidation of benzene. The amount increases with H_2O and O_2 . Other surface products containing carboxylates or carbonyl groups are formed. The extracted surface products may not be true surface products.

Phenoxy groups may form phenol especially in acidic extract solutions whereas in most of the studies, adsorbed phenol was shown as the surface species on TiO₂ (Degussa P25) (Table 2.3). Larson *et al.* [54] studied the initial steps in photocatalytic oxidation of benzene, toluene, p-xylene, mesitylene, benzyl alcohol, benzaldehyde, and m-cresol adsorbed on TiO₂ thin film. Adsorbed aromatics were oxidized by O₂ photocatalytically in the absence of gas-phase aromatics. The surface compounds were characterized by temperature programmed oxidation and desorption. Benzene and methyl benzenes oxidize rapidly at 273 and 300 K to form adsorbed intermediates that are more strongly adsorbed and less reactive than original aromatic, which is relatively weakly adsorbed on TiO₂. The rates of photocatalytic oxidation of benzene to CO₂ are slow relative to complete oxidation of alcohols or chlorinated hydrocarbons. The intermediates do not appear to be alcohols or aldehydes formed by oxidation of a methyl group, or do they correspond to addition of a hydroxyl to the aromatic ring. M-cresol does not photocatalytically oxidize.

The species formed during radical chemistry are diverse. However, a comment can be made as the last steps of degradation mechanism are the oxidation of simple molecules such as formic acid, formate, carbonate and formaldehyde since the end product formed is mostly CO₂. A model degradation mechanism for formaldehyde is given below (Equation 2.7-14) [75].



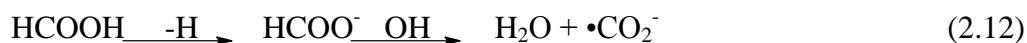


Table 2.3 Less active intermediates and surface products formed from benzene on TiO₂ surfaces due to radical chemistry.

Catalyst used	Observation on color change	Extracted solvent	Observed products (gas Phase)	Observed products (surface extract)	Reference
TiO ₂ (Degussa P25)	Dark to light Yellow	Water	CO ₂ , CO	1,2,3,4,5,6,7	Jacoby <i>et al.</i> [67]
TiO ₂ (Degussa P25)	Yellow	Water	CO ₂	1,2,5,8,9	D'Hennez <i>et al.</i> [68]
TiO ₂ (P25)	Not mentioned	Ftir	CO ₂ , CO	10,11,12	Wu <i>et al.</i> [63]
TiO ₂ , TiO ₂ /Sr ₂ CeO ₄	Yellow	Ether	CO ₂	13,14	Zhong <i>et al.</i> [64]
TiO ₂ (Degussa P25)	Not mentioned	FTIR-ATR GC/MS	All in gas phase	15,16,17,9	Wang <i>et al.</i> [61]

1 phenol (hydroxybenzene), **2** hydroquinone (1,4 benzenediol), **3** catechol (1,2 benzenediol), **4** resorcinol (1,3 benzenediol), **5** benzoquinone (2,5-cyclohexadiene, 1,4-dione), **6** oxalic (ethanediodic) acid, **7** malonic (propanediodic) acid, **8** acetic acid, **9** formic acid, **10** phenoxy, **11** carboxy groups, **12** carbonyl groups, **13** ethyl acetate, **14** (3-methyl-oxiran-2yl)-methanol, **15** 1,5-hexadien-3-yne, **16** 2,4-hexadiyne, **17** 1,3-hexadien-5-yne

2.1.2.3 Regeneration Studies

Cao *et al.* [76] observed apparent deactivation of various titania catalysts during the photocatalytic oxidation of gas phase toluene. After prolonged use with flow reactor, toluene oxidation rates were observed to pseudo steady-state levels, and yellowish discoloration was observed. The deactivated catalyst samples were heated to either 350°C or 420°C in air in order to “burn out” strongly bound intermediate species via high-temperature oxidation. Treatment at 350°C for 2 h was reported to reduce catalyst discoloration and allow a partial recovery of the higher initial oxidation rates seen with fresh catalysts. Regeneration at 420°C allowed complete recovery and returned the catalyst samples to their original white color. Regeneration under air and UV atmosphere without contaminant may be considered as a practical approach than thermal generation particularly in indoor air cleaning systems due to low operating and capital cost. However to oxidize the species is a slow process and requires long time. Jacoby *et al.* [67] regenerated the catalysts in 20 h for complete removal of the discoloration and recovery of the normal catalyst activity. D’hennezel *et al.* [68] removed discoloration of catalyst and regained the activity after 16 h. The benzene discoloration could not be removed completely. Pinna *et al.* [77] studied ethyl benzene oxidation on anatase commercial powders. High surface area anatase is able to adsorb large amount of aromatics, thus giving a decisive contribution to the abatement, even in the dark. Anatase powder darkens until becoming brown. A CO₂ peak due to combustion of carbonaceous species is observed around 400°C with TPO. Darkening behavior is not observed when anatase has been impregnated with KOH, which means basic nature of cement prevents this phenomenon.

2.1.2.4 Application of Photocatalytic Activity to Cement Based Materials

2.1.2.4.1 Cement Structure

Cements solidify and harden both in air and under water. They are hydraulic binders. Hydraulicity is the ability of a material to set and harden under water. Gypsum ($\text{CaSO}_4 \cdot 2\text{H}_2\text{O}$) and lime (CaCO_3) is not resistant to water [78]. Cements are made from limestone and clay, limestone being the major constituent. The hydraulic components (SiO_2 , Al_2O_3 , Fe_2O_3) are contained in the clay. The finely ground raw marl meal is fired in a rotary kiln at 800-1450°C to form cement clinker. The cement clinker is ground to fine cement with the addition of plaster rock or anhydrite as a retarder [79]. A typical composition of ordinary Portland cement is given in Table 2.4. Dry cement consists of four main oxide phases: Tricalciumsilicate [$3\text{CaO} \cdot \text{SiO}_2$ or C_3S], dicalcium silicate [$2\text{CaO} \cdot \text{SiO}_2$ or C_2S], tricalcium aluminate [$3\text{CaO} \cdot \text{Al}_2\text{O}_3$ or C_3A], and tetracalcium alumino-ferrite [$4\text{CaO} \cdot \text{Al}_2\text{O}_3 \cdot \text{Fe}_2\text{O}_3$ or C_4AF]. Cement also contains gypsum that is added to control setting process. C_3S and C_2S constitute approximately 75% by mass of dry cement [80]. The compound composition of Portland cements or clinkers can be determined approximately by using Bogue's equations (Equation 2.15-2.18) [78].

$$\text{C}_3\text{S}\% = 4.071 \times (\text{CaO}\%) - 7.6 \times (\text{SiO}_2\%) - 6.718 \times (\text{Al}_2\text{O}_3\%) - 1.43 \times (\text{Fe}_2\text{O}_3\%) - 2.852 \times (\text{SO}_3\%) \quad (2.15)$$

$$\text{C}_2\text{S}\% = 2.867 \times (\text{SiO}_2\%) - 0.7544 \times (\text{C}_3\text{S}\%) \quad (2.16)$$

$$\text{C}_3\text{A}\% = 2.650 \times (\text{Al}_2\text{O}_3\%) - 1.692 \times (\text{Fe}_2\text{O}_3\%) \quad (2.17)$$

$$\text{C}_4\text{AF}\% = 3.043 \times (\text{Fe}_2\text{O}_3\%) \quad (2.18)$$

When cement is mixed with water, chemical reactions take place that result in the formation of hydration products. The reactions are exothermic (Heat of hydration is 120, 62, 207,100 cal/g for C_3S , C_2S , C_3A and C_4AF respectively [81]). Gelation starts at the grain boundaries of the cement and ends with the complete transformation of the cement grain to hydrate. The smaller the grains of cement, the more rapidly the cement gel transforms to solid hydrated cement. The hydration of larger grains can take years. Dehydration can interrupt the hydration process; the addition of water can reactivate it. The hardened product is water resistant [79].

The two silicate phases C_3S and C_2S , give calcium silicate hydrate (C-S-H) and calcium hydroxide [$Ca(OH)_2$] as hydration products, which constitute approximately 50-60% and 20-25% of the total volume of the hydrated product respectively. Hardened cement paste contains C-S-H gel, crystals of calcium hydroxide, ettringite, minor residues of the original unhydrated cement, and residues of the original water-filled spaces in the fresh paste. C-S-H gel is the main component of the cement paste and is responsible for the strength and microstructure of cement paste. Strength comes from covalent bonding (~65%) and Van Der Waals bonding (~35%). C-S-H gel exists in various forms such as fibrous particles, honeycombs, flattened particles and irregular grains. The bulk volume of C-S-H gel requires 60% more volume after full hydration. Gel contains high surface area which is between 100-700 m^2/g . C/S ratio changes between 1.1-2. H ratio varies too much. C-H or $Ca(OH)_2$ has much higher crystallinity. It keeps the solution alkaline (pH 12.4-13.5). When cement paste is combined with fine aggregate (maximum particle size 4.75 mm), it forms a mortar, and when cement paste is combined with fine and coarse aggregate, it forms concrete [80].

Pores in cement paste matrix can be classified as gel pores, capillary pores, hollow-shell pores and air voids. Gel pores takes place in C-S-H matrix and they are few nanometers in size. Since pore dimension is an order of magnitude bigger than water molecule, the movement of water does not

contribute much to cement paste permeability. Gel pores occupy about 28% of the total volume of the gel. Capillary pores are initially water-filled spaces and during hardening they are converted to interconnected channels or if the cement paste is dense enough, cavities interconnected by gel pores. Their size changes from 2 nm to 10 μm . The volume of the capillary pores would be about 20% of the total volume of the paste. The fluid contained in capillary pores is not pure water, but an ionic solution that is in equilibrium with the hydrated paste. The water in capillary pores is almost completely evaporable at relative humidities below about 40%. At above 40%, capillary condensation occurs. Air voids form during mixing and placing of cement mixture. The size changes up to several millimeters [80].

The strength of a hardened cement paste is due to the presence of a continuous three-dimensional network of hydrate phases which can resist external stresses without being broken down. The pores of the paste have an adverse effect on strength and above certain porosity the strength drops to zero. Pores of different size affect the strength unequally. Generally, pores with greater radii are more detrimental than very fine gel pores [81]. Strength of concrete depends on water/cement ratio of the concrete mix, quality of the mixing water, properties of the cement and aggregates, mixing, transportation, placing and consolidation operations, curing conditions and age of concrete [78].

Portland cement is available in different forms such as, high-early-strength, hydrophobic, white, colored, blast furnace slag, pozzolana, alumina, gypsum alumina Portland cement. White cement is mentioned since it is used in this study.

2.1.2.4.1.1 White Cement

The manufacture of white Portland cement requires suitable raw materials and special care against contamination during production. The grey color of ordinary Portland cement is due to the iron oxide present, and for white, the content of this needs to be kept low. The raw materials are suitable limestone or chalk, and china clay, both of which must be low in iron. Cryolite (sodium aluminium fluoride) has at times been added as a flux to aid in burning. Contamination with iron, during the preparation of the raw mix and burning has to be avoided. The cement is burnt in a rotary kiln, usually with an oil or gas fuel to avoid the contamination with coal ash which is inevitable when pulverized coal is used for firing. The presence of small quantities of manganese oxide is said to have marked influence on the color of white cements [81].

Table 2.4 Typical composition of binders used in construction industry [81]

	British white cements	Tiel white cement	Ordinary Portland Cement	Limestone	Clay
CaO	67.70	67.43	64.1	52.72	1.61
SiO ₂	22.13	21.56	22.0	2.16	60.48
Al ₂ O ₃	4.07	0.77	5.5	1.09	17.79
Fe ₂ O ₃	0.46	0.53	3.0	0.54	6.77
MgO	0.46	1.72	1.4	0.68	3.1
Na ₂ O	0.11	-	-	0.11	0.74
K ₂ O	0.12	-	-	0.26	2.61
SO ₃	2.39	0.89	2.1	0.02	0.21
Loss on ignition	2.64	6.48	-	42.39	6.65

A white cement is manufactured in France from the well-known Tiel deposits of iron-free limestone. These deposits, known as Chaux du Tiel, contain sufficient clay matter to yield a hydraulic cement. This material owing to its physical nature, requires only light burning and the product is akin to an eminently hydraulic lime. As is common with the French hydraulic lime, it is partially hydrated in such a way as to hydrate the free lime present, but not the calcium silicates. Its composition is such that it falls outside the limits of Portland cement specifications and its physical properties are more closely similar to those of a hydraulic lime [81]. Composition analyses of white cements are shown in Table 2.4.

2.1.2.4.1.2 Titania in Cement Matrix

Titania occurs to a small extent, about 0.2-0.3 % in all Portland cements, being derived from the clay or shale. It is a more important constituent of high alumina cement, where about 1.5-2% is usually present, when it is derived from bauxite. Kühl found that in a Portland cement the substitution of silica by titania in small amounts slightly increased the strengths, but for larger amounts a reduction in strength occurred. The optimum content was found to be 4.5%. Kühl suggests that a compound $3\text{CaO}\cdot\text{TiO}_2$ is formed and early workers on the system CaO-TiO_2 claimed to have prepared both $3\text{CaO}\cdot\text{TiO}_2$ and $2\text{CaO}\cdot\text{TiO}_2$; there is however, now good evidence that the maximum amount of lime combined corresponds to a ratio of $3\text{CaO}\cdot 2\text{TiO}_2$. Although behaving in many respects as a separate compound, it seems likely that $3\text{CaO}\cdot 2\text{TiO}_2$ is a solid solution of CaO in one of the polymorphic forms of $\text{CaO}\cdot\text{TiO}_2$. The system $\text{CaO-CaO}\cdot\text{Al}_2\text{O}_3\text{-CaO}\cdot\text{TiO}_2$ contains no ternary compounds, each of aluminates being in equilibrium with CT solid solution; a few percent of CA or C_{12}A_7 in solid solution in CT

stabilizes it in the optically isometric form in which it is usually found in nature, with refractive index 2.38, density 4.05 [81].

2.1.2.4.2 Clay

Clay is the cheapest and the most abundant natural binding agent. Its density ranges between 1500 kg/m^3 and 1700 kg/m^3 . Clays are available in several colors such as white, yellow, red, and brownish-yellow (Table 2.4) [82].

2.1.2.4.3 Gypsum

Calcined gypsums harden in air. The raw material, plaster rock, is found as dehydrate form in nature (hydrous calcium sulphate). Aiming to remove crystallized water partially or completely, it is fired in a rotary kiln either at low temperatures, of up to 190°C , or at high temperatures, up to 1000°C , in which Plaster of Paris or anhydrous gypsum is formed, respectively. If the powdered gypsum is mixed with water, the gypsum reacts exothermically with water to form calcium sulphate dehydrate ($\text{CaSO}_4 \cdot 2\text{H}_2\text{O}$) [79].

2.1.2.4.4 Lime

Quicklime (CaO , calcium oxide) and carbon dioxide are formed when limestone is fired at temperatures below sintering limit of 1250°C . The quicklime is slaked by adding water. The slaked lime (hydraulic lime, lime paste, calcium hydroxide) almost doubles its volume as it expands. Slaked lime ($\text{Ca}(\text{OH})_2$) hardens back to limestone (CaCO_3) when mixing water is added, using CO_2 from air. The water liberated evaporates (Table 2.4) [79].

In addition to these, silicate binders such as potassium water glass $K_2O.nSiO_2.H_2O$ and calcium aluminate binders ($CaO.Al_2O_3$ and $CaO.2Al_2O_3$) are also used in construction industry. The hydration and production reactions of some of the mentioned binders are given in Table A.1 in Appendix A.

2.1.2.4.5 Plastering

Plastering is a single-or multilayer coating applied to walls or ceilings with a defined thickness (other coatings as a top coat are also possible). Its final properties develop only after hardening.

The most important binders used for plaster today are hydraulic or eminently hydraulic limes and cements. The type of binder determines the strength, the hardening time, the frost resistance, the salt resistance and the water resistance of the plaster. The compressive strength of the mortar increases in the following order: non-hydraulic lime, hydrated hydraulic lime, hydraulic lime, eminently hydraulic lime and cement [79].

The major component of plaster by volume is the aggregates. The mortar also contains binders to bind the components and binders are responsible for the hardening process and hardening type, as well as much smaller quantities of admixtures [79]. Types of plasters are given in Table 2.5.

2.1.2.4.6 Grout

Grout is a construction material used to embed rebars in masonry walls, connect sections of pre-cast concrete, fill voids, and seal joints (like those between tiles). Grout is generally composed of a mixture of water, cement, sand, often color tint, and sometimes fine gravel (if it is being used to fill the cores of cement blocks). It is applied as a thick emulsion and hardens over

time, much like its close relative mortar. Main varieties include: Tiling grout (either urethane, cement-based or epoxy), flooring grout, resin grout, non-shrink grout, structural grout and thixotropic grout. Structural grout is used in reinforced masonry to fill voids in masonry housing reinforcing steel, securing the steel in place and bonding it to the masonry. Non-shrink grout is used beneath metal bearing plates to ensure a consistent bearing surface between the plate and its substrate [83].

Ceramic tiles should be constructed with gaps changing according to used place and aim. The main reason of leaving gap between tiles is to give relaxation spaces due to thermal expansions occurring. To tolerate constructional (earthquake), human and machine movement, these gaps are necessary. To leave gaps between tiles is important, but not enough. Unlike hard materials such as white cement and gypsum, using grout between gaps, gives the elasticity under stress [84].

2.1.2.4.7 Other Components used in Mortars

2.1.2.4.7.1 *Aggregates*

Aggregates constitute the major part of mixed plaster by volume and affect the properties of plaster such as porosity, density, weather-frost resistance and compressive strength. Aggregates are classified according to their structure and purpose:

- Dense structure sand, crushed sand, gravel, granular materials
- Porous structure, pumice, tuff, expanded clay, crushed brick
- Hydraulic: Trass, Pozzoulana and Santorin earth
- Colored: Black basalt, schist, colored quartz sand, porphyry, green syenite.
- Glittering: Mica, crushed shells, cullet
- Workable by a stonemason: Shell limestone, sandstone, limestone and tuff stone granulate.

Table 2.5 Types of plasters [78]

Plaster Type	Major Constituent	Areas of Application	Advantages	Disadvantages
Clay Plaster	Clay	Dry interior and exterior surfaces	Cheapest	Moisture
Gypsum Plaster	Gypsum	Closed Spaces		Water soluble
Loam Plasters	Alumina Silicate, sand	Base coat plaster, interior plaster, usage under rain with suitable additives such as casein, fine fiber, dung	Interior climate regulation by adsorbing and releasing water, retains heat, easy to work, cheap, adsorption of smell and chemicals	Crack formation due to swelling and shrinking with changing water content
Lime-cement pla. Cement Plasters	Lime, cement Portland cement, quartz sand	Interior places to plaster wet rooms, surfaces with water contact with density increasing additives.	Water resistance properties Frost damage Watertight	Stiff, cracking Limited water permeability
Lime-gypsum-sand Plasters	Lime, gypsum, sand	Interior work due to gypsum	Increased strength due to gypsum	
Silicate Plaster	Potassium water glass	Finish coat for exterior surfaces	Good vapor permeability, high resistance to acidic and water materials	
Silicone Plaster	Silicone resin emulsion		High vapor permeability Good water repellent properties	

Grain sizes change from compact to coarse, which influence the texture of plaster. A mixture different grain sizes can be used. Coarse grades cannot be applied by machine. Grain type and size influence the amount of binder [79].

2.1.2.4.7.2 Admixtures

Admixtures are generally organic originated materials described in recipes and patents, which is manufacturer specific. They change the properties such as porosity, elasticity, adhesion with the surface, setting time and water repelling capability. The examples are given in Table A.2 in Appendix A [79].

2.1.2.4.7.3 Pigments

Pigments can be classified as organic or inorganic pigments, which are chemically manufactured or mineral originated, respectively. Pigments should have resistances to sunrays and alkali attack for retaining its color. Natural pigments can be classified as;

- Earth pigments, which are cleaned, dried, finely ground ores
- Mineral pigments, made by heating sulphur, clay, soda
- Spinel pigments, such as volcanic minerals [79].

Commonly used color pigments are

- Black pigments: carbon black, graphite, bone black, and magnesium oxide.
- Yellow pigments: ochre and sienna.
- Red pigments: iron, minium (red ocher), mummy, and chrome red
- Blue pigments: ultramarine blue and cobalt blue
- Brown pigments: raw and burnt umber.
- Green pigments: chrome green (chromium oxide).

- White pigments: calcium carbonate (chalk), white cement, and white marble dust [82].

2.1.2.4.8 Activity Studies with Cement Based Materials

2.1.2.4.8.1 Activity Studies in Gaseous Phase

Strini *et al.* [73] observed 3-10 times decrease in photocatalytic oxidation activity of Degussa P25 in Portland cement samples using (BTEX- Benzene, toluene, ethyl benzene and o-xylene) when compared to pure Degussa P25 activity. Non- linear dependency was observed for TiO₂ amount and due to relative loss of activity at higher concentrations. In addition, oxidation rates are linearly correlated with BTEX concentrations (0.2-5.8 $\mu\text{mol}/\text{m}^3$) and UV-A light intensity (750-1350 $\mu\text{W}/\text{cm}^2$). For 1% TiO₂ added cement, oxidation rates for BTEX are 0.16, 0.76, 1.24, 1.29 $\mu\text{mol}\cdot\text{m}^{-2}\cdot\text{h}^{-1}$ respectively.

The application of titanium dioxide in paving blocks is patent protected for the European market by Mitsubishi Materials Corporation as well as Italcementi S.p.A. Both patents comprise the application of TiO₂ in the functional surface layer of double layer paving blocks having enhanced NO_x cleaning potential and or capable of abating organic and inorganic pollutants. The thickness porosity as well as the surface texture of the functional surface layer is claimed by the patents in different ways and is therefore varying in the same way as the concentration of titanium dioxide. Products containing titanium dioxide started in 1997 in Japan. In 2002, investigations to the application of a cement based asphalt slurry seal have been conducted in Italy. In the course of a growing environmental consciousness and new prescriptive limits for nitrogen dioxide there is an urgent need to strengthen research in this

area. According to Council directive 1999/30/EC [85], from January 2010, the limit values for nitrogen dioxide and oxides are reduced by 20% [86].

Kawakawi *et al.* [87] studied characteristics of NO_x removal, physical properties and mechanical properties of cement mortar with three types of TiO₂. For NO_x removal, TiO₂ with high surface area showed best performance. NO_x abatement was proportional with TiO₂ content up to 15%. Washed specimen performance was 15 % higher than untreated specimen. Strength and modulus of elasticity decreased linearly with the increase of the TiO₂ content.

Guerrini *et al.* presented the results of road and sidewalk project in Bergamo, Italy. The road section involved in the project is 500 m long and has a surface area of 12000 m². A clear demonstration of depolluting activity was obtained from measurements carried out two different distances from the ground. The statistical data must be correlated to daily local pollution levels and with weathering data [88]. In another test site in Antwerp, a good efficiency of NO_x reduction was obtained. It was reported that the relative humidity is an important parameter. By washing the surface, the activity is regained [89]. Chrispino *et al.* studied the composition of photocatalytic pavement mortar in terms of both water content and typology of fluidizing substances in order to allow the achievement of a photocatalytic thickness of 1-1.5 cm which is able to match economical and technical demands [90].

The surface of TiO₂ was investigated using XPS. TiO₂, Ti-OH and Ti-OH₂ were observed on the surface from O 1s peak. Only one oxidation state of Ti detected. The surface was subjected to NO_x and no change was observed with reactant concentration and UV irradiation [91]. The photocatalytic degradation rates of benzene and toluene in gas phase using TiO₂ added - cement based materials are shown in Table 2.6.

2.1.2.4.8.2 Activity Studies in Liquid Phase

TiO₂ added cement based coatings have been used in self cleaning studies such as termination of algae [92] and fungi [93], oxidation of chemicals such as 3-nitrobenzenesulfonic acid [94,95], 4-nitrotoluenesulfonic acid [94], oxidation of dyes such as acid orange-7 [95,96], Rhodamine B [97], methyl orange [98]. The changes in concentration or color has been followed by HPLC [94,95] and UV-Vis spectrophotometer [99,95,96] or chroma-meter [97]. In liquid phase studies, the effect on photocatalytic activity can be inspected easily for chemicals such as H₂O₂ [99]. However, pH effects become important in liquid phase studies [99,26]. Interaction of basicity of cement surface and acidity of TiO₂ surface may sweep the OH groups on TiO₂ surface and influence the reaction kinetics [26,100]. To know point of zero charge is important, which is 6.3-6.6 for Degussa P25 [26,100].

Lackhoff *et al.* showed the decreasing photocatalytic activity of TiO₂-cement mixtures as compared to pure TiO₂ and higher activity of Degussa P25 than UV100 (anatase-around 250 m²/g surface area) by inspecting atrazine degradation. Degussa P25 has been one of the reference samples in photocatalytic studies, which has 80% anatase and 20% rutile and 50 m²/g surface area. The effect of carbonation of cement was followed by Raman Spectroscopy [26,98] and the effect to the photocatalytic activity is shown. The effect of TiO₂ to the hydration kinetics was studied by NMR (Nuclear Magnetic Resonance) relaxometry. Degussa P25 and UV 100 have increased hydration speed of white cement. Observation of short relaxation times after fast hydration stage is due to dense porous structure. The addition of TiO₂ (Degussa P25 and UV 100) to the cement structure have increased the resistance to compressive strength, which verifies the results of NMR relaxometry of dense porous structure [26].

Table 2.6 Literature survey for photocatalytic degradation of benzene and toluene using TiO₂ added cement based materials.

Molecule Used	Experimental Conditions (Type of reactor-initial concentration-total flow rate-conversion-RH-temperature)	Application	Degradation Rates		References
			$\mu\text{mol.g}^{-1}.\text{h}^{-1}$	$\mu\text{mol.m}^{-2}.\text{h}^{-1}$	
Benzene	Flow-25~70 ppb-100 ml/min-NA- 50%-23°C.	Mixture with white cement or dispersed TiO ₂ film (1% TiO ₂ addition)	0.016 (for TiO ₂ film)	0.16	Strini <i>et al.</i> [73]
Toluene	Flow-26 ppb-2L/min-63%-47%-23°C.	Dispersed on corrugated sheets and roofing tiles (S5-300B anatase in water %17.3 pH=12, 330 m ² /g in dry form Millenium chemicals)	0.0061	5.56	Demeestre <i>et al.</i> [17]
Toluene	Flow-12 ppm-170 ml/min-86%-41%-25°C.	Sol gel coating or dipping of cements to the dispersed TiO ₂ powder	-	521	Ramirez <i>et al.</i> [101]

NA: Not available

Guerrini *et al.* [102] presented the colorimetric results taken from the pioneer works of the photocatalytic cements 'Dives in Misericordia' Church in Rome, Italy and "Cite de la musique et des Beaux-arts" of Chambéry, France. After 6 years, the maintenance of the primary color has been confirmed. b^* value (represents color tones change between yellow and blue) variations, are due to the presence of inorganic substances on the surface. If a water washing is applied to the surface of the panels, the primary color is completely recovered.

Giannantonio *et al.* [93] designed for testing the effects of different concrete compositions and exogenously added nutrients on fungal colonization and fouling. A strong positive relationship was observed between tile water-to-cement ratio and the amount of biofouling. In addition, cement containing photocatalytic titanium dioxide and exposed to artificial sunlight strongly inhibited fungal colonization and fouling. Mortar tiles coated with form-release oil and incubated with sterile rainwater were also capable of supporting fungal colonization.

Watts *et al.* [103] mixed TiO_2 powder with varying concrete sealer formulations and applied to prepared concrete surfaces within PVC batch reactors. A solution of 4-chlorophenol in de-ionized water, with an initial 4-chlorophenol concentration of 4 mg/L, was added to each open reactor. The photocatalytic efficiency of each TiO_2 -sealer was determined through bulk solution sampling while a reactor was exposed to continuous UV light. Through analysis of mean 4-chlorophenol concentrations, the disappearance of 4-chlorophenol from solution was attributed solely to the presence of TiO_2 in the sealed concrete surface of a UV exposed reactor. The rate of disappearance increased when the mass percent of TiO_2 in the sealer was increased. The zero-order reaction rate constants ranged from 0.135 to 0.2873 $\text{mg L}^{-1}\text{h}^{-1}$.

There are studies in the literature such as photocatalytic activity of TiO_2 on pumice stone [95,96,104]. Although, pumice stone is a soft material, it can be fixed to a hard surface in the form of pellet [4]. In these studies, pumice

stone with TiO_2 is presented as a solution to disinfection of waste water systems [95,96,104].

2.1.3 Enhancing Self Cleaning Effect

Photocatalytic effect can be enhanced with superhydrophilic or superhydrophobic surface properties. On superhydrophobic surfaces, the water molecules are repelled, which prevents drying of water and deposition of dirt on the surface. In superhydrophilicity case, the water contact angle with the surface was so low that, water molecules flow on the surface, disturbs the interaction between the surface and the dirt and remove the surface impurities by the help of gravitational force.

2.1.3.1 Superhydrophilicity

Superhydrophilicity effect was first observed by Fujishima group in Japan in 1997 [105]. They observed the decreasing of contact angle between water and the surface to very small angles which means spreading on the surface. Superhydrophilic surfaces are created with TiO_2 which requires UV activation of the surface. This limits the usage in indoor applications. Another problem is the stability of superhydrophilic character. After obtaining superhydrophilic surfaces by UV illumination of TiO_2 , contact angle goes up and is restored early comparatively in a dark place. It is desirable that the contact angle rises slow in a dark place, and maintains low angles for a long time, because if actual use is considered, it is not always irradiated by UV light, such as sunlight. In order to improve these characteristics, Toto Ltd. and Fujishima group found out that upon addition of SiO_2 , stable hydrophilicity was achieved in dark. The contact angle of water was low immediately without

any initial lag time. In their procedure, TiO_2 sol and SiO_2 sol were applied together or sequentially using air spray. After drying at RT, calcination at 800°C -1h was done [106]. This preparation method is similar to layer by layer deposition (LbL) technique, which is used to adsorb oppositely charged nanoparticles sequentially first discovered by Iler in 1966 [107]. Using LbL technique, TiO_2 and SiO_2 bilayer films were successfully deposited from aqueous commercial suspensions of SiO_2 and TiO_2 by dip coating technique [108]. The pH of the solutions is adjusted to 3 by HCl. There is a calcination period at 550°C for 3h. The thicknesses were 7 nm and 22 nm for TiO_2 and SiO_2 layers respectively. Preparation of TiO_2 sol from TiCl_4 and mixing with SiO_2 particles in solution is also used for obtaining strong adherence and superhydrophilic properties [109].

In addition to stability of superhydrophilicity, the photocatalytic activity of the SiO_2 - TiO_2 binary oxides have also increased according to Guan *et al.* [110]. This increase in photocatalytic activity has been explained by the increase of the acidity of TiO_2 - SiO_2 surface [110,111], where a model is proposed by Tanabe *et al.* [112]. By tuning SiO_2 - TiO_2 molar ratio, superhydrophilic and photocatalytic properties can be arranged. They obtained highest hydrophilic-self cleaning effect in 30-40 mol% SiO_2 addition, whereas best photocatalytic effect was observed with 10-20% SiO_2 addition. Guan *et al.* used a classic sol-gel synthesis starting from TEOS (Tetraethylorthosilicate) and TBOT (tetrabutylorthotitanate) to synthesize the films.

Lee *et al.* [113] revealed that, during mixed film calcination, transformation from amorphous to anatase phase, as well as transformation from anatase to rutile phase, were shifted toward higher temperatures with increasing the SiO_2 content. Yu *et al.* [114] found that SiO_2 suppress the TiO_2 crystal growth, since the contact between TiO_2 particles are prevented by SiO_2 during thermally activated growth.

Fujishima group [115] used biomimetic approach to create stable wettability and TiO_2 colorization. Polystyrene film was coated by dip coating

and stabilized in 100°C for 30 min. The film was treated with 7% ethanol solution of polyethylenimine. This treatment makes the polystyrene hydrophilic. The film is immersed to a water suspension containing 10% TiO₂ solution. The film was calcined to remove the polymer films and solidify TiO₂ network. This type of templating also result in TiO₂ colorization which can be tuned by size of polystyrene spheres used to create template.

Hou *et al.* also used polystyrene/TiO₂ mixture in a different way [116]. Polystyrene was dissolved in tetrahydrofuran and mixed with TiO₂ nanoparticles for 1 h. The heating above 60°C transformed the coating to superhydrophobic form. The switching mechanism to superhydrophilic state is the UV light. To regain superhydrophobic property, the coating is heated to 180°C.

SiO₂-TiO₂ bilayers are also used for increasing transmittance of the films. A similar effect was observed by coating TiO₂ sol on commercial PET (Polyethylene terephthalate) films. The obtained films were dried at room temperature overnight. The obtained films showed superhydrophilic, photocatalytic properties with increasing transmittance [117].

Another method used in creating superhydrophilic surfaces is increasing surface roughness [118]. This method also wets the surface and there is no need to UV activation. Wenzel equation defines roughness as

$$\cos \theta_o = r \times \cos \theta \quad (2.19)$$

where θ_o and θ are the macroscopic (apparent) and intrinsic (Young) contact angles measured on rough and flat surfaces of the same material, respectively, and r is the roughness factor. Roughness enhances the spread of liquid, and capillary forces dominate wicking of the liquid into the structure of textured materials [119].

Roughness can be created by sol-gel process modifying by some polymer such as PEG (polyethylene glycol) incorporation. PEG 2000 with

0.5% addition showed superhydrophilicity after calcinations at 550°C. Using ordered surfaces created by some templating procedure is also used for creating roughness [115,117].

Some studies took place to obtain superhydrophilic surfaces with natural drying. One of the methods is to use polymer formulations such as PEDT (Polyethylenedioxythiophene):PSSH (Poly(styrenesulfonate)) polymer blend to form nanosegregants and water attracting surfaces [120] by the help of water capturing sulfonic acid groups.

2.1.3.2 Superhydrophobicity

Superhydrophobicity was introduced in 1996 by Onda et al [121,122] to describe water-repellent fractal surfaces, made of a hydrophobic material, on which water drops remain as almost perfect spheres and roll off such surfaces leaving no residue. Today superhydrophobic surfaces are defined as textured materials (and coatings) on (nonsmooth) surfaces on which water forms contact angles 150° and larger, with only a few degrees of contact angle hysteresis [119].

The practical usage of water repellent surfaces can be waterproofing of clothes, concrete or paints, antirain windshields and window panes. When water repellent surfaces are used;

- Surfaces which have low surface energy (hydrophobic) will form, so less dust particles settle on them
- The rain will wash the surface and taking the dust with the water drop.

The challenges to industry are;

- To build a permanent superhydrophobic surface is hard due to aging of these surfaces, the microtextures are easily damaged by simply rubbing.
- The textures can be filled with oily substances and it is difficult to remove them from microstructures [123].

The paint industry does not create microtextures on the surface, but create superhydrophobic surfaces by using silicon based oils. Silicon based materials are used in silicon or plastic paints to create water droplet effect. However, one disadvantage of droplet effect seen on the paint surface is a dusty trail formation during slipping down from the surface of a vertical wall.

2.1.3.3 Inorganic Resin Selection

The resins can be alkyd, phenol-formaldehyde, amino, epoxy, polyurethane type resins which forms solvent based paints. Polyvinyl acetate, polyacrylates and their copolymers are used in emulsion paints or plastic paints which have water based formulations. All of these formulations are organic type resins which contains C-C bond [124].

Inorganic type resin formulations are silicon based polymers. The bond strength of the Si-O siloxane bond is about 108 kcal/mole. It is considerably higher than 83 kcal/mole for the C-C carbon bond of organic polymers. The higher bond strength provides the basis for their improved durability and heat resistance compared to carbon based organic systems. Inorganic siloxane bonds are virtually unaffected by sunlight and UV attack. By comparison, organic coatings based on acrylic or polyurethane binders exhibit fading and gloss in 2 to 5 years exterior exposure. The Si-O bond is already oxidized and, consequently, atmospheric oxygen and most oxidizing chemicals do not affect coatings based on siloxane binders [125].

Silicate binders are not considered acceptable for broad use in coatings because of their poor film properties. Heat curing limited the practicality of silicone coatings, particularly on large structures. A significant advance was made in 1978 with the introduction of ambient cure binders on the hydrolysis of trialkoxysilane. Subsequent development of new silane and silicate precursors led to formulation of polysiloxane coatings with improved film

properties [125]. Two families of products are used in the coating industries: silicone polymers as additives and silicone resins as the main component, or binder. At low levels, silicone polymers are used to ease application of paints. The surface properties of silicones enable a paint to wet a substrate easily and give it a smooth appearance once dry. Here silicones are behaving as performance enhancing additives during the coating application. They are effective at an addition level of a fraction of a percent (Table 2.7) [126].

In contrast to the low-level use of silicone polymers as additives, silicone resins can be major components of the coating, where they are used as binders or co-binders, imparting important benefits such as durability throughout the life of the coating. Silicone resins offer resistance to weathering in paints for exterior surfaces such as bridges and metal cladding on buildings. Silicone resins have greater resistance to high temperatures than organic resins and are used in paints for ovens, chimneys, car exhausts and barbecues [126].

Silicone hydrophobicity limits wetting and surface contact with any water based media. However, water vapor can diffuse through most silicone polymer coatings, which is advantageous in some applications like masonry treatment [126]. Addition of as little as 10% silicone can significantly increase the gloss retention and chalking resistance.

Table 2.7 Silicones in coatings and benefits according to usage ratio [126].

Silicone as performance-enhancing additives (0.1-5.0 %)	Silicone resins and intermediates (30 – 100 %)
Foam control	Weather resistance
Substrate wetting	Heat resistance
Leveling	
Adhesion	
Surface slip	

Phenyl groups attached to silicon are far more resistant to thermal oxidation than methyl groups. So, most silicone resins for high temperature applications have a combination of methyl and phenyl substituents to achieve required balance of heat stability, flexibility and compatibility with organic resins [126].

2.2 VISIBLE LIGHT PHOTOCATALYSIS - METAL AND ANION DOPING¹

The “holy grail” of photocatalysis research is to find photocatalysts that are active in visible light region, such that solar energy can be utilized. Therefore, modifying the semiconductor band gap for effective visible light utilization constitutes a significant amount of research in photocatalysis. There are various methods for introducing visible light activity to photocatalysts.

- metal and anion doping
- dye sensitization
- shuttle redox mediator
- oxygen-deficient TiO₂ and composite semiconductors.

One of the used techniques in obtaining visible light activity is doping the photocatalysts with metal and non-metal ions. The method used for doping may change the crystalline structure and morphology. Impregnation, coprecipitation, sol-gel methods, metal-ion implantation and RF magnetron sputtering techniques are used for doping [127].

The effect of metal ion dopants on the photocatalytic activity is made up from the sum of changes which occurs in:

¹ This section is adopted with permission from Inderscience Publishing Group, Deniz U., Oymak M.M., Bahar I., “CO₂ Utilization by Photocatalytic Conversion to Methane and Methanol” International J. Global Warming, 3 (2011) 142-62.

- . The light-absorption capability of the TiO₂ photocatalyst;
- . Adsorption capacity of the substrate molecules at the catalyst's surface;
- . Interfacial charge transfer rate.

The main objective of doping is to induce a batho-chromic shift (i.e., a decrease of the band gap or introduction of intra-band gap states, which results in more visible light absorption) [127]. The ability of a dopant to function as an effective trap is related to dopant concentration, energy level of dopants within TiO₂ lattice, their d electronic configuration, the distribution of dopants within the particles, the electron donor concentration, and the incident light intensity. Dopant should act as both electron and hole traps, since trapping one of them leads to combination of other with its mobile counterpart [128].

Titania is doped with alkaline earth (Ca⁺², Sr⁺² and Ba⁺²) [129], Fe⁺³ [130], Cr⁺⁶ [131] and rare earth ions (La⁺³, Sm⁺³, Ce⁺³, Pr⁺³, Gd⁺³, Er⁺³, Nd⁺³) [132]. Substitution of Ti⁺⁴ by dⁿ metallic ions in TiO₂ lattice lead to allowed energy states in the band gap of TiO₂, which results in visible light active transitions due to e⁻ transfer from this energy level to CB of TiO₂. One of the reasons of the red shift is homogenous Ti⁺⁴ substitution; another one is the formation of metal clusters [132]. If shift changes with dopant concentration, it may be due to the metal ion incorporation. The change in the red shift with respect to the annealing temperature can be attributed to the formation of metal clusters [127]. The reason of the shift is important since it changes photocatalytic activity. The extent of red shift is given in the order of V>Cr>Mn>Fe>Ni and depends on the amount and type of the metal ions implanted [133]. Synthesis techniques such as metal ion implantation and impregnation give different trends in UV-Vis absorption spectra in Cr-doped TiO₂. Anpo *et al.* claimed that modification of electronic state of TiO₂ by metal ion implantation is related with strong and long distance interaction between metal and TiO₂, which is the result of highly dispersed metal ions in the deep bulk of catalysts. The surface properties do not change much by this method.

The formation of impurity energy levels, which is due to metal oxide cluster formation is observed in impregnated Cr-doped TiO₂ [133].

An enhancement of the intrinsic adsorption edge of TiO₂ from 380 nm to higher wavelengths and a higher absorbance in the range of 400–650 nm compared to bare titania (both dependent on the iron content) is observed for iron doping. Iron cations occupy substitutional positions because of the similar radius of Fe³⁺ and Ti⁴⁺ and form solid solutions with titania at low concentrations (<1 at % Fe). The presence of iron catalyzes the anatase to rutile transformation, with rutile being detected even at 400°C [127]. Fe-doped TiO₂ photocatalysts showed improved rates of oxidation of 2,4-dichlorophenoxyacetic acid [134], and o-cresols [135]. Yu *et al.* prepared Fe grafted TiO₂ using anatase and rutile samples [136]. The highest activity was obtained for Fe grafted rutile sample calcined at 950 °C and pH adjustment at 2 during synthesis of the sample. The pH adjustment is important since at higher pH values formation of Fe₂O₃ is favored during impregnation at 90°C, which does not show photocatalytic activity. Another reason of activity increase is high crystallinity of the TiO₂. They used 0.05 wt% Fe/TiO₂, which they calculated as optimum in their previous study. Yu *et al.* observed highest photocatalytic activity with 0.5at% Fe using TiO₂ nanotubes as supports. Degussa P25 also shows some visible light activity due to its rutile content [137]. There are at least two effects competing with each other giving rise to an optimum Fe content. For higher concentration of Fe, the activity decreases, since recombination rates increase. The recombination rate through tunneling between the trapped charge carriers depends on the distance R separating the e⁻/h⁺ pairs according to Equation 2.20

$$k_{\text{recomb}} \propto \exp(-2R/a_0) \quad (2.20)$$

where a_0 is the radius of the hydrogenic wave function of the trapped carriers. Therefore recombination rate increases exponentially with the dopant

concentration because the average distance between trap sites decreases with increasing number of dopants for each particle. For a 4 nm diameter particle, there is only 1 dopant per ion per particle at 0.1%, 5 at 0.5%, 30 at 3.0% [128]. As a conclusion, there is an optimum trapping site concentration, which depends on particle size, and exceeding leads to increase of recombination sites.

Anion doping such as N [138,139,140,141], C [142], S [143], B [144] and F [145] were reported in shifting absorption spectra of TiO₂ to visible light region. Following Asahi's pioneering work, N-doped TiO₂ became one of the most studied anion doping systems. Nitrogen is either substitutionally or interstitially doped within the TiO₂ system, which gives XPS N 1s peaks at 396 eV and 400 eV, respectively [146]. The origin of visible light activity is still in debate whether it is caused by band gap narrowing model [138] or formation of localised mid-gap states above the valence-band edge [146]. According to a theoretical calculation using spin-polarized plane-wave pseudopotential method based on a density functional theory, N 2p states are still localized lying slightly above the top of O 2p valence band for 12.5% N doping. At least 20% N doping is needed to mix the N 2p state with the O 2p valence band, but in reality, this forms TiN structure [147].

Asahi reported that nitrogen doping offered visible light (VL)-photocatalytic activity to TiO₂, without any loss of UV-activity, for the decoloration of methylene blue solution and degradation of gaseous acetaldehyde [138]. Irie *et al.* [148] studied degradation of gaseous 2-propanol. Sakthivel *et al.* [139] studied degradation of 4-chlorophenol, benzene and acetaldehyde. These studies [148,139] showed that nitrogen doping only offered modest visible light activity to TiO₂, but at the same time lowered the UV-activity. Yates *et al.* [149] studied degradation of stearic acid molecules and observed almost no visible light activity for N-doped TiO₂. It thus seems that the preparation history, which dictates the types and level of nitrogen doping

and the concentration of oxygen vacancies, greatly influences the photocatalytic activity [4].

There is overwhelming spectroscopic and chemical evidence for the presence of point defects on samples sputtered and annealed in UHV. These are attributed to vacancies in the bridging oxygen rows [1]. Oxygen vacancies are found to be color centers which respond to visible light region [35]. TiO_{2-x} systems show weak absorption of 400-500 nm which is prepared by H_2 plasma treatment of powder form of TiO_2 [150] and they are able to oxidize nitrogen under visible light. Same research group oxidized 2-propanol and benzoic acid under visible light [151]. The same activity for acetone degradation was observed after 120 days of sunlight irradiation of the prepared catalyst.

2.3 SURFACE CHARACTERISTICS OF A METAL OXIDE

Acidity and basicity depend on the nature of the oxide and depend on the charge and radius of metal ions. Other factors influencing the character of the metal-oxygen bond are the coordination number, the filling of the d orbitals, and the nature of the other ligands [152].

Some of the adsorption forms occur preferentially at surface, depending on the physicochemical properties of the chosen oxides which are themselves strongly dependent on preparation techniques, starting materials, and the different pretreatments they are subjected to. Each of these adsorption types can be considered as a form of chemical reaction between the adsorptive and the surface and can be associated to a different strength of chemisorption [152]. NH_3 and CO_2 possible interactions with a metal oxide are shown in Figure 2.1;

(a) Hydrogen bonding via one of its hydrogen atoms to a surface oxygen atom (or to the oxygen of a surface hydroxyl group). It is the weakest mode of interaction.

(b) Transfer of proton from surface hydroxyl to the adsorbate. It occurs with the surface acting as a Bronsted acid.

(c) Coordination to an electron-deficient metal atom. It takes place with the solid acting as a Lewis acid. It is the strongest mode of interaction.

If hydrogen bonding or adsorption onto a Bronsted acid site takes place, the interaction will involve neighboring anions or hydroxyl groups. If adsorption is via coordination to the metal cation, the gas phase basicity is the more appropriate measure of the acid strength of the metal. Lewis acidity can be created by dehydroxylating the surface.

(d) apart from this, the dissociation of ammonia with the formation of surface NH_2 (or NH) and OH species and a complete transfer of protons to the ammonia molecules from Bronsted sites to produce adsorbed NH_4^+ ions are also quite feasible ways of ammonia adsorption.

There exists no simple relationship between the stability of individual surface species and the acidic strength of the binding surface sites. The stability of the adsorbed species is given not only by its own thermodynamics but also by the thermodynamics of the surface site [152].

Concerning carbon dioxide adsorption, CO_2 molecules can be adsorbed on positive and negative surface sites. The adsorbed CO_2 (carbonate forms) may then block surface sites. The different ways of CO_2 adsorption on the surface of oxides can be summarized:

(e) Adsorption on a hydroxyl group with formation of a superficial hydrogenocarbonyl ion;

(f) Adsorption on the metal cation and dissociation of the resulting bonding;

(g) Adsorption on the metal ion and the neighboring oxygen ion and formation of a bidentate carbonate;

(h) Adsorption on the oxygen vacancy and formation of a superficial carbonyl group;

(i,j) adsorption on the metal ions with participation of oxygen in excess and formation of a monodentate carbonate [152].

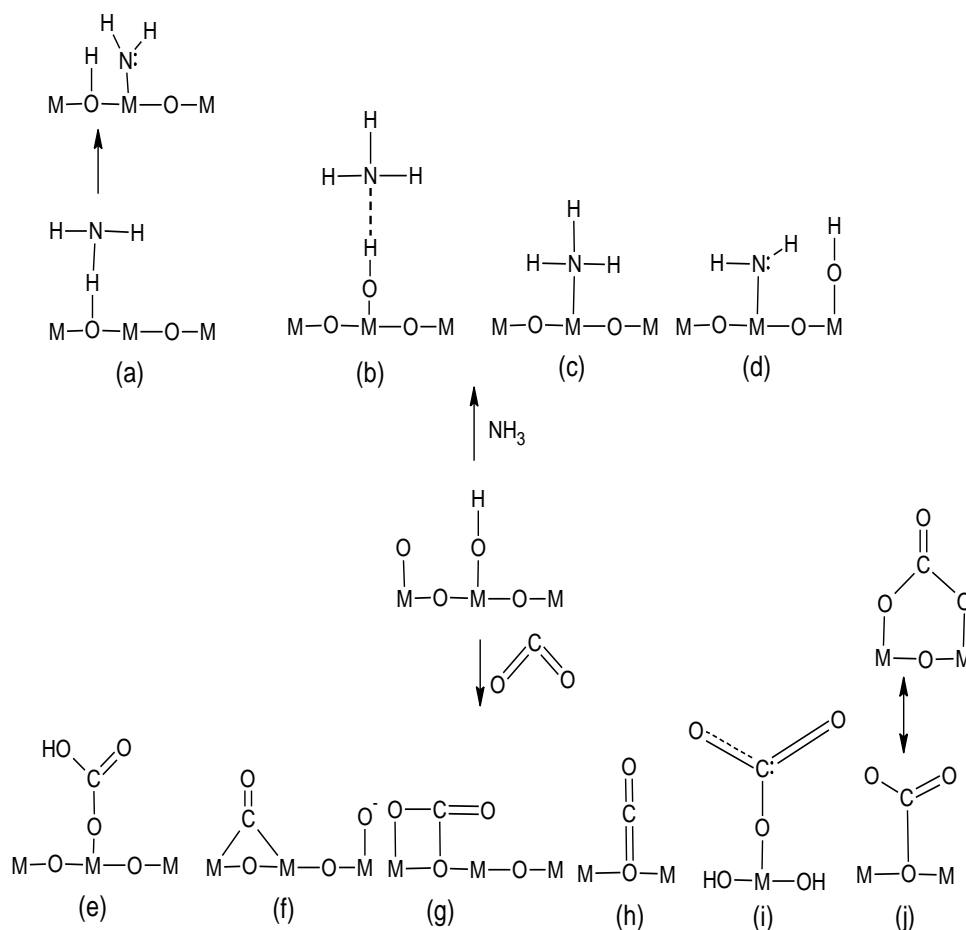


Figure 2.1 Possible surface interactions of NH_3 and CO_2 with metal oxide surfaces [152].

2.3.1 What Are The Possible Probe Molecules to Measure The Acidity and Basicity?

2.3.1.1 Acidic Probe molecules

The ideal probe molecule should not be specific to basic sites and not be amphoteric. It should not interact with several basic sites or give rise to chemical reactions. CO₂ (pK_a = 6.37) is commonly used to characterize basic sites but it may react with hydroxyls and framework oxide ions to give carbonated species. SO₂ is another molecule used in basic site determination (pK_a=1.89), which is more acidic than CO₂ and thus the results are more precise. Pyrole is another option, however particularly at low temperatures, shows some amphoteric character [153]. Benzoic acid is used in another study to determine the basic sites of TiO₂ using UV-Vis technique [154]. CH₂Cl₂ and CHCl₃ are used as acidic probes in inverse gas chromatography method [155].

2.3.1.2 Basic Probe molecules

Ammonia (pK_a = 9.24, proton affinity in gas phase = 857.7 kJmol⁻¹) and pyridine (pK_a=5.19, proton affinity in gas phase = 922.2 kJmol⁻¹) are favored molecules to probe the overall acidity of metal oxides, since both Lewis and Bronsted acid sites retain these molecules. Infrared spectroscopy is used to distinguish these two sites. Ammonia is among the smallest strong basic molecules; its diffusion is not affected by porosity. Ammonia adsorption isotherms are type 1. The adsorption capacities of large pore zeolites for benzene and pyridine vapors are practically equal. The adsorption rate of pyridine is substantially lower than the adsorption rate of benzene due to its electronic structure [153]. Methyl acetate, tetrahydrofuran, diethyl ether are used as basic probe molecules in inverse gas chromatography [155].

NO can be employed as a probe to identify Lewis acid sites and characterize their density and strength. NO may disproportionate into N₂O and

oxygen and is also likely to form nitrosyl complexes with transition metal ions. CO and N₂ adsorption at low temperature provide a powerful tool for characterizing acid sites [153].

2.3.2 The Techniques Used to Measure Surface Acidity and Basicity

The amount of acidic and basic sites of TiO₂ can be calculated using methods such as chemisorption technique, UV-Vis spectroscopy, adsorption microcalorimetry, FTIR spectroscopy, inverse gas chromatography method. UV-Vis technique and chemisorption technique gives total number of Lewis and Bronsted acidic sites. By using chemisorption technique, with a careful vacuum treatment, differentiation between strong sites (Lewis) and weak sites (Bronsted) can be done. The sites further can be differentiated by evolved heat using adsorption microcalorimetry or different vibrations of the surface bound molecules using FTIR spectroscopy. In this thesis study, FTIR spectroscopy with Diffuse Reflectance equipment has been used with CO₂ and NO as probe molecules.

2.3.2.1 FTIR Spectroscopy

A review of infrared spectroscopic species from ammonia adsorption on most metal surfaces is studied by Tsyganenka *et al.* for both anatase and rutile [156]. The differences in vibrational behavior were shown for two polymorph structure. No Bronsted acid sites were observed for TiO₂. A review of infrared spectroscopic species from reactive adsorption of CO₂ on metal surfaces is published by Busca *et al.* [157]. Another review from the same group shows benzene, ammonia, pyridine, CO and CO₂ adsorption to the 4 different anatase powders [158]. CO₂ adsorption and CO adsorption at 77 K for determination of

acidic and basic sites of Degussa P25 and TiO₂ (Merck) are given by Martra *et al.* [159]. Hadjiivanov *et al.* studied benzene and ammonia adsorption with FTIR on Degussa P25 and TiO₂ prepared by sol-gel method [160].

2.3.2.1.1 Theoretical Background for DRIFTS

Infrared reflection spectrometry has found a number of applications, particularly for dealing with solid samples that are difficult to handle, such as polymer films and fibers, foods, rubbers, agriculture products, and many others. Mid-infrared reflection spectra, while not identical to the corresponding absorption spectra, are similar in general appearance and provide the same information as do their absorption counterparts. Reflectance spectra can be used for both qualitative and quantitative analysis. Most instrument manufacturers now offer adapters that fit into the cell compartments of infrared absorption instruments and make it possible to obtain reflection spectra [161].

Reflection of radiation is of four types: Specular, diffuse, internal, and attenuated total reflection (ATR). Specular reflection is encountered when the reflecting medium is a smooth polished surface. Here the angle of reflection is identical to the incident angle of radiation. If the surface is made up of an infrared absorbent, the relative intensity of reflection is less for wavelengths that are absorbed than for wavelengths that are not. Thus, a plot of reflectance R , which is the fraction of the incident radiant energy that is reflected, versus wavelength or wave number provides a spectrum for a compound that is similar in general appearance to a transmission spectrum for the species. Specular reflection spectra find some use for examining and characterizing the smooth surfaces of solids and coated solids but is not as widely used as diffuse and total reflection spectra [161].

Diffuse Reflectance Infrared Fourier Transform Spectrometry (DRIFTS) is an effective way of obtaining infrared spectra directly on

powdered samples with a minimum of sample preparation. The rough surface may be a continuous solid, such as a painted surface, fabric, an insect wing or a piece of wood, or it may be a powder that has just been dumped into a sample cup, not pressed into a glassy pellet [162]. In addition to saving time in sample preparation, it permits conventional infrared spectral data to be gathered on samples that are not appreciably altered from their original state. The widespread use of diffuse reflectance measurements had to await the general availability of Fourier transform instruments in the mid-1970s because the intensity of radiation reflected from powders is too low to be measured at medium resolution and adequate signal-to-noise ratios with dispersive instruments [161].

Diffuse reflection is a complex process that occurs when a beam of radiation strikes the surface of a finely divided powder. With this type of sample, specular reflection occurs at each plane surface. However, since there are many of these surfaces and they are randomly oriented, radiation is reflected in all directions. Typically, the intensity of the reflected radiation is roughly independent of the viewing angle [161]. Ideally, the beam should penetrate about 100 μm into the sample. A large collecting mirror or, for NIR, an integrating sphere, is used to collect the scattered radiation [162].

The diffuse reflectance experiment requires that the incident beam penetrate into the sample, but the path length is not well defined. The path length varies inversely with the sample absorptivity. The resulting spectrum is distorted from a fixed path absorbance spectrum and is not useful for quantitative analysis [162]. A number of models have been developed to describe in quantitative terms the intensity of diffuse reflected radiation. The most widely used of these models was developed by Kubelka and Munk [1]. Application of the Kubelka-Munk equation is a common way of making the spectral response linear with concentration [162]. Fuller and Griffiths in their discussion of this model show that the relative reflectance intensity for a powder $f(R'\infty)$ is given by Equation 2.21

$$f(R_{\infty}^l) = \frac{(1-R_{\infty}^l)^2}{2R_{\infty}^l} = \frac{k}{s} \quad (2.21)$$

where R_{∞}^l is the ratio of reflected intensity of the sample to that of a nonabsorbing standard, such as finely ground potassium chloride or KBr. The quantity k is the molar absorption coefficient of the analyte, and s is a scattering coefficient. For a dilute sample, k is related to the molar absorptivity ϵ and the molar concentration of the analyte c by the relationship

$$k=2.303 \times \epsilon \times c \quad (2.22)$$

Reflectance spectra then consist of a plot of $f(R_{\infty}^l)$ versus wave number [161]. The Kubelka-Munk equation gives absorbance-like results for diffuse reflectance measurements, as can be seen by comparing it to Beer's Law,

$$A=a \times b \times c=K \times c \quad (2.23)$$

for a fixed path length. In Beer's Law, K is a proportionality constant based on absorption coefficient and the path length. $\frac{2.303 \times \epsilon}{s}$ is also a proportionality constant, but based on the ratio of absorption coefficient to scattering coefficient. The term $f(R_{\infty}^l)$ can be considered a "pseudoabsorbance" [162].

2.3.2.1.2 CO₂ Adsorption Using FTIR Spectroscopy

CO₂ is adsorbed reversibly at RT (100-300 torr). The peak intensity increases with pressure of the adsorbed gas. The species observed on the surface changes according to pretreatment temperature [163]. Peak assignments of CO₂ adsorption on TiO₂ are given in Table 2.8.

Table 2.8 Peak assignment literature survey related with CO₂ adsorption on TiO₂.

Reference	Other CO ₂ Related Peaks	Carbonate-Bicarbonate Related Peaks
Yates <i>et al.</i> [164]		1580 and 1320 cm ⁻¹ (CO ₂ ⁻ derivatives)
Primet <i>et al.</i> [163]	3609 and 3716 cm ⁻¹ (Gas phase CO ₂ peaks)	1670 (shoulder), 1555, 1420, 1340 and 1220 cm ⁻¹ (1220 cm ⁻¹ can be related with δ(OH) vibration. Since this peak series are observed on hydroxylated TiO ₂ , it may be assumed that they are bicarbonate originated peaks. Bicarbonates can easily be vacuumed at 25°C, they concluded that basic character is not strong.)
Martra <i>et al.</i> [159]	1630 cm ⁻¹ (CO ₂ can also partly contribute to the peak). 2351 cm ⁻¹ (Linearly adsorbed CO ₂ for Degussa P25). 2347 cm ⁻¹ (For Merck sample, due to carbon dioxide molecules linearly adsorbed on Ti ⁴⁺ ions)	1578 and 1359 cm ⁻¹ (Monodentate carbonate) 1672, 1243 and 1053 cm ⁻¹ (Bidentate carbonate groups) 1630, 1430, 1408 and 1221 cm ⁻¹ (Bicarbonate species) 1595 and 1315 cm ⁻¹ (Due to the asymmetric and symmetric stretching modes of monodentate carbonate species formed on Lewis acid–base pairs in defect position (edges, steps, corners)).
Busca <i>et al.</i> [158]	2376 cm ⁻¹ (Interactions of two CO ₂ molecules on single metal center) 2280 cm ⁻¹ (Adsorbed ¹³ CO ₂) 2350 and 2360 cm ⁻¹ (Two different Lewis acid center, where acidity observed at 2360 cm ⁻¹ is stronger than 2350 cm ⁻¹ peak).	

2.3.2.1.3 NO Adsorption Using FTIR Spectroscopy

The coordination chemistry of the NO molecule is complicated because NO has an electron in the antibonding $2\pi^*$ orbital. NO molecule exhibits both electron donor and acceptor behavior [165]. Easy determination of the nature of N_xO_y adspecies is difficult; large number of compounds which may coexist on the surface due to formal oxidation state of nitrogen (1-5), overlap of some band such as N-O stretching modes around 1870 cm^{-1} for NO, $(NO)_2$ and N_2O_3 [166].

When NO is adsorbed on reduced surfaces, dinitrosyls are expected. On oxidized surfaces, oxidation of NO occurs. When NO is co-adsorbed with excess oxygen, NO_2 , N_2O_4 and nitrates are expected. Stability is important phenomena in determining surface species. Generally non charged species such as NO, $(NO)_2$, N_2O_4 , NO_2 are removed easily. Ionic species such as nitrites, nitrates and nitrosyls are not removed by vacuum. For surface nitrates, stability is ordered from highest to lowest as bridged, bidentate and monodentate nitrates for same cationic sites. No reaction between NO_2^- and NO is expected. However, nitrates can oxidize NO. Many NO_x species absorb at $1650\text{-}1600\text{ cm}^{-1}$. However, NO_x interaction with surfaces is often accompanied by water evolution. Typical adsorbed water $\delta(H_2O)$ band is seen at 1620 cm^{-1} . It is not easy to distinguish water from N_xO_y species unless dehydroxylated surface is utilized. Surface nitro, nitrito or nitrato species are generally produced after $NO+O_2$ co-adsorption on samples having Lewis acidity [166].

With a minor admixture of O_2 in NO, IR bands of nitrates increase sharply [167]. NO interaction with TiO_2 is weak, and produces N_2O as gas product on rutile phase [168]. There are some IR studies without illumination of UV light. Dines *et al.* [169] report IR and Raman spectra of NO and NO_2 adsorption on anatase, leading to the formation of bridging, monodentate and bidentate nitrate species. These species, together with nitrite also detected by

Hadjiivanov *et al.* [170] when anatase sample was exposed to NO_2 . Degussa P25 was exposed to NO which results formation of NO^- and $\text{N}_2\text{O}_2^{-2}$ and nitrates species. When $\text{NO}+\text{O}_2$ was used, nitrates concentration increased and NO^+ formed [171]. For UV illuminated TiO_2 , NO was adsorbed on TiO_2 in the form of bidentate nitrites and nitrates by reacting with OH groups and peroxy species. Adsorbed nitrites were transformed into nitrates in seconds detected by in-situ FTIR [172]. The peak assignments related with NO adsorption is given in Table 2.9.

2.3.2.1.4 Benzene Adsorption on TiO_2

Nagao *et al.* [173] and Suda *et al.* [174] studied benzene, toluene and chlorobenzene adsorption on rutile surface by chemisorption and FTIR. The IR adsorption band due to C-C stretching vibration of the aromatic ring shifted to the lower wave number with reference to the case of gaseous state, showing that these molecules are adsorbed through the formation of $\text{Ti}^{+4}-\pi$ electron type complex on dehydroxylated surface and by the formation of a $\text{OH}-\pi$ electron type complex on hydroxylated surface. Multilayer adsorption $\pi-\pi$ interactions are also included in addition to $\text{Ti}^{+4}-\pi$ interactions. The second interaction also has to be true since the band disappears in the IR spectrum after vacuum treatment at RT but irreversible adsorption is measured by chemisorption technique. Hadjiivanov *et al.* [160] studied benzene co-adsorption after ammonia. The spectra also show the same band at 1478 cm^{-1} formation after adsorption of ammonia. Since ammonia should cover acidic Ti^{+4} sites, the band should appear due to $\pi-\pi$ interactions.

Table 2.9 Peak assignment literature survey related with NO adsorption on TiO₂.

Reference	Other Peaks formed due to NO adsorption	Nitrate-Nitrite Related Region
Hadjiivanov <i>et al.</i> [166]	1368-1359 cm ⁻¹ (ν _s (NO ₂ for N ₂ O ₄ formation) 1764 cm ⁻¹ (ν _{as} (N-O),trans-(NO) ₂). 1758-1730 cm ⁻¹ with a shoulder at 1710 cm ⁻¹ (ν _{as} (NO ₂) for N ₂ O ₄ formation) 1845 cm ⁻¹ and 1905 cm ⁻¹ (Characteristic gaseous NO peaks) 1914-1900 cm ⁻¹ (ν(NO) of mononitrosyl species)	1260 cm ⁻¹ (ν _{as} (NO ₂)), 1330 cm ⁻¹ (ν _s (NO ₂)) 1380 cm ⁻¹ (ν _{as} (NO ₃)) 1542 cm ⁻¹ (Nitro-nitrito (NO+NO ₂ Adsorption)) 1545-1190 cm ⁻¹ (Monodentate nitrate (NO adsorption)) 1550,1450 cm ⁻¹ (Nitro-nitrito (NO ₂ Adsorption)) 1582-1302 cm ⁻¹ (Monodentate nitrate (NO+NO ₂ adsorption)) 1622-1322 cm ⁻¹ (Bridging nitrate (NO adsorption)) 1612-1241 cm ⁻¹ (Bidentate nitrate (NO+NO ₂ adsorption)) 1620-1610-1580-1220 cm ⁻¹ (Bridging nitrate (NO ₂ adsorption))
Guglielminotti <i>et al.</i> [175]	1920 cm ⁻¹ (Adsorbed NO ₂)	
Hadjiivanov <i>et al.</i> [170]		1380 cm ⁻¹ , 1410 cm ⁻¹ , 1580 cm ⁻¹ , 1610 cm ⁻¹ and 3500 cm ⁻¹ (Assigned to Ti-O ₂ -NOH species after NO ₂ adsorption on anatase)
Dines <i>et al.</i> [169]	3675 cm ⁻¹ (Perturbation occurred after NO ₂ adsorption and is assigned to interaction with monodentate nitrato not formed from NO.) 3720 cm ⁻¹ (Adsorption of both NO and NO ₂)	1190 cm ⁻¹ (The broad band due to lower band of bridging nitrato species) 1240 cm ⁻¹ (Lower band of bidentate nitrato species) (Bidentate species is formed harder on the surface than bridged species and also

Table 2.9 (Continued)

	led to the perturbation of band which must be placed adjacent to adsorption sites forming bridged or bidentate nitrate.)	removed easily by evacuation at elevated temperatures.) 1586 cm ⁻¹ (Bidentate nitrate) 1610 cm ⁻¹ (Bridging nitrate) (different behavior due to initial appearance pressure and vacuum disappearance)
Nakamura <i>et al.</i> [176], Pozdnyakov <i>et al.</i> [177]		1192 cm ⁻¹ (Bidentate nitrite)
Belanger <i>et al.</i> [178]	2263 cm ⁻¹ (NO ₂ adsorption)	
Mccormick <i>et al.</i> [179,180]	2100-2400 cm ⁻¹ region (Related with NO ⁺ or NO ₂ ⁺ formation due to adsorption of NO ₂ ⁻ and NO ₃ ⁻ fragments) 2267-2250 cm ⁻¹ region (Assigned to NOH ⁺ species)	
Wu <i>et al.</i> [172]	3700-3550 cm ⁻¹ region (H bonded OH groups) 3750-3700 cm ⁻¹ region (Assigned to surface free OH groups). 3600-3400 cm ⁻¹ region (Corresponds to H bonded OH groups, $\nu(\text{OH})$ of NO-H (3565 cm ⁻¹) and isolated $\nu(\text{H}_2\text{O})$ (around 3456 cm ⁻¹)). Lower frequencies than 3400 cm ⁻¹ corresponds to undissociated $\nu(\text{H}_2\text{O})$ region	1192 (Bidentate nitrite $\nu(\text{NO}_2)$) 1458 (Symmetric stretching mode of bidentate nitrate $\nu(\text{NO}_3)$) 1508 (Monodentate Nitrate $\nu(\text{NO}_3)$) 1525 (Monodentate Nitrate $\nu(\text{NO}_3)$) 1540 (Monodentate Nitrate $\nu(\text{NO}_3)$) 1576 (Bidentate nitrate $\nu(\text{NO}_3)$) 1620 (Adsorbed, undissociated water, $\delta(\text{H}_2\text{O})$)

Table 2.9 (Continued)

Hadjiivanov <i>et al.</i> [171]	1920-1840 cm ⁻¹ (NO)	1170 cm ⁻¹ (NO ⁻)
	1930 cm ⁻¹ (N ₂ O ₃ , Possibly NO)	1335 cm ⁻¹ (Hyponitrites)
	2210-2150 cm ⁻¹ (NO ⁺)	1520-1280 cm ⁻¹ (Nitro species, possibly monodentate nitrates)
	2242, 2231 cm ⁻¹ (N ₂ O, weak adsorption)	1578, 1572- 1250-1220 cm ⁻¹ (Bidentate nitrates) 1644-1628 -- 1220-1175 cm ⁻¹ (Bridged nitrates)
Kantcheva <i>et al.</i> [181]	1715 cm ⁻¹ (σ (NO), ON-Ti ⁴⁺ -ONO ₂ ⁻)	1160 cm ⁻¹ (σ (NO), Ti ⁴⁺ -NO/NOH)
	1843 cm ⁻¹ (σ (NO), ON-Ti ⁴⁺ -NO/NOH)	1505-1286 cm ⁻¹ (Split σ_3 , NO ₃ ⁻ monodentate)
	1913 cm ⁻¹ (σ (NO), ON-Ti ⁴⁺ -ONO ₂ ⁻)	1555-1215 cm ⁻¹ (Split σ_3 , NO ₃ ⁻ bidentate)
	2210 cm ⁻¹ (σ (NO), NO ⁺)	1580-1215 cm ⁻¹ (Split σ_3 , NO ₃ ⁻ bidentate)
	3565 cm ⁻¹ (σ (NO), Ti ⁴⁺ -NOH)	1615-1215 cm ⁻¹ (Split σ_3 , NO ₃ ⁻ bidentate) 1630-1625--1215 cm ⁻¹ (Split σ_3 , NO ₃ ⁻ bridged)

2.3.3 Surface Acidity Correlation with Photocatalytic Activity

Papp *et al.* [182] showed that there was a linear relationship between surface acidity and photocatalytic activity of Degussa P25 indicated by n-butylamine titration procedure established by Tanabe [183]. The photocatalytic activity decreased with increasing annealing temperature, which is increased from 250°C to 500°C. This also decreased the surface acidity. They also showed there is an optimum amount of MoO₃ and WO₃ which gives maximum amount of photocatalytic activity and also acidities.

Martra *et al.* [159] studied Merck TiO₂ and Degussa P25 using FTIR spectroscopy and used benzaldehyde to observe photocatalytic activity which is an intermediate formed during toluene photooxidation. They showed that Degussa P25 has changed benzaldehyde to hemiacetic-like species whereas TiO₂ Merck slightly disturbed the structure. They also used CO at 77K to measure the acidic sites and CO₂ at RT to measure the basic sites of TiO₂. This analysis showed that Degussa P25 showed both acidic and basic activity as expected from all amphoteric oxides but TiO₂ Merck did not show any basic activity.

Kozlov *et al.* [154] studied photocatalytic decomposition of acetone to observe the activity differences between an untreated Hombikat UV 100 TiO₂ and H₂SO₄ treated TiO₂ sample. They decreased the basic sites and increased the acidic sites by the treatment. They observed increase in photocatalytic activity with increasing acidic sites. The activity increased 20-30%. They measured acidic sites by pyridine adsorption and used benzoic acid to measure the basic sites. The increasing molarity of H₂SO₄ increased the acidic site increase effect on TiO₂. The specific surface area did not change significantly during treatment.

2.4 PATENT SUMMARY

A patent survey was conducted and given in Table 2.10 since there was a parallel project to this thesis work with Kalekim Company, where there is a chance of commercialization of the products. In this patent survey, WIPO is searched for KR, EP (European Patent), WO (World Organization) and Espacenet for JP and US patents. Especially JP patents were included due to high research in this topic.

The self-cleaning technology is solving its own problems coming from economic reasons such as efficient usage of the photocatalytic material or using recycled materials. The technology adapted itself according to customer needs such as transparency, bio-organism resistance or long-term stability, which means to overcome binder problems. Maybe the most important need for the customers is the usage of the photocatalytic technology in indoor environments or utilization of visible light more effectively, which is still a challenge for the scientific community. Various applications adapted self-cleaning technology and produced commercially available products.

Deposition of TiO_2 particles near the surface increases the effective usage of the particles mainly due to higher UV accessibility. Depth of the application area and application time are some parameters mentioned in the section on patents related to particle deposition near surface.

The organic material of paints and coatings, such as binders and additives, can be decomposed due to the aggressive nature of radicals. This leads to removal or chalking of TiO_2 , which also means deterioration of the paint. This self-degrading effect may result in relatively high quantities of organic compounds, like aldehydes and ketones. These compounds are quite stable indoor air pollutants and may decrease the quality of the air [184]. In preventing degradation of binder using inorganic systems part, patents to reduce or prevent this phenomenon were investigated.

The studies have demonstrated that titanium dioxide deactivates a wide range of pathogenic microorganisms. In general, bio-particulates affect the hygienity of the surfaces. Hygiene conditions are important, where the concentration of bioorganisms can be high such as hospitals, or hygiene conditions are maximized at homes due to infant raising. It is thus expected in the near future that self-sterilizing TiO₂ materials may have many medical applications. At least, hospital room walls, medical instruments, and hospital uniforms can all be coated with self-sterilizing TiO₂ materials [184].

To increase the utilization of sunlight, wavelengths on visible range should be included to the region where photocatalytic activity occurs. Visible light activity is also important for indoor environments, where lightning includes less UV intensity than classical UV sources. There are various methods that can be used in utilization of visible light activity [184,185,186,187,131,188,189].

Construction is a convenient sector for using recycled materials. The materials are generally used as aggregates, where the size and amount of particulates are important in mix design. The use of recycled materials in photocatalysis is either using photocatalytic coating materials in the production of classical products such as pavements or coating directly the recycled products such as diatomaceous earth.

Nitrogen oxides (NO_x) are the generic term for a group of highly reactive gases, most of them emitted in air in the form of nitric oxide (NO) and nitrogen dioxide (NO₂). Nitrogen oxides are for instance formed when fuel is burned at high temperatures, as it is the case in combustion processes in automobiles. One of the European Union (EU) directives (1999/30/EC) established limit value for concentrations of the most representative air pollutants. However, NO_x exceeds the maximum allowed limit, especially in urban areas [190]. Photocatalysis is utilized in places such as roads, pavements, buildings near roads with heavy traffic, where high NO_x emissions are present.

Transparency is mostly based on particle properties. It is obtained when particles transmit visible light. In practical terms, reduction in the crystal size of a TiO_2 product leads to an optimum size of TiO_2 of the order of 20–50 nm where the ultraviolet spectrum of light (200–400 nm) is effectively scattered from the particles while the visible wavelengths are transmitted through the material. The material thus appears virtually transparent to the naked eye [191]. This kind of property is utilized in coatings.

Plasters and joints are also application surfaces which photocatalysts can be incorporated. They are specifically included, since the application areas of this thesis are on these products. TiO_2 mediated self cleaned cement based materials with different applications were shown such as filter unit, tooth bleaching agent, and air filter. A company based approach and search was also included for some big companies such as Italcementi S.p.A. and Toto Ltd.

Table 2.10. Patent survey on TiO₂ mediated self cleaning cement based materials.

Comments on Patents	Reference
Patents Related with Particle Deposition Near Surface	
Road surface application formed by injecting or spraying a mixture comprising TiO ₂ , cement, a filler and water on the surface.	[192]
Pavement construction method. The coating solution is applied when the hardness of cement solution is 1/3-2/3 of its final hardness.	[193]
Application on the tile surface, which is processed by molding, press working, drawing-out and steam-curing and following photocatalytic material spraying of dry-mix of powdery-granular carbon cement [100-300 pts.], mixing these with water [30-150 pts.], coloring inorganic pigment [10-20 pts.], efflorescence preventing agent [1-10 pts.] by weight.	[194]
Concrete block processing technique to increase the adhesion of concrete and photocatalyst without using organic adhesive. Photocatalyst powder-cement-water is sprayed on natural aggregate-cement paste layer.	[195]
Roofing material with a surface thickness of at least 0.5 mm. When the thickness is smaller than this, uniform molding of the surface layer is difficult, and the quantity of titanium oxide is too insufficient to function as photocatalyst.	[196]
Composition containing TiO ₂ powder-cement-sand-inorganic pigment applied to 1 μm-2 mm depth.	[197]
Photocatalytic TiO ₂ coating cured at RT which is applied to a depth of 0.01-2 mm on the surface of concrete.	[198]
Recipe for adding antifouling ability to water contacting places. Cement/photocatalyst (4/6-8/2 by weight) layer with a thickness of 0.01-0.5 mm. Viscosity improver methyl cellulose, surface active agent such as polycarboxylate and 25-35 wt% water is used if necessary.	[199]
Cement base surface colored board which is processed by molding the kneaded mixture, press forming (20-35 kg/cm ²), curing for a period of time and application of photocatalyst. The recipe is Portland cement (100 pts. wt.),	[200]

Table 2.10 (Continued)

synthetic resin emulsion diluted with water (200 pts. wt.), blue-colored silica sand (200 pts.wt.), a blue pigment (0.4 pts.wt.) and glass fiber (30 mm in length-0.8 pts.wt.)	
Patents Related to Preventing Degradation of Binder Using Inorganic Systems	
Coating liquid comprising photocatalyst particles and alkali metal silicate binder in which borate, boric acid or their mixtures are included.	[201]
Long lasting photocatalytic paint with antifouling and antibacterial properties containing potassium silicate instead of common organic binders. The mixture of titanium dioxides chosen has high specific surface area.	[202]
Inorganic ceramic paint (100 pts. wt. molar ratio $n\text{SiO}_2/\text{K}_2=2.5-7.0$), far infrared ray-emitting material (5-40 pts.wt.), anion emitting material (1-30 pts.wt.), photocatalyst (0.5-10 pts.wt.), antibacterial powder (0.1-5 pts.wt.).	[203]
Composition of fluorinated polymer which shows resistance to degradation containing a vinyl ester and/or vinyl ether, and a fluoroolefin, or cement or silicon based polymer.	[204]
2 layer coating process. First layer includes only resistant binder sprayed and dried at 200°C. Second layer includes photocatalytic material and binder. The binder amount changes w.r.t. first layer binder; 5-40% if binder is cement and/or gypsum, 20-98% if not.	[205]
Bio-organism Deactivation	
Homogenous coating (pH 5-9) composition consisting of TiO_2 dispersed particles with average primary (5-50nm) and dispersed particle diameter (10-100nm), an alkoxy silane hydrolysis-polycondensation product, a polymer dispersing agent, an organic amine, and silver particles if necessary. In addition, application of the composition is explained.	[206]
Roof materials subsuming mineral core, colloidal silica, a metal oxide, an exterior coating including clay, a photocatalytic particle (<100nm)	[207]
Inorganic composition containing Mn^{+2} and/or Mn^{+4} (1-50 wt%) and TiO_2 (50-99 wt%)	[208]
Recipe including TiO_2 , WO_3 with additional metal such as Fe, Ni, C, Cu, CO2P. 5 wt% carbon can be utilized for enhancing the effect.	[209-210]
Recipe including 5-50 wt% of TiO_2 , Pt- TiO_2 , Pt WO_3 -Pt- WO_3 , WO_3 .	[211]

Table 2.10 (Continued)

Composition containing silicate agent (binder) and dispersed photocatalyst particles.	[212]
Patents on Visible Light Activity	
Mortar formulation containing sand, colored quartz, magnesia (MgO) and cement having similar particle sizes. Quartz color changes from white, transparent, gray, brown, yellow, red, purple, green, blue, and black.	[213]
Manganese containing recipe using hydrated manganese dioxide sol, titanium solution and NH ₃ solution with changing Mn/Ti ratio 0.01/100-33/100.	[214]
Pt solution (with little yellow-hunter scale $b^* < 6$) containing halogenated Pt compounds loaded on TiO ₂ by heating and mixing (pH < 5). pH is adjusted to 5 or less and solution is neutralized if necessary. The surface area is 10-100 m ² /g.	[215]
Patents On Compositions Containing Recycled Particles	
Pavement block with NO _x removal property. Recycled material used is papermaking sludge incineration ash with a particle size of 0.15-1.2 mm as water retentive material.	[216]
Two layer pavement block construction. Base layer is composed of waste stone, cement, water and admixtures. Top layer is formed from crushed aggregates (1400~2000 kg/m ² particle size below 13 mm), cement (400~800 kg/m ²), scarlet powder (20~300 kg/m ²), water (80~200 kg/m ²), admixture (0.2~2.0 wt.%), anatase TiO ₂ (1~10 wt.%) and 1-10 wt.% porous basalt (average particle diameter 30-100 nm) and basalt powder (average particle diameter 75-200 μm)	[217]
Mortar preparation method by coating photocatalyst onto recycled expansion perlite and vermiculite particles, and additionally waste wood thermal treatment to obtain charcoal particles. Mixing of formed particles (particle sizes are adjusted to 4500-6000 blain) with cement, additive and water. The patent also includes method of preparation of recycled perlite and vermiculite particles.	[218]
Air purifying panel which contains a selected material from the group of blast furnace slag, steel slag and MSW (municipal solid waste)/MSWI bottom ash.	[219]
Mixture of TiO ₂ with diatomaceous earth waste obtained from a process of filtration.	[220]
Patents Related To NO_x Removal	

Table 2.10 (Continued)

Transparent coating liquid consisting of TiO ₂ particles, silicon based material containing minimum one polysiloxane compound, particles with HNO ₃ removal ability such as magnesium carbonate, calcium carbonate and their mixtures. (* contains additional opacifying agent and photocatalyst particle size changing from 1-50nm)	[221, 222*]
Iron oxide particles coated with TiO ₂	[223]
Roofing membrane including two layers, where base layer containing either a bituminous membrane, a plastic or metal panel. The second layer is obtained by mixing the base layer with granules obtained from anatase TiO ₂ , and a silicate or phosphate binder by pressing or calendaring on the hot bituminous blend.	[224]
Ceramic formulation containing scoria aggregate (67 wt% containing TiO ₂ (≥2 wt%) with particle size of 0.08-40 mm), water (10 wt%), cement (22 wt%) water reducing agent (<1 wt%) and photocatalyst (< 1 wt%). Composition is cured and cut.	[225]
Sound proof wall application comprising cement, TiO ₂ powder, light weight aggregate. Surface layer has a porous structure.	[226]
Cementitious coating film applied to outer surface of the road consisting of an adsorbent, a photocatalyst, alkaline earth metal salt and aggregate or a foaming agent.	[227]
Shotcrete formulation including TiO ₂ (5-40 wt% with 10-110 m ² /g surface area), Portland cement (50-90 wt% with 3060-4500 cm ² /g surface area), silica fume (3-15 wt% with 15-30 m ² /g surface area). 5-30 wt% adsorbent such as zeolite or activated carbon is added if necessary.	[228]
Patents On Transparent Coatings	
Formulation consisting of TiO ₂ , sulfur, fluorine and carbon applied to cement based surfaces. The crystallite particle size is 1 nm. The molar ratio of the TiO ₂ to the sulfur, fluorine and carbon is 99.75:0.25:0.906:1.314 respectively.	[229]
Composition including metal or metal oxide particles, titanium compound, organosiloxane oligomer and a silane compound.	[230]
Stable (at basic, neutral and acidic pH) sol preparation method using alpha-hydroxy acids with TiO ₂ (particle size < 10 nm). The method involves thermal treatment of suspension.	[231]

Table 2.10 (Continued)

Stable sol formulation is formed by precipitating amorphous TiO ₂ using organotitanium compounds, water soluble titanium salts. The amorphous TiO ₂ is redispersed and peptized to form a translucent or transparent mixture.	[232]
Processing and application method patent utilizing photocatalytic activity on mineral insulation wool or in glazing as building material.	[233]

Patents on Plaster and Joints

Formulation is formed by mixing plaster with materials such as sepiolite, vinylon chip or natural hemp fiber, scallop shell powder, slaked lime, modified titanium oxide, cmc or metrose and inorganic pigment. The mixture is cured with water or is baked at a high temperature of 600-650°C and molded.	[234]
Plaster recipe is obtained by mixing white shirasu (55-75 wt%), plaster (15-30 wt%), slaked lime (15-40 wt%) of a hardener, white cement (5-15 wt%), a tie rod, an inorganic pigment (0.1-5 wt%), vinylon chip (0.1-3 wt%), and titanium oxide (0.2-5 wt%).	[235]
Formulation consisting of commercial titanium oxide powder Jupiter, slaked lime as hardener (20-35 wt%), white cement (5-15 wt%), vinylon chips (0.1-1 wt%), white volcanic ejecta (40-65 wt%), plaster (20-35 wt%). The mixture is mixed with water.	[236]
Recipe containing diatomaceous earth (20-40 wt%), air hardening material such as dolomite plaster and slaked lime (2-30 wt%), hydraulic material such as Portland cement (10-40 wt%) and a photocatalyst (< 5 wt%).	[237]
Formulation including alkali metal silicate, water hardenable material such as cement based powders and photocatalytic material. The mixture is kneaded with water to form a pasted joint material.	[238]
Formulation containing minimum one of the SiO ₂ -Al ₂ O ₃ powder and CaO-SiO ₂ powder and photocatalytic oxide.	[239]
Recipe comprises a hydraulic material, an antimicrobial agent and/or a photocatalytic metal oxide, and particulate aggregate (<10 μm)	[240]
Dry construction method of tiles and joint fiber where a guide member is used to align the tiles in partitioning spaces.	[241]

Table 2.10 (Continued)

Patents on Cement Based Materials With Different Applications	
Dew-point evaporative cooler containing water, UV radiation source (natural sunlight or electrical powered by solar panel) and catalyst (preferred is TiO ₂).	[242]
Tooth bleaching formulation comprising a chemical compound generating hydrogen peroxide in aqua, titanium dioxide, phosphoric acid, condensed phosphate, and an inorganic or organic thickening material.	[243]
Cementitious building material reinforced with fiber for exterior wall cladding and roofing usage with air purification activity.	[244]
Monolithic building element which can be used in exterior, interior places such as roofs, walls and siding of building and floors.	[245]
Photovoltaic cell surface coating for maintaining cell efficiency.	[246]
Manufacturing method for extruded cement panel. Photocatalytic and superhydrophilic surface obtained by spraying photocatalytic solution.	[247]
Coating composition evaporating at room temperature subsiding xylene, polyalkylphenylsiloxane, composite photocatalyst powder, hydrophilic fumed silica and antibacterial powder.	[248]
Filter production method formed from multilayers.	[249]
Disposal container and facility for radioactive waste.	[250]
Air purifier with a UV source (350-400 nm, 100-150 Lux). Formulation contains TiO ₂ (5-15 wt%), binding agent (13-30 wt%) such as cement, colloidal silica, wood chip/clay balls, polyorganosiloxanes and sand (70 wt%) if necessary and water. Part of the cement can be changed by pozzolana. The coating further comprises metallic oxides of coloring.	[251]
Sound absorbing and air purifying surfaces, containing TiO ₂ , at least one hydraulic binding agent such as siliconized compound and cement, minimum one sound absorbing material and water.	[252]
Photocatalytic bituminous road surface (thickness 10-60 mm) formulation comprising plasticizing admixture, a photocatalytic material, amorphous silicon dioxide, and cement mortar.	[253]
Grass proofing package obtained using granular solidified mixtures including porous waste based on SiO ₂ and	[254]

Table 2.10 (Continued)

Al ₂ O ₃ , water and blast furnace cement and deposited photocatalyst on inside and/or outside surface of granular material.	
Photocatalytic cement containing films used on galvanized steel sheet containing an epoxy film layer (to prevent water access) in the middle.	[255]
Wooden cement board with adsorption and antifouling property by spraying a mixture containing an active carbon, and photocatalyst with water glass.	[256]
Comments On Studies of Companies with High Number of Patents In the Field	
Italcementi	
An organic additive formulation containing a cellulose ether, a melamine resin, a polymer selected from ethylene polymer, an acrylic polymer, and a terpolymer consisting of co-monomers minimum one ester of acrylic acid with an alcohol and minimum one ester of vinyl alcohol with a carboxylic acid, or alternatively a styrene, an acrylic or butadiene latex and chemically modified starch.	[257]
Patents on hydraulic binders	[258,259,260, 261]
Application patent to road surfaces (depth of filling 30-50 mm)	[262]
Cement paving strengthened with fibrose material.	[263]
Measuring method of photocatalytic activity which utilizes electromotive force generated between two electrodes (graphite) placed in contact with illuminated area and darkened area of material. For repeatability of the method, the specimens are subjected to the same procedure 5 times.	[264]
Doped TiO ₂ with a metal from groups I-VA, and actinide and lanthanide series.	[265]
Patent on carbon-doped TiO ₂ recipe	[266]
Patent on metakaolin supported TiO ₂	[267]
Patents on calcium titanate containing structures	[268-269]

Table 2.10 (Continued)

Toto Ltd.	
Film formation method. Tetraethylsilane is reacted to form amorphous silica by hydrolysis and dehydration condensation polymerization. Anatase type titania sol is applied burned and irradiated with 0.3 mW/cm ² UV for one day to develop hydrophilicity.	[270]
A lightening apparatus patent which contains a superhydrophilic photocatalytic layer for tunnel or road usage. Cleaning of the cover glass is easily done by jetted water from a car.	[271]
Transparent photocatalytic coating composition excited by light for obtaining ultra-hydrophilic properties. Precious metals such as Pd, Rh, Os, Ru, Pt is added to a photocatalyst of ZnO, SnO ₂ , WO ₃ , TiO ₂ , SrTiO ₃ , Fe ₂ O ₃ , Bi ₂ O ₃ and coated on a plate such as asbestos panel.	[272]
Superhydrophilic road marker composition easily cleaned with rain.	[273, 274]
Paving surfaces with photocatalyst-contained layer provided with superhydrophilic property which is easily cleaned by rain.	[275]
Cold reserving show case coating to prevent condensation of droplet in the inner surface of glass. Freshness is preserved due to oxidation reactions of gases such as ethylene and acetoaldehyde.	[276]
Superhydrophilic bathroom member coating to prevent sticking of soap scum or fats and to create easily cleaned surfaces. Microorganisms are killed due to photo-oxidation reactions.	[277]
Coating formulation used in a bowl for a wash stand application. The surface is irradiated with UV source to gain hydrophilic properties.	[278]
Patent on glass surface coating for interior usage with a short-wavelength and visible light lamp.	[279]
Coating film formulation for patient's room excited with a florescent light source (intensity of UV rays is not less than 0.001-1 mW/cm ² , preferable 0.01-0.1 mW/cm ²).	[280]
Hospital usage coating formulation for bio-organism deactivation.	[281]
Cement based joint formulation with antifouling properties containing a hydraulic material, a photocatalytic metal oxide (anatase TiO ₂), particulate aggregate (<10 μm), antimicrobial proof agent.	[282]

Table 2.10 (Continued)

Sticker type of coating to give photocatalytic activity (deodorizing) to the preinstalled tiles and fixing of the article by heating and cooling.	[283]
Fibrous-hollow photocatalyst material for usage in liquid phase decomposition reactions. The inner diameter of hollow photocatalyst is between 3 and 8 nm.	[284]
TiO ₂ particles designed to use in cancer treatment by UV radiation. Particles bind a hydrophilic polymer which is capable of bonding with a molecule that identifies the cancer cell.	[285, 286]
Activity measurement technique using working and counter electrode in a dye containing electrolytic medium.	[287]
Activity measurement technique by utilizing pH measurement due to OH radical concentration in an alkali halide aqueous solution	[288]
Device for coating of photocatalytic material by heating.	[289]

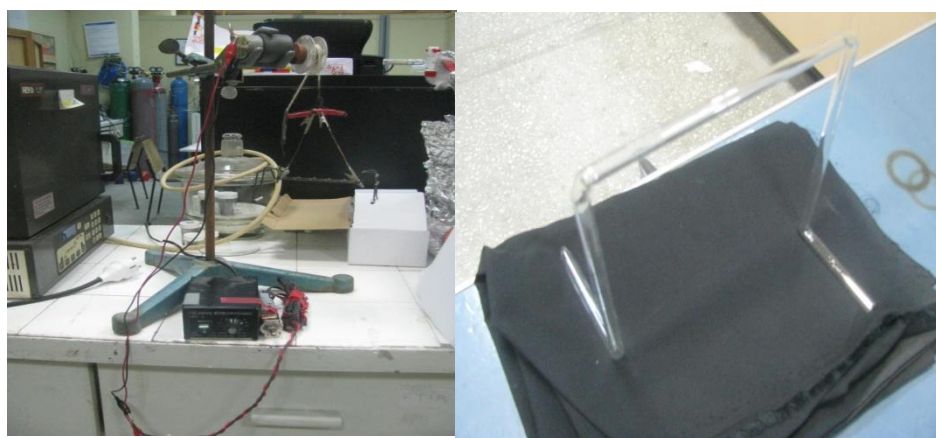
CHAPTER 3

EXPERIMENTAL

3.1 SOL-GEL COATED SAMPLES

3.1.1 Preparation of the Samples

The sol was prepared by mixing $\text{Ti}(\text{OC}_3\text{H}_7)_4$, $\text{C}_2\text{H}_5\text{OH}$, CH_3COOH , H_2O at the ratio [15:90:1:1] respectively [31]. $\text{Ti}(\text{OC}_3\text{H}_7)_4$ - $\text{C}_2\text{H}_5\text{OH}$ solution was mixed separately and added to $\text{C}_2\text{H}_5\text{OH}$ - CH_3COOH - H_2O solution during stirring. In order to keep the selected ethanol ratio constant, half of the required amount was used to prepare each of the two solutions. The solution was mixed for 15h. A dip coating procedure was applied by using a home-made apparatus for dipping [Figure 3.1a]. The glass beads were aligned vertically to a glass rod and these rods were hanged to a glass apparatus [Figure 3.1b]. The glass beads were dip-coated (dipping-pulling rate: 7.5 cm/min - 10 min holding in the solution) 1-3-5 times with the sol, dried at 120°C and calcined in the end at 450°C for 5 h. Several layers were coated as such. Pt incorporated into the structure by adding Pt precursor ($\text{Pt}(\text{NH}_3)_4\text{Cl}_2 \cdot \text{H}_2\text{O}$) into the solution in 0.1 mol %. These samples are indicated as (Pt(in)- TiO_2). In addition, for reaction tests in series, Pt was dip-coated on the surface of 5 times coated Pt(in)- TiO_2 glass beads by the same procedure using Pt precursor dissolved in water. These samples are indicated as (Pt(on)-Pt(in)- TiO_2). The samples were further calcined at 450°C for 5 h for Pt activation.



(a)

(b)

Figure 3.1 a) Home made dipping apparatus b) Glass apparatus

3.1.2 Characterization of the Samples

The XRD measurements of the catalysts were performed using Rigaku D/Max 2200 PC X-Ray Diffractometer using $\text{Cu-K}\alpha$ radiation. BET measurements were done with Micromeritics Gemini V Surface Area and Pore Size Analyzer. HR-TEM analysis was performed on a JEOL JEM 2100F field emission gun scanning transmission electron microscope operating at an accelerating voltage of 200 kV using a single tilt holder. Specimen was prepared after scraping the film by a scalpel from the glass substrate as powder, dispersing this powder in ethanol in an ultrasonic bath for 10 min. The solution was dropped on copper grids covered with lacey carbon films.

3.2 CEMENT BASED MATERIALS

3.2.1 TiO₂ Powder Selection

15 commercial samples were used in this study. The samples were coded S1 to S15. The manufacturer and the manufacturer specified properties for these samples are given in Table 3.1. Six samples were selected for photocatalytic benzene oxidation experiments based on their surface areas S8 (11 m²/g), S9 (77 m²/g), S12 (300 m²/g), based on their surface treatment S1 (organic surface treatment, 11 m²/g), S8 (untreated, 11 m²/g), and based on anatase-rutile ratio S15 (pure rutile (16 m²/g), S13 (80% anatase + 20 % rutile, 50 m²/g).

3.2.2 Sample Preparation

3.2.2.1 Cement Based Sample Preparation

The powder materials were mixed with a tumbler. The mortar was mixed with 33% water and applied into the sample containers. The samples were cured for 28 days at 23°C and 50% relative humidity. The samples were weighed before TiO₂ deposition. TiO₂-water solution was deposited on the grout samples using a syringe. The samples were left for air drying one day. To adjust the sample similar to the initial sample weight, drying was done around 10 min at 105°C. For photocatalytic benzene degradation experiments, TiO₂-grout or plaster samples were used once and the total weight of the used samples in the experiments were 9.44 g (~20 cm² area). (Figure 3.2a-Appendix B).

Table 3.1 Structural properties of TiO₂ samples used in this study.

TiO ₂ Code	Producer	Product Name	Density (g/cm ³)	Particle Size (nm)	Composition	TiO ₂ %	TiO ₂ phase	Surface Area** (m ² /g)
S1	Huntsman	Tioxide AHR	3.85	150	-	99	A	-
S2	Kemira	Kemira AN	3.9	180	-	98.5	A	-
S3	Kerr Mc Gee	Tronox A-K-350	-	5	>99% A	-	A	-
S4	Millennium Chemicals	PC 105	3.8	15-25	>99% A	97.2	A	85
S5	Millennium Chemicals	PC 500	3.8	5-10 nm	>99% A	83.9	A	> 350
S6	Millennium Chemicals	Tiona AT-1	3.8	300 nm	98% A	98.5	A	< 10
S7	Sachtleben	Hombikat UV 100	-	<10 nm	90% A	99	A	> 250
S8	Sachtleben	Hombitan LW	3.9	-	A	98.5	A	-
S9	Sachtleben	Hombikat N100	-	20 nm	A	98	A	100
S10	Tayca Corporation	TKP-102	2.5-4.2	15	A	>92	A	110
S11	Tayca Corporation	AMT-100	2.5-4.2	6	A	93	A	280
S12	Tayca Corporation	TKP-101	2.5-4.2	6	A	83	A	300
S13	Degussa	Aeroxide P25	3.8	21	80% A + 20% R	99.5	A + R	50 +/- 15
S14	Sachtleben	Hombitan LW-C	3.9	-	60% A + 40% R	99	A + R	-
S15	Kronos Titan	Kronos 2300	4.1	-	R	94	R	-

* A: Anatase R:Rutile, ** Manufacturer's data.

3.2.2.2 Sample Preparation for Visible Light Studies

Fe-doped TiO₂ was prepared by an incipient wetness impregnation method. 0.2 g Degussa P25 was mixed with 25 ml of ferric nitrate (Fe(NO₃)₃) aqueous solution. pH of solutions were adjusted to 4 with a dilute nitrate acid solution (0.1 M). Suspensions were stirred for 0.5 h and placed at RT for 48 h. Then, solution was dried in an oven at 105°C for 5 h to evaporate the water. Dried samples were ground and calcined at 500°C in air for 1.5 h. Fe/Ti atomic ratios were adjusted as 0.25, 0.5 and 1.0. Color changed from white to slight red with increasing Fe amount. For photocatalytic benzene degradation experiments, the powder was coated on glass slides.

3.2.2.3 Sample Preparation for Pure TiO₂ Studies

Pure TiO₂ activity was investigated by coating TiO₂ powders on glass slides by water. The soda-lime glass slides were dried at 105°C. The slides were used at least after 1 day of drying period. For photocatalytic benzene degradation experiments, the glass slides were cut conveniently to fit inside reactor before coating. The coatings were used once for each experiments.

3.2.2.4 Sample Preparation for Coating Studies

3.2.2.4.1 Direct Addition to Paint Formulation

S13 has been used as additive to the solvent based formulation in 1% and 5% ratios. Around 0.02 g grout marker paint (Edding 8200) was used to coat one side of the glass slide (5 cm²).

3.2.2.4.2 Solution Deposition using Grout Maker

S8 was used in water and applied to the surface by using a commercial grout marker manifold (Edding 8200).

3.2.2.4.3 Binding using White Cement

For preparation of binding with white cement, S9 sample was used (0.01 g). White cement (0.3-0.5 g) mixed with water (0.5-1 g) transferred to the grout surface. 0.01 g TiO_2 is transferred to the surface in approximately one minute during curing period of the white cement.

3.2.2.4.4 Coating Study with a Commercial Binder

A formulation was studied by using a commercial binder (Aykim Sylon S300) and S13. S13 (5wt.%) and binder (10 wt.%) was mixed with water and stirred under cold bath for 30 minutes. The solution was deposited on glass slides. After initial drying, the glass slides were calcined at different temperatures for 3h. The coating also subjected to boiling water and water at RT treatments.

3.2.3 Photocatalytic Reactivity Experiments

Gas phase photocatalytic oxidation of benzene with H_2O was carried out in a reaction cell (48 ml) which is connected to a pyrex manifold (215 ml) (Figure 3.2b-Appendix B). The manifold is connected to a vacuum pump and to an injection port. The degradation of benzene was monitored using a gas

chromatography instrument (Varian 3900) equipped with an FID detector and Poraplot Q as capillary column. The experiment has been done around atmospheric pressure and room temperature. 100 W UV light (~365 nm) (black light) was used in the studies. CO₂ verification experiments were done by using an Hp 5800 with a TCD detector and Propaq Q as column.

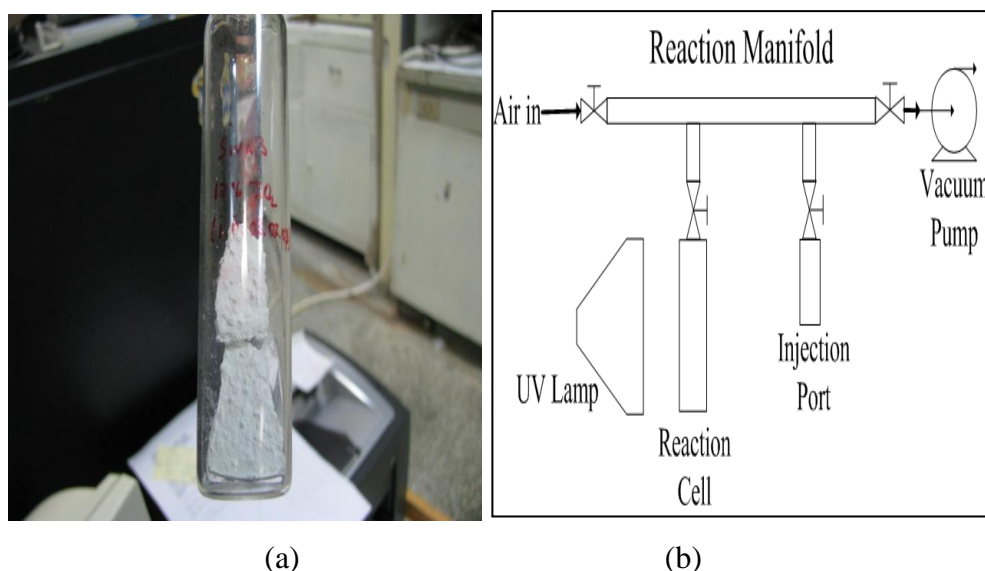


Figure 3.2 a) Sample placed in a reactor. b) Experimental set up.

3.2.4 Characterization of the Samples

DRIFTS measurements have been done using a Pelkin Elmer FTIR (Spectrum 100 series) equipped with a DRIFT cell (Pike) and MCT (Mercury Cadmium Telluride) detector. NO adsorption studies have been done with 15 TiO₂ powders used in this research using DRIFTS. CO₂ adsorption studies

have been done for 15 TiO₂ powders used in this research, 10% S8-grout, S8-on grout sample and grout samples without TiO₂ using DRIFTS.

XRD measurements of the catalysts were performed using Rigaku D/Max 2200 PC X-Ray Diffractometer using Cu-K α radiation.

BET measurements were done with Micromeritics Gemini V Surface Area and Pore Size Analyzer. The powder for the analysis was obtained by scratching the sample face to be analyzed.

Simultaneous differential thermal gravimetric analysis (DTGA) has been done with Shimadzu DTG-60H model equipment.

UV-Vis analysis (PG instruments Ltd., T80+ UV/Vis Spectrometer-transmittance mode) has been done by coating the glass with TiO₂ powder dispersed in water or ethanol. The samples are dried until dispersants are evaporated. The spectra were taken between 200 to 800 nm.

UV-Vis measurements were done by using Shimadzu-UV 2300 with Diffuse Reflectance apparatus. The samples were used as powder. They were scratched from surface of the grout samples.

Raman spectra of TiO₂ coated glass slides were obtained with Renishaw in via Raman Microscope system, using 532 nm argon ion laser with power of 30 mW for sample excitation.

SEM Images were taken using Zeiss-Leo Supra 35 VP Field Emission SEM system.

CHAPTER 4

RESULTS

4.1 CHARACTERIZATION

4.1.1 X-Ray Diffraction Measurements

XRD measurements were done for 15 commercial TiO₂ powders (12 anatase, 2 anatase+rutile mixture, 1 rutile). The crystalline phases indicated by the manufacturers were confirmed. The diffraction patterns are shown in Figure 4.1. The broadening of the crystalline anatase peaks are observed for the smaller particle size TiO₂ powders such as S3, S5, S7, S11, S12. XRD patterns showed strong diffraction peaks at 27°, 36° and 55° indicating TiO₂ in the rutile phase. For the anatase phase, XRD patterns exhibited strong diffraction peaks at 2θ of 25° and 48°, where 25° shows <101> of TiO₂ anatase structure.

4.1.2 BET Measurements

BET measurements were done for 15 commercial TiO₂ powders to determine the surface area of the samples. The measurements were compared to the manufacturer's specification data in Table 4.1. The BET measurements agreed to within 30% of the manufacturer's specifications.

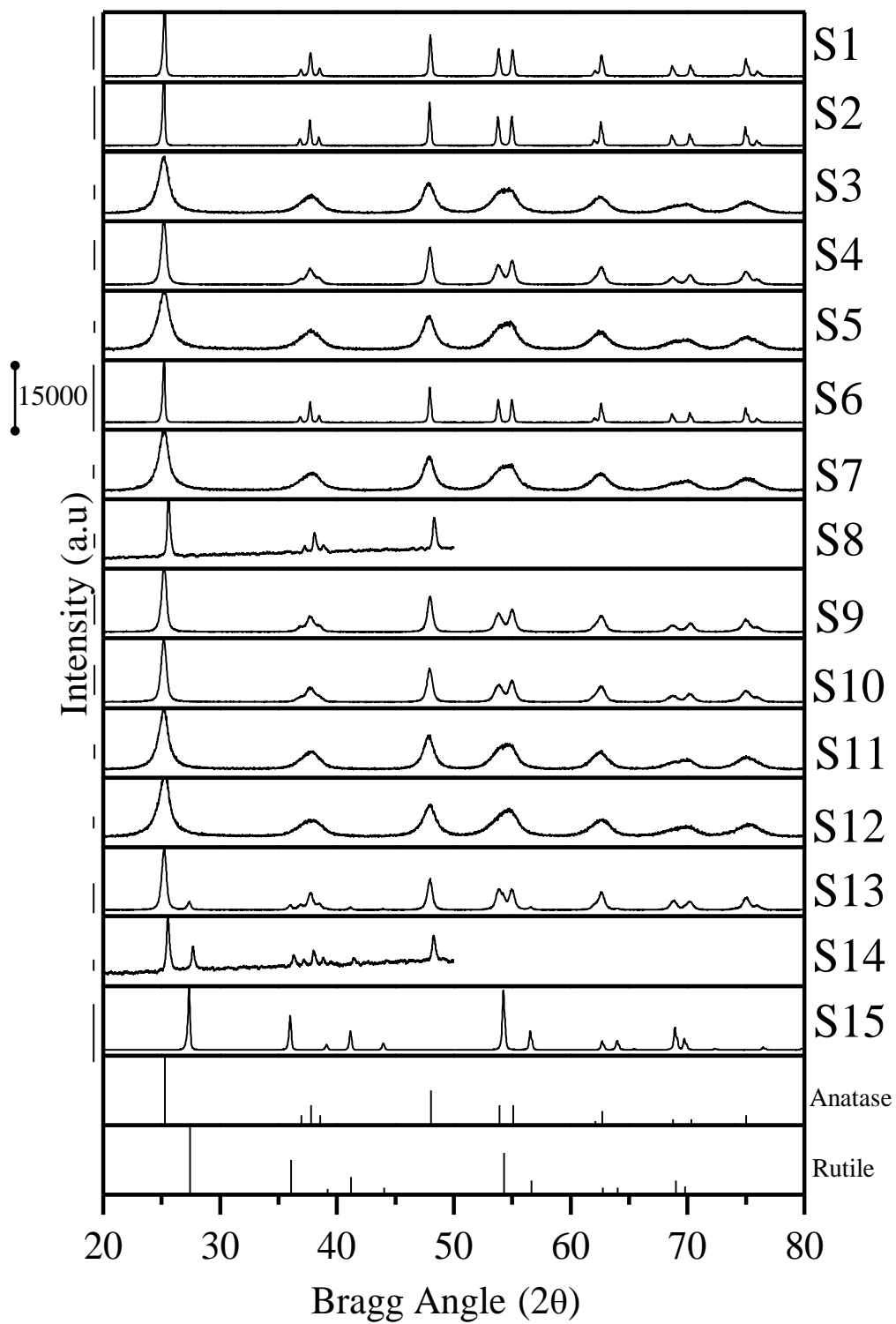
Figure 4.1 X-Ray Diffraction Results of TiO_2 powders

Table 4.1 BET results comparison for TiO₂ powders (A = anatase, R = rutile)

TiO ₂ Code	TiO ₂ phase	Data from manufacturer (m ² /g)	This study (m ² /g)
S1	A	-	11
S2	A	-	2
S3	A	-	266
S4	A	85	72
S5	A	> 350	278
S6	A	< 10	9
S7	A	> 250	258
S8	A	-	11
S9	A	100	77
S10	A	110	81
S11	A	280	253
S12	A	300	265
S13	A + R	50 +/-15	51
S14	A + R	-	21
S15	R	-	16

4.1.3 TGA Measurements

The TGA analysis has been done for 10% S1-grout sample (Figure 4.2). The sample lost 1.8% of its weight at 110°C. 5.2% of its weight has been lost till 500 °C. 1.8% of the weight loss is due to change in water content of the sample. After analysis, the sample weight was recorded and it was observed that all the water loss has not been recovered by the sample. The reason maybe the water content in the pores of the matrix which is not easily evaporated under room conditions has been evaporated under 110°C or simply the drying period still continues after curing period. The weight loss till 500°C may be due to CO₂ loss from the structure.

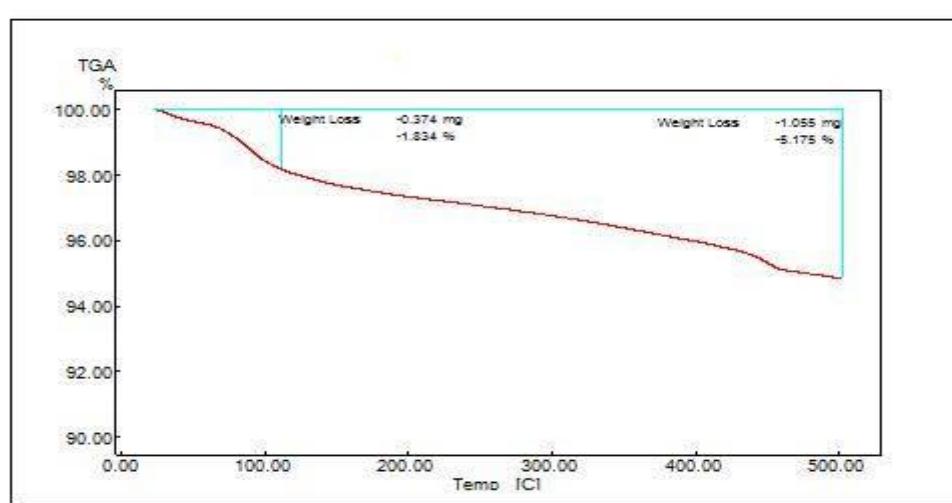


Figure 4.2 TGA results for cured sample S1.

4.1.4 UV-Vis Measurements

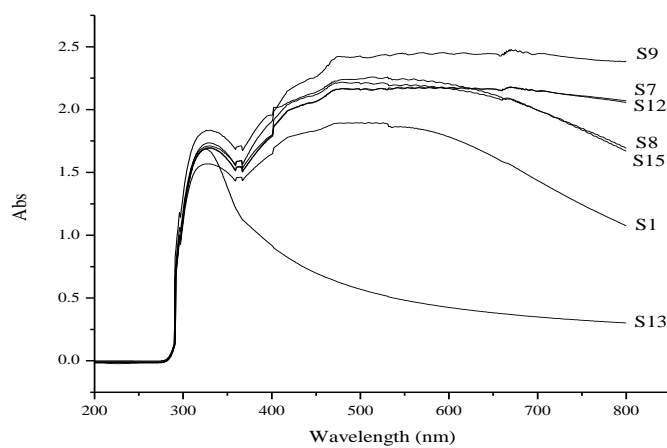


Figure 4.3 UV-Vis spectra for selected TiO₂ powders.

UV-Vis analysis has been done in transmittance mode for 7 selected TiO₂ powders. The powders were coated on soda-lime glass. Soda-lime glass is used in the reference cell (Figure 4.3). The measurements were done once. There is a significant transparency observed for S13 sample.

4.1.5 Surface Characterization using CO₂ and NO as Probe Molecules on TiO₂ with DRIFTS

DRIFTS studies were performed using Pelkin Elmer (Spectrum 100 Series) Spectrometer with Pike DRIFTS cell connected to a home built gas manifold capable of holding vacuum up to 10⁻⁵ Torr. The sample was used as received. The system was evacuated for 10 min to remove air. Subsequently, known amounts of intended gases were dosed onto the sample.

4.1.5.1 CO₂ Adsorption Studies

The sample cell was vacuumed for 30 minutes prior to the introduction of CO₂. 1 torr of CO₂ was introduced. The DRIFTS spectrum was recorded after allowing the system to equilibrate for 20 min. DRIFTS spectra under 5, 10, 50, and 500 Torr were recorded accordingly. After the adsorption experiments, DRIFTS spectra were recorded after 10 min vacuum.

Over 15 TiO₂ powders characterized by DRIFTS, monodentate, bidentate and bicarbonate structures were observed on the surface (Figure 4.4). The difference observed on different powders indicate the difference in the surface characteristics and reactivity of these samples.

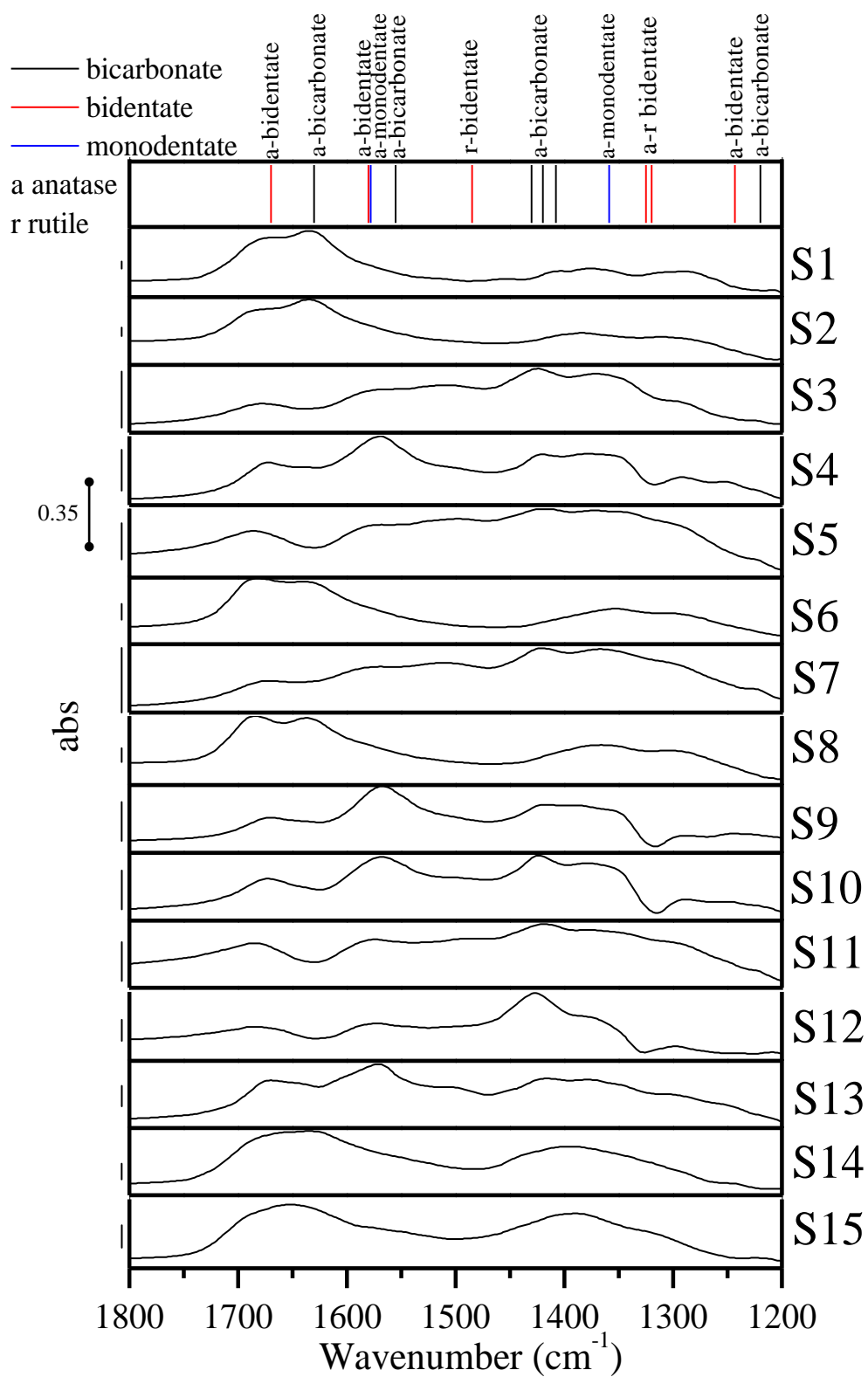


Figure 4.4 Comparison of carbonate region for 15 TiO_2 powders

S8 has been studied as pure, in the grout (10%), and on the grout (top coating) (Figure 4.5, Figure C.1 in Appendix C). The peaks due to, the broad peak between $3500\text{-}3000\text{ cm}^{-1}$ is more intense at 10% S8 and grout samples, which results from OH groups of residual water and surface bound OH groups. This region has also reduced after drying procedure (Figure C.1). The absorbance of $1400\text{-}1200\text{ cm}^{-1}$ region is low for grout and 10% S8 (this region for 10% S8 was removed from the graph, since there is too much noise). A peak is observed at 1750 cm^{-1} on grout sample. S8 integration to the grout matrix, increased the intensity of the carbonate related peaks or adsorption of CO_2 in all cases. Pure S8 and top coating has similar absorption peaks in the carbonate region. The bicarbonate peak at 1630 cm^{-1} [159,] is not observed for grout. Traces of water also contribute to the 1630 cm^{-1} peak [159]. The peaks seen on S8 top coating at 1550 cm^{-1} [163] and 1430 cm^{-1} [159,163] are attributed to bicarbonate species and these peaks are not seen on the other samples (Figure 4.5).

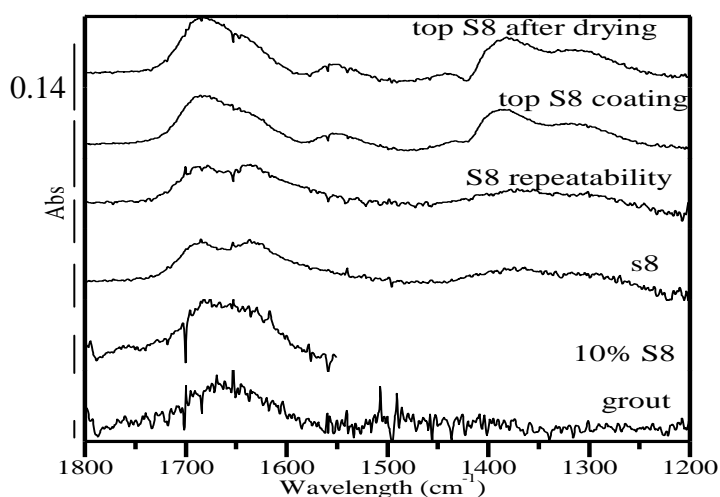


Figure 4.5 DRIFTS spectra comparison of pure powder, coating and grout applications using S8 on carbonate ($1800\text{-}1200\text{ cm}^{-1}$) region.

4.1.5.2 NO Adsorption Studies

The DRIFTS studies over these samples were also conducted for NO_x adsorption. The experiment was performed by sending NO+argon (10% volume) incrementally at 1, 50, 100, 250, 700 Torr mixture allowing 20 minutes for adsorption equilibrium. At the total pressures indicated NO pressures were 0.1, 5, 10, 25, 70 torr in the cell. The cell was vacuumed afterwards for 5-10 minutes.

Keeping in mind the interactions with water $\delta(\text{H}_2\text{O})$, 15 different TiO₂ powders were characterized by using NO as a probe molecule. Nitrite and nitrate formations were observed (Figure 4.6). The characterization of the peaks was mainly based on comprehensive review of Hadjiivanov [166]. On the surface of cement, NO can also adsorb as Ca(NO₃)₂ [4].

NO₂⁻ or NO₃⁻ ions are negatively charged fragments. Therefore, there are several possibilities of their formation on the surface: (1) They replace another negative fragment (e.g., an OH group), (2) another, counterpair cation (e.g., NO⁺) is formed simultaneously, or (3) a surface cation is oxidized. For cations with a stable oxidation state, the latter possibility can be rejected, but it is very probably realized on real catalysts, because the NO-conversion catalysts are based, as a rule, on cations easily changing their oxidation state [166].

Similar adsorption bands are observed for S1, S2, S6, S8, S14, S15 samples in nitrite-nitrate region (Figure 4.7). These samples have surface areas lower than 16 m²/g. S3, S4, S5, S7, S9, S10, S11 and S13 samples, which have surface areas around 50-350 m²/g have shown similar characteristics in nitrite-nitrate region (Figure 4.8).

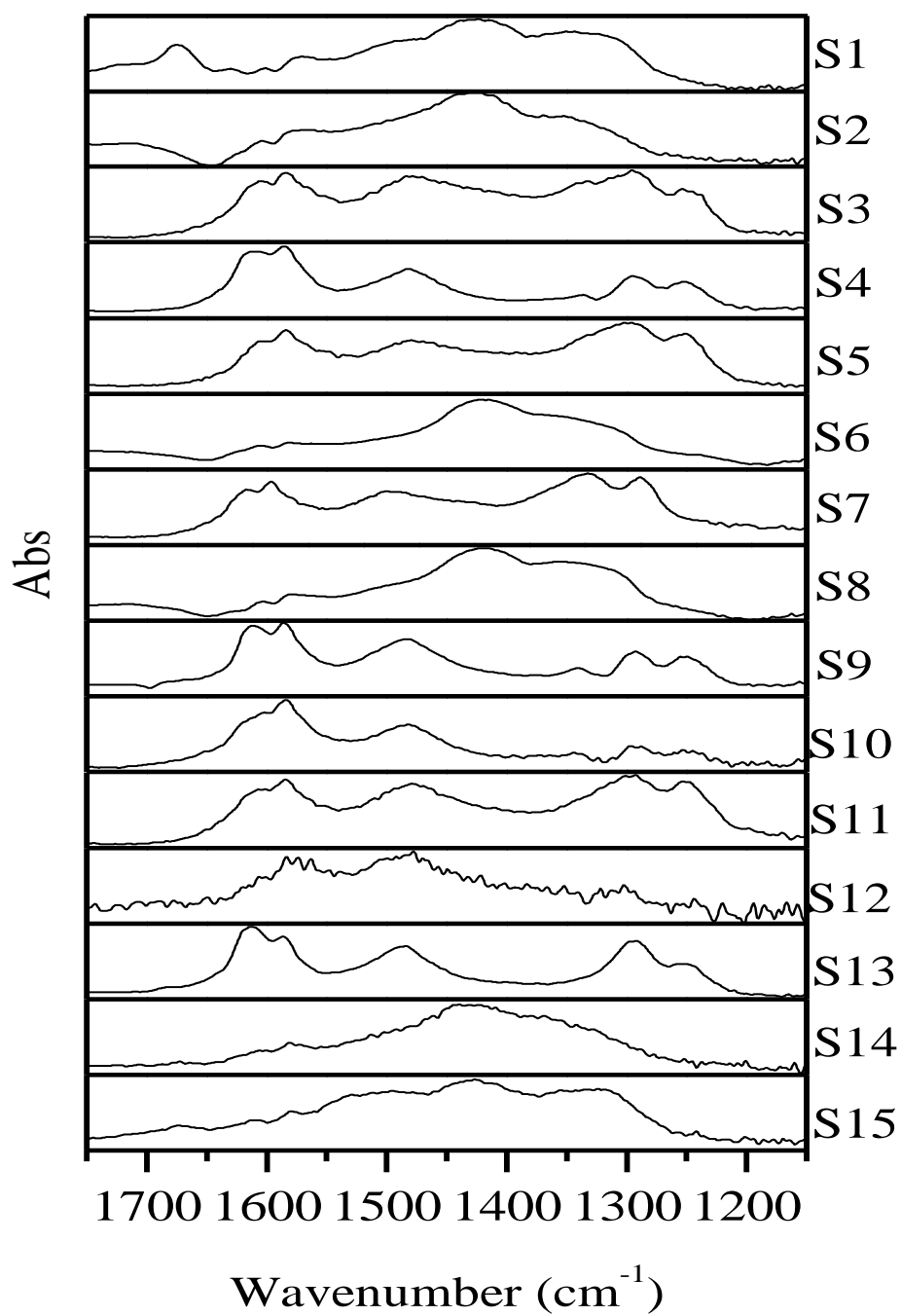


Figure 4.6 Changes in the nitrite-nitrate region of 15 TiO₂ powders

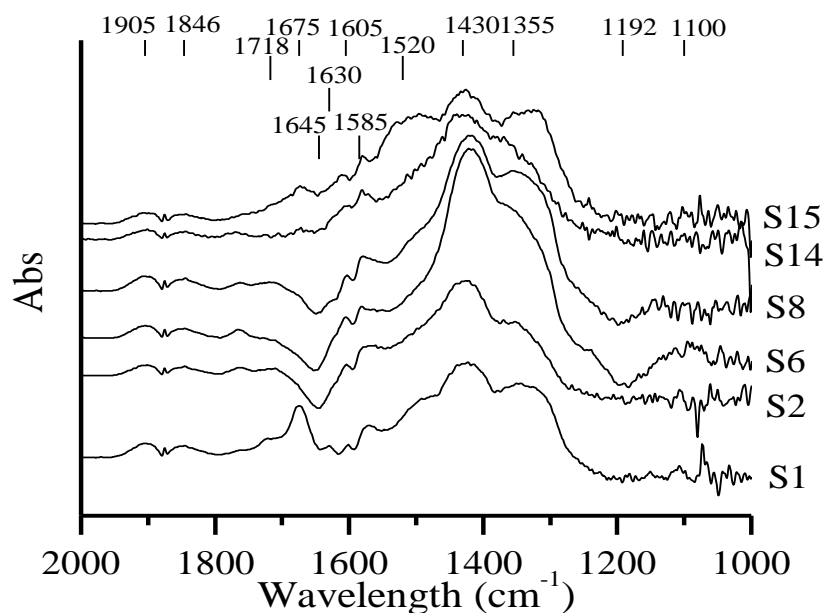


Figure 4.7 NO adsorption spectrum of nitrite and nitrate region for S1, S2, S6, S8, S14, S15 samples under 70 torr NO atmosphere at RT.

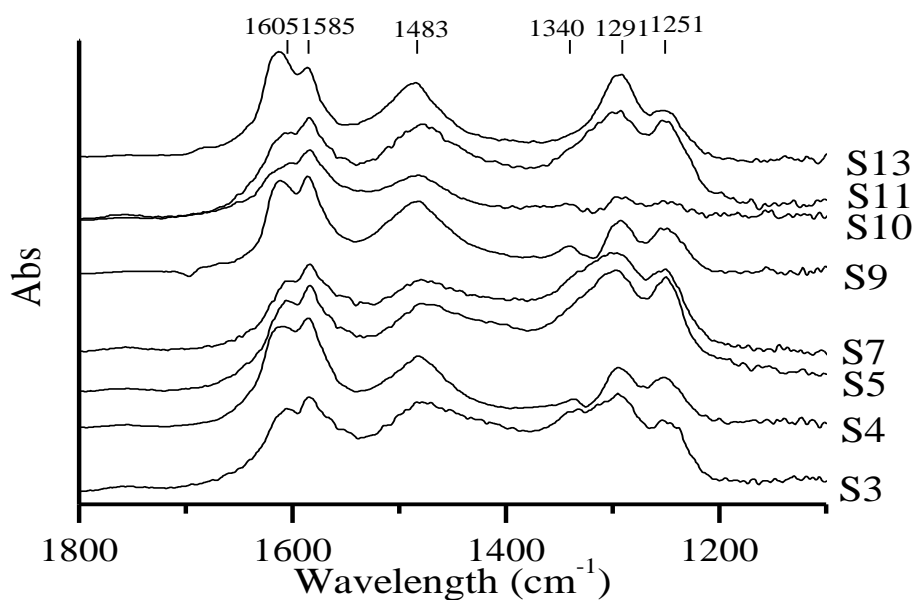


Figure 4.8 NO adsorption spectrum of nitrite and nitrate region for S3, S4, S5, S7, S9, S10, S11, S13 samples under 70 Torr NO atmosphere at RT.

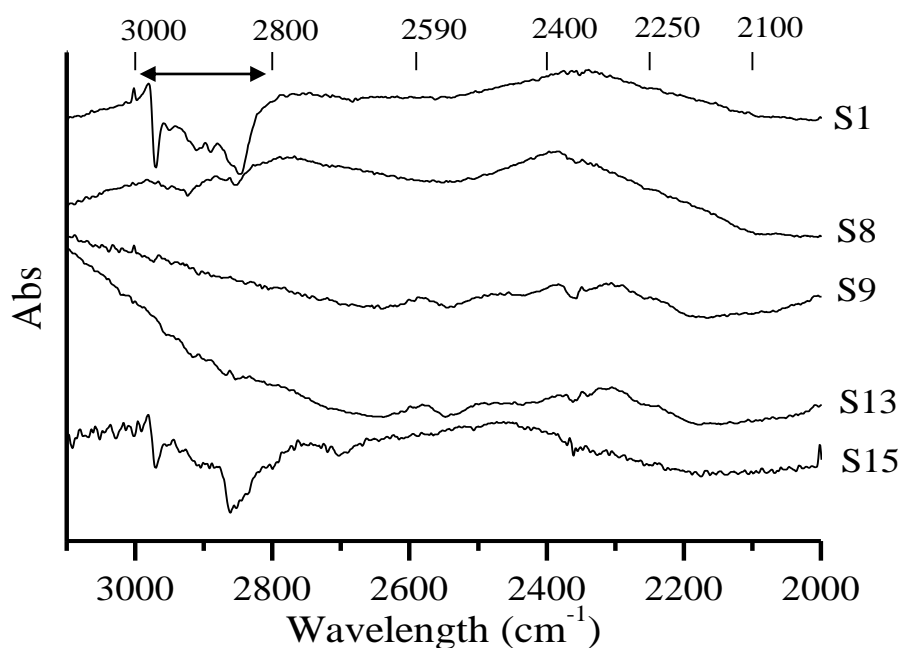


Figure 4.9 NO adsorption spectrum for S1, S8, S9, S13, S15 samples under 70 Torr NO atmosphere at RT.

There is negative peak formation and gradual decrease at 2800-3000 cm^{-1} region which is assigned to C-H stretching for S1, S2, S6, S8, S14, S15 samples (Figure 4.9). The peaks are more intense for S1 and S15. For S1 an organic treatment is done to the product and S15 contain aluminum compounds due to data taken from the supplier. There is no peak formation for S3, S4, S5, S7, S9, S10, S11, S12 and S13 samples at 2800-3000 cm^{-1} region. The peak assignments are given in Appendix D.

4.1.6 Search for Ti-O-Si bond: Raman Characterization of Degussa P25 on Glass

The Raman characterization was done for Degussa P25 samples on glass (0.004 g coating on 2 cm²-10 cm²-20 cm²). The general spectrum was recorded in beginning and anatase peaks were detected below 650 cm⁻¹. The bands between 300-800 cm⁻¹ and 800-1200 cm⁻¹ regions were inspected separately to get rid of the high intensity peak of anatase at 144 cm⁻¹. According to literature, Si-O-Ti linkages are seen on 950 and 1100 cm⁻¹ peaks. The literature is given below. The peaks around 950 and 1100 cm⁻¹ were detected for 10 cm² and 20 cm² coatings (Figure 4.10).

Anatase peaks were given in literature as 144,197,399,515,519,640 cm⁻¹ [290,291]. The bands at 952 and 1100 cm⁻¹ are associated with vibrational modes involving SiO₄ units linked with titanium atoms. Raman band at 805 cm⁻¹ is assigned for Si-O-Si symmetric stretching vibrations. The band at 430 cm⁻¹ is assigned to coupled combinations of Si-O-Si and O-Si-O bond bending vibrations. The bands at 488 and 605 cm⁻¹ is attributed to defects in network [292]. For TiO₂-SiO₂ glasses, the Raman active bands at 935 and 1105 cm⁻¹ belong to the vibrations of mixed Si-O-Ti linkages [293]. 950 cm⁻¹ band is associated with Si-O-Ti bridges which becomes more intense upon heating [294]. The bands at 970 and 1115 cm⁻¹ cannot be related to Ti-O vibrational modes since all solid titania compounds possess Raman bands below 900 cm⁻¹ [295]. A peak at 1058 cm⁻¹ was also observed in another study [296].

According to a micro-Raman study of a windows glass (SiO₂ (72%), Na₂O (15%), and CaO (8%)), the spectra showed peaks at 450, 560, 600, 800, 950 and 1100 cm⁻¹. 950 and 1100 cm⁻¹ bands are attributed to Si-O stretching vibration modes of Q2 and Q3 species respectively [297]. The Raman spectrum of empty glass was obtained. The peaks at 1096, 989 and 942 cm⁻¹ were also seen in empty glass reference in Figure 4.10. The peak at 1048 cm⁻¹ was not observed in empty reference.

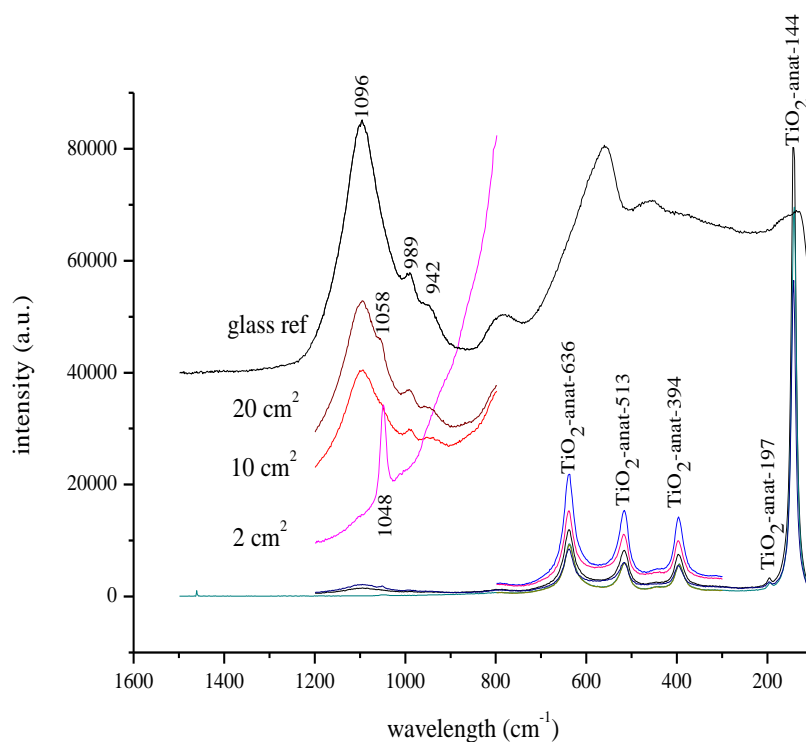


Figure 4.10 Raman spectra of S13 coatings on glass slide for different coating areas (deposited amount is 0.004 g for all coatings).

4.1.7 SEM Analysis

High surface area sample (S12), low surface area sample (S8), low surface area sample with organic surface treatment (S1) and low surface area rutile sample (S15) were used in SEM secondary electron analysis (Figure 4.11). Obtained secondary electron images show TiO_2 particles lower than 100 nm for S12 sample and TiO_2 particles between 100 and 250 nm are observed for S1, S8 and S15 samples. Another important observation is TiO_2 agglomerates seen in μm range.

When secondary electron images in different magnifications are inspected, the homogenous distribution of S1 particles were not observed on 10% S1-Plaster samples (Figure 4.12a-b-c). Another confirmation is from the EDX analysis. When regional elemental analysis and a point elemental analysis in that region are compared in terms of at % ratios of Ti/Ca, the homogeneity of S1 in plaster is not observed (13.31/8.66 for regional and 6.3/2.49 for point analysis)(Figure 4.12d-e).

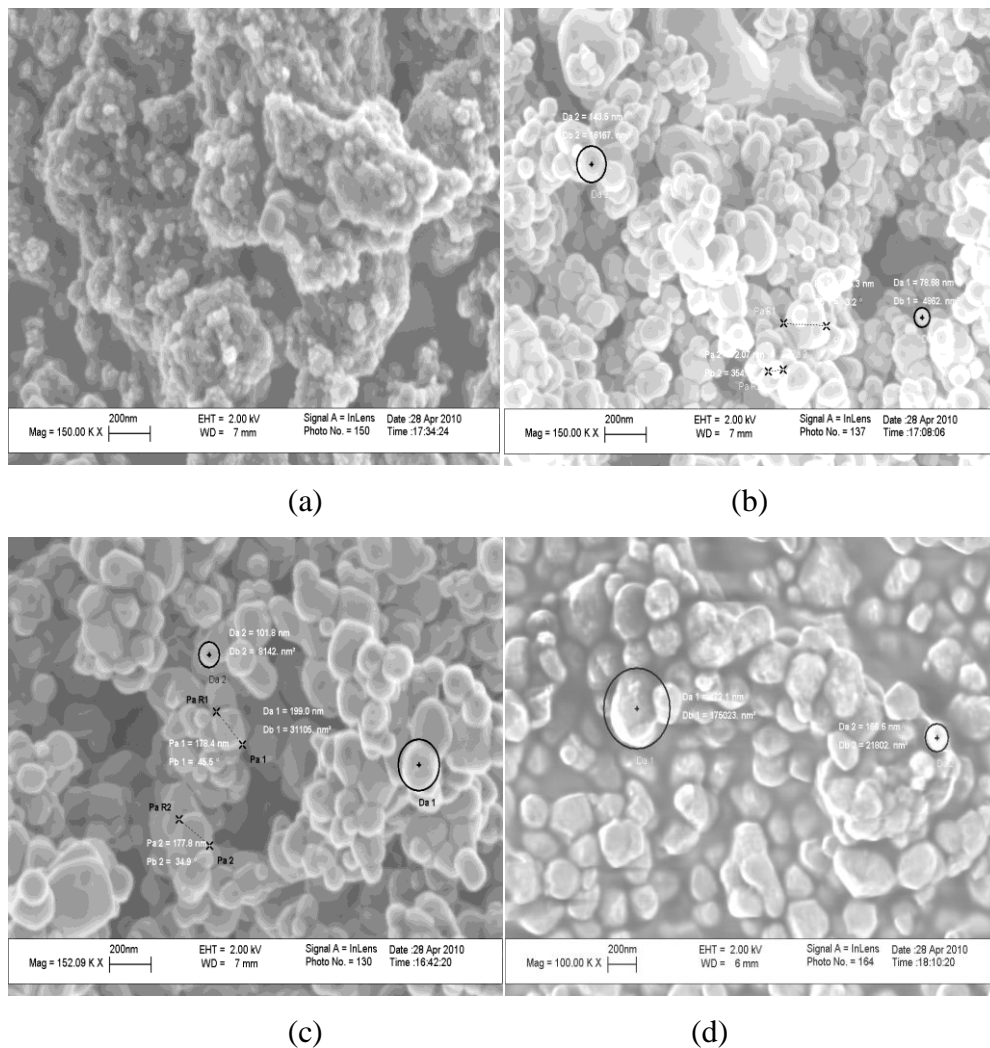


Figure 4.11. SEM images of (a) S12, (b) S8, (c) S1, (d) S15 [298].

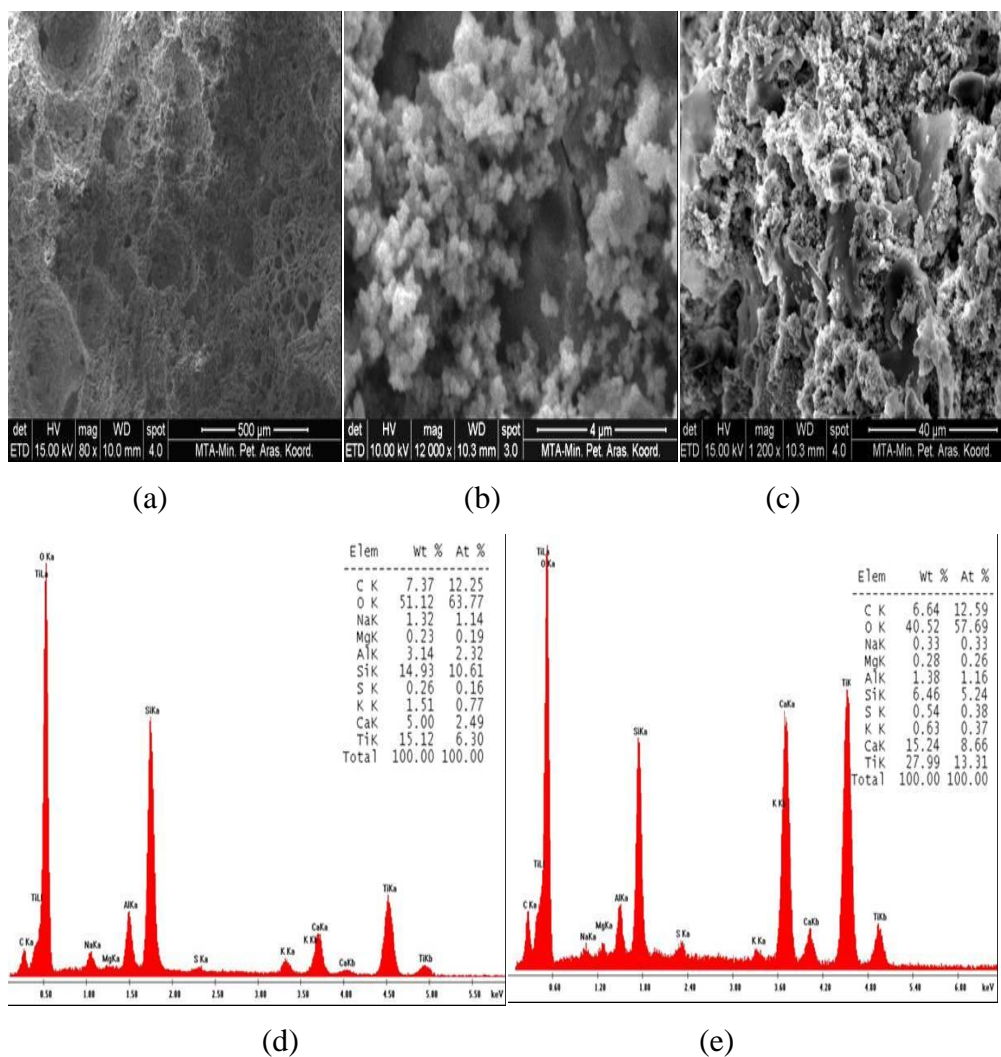


Figure 4.12 SEM Images (a), (b), (c) and point (d) and regional (e) EDX analysis of 10 % S1-plaster [298]

4.2 PHOTOCATALYTIC BENZENE OXIDATION EXPERIMENTS

4.2.1 Kinetic Screening Tests on Photocatalytic Benzene Oxidation

In these preliminary kinetic screening studies, the change in benzene amount was observed in the batch reactor by changing parameters of the study such as light source, sample type and TiO₂% in the samples. In this experimental procedure, benzene and water was injected with a syringe (1 μl) to the reaction cell at RT and atmospheric air pressure. After initial adsorption and diffusion period, UV light is activated. Benzene oxidation graphs include 2 parts: First stage gives the adsorption period of the benzene on the manifold and sample in the dark period. After dark adsorption equilibrium is reached, UV or visible light is activated and increase in the desorption of the benzene is observed due to temperature increase. Benzene amount in the gas phase makes a peak and begins to decrease due to degradation of benzene. The problem in quantification comes from the beginning of UV light activation. In this period, the increase in the benzene amount is observed, however at the same time, photocatalytic degradation of benzene is expected. However as mentioned before, these pre-results indicated an increase in the slope or an increasing amount of benzene decrease with respect to TiO₂%, which means the oxidation activity increased with increasing TiO₂%. They showed low visible light activity for both samples (shown in visible light studies Figure 4.19-4.20). The grout and plaster samples showed similar behavior with respect to benzene. The samples were compared for the same TiO₂ content in Figure 4.13. Grout and plaster samples followed similar trends under UV light. There are differences observed due to initial adsorption amounts. Rutile sample (S15) showed no photocatalytic activity (Figure 4.14a). The grout sample without TiO₂ showed no photocatalytic activity (Figure 4.14b).

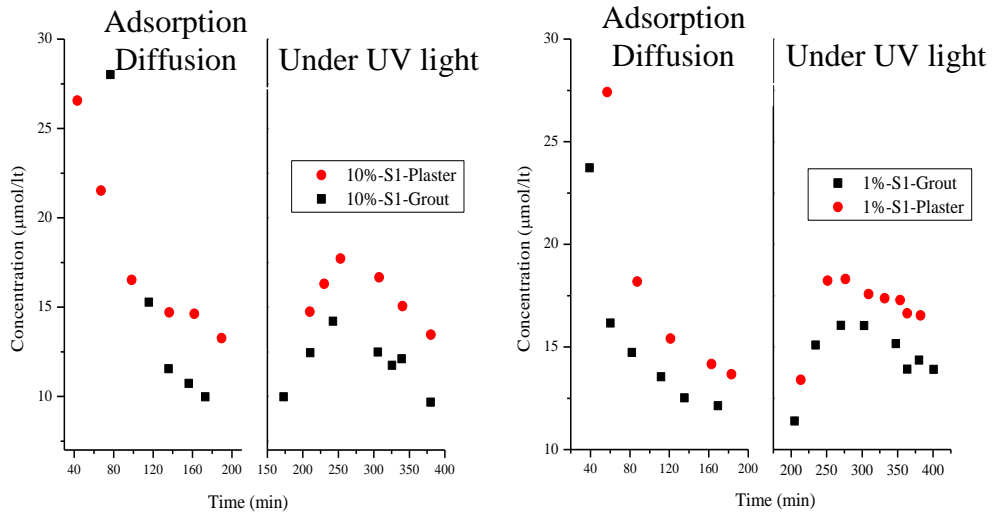


Figure 4.13 Comparison of the grout and plaster samples (S1) for the same TiO₂% under UV light.

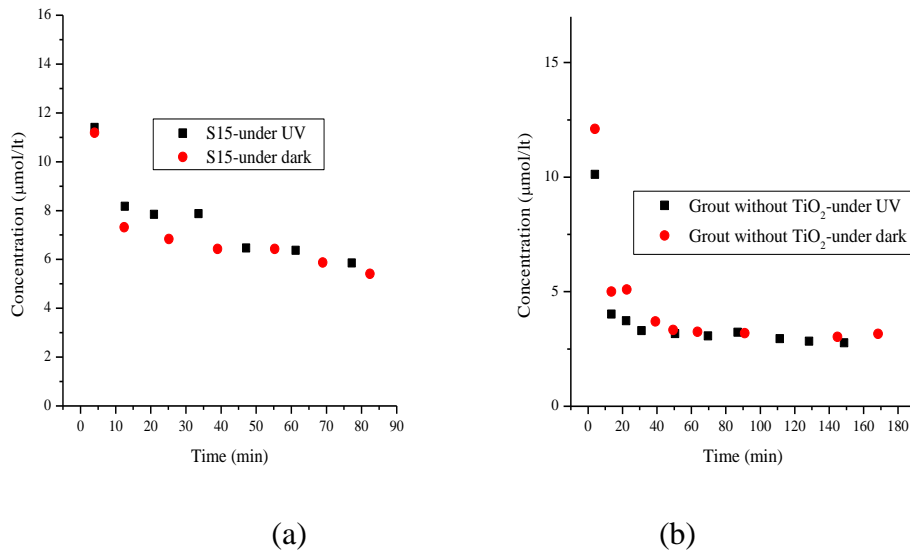


Figure 4.14 (a) Pure rutile (S15) coating, (b) Pure grout sample.

From these kinetic screening tests, for the sake of decreasing sample amount, it was decided to proceed with grout samples and UV light irradiated experiments were done for photocatalytic benzene oxidation. The rutile sample was not used in further studies.

4.2.2 Photocatalytic Benzene Oxidation Studies

It is common to approximate the photocatalytic oxidation rates over illuminated TiO₂ by the Langmuir-Hinshelwood kinetics model.

$$r = \frac{dC}{dt} = k \frac{KC}{1+KC}$$

where r is the oxidation rate of the reactant, C the concentration of the reactant, t the illumination time, k the reaction rate constant, and K is the adsorption equilibrium constant of the reactant.

When the chemical concentration C is small, the equation can be simplified to an apparent first-order solution in a batch type reactor. Generally first-order kinetics are appropriate for the entire concentration range up to few ppm and several studies were reasonably well fitted by this kinetic model [45,299,300]. Reaction rate constants k can be calculated from the slope of trend lines of $\ln(C_{a0}/C_a)$ vs. time graphs, where C_a is the concentration of benzene at given time and C_{a0} is the initial benzene concentration (Equation 4.38-4.40).

$$\frac{d}{dt}(C_a) = -k \times C_a \quad (4.38)$$

$$\int_{C_{a0}}^{C_a} \frac{dC_a}{C_a} = - \int_0^t k \times dt \quad (4.39)$$

$$\text{Ln} \left(\frac{C_{a0}}{C_a} \right) = k \times t \quad (4.40)$$

The results are shown for 10% TiO₂ added samples in Figure 4.15. The trend line was drawn by linear regression. There is a significant difference in trend lines of UV irradiated and dark experiments. (The results for UV experiments and dark experiments are given in Table 4.5 and Table G.1, respectively.)

In the calculations, approximately first 20 minutes of the reaction is omitted since this part of the reaction includes initial adsorption period and UV degradation period together. This type of calculation can be used as a preliminary evaluation. Reaching steady state at the beginning of the experiment is necessary to get rid of initial adsorption effects. Flow type reactors such as recirculating flow reactor or packed bed reactor can be used as alternatives in the experimental set up. Recirculating flow reactor circulates the flow by feeding and discharging low amount of make up and effluent gas. Packed bed reactor can also be used under low flow rates and so high residence times. During operation, following an initial equilibration period, all mass flows inside the system such as reactant adsorption and desorption on sample and on reactor surfaces, catalytic reactant oxidation, reactant vented out to reactor reach a steady state equilibrium. The data measured after equilibrium ensures that the resulting activity is obtained under defined, uniform and time-constant conditions. In a typical flow system, dry air is used as carrier gas. The flow rate of the system and concentration of benzene and water are adjusted using mass flow controllers. A dead volume is left for mixing of gases before sample cell. The outlet of reactor cell can be directly fed to the Gas Chromatography or a syringe can be used by taking sample from sample port

after reactor cell and inject to the Gas Chromatography indirectly. A schematic diagram is given in Figure 4.16.

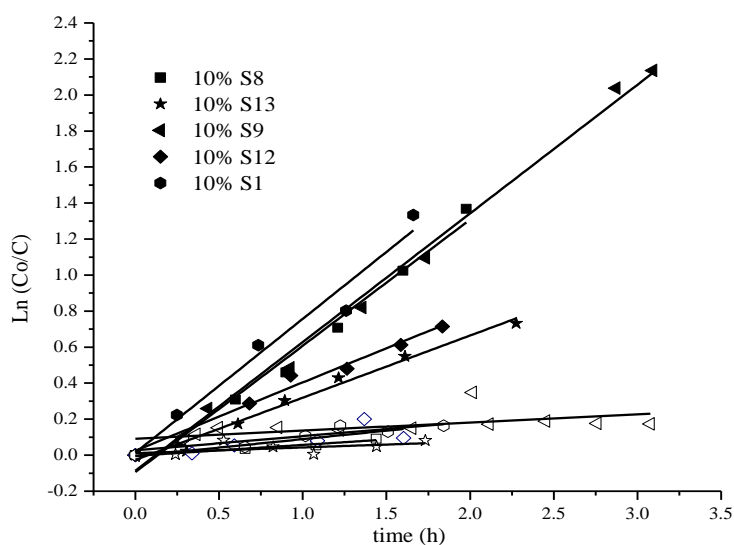


Figure 4.15 Illustrative diagram that shows trend lines for UV irradiated and dark experiments of 10% TiO_2 added grout samples. Full symbol represents UV experiments, whereas empty symbol represents experiments conducted in dark conditions.

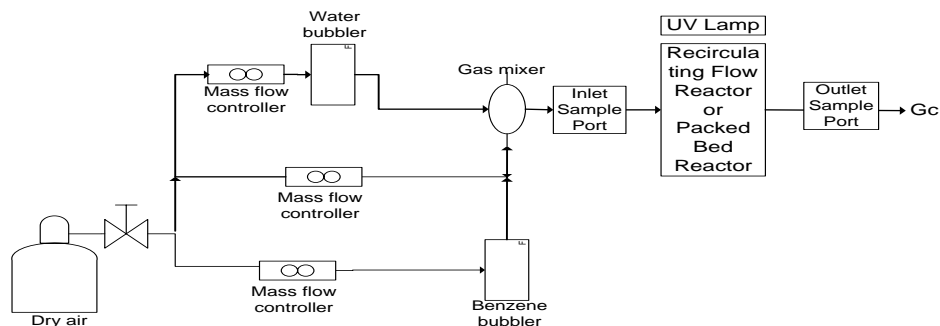


Figure 4.16. Typical flow system diagram for photocatalytic benzene oxidation reaction.

UV data can be subtracted from a reference data for correction of this stage. However, the initial concentration is not exactly same (around 200-300 ppm) for all experiments due to unavoidable injection errors. In addition, the empty reactor test is not taken as reference for correction due to additional adsorption on the sample and the dark experiments were not carried out for all experiments.

In this experimental procedure, prior to the reaction measurements, the system was vacuumed for 30 minutes. The benzene was injected with a syringe (0.2 μ l) through injection port to the manifold (85°C) and allowed to evaporate. Before allowing benzene to the reaction cell, UV irradiation was applied for 1 hour to the reaction cell. Some of the experiments were done twice for each sample by exposing the sample to UV light and not by covering with aluminum foil (UV and dark experiment).

4.2.2.1 Pure TiO₂ Coatings

TiO₂ coatings were successfully deposited on glass lamels in expected amounts (Table 4.2).

Table 4.2 Pure TiO₂ coating study on glass lamels.

TiO ₂ Code	Total Weight	Coated Amount (g)	Expected Coating Amount (g)	error %
S1	0.4733	0.0037	0.0038	2.7
S8	0.5597	0.0036	0.0038	5.6
S9	0.5084	0.0038	0.0038	0
S12	0.4353	0.0036	0.0038	5.6
S13	0.4921	0.0038	0.0038	0

The commercial TiO₂ samples were coated on 2 cm² glass slides with similar amounts. The results were shown in the Table 4.3.

Another important parameter in coatings is the dispersion on the surface. There are dispersion problems for some commercial samples, which is apparent when thinner coatings have to be made. TiO₂ which has good dispersive abilities on glass surface is Degussa P25. The coating amount can be reduced easily and specific activity increases 7 fold (Table 4.4). The highest activity will be for the thinnest coating. Degussa P25 also shows transparency, which means the particle agglomeration, is not that much due to interactions or repulsive forces between particles on glass. The coating thickness will not be minimized since it is inapplicable to paint type of coatings.

Table 4.3 Pure TiO₂ coating activity results on 2 cm² glass slides.

Sample Code	Coating Amount (g)	k (1/h) (UV)	k (1/h*g _{cat}) (UV)
S1	0.0037	0.300	81
S8	0.0036	0.576	160
S9	0.0038	0.668	176
S12	0.0036	0.469	130
S13	0.0038	0.574	151

Table 4.4 Comparison of activity change with coating amount for the same coated area (2 cm²) for S13 sample.

Sample Code	Coating Amount (g)	k (1/h) (UV)	k(1/h×g _{cat}) (UV)
S13 (Degussa P25)	0.0003	0.351	1170
	0.0038	0.574	151

4.2.2.2 Comparison of the Results on Glass and on Grout

The UV oxidation results were similar for different TiO₂ coatings. And it was seen that the activity was better when TiO₂ was coated on the surface. The reason should lie that UV activated TiO₂ increased when TiO₂ is on the surface. To show this, TiO₂ has been coated to different coated surfaces as 2-5-10 cm². The increase in the rate constant showed that, more TiO₂ on the surface is active as the coated surface become large. This also meant that, TiO₂ coating was much more effectively utilized. Same experiment procedure was applied on grout samples but the rate constant seemed independent from coated surface area.

Preliminary kinetic studies made on TiO₂ added cement based materials showed that the activity is not correlated with the amount of TiO₂. Below the possible reasons are discussed:

4.2.2.2.1 The Particles in the Bulk are not Accessible

A set of experiments was done with S13 or Degussa P25, same amount of sample was coated to different coated areas 2-5-10 cm², and it was observed that specific activity increased for the same amount of catalyst, which means increased amount of TiO₂ under UV activation or in a different way, the particles in the bulk are not accessible (Figure 4.17).

4.2.2.2.2 The Contents of Grout Interact with TiO₂

Same systematic experiment series have been applied to grout samples coated with TiO₂. It was seen that, increasing the UV exposed area did not increase the activity as expected from pure Degussa P25 experiments on glass. The grout surface is more alkaline compared to glass. This may affect the

dispersion of Degussa P25 (during drying) on the surface of the grout which leads to loss of activity due to agglomeration (Figure 4.18). The shadowing of the particles in cement media can be important.

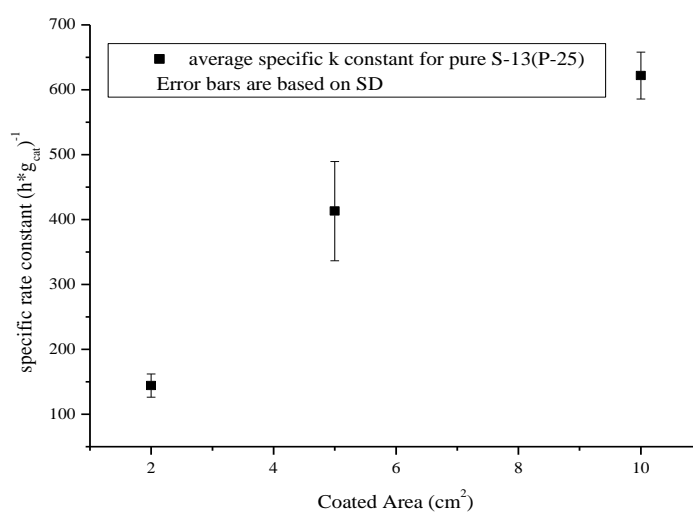


Figure 4.17 Specific rate constant vs. UV illuminated area for Degussa P25 on glass (The experiments were repeated 3 times and the results are given in Appendix F-Table F.1).

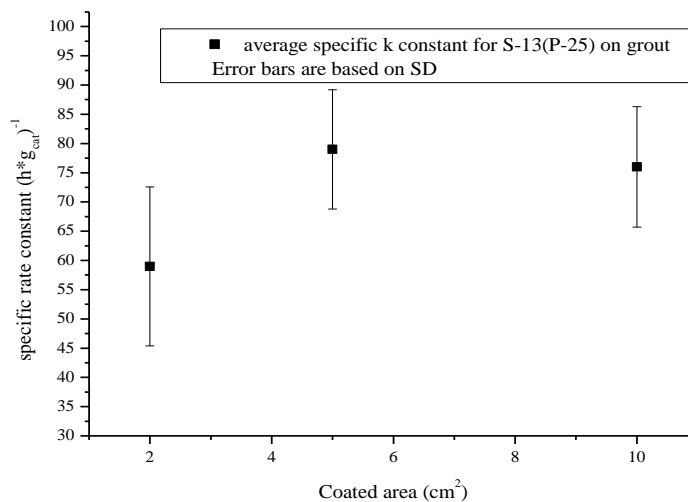


Figure 4.18 Specific rate constant vs. UV illuminated area for Degussa P25 on grout (The experiments were repeated 3 times and the results are given in Appendix F -Table F.2).

4.2.2.3 Cured Cement Based Materials Studies

4.2.2.3.1 Bulk Addition Studies

Due to particle interaction between TiO₂ and grout, an experiment set was designed in order to select TiO₂ with highest activity (Table 4.5). The activity test results were shown for bulk addition of TiO₂ for 10% and 1%. S9 sample showed highest activity. Due to the similar results with grout sample without TiO₂ and comparable errors resulting from measurements, the activities of the 1% TiO₂ addition were not commented. However there is an increase with increasing TiO₂ content.

Table 4.5 Bulk addition of TiO₂ samples in grout under UV source

Sample Code	Rate constant (1/h) (UV)	Rate Constant (1/h×g _{cat})
10% S1	0.556 (±0.093)	0.589 (±0.099)
10% S8	0.470 (±0.205)	0.498 (±0.217)
10% S9	0.756 (±0.109)	0.801 (±0.116)
10% S12	0.509 (±0.146)	0.540 (±0.155)
10% S13 (P25)	0.414 (±0.092)	0.439 (±0.098)
1% S1	0.161	1.706
1% S8	0.126	1.335
1% S9	0.086	0.911
1% S12	0.150	1.589
1% S13	0.115	1.218
Grout Sample without TiO ₂	0.087	--

* The 10% TiO₂ addition experiments were repeated three times and results were given in Appendix F -Table F.3.

** 9.44 g grout is used in the experiments including TiO₂ mentioned as %.

Aissa *et al.* [301] characterized titania (PC105-85 m²-average 20 nm particle size) added mortars by using Raman mapping of the surface, Diffuse Reflectance-UV-Vis technique. They define occurrence rate or presence probability and showed that this value reaches 100% even at 5% TiO₂ additions. They used a flow reactor and in-line photoacoustic analytic spectrometer to analyze the removal of formaldehyde. They inspected the behavior in the dark and under UV light. In Table 4.6, the rate ratios were compared with the ratio of our 10% and 1% TiO₂ added grout results. The results are comparable to each other for most of the TiO₂ samples.

Table 4.6 Comparison of bulk added TiO₂ samples in grout results with Aiessa *et al.* study.

	10% / 1% rate ratio
Aiessa <i>et al.</i>	2.50
S1	3.18
S8	3.56
S9	7.80
S12	1.70
S13	1.86

4.2.2.3.2 Coating Studies on Grout

S13 (Degussa P25) samples has been applied on the surface and the results were shown in Table 4.7. The increase in activity is obvious when TiO₂ is applied on the surface due to increased number of active sites on the surface, which also means there is inactive sites buried in the bulk of the material.

Table 4.7 Activity comparison of TiO₂ in the bulk and on the surface.

Pure S13	k (1/h) (UV)	k(1/h×g _{cat}) (UV)
In the bulk ~20 cm ² 0.944 g	0.33	0.34
In the bulk ~20 cm ² 0.0944 g	0.12	1.22
On the surface ~20 cm ² 0.01 g	0.53	53

Table 4.8 Activity results of coating studies on grout under UV light.

Sample Code (0.01 g coating)	Rate constant (1/h) (UV)	Rate constant (1/h×g _{cat}) (UV)
S1	1.016 (±0.257)	101.6 (±25.7)
S8	0.566 (±0.160)	56.6 (±16.0)
S9	1.280 (±0.231)	128 (±23.1)
S12	0.806 (±0.191)	80.6 (±19.1)
S13	0.526 (±0.220)	52.6 (±22.0)

*The experiments were repeated three times and the results are given in Appendix F -Table F.4.

** 9.44 g grout is used in the experiments.

A coating study was done on the grout surface and the results are shown in Table 4.8. The highest results are observed for S9 sample, followed by S1 and S12. The activities are higher than bulk addition of the samples. The order of TiO₂ samples according to activity is same with the bulk addition experiments.

In the light of these experiments, it was concluded that S9 sample shows the highest activity in the grout media.

4.2.2.3.3 Experiments done with Plaster Samples

By using S9 sample, the bulk addition and surface coating experiments were done for plaster samples. The results are similar as shown in Table 4.9

Table 4.9 Comparison of activity results done with plaster and grout.

Sample Code	Rate constant (1/h) (UV)	Rate constant (1/h×g _{cat}) (UV)
S09 on grout - 0.01 g	1.28	128
S09 on plaster -0.01 g	1.17	117
S09 in plaster additive 10%	0.65	0.69
S09 in grout additive 10%	0.76	0.80

* 9.44 g grout and plaster is used in the experiments including TiO₂ mentioned as %.

4.2.2.4 Visible Light Studies

4.2.2.4.1 Kinetic Screening Tests on Photocatalytic Benzene Oxidation

Due to absorption of TiO₂ starting from UVA to deeper UV region, visible light studies are needed for modification of TiO₂ for the indoor usage or utilization of sunlight more effectively. Similar results were obtained in kinetic screening tests. By changing light source, the decrease in the activity was observed both for plaster and grout samples with 1-10% TiO₂ addition (Figure 4.19-4.20).

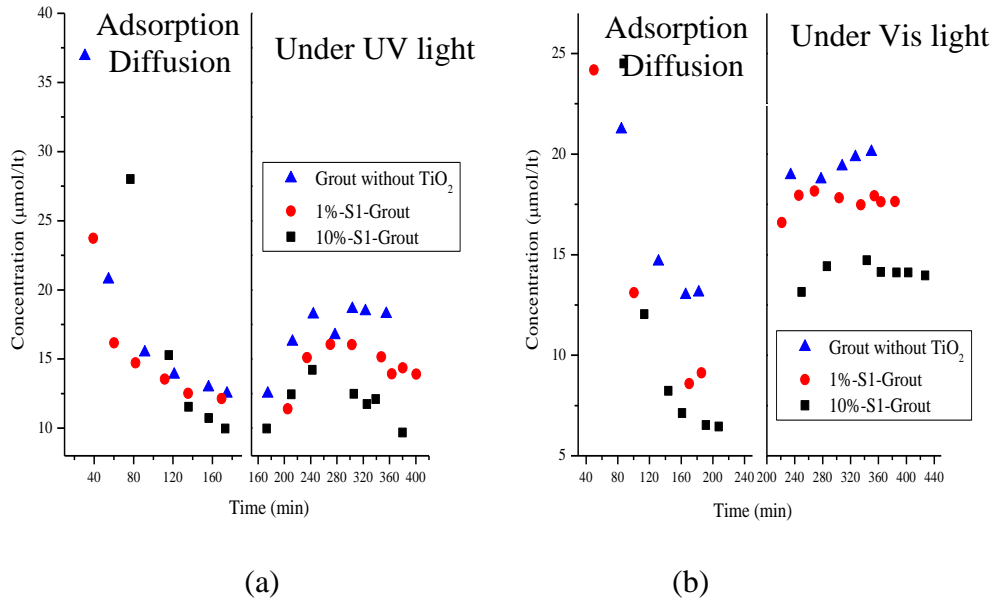


Figure 4.19 Photo-oxidative benzene degradation for grout samples under a) UV light b) Visible light

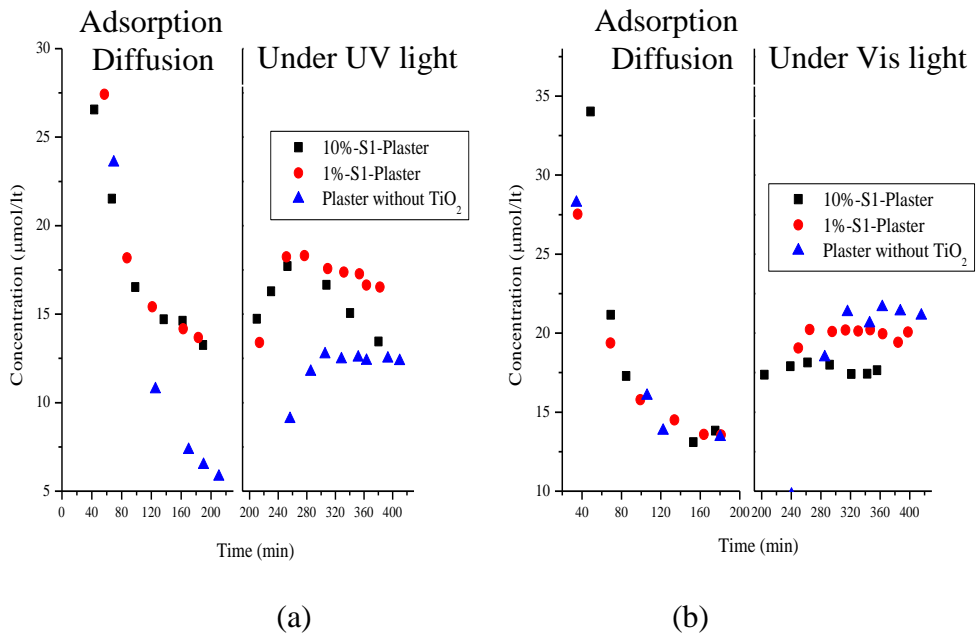


Figure 4.20 Photo-oxidative benzene degradation for plaster samples under a) UV light b) Visible light.

4.2.2.4.2 Fe Addition by Wet-Impregnation Method

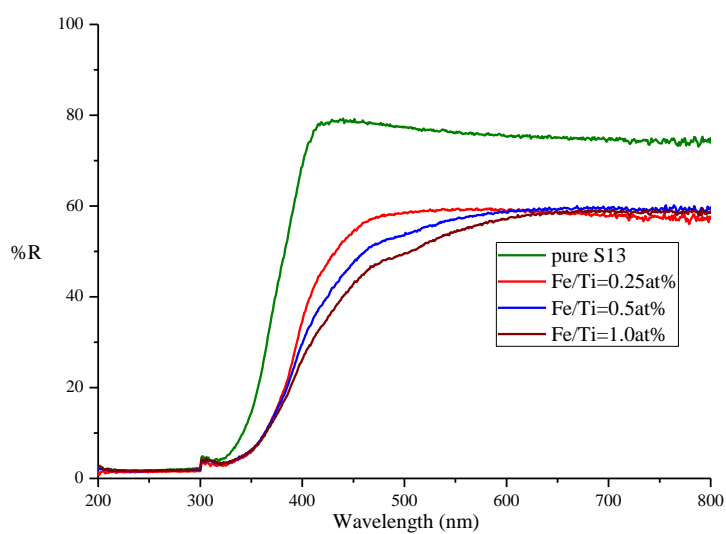


Figure 4.21 UV-Vis spectrum comparison of Degussa P25 coatings with different Fe loadings.

Table 4.10 Visible light activity results of Degussa P25 coatings with different Fe loadings.

Sample Code	k (1/h)	k (1/h \times g _{cat})
S13 (P25)	0.24	24
0.5 at% Fe/Ti	0.24	24
1.0 at% Fe/Ti	0.27	27

Fe is a convenient element for visible light studies due to economical reasons. Fe is loaded to TiO₂ by incipient wetness impregnation method. The increase in visible light absorption is observed with increasing Fe loading (Figure 4.21). Red shifts of this type can be attributed to the charge transfer transitions between metal ion d electrons and TiO₂ conduction or valence band [128]. The activity changes due to Fe loading are shown in Table 4.10. Fe loading by incipient wetness impregnation did not increase visible light activity.

4.2.2.5 Changes in Initial Adsorption with Sample and Water Amount

In the beginning of the experiment, the initial adsorption of benzene covers the surface of TiO₂. Initial adsorption amount changed with increasing sample amount and with water content (Figure 4.22). To observe the changes, sample amount was increased and the sample was dried in the oven and let it come to equilibrium in room conditions. The result shows us that the water and benzene adsorb on the same sites which cause competition for the sites. A similar observation was also done by Jacoby *et al.* [67].

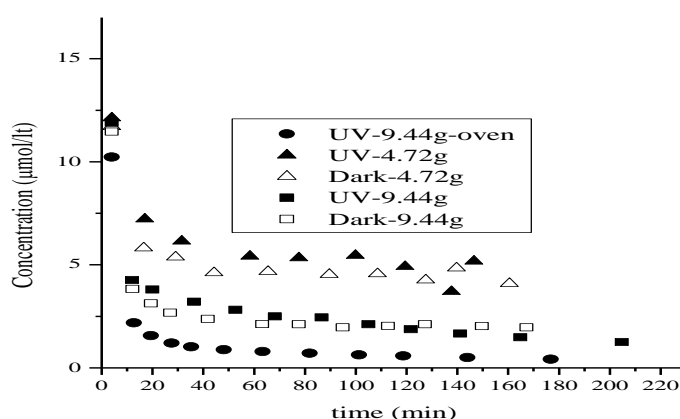


Figure 4.22 Effect of grout amount increase and water content change on 10 % S13 sample activity under dark and UV conditions.

4.2.2.6 Experiments done in the Dark Conditions

The aim of doing dark experiments is to eliminate other effects that will decrease benzene in the reactor such as diffusion of benzene to the sample. By differentiating these effects, benzene decrease due to photocatalytic UV degradation is determined.

The grout sample without TiO_2 and dark experiments done for 10% TiO_2 added grout samples were compared with each other (Figure 4.23). The results followed a similar trend line. Due to this similarity the catalytic effect of TiO_2 in the grout samples was neglected for dark experiments. The effect was attributed to the whole sample. The dark experiments for 1% TiO_2 added grout samples were excluded since similar results would be expected. Dark activities for 10% TiO_2 addition are used for calculating 1% TiO_2 addition and TiO_2 coatings on grout experiments.

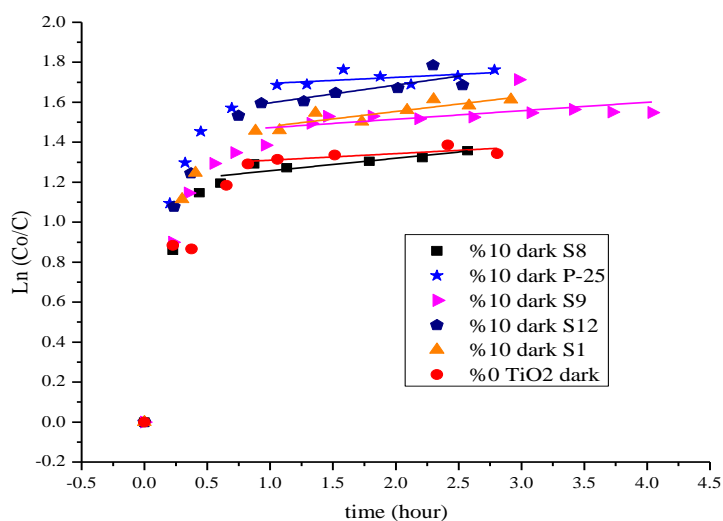


Figure 4.23 Comparison between dark experiments using 10% TiO_2 added samples and grout sample without TiO_2 . The results are given in table form in Appendix G-Table G.1.

The pure TiO_2 samples were also subjected to dark experiments. The dark experiments of pure samples followed much similar trend lines. The pure TiO_2 samples showed higher dark activity compared with TiO_2 added grout samples (Figure 4.24).

Dark experiments followed a similar trendline for similar experimental sets as shown in Figure 4.23 and Figure 4.24. The dark activities were averaged for similar experiments and subtracted from UV illuminated results. By this way, benzene elimination due to diffusion was eliminated and it was assured that the remaining activity was due to benzene degradation.

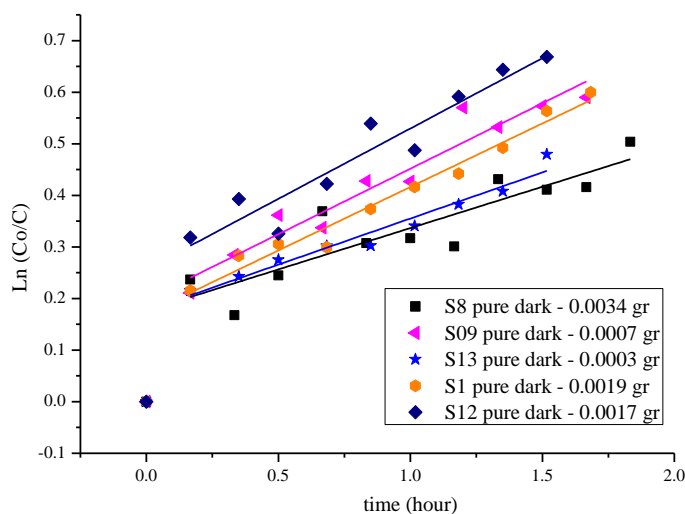


Figure 4.24 Dark experiment results for pure TiO_2 samples. The results are given in table form in Appendix G-Table G.2.

4.2.2.6.1 Mass Transfer Limitations due to Thickness of the Coating and TiO₂ Concentration

There is a change in the dark absorption amounts with increasing thickness of TiO₂. This means there is an internal mass transfer limitation for TiO₂ coatings (Table 4.11). It is also possible to see that the effect becomes less important with decreasing thickness of the sample.

Table 4.11 Dark activity results for S13 with different thickness.

Pure S13 (0.004 g)	k (1/h)	k (1/h×g _{cat})	k (1/h×cm ²)
~2 cm ²	0.193	50.8	0.097
~10 cm ²	0.267	66.8	0.027
~20 cm ²	0.5	131.6	0.025

Table 4.12 Dark activity changes due to particle size and surface areas

2 cm ² coating	Coating Amount (g)	k (1/h) (dark)	Particle Size (nm)	Surface Area (m ² /g)
S1	0.0037	0.163	150	11*
S8	0.0036	0.164	-	11*
S9	0.0038	0.257	20	100
S12	0.0036	0.229	6	300
S13	0.0038	0.193	21	50

* The data is measured using BET. Other data given is taken from the companies.

Same amount of TiO_2 samples used in this study are coated on glass and dark activity is observed in Table 4.12. As seen, there is a slight increase in the adsorption activity with decreasing particle size. Pore volume increases with decreasing particle size. Therefore, diffusion of the benzene increases.

4.2.2.7 CO_2 Measurement for Verification of Benzene Degradation

Three experiments were done using S13 coated glass slides. In Figure 4.25, the sampling time from the reactor was different for benzene and CO_2 analysis. The ratio of CO_2 to benzene was not shown. In Figure 4.26, two other experiments with similar sampling times were shown. The benzene conversion and formation of CO_2 followed a similar increasing trend. The $\text{CO}_2/6$ to benzene ratio increased near 1 at the end of the experiment. The initial CO_2 concentrations were assumed zero. So the conversion to CO_2 was achieved in benzene degradation experiments, which means the surface is self cleaning itself.

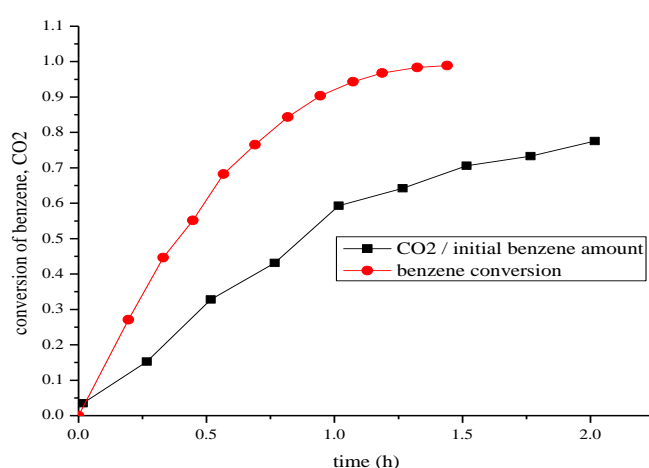


Figure 4.25 Benzene degradation justification by measuring CO_2 with TCD detector 1st experiment.

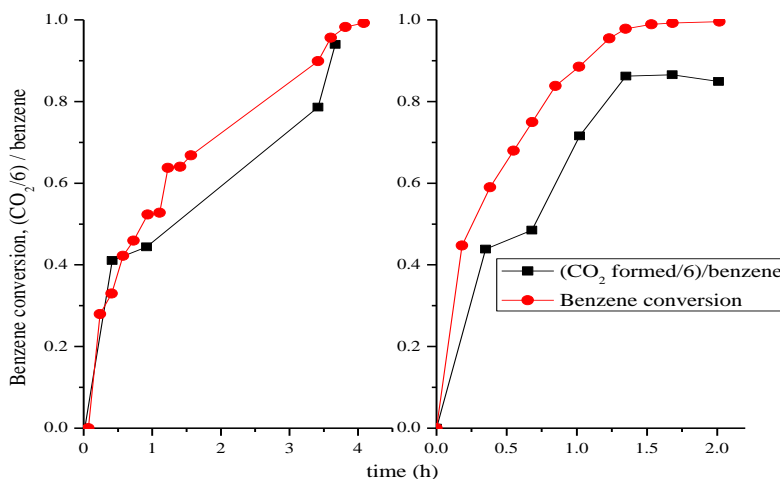


Figure 4.26 Benzene degradation justification by measuring CO_2 with TCD detector. 2nd and 3rd experiment.

4.2.2.8 Stable Coating Project on Surface: Coating Formulation Studies

Paints for exterior surfaces are exposed to sunlight in wet, dry, hot and cold conditions. The combination of UV radiation, variable temperature and humidity rapidly degrades organic polymers, roughening the coating surface and exposing the pigments. To the coating user, this is observed as loss of gloss and chalking (loose pigment on the paint surface) [126]. To reduce the chalking of the TiO_2 pigment, pigment has to be bound to the surface by using a binder matrix or resin.

4.2.2.8.1 Addition to a Paint Formulation

S13 has been used as additive to the solvent based formulation in 1% and 5% ratios. Around 0.02 g paint was used to coat one side of the glass slide (5 cm^2). By adding S13 to paint, chalking was prevented. The results were given in Table 4.13. The activity was almost none when compared with pure results. (The dark experiments were not performed and subtracted from UV irradiated results for this case. However, $k_{\text{average}} = 0.5$ for 20 cm^2 pure TiO_2 on glass). The decrease of activity is due to cloaking of S13 by the pigment in paint, which is rutile TiO_2 powder. S13 sample should be integrated in a resin, which has no pigment inside. A simple finger testing was applied to the coating (Figure 4.27).

Table 4.13 Activity comparison of pure S13 and S13 in the paint.

S13 on glass slide (UV)	$\sim 2 \text{ cm}^2$		$\sim 5 \text{ cm}^2$ (5% additive)		10 cm^2		$\sim 20 \text{ cm}^2$ (1% additive)	
	k (1/h)	k (1/h \times g_{cat})	k (1/h)	k (1/h \times g_{cat})	K (1/h)	k (1/h \times g_{cat})	k (1/h)	k (1/h \times g_{cat})
$\sim 0.001 \text{ g}$ in paint	-	-	0.20	200	-	-	0.20	204
0.004 g pure powder activity	0.57	144	1.65	413	2.49	622	5.45	1435



(a)

(b)

Figure 4.27 Finger testing of a) addition to commercial paint, b) S8 after deposition with water solution.

4.2.2.8.2 Application using Commercial Grout Marker Manifold

A commercial grout marker was inspected. The parts were disassembled and the ink inside was removed. TiO_2 solution was put inside and the equipment worked for TiO_2 solution as well (S8).

S8 solution has been deposited to the glass slides and the solution concentration checked. The concentration was equal or higher than the prepared solution. No blockage occurred on the tip of the marker.

4.2.2.8.3 Using White Cement as Inorganic Binder

S9 and white cement were used together to bind TiO_2 powder in a more rigid way. White cement is applied to surface first and curing reactions were started by adding water. S9 was loaded to the surface before drying or finishing of the curing. By this way, retaining of maximum amount of TiO_2 on the surface is aimed with binding to the surface at the same time. The results are given in Table 4.14. The results are similar to each other. A simple finger testing was applied to the coating (Figure 4.28). This study was done to show

binding ability of inorganic media. The more practical approach is to apply S9 during curing of grout and plaster surfaces. Before commercial application, feasibility and mechanical studies have to be applied.



Figure 4.28 Finger testing of a) S9 sample a) without and b) with white cement binder.

Table 4.14 Surface binding studies on grout media.

Sample code (0.01 g S09)	k (1/h) (UV)	k (1/h×g _{cat}) (UV)
S09	1.29	129
S09 with white cement	1.13	113

4.2.2.9 Precipitation Study

During surface coating studies, it was observed that some of the solutions become precipitated very fast after magnetic stirrer is stopped. An

experiment is done to show this behavior. As seen in Table 4.15, S12 sample precipitate compared to the S8 sample.

Table 4.15 Observation on precipitation speeds of TiO₂ powders

Time min	S8		S12	
	Coating amount (g)	Expected Coating Amount (g)	Coating amount (g)	Expected Coating Amount (g)
0	0.0022	0.0020	0.0021	0.0020
10	0.0022	0.0020	0.0006	0.0020
20	0.0021	0.0020	0.0003	0.0020
30	0.0021	0.0020	0.0003	0.0020
60	0.0020	0.0020	0.0002	0.0020

4.2.2.10 Precision of the Experiments

Table 4.16 represents the standard deviations and R² test results for selected results. The R² test score ranges between 0 and 1. Test indicates the consistency between data points and the line drawn by applying linear regression. Test gives high score (near to 1), if the data is well-matched with the trend line. The consistency decreases in the dark experiment results and some of the 1% TiO₂ added grout UV results. The standard error remains similar for all the experiments. Thus, the inconsistency increases as the slope or trend line decreases to small values or low activity. The averaged standard error was found as 0.026 for all experiments. The averaged error results from experimental errors due to changes in the ambient air (humidity, temperature), and injection errors.

Table 4.16 Standard deviations and R^2 test results for selected bulk addition experiments

Sample Code	Standard error – R^2 test	k (1/h) (dark)	Standard error – R^2 test
10% S1	0.075 - 0.96	0.075	<u>0.021 - 0.69</u>
10% S8	0.039 - 0.98	0.058	0.008 - 0.95
10% S9	0.027 - 0.99	0.043	<u>0.021 - 0.26</u>
10% S12	0.025 - 0.98	0.089	<u>0.034 - 0.57</u>
10% S13	0.020 - 0.98	0.030	<u>0.021 - 0.17</u>
1% S8	0.018 - 0.96	0.065	<u>0.026 - 0.28</u>
1% S09	<u>0.034 - 0.44</u>	--	
1% S13	0.018 - 0.91	--	
1% S01	0.022 - 0.94	--	
1% S12	<u>0.033 - 0.85</u>	--	
Grout with no TiO ₂ additive	<u>0.023 - 0.72</u>	0.033	<u>0.014 - 0.52</u>

*The R^2 test results lower than 0.9 are shown as underlined.

4.3 SUMMARY OF THIS CHAPTER

XRD, BET, TGA, UV-Vis, SEM techniques were used to characterize commercial TiO₂ samples. A careful elimination was applied for the reduction of TiO₂ sample size and parameters used in the photocatalytic benzene oxidation experiments with the help of preliminary and characterization studies. Pure TiO₂ coatings were prepared and experiments were done under UV and dark conditions. The experimental set which shows inaccessible particles in the bulk was done by using pure samples. Same set of experiments were done by using cured grout samples as support and grout-TiO₂ interaction was shown. Another experimental set was done by using 10% and 1% TiO₂ inside the bulk grout and S9 was determined as the TiO₂ which shows the highest activity. Since there have been inaccessible sites by UV light when TiO₂ is embedded in the grout, for achieving best utilization of TiO₂, grout

surfaces were coated with TiO₂ and the activities were determined. An increase in the activity was observed and compared with the bulk added TiO₂. TiO₂ order of activity remained the same. In kinetic screening tests, it was decided to design experiments with grout sample due to similar structure of materials. Verification experiments were done by using S9 sample both in the plaster and on the plaster. Similar activities were observed. In addition to these experiments, for effective utilization of visible light, Fe was added by incipient wetness impregnation method to Degussa P25. Visible light absorbance increased; however, the activity did not increase under visible light. Initial adsorption amount changed with sample size and also water content, which shows both water and benzene adsorb on same sites. The experiments done under dark conditions showed that, dark activity was analogous for experiments done in similar samples. Mass transfer limitations were observed and changed due to thickness of the coating and TiO₂ concentration. CO₂ verification experiments were done to show that benzene decrease also indicates the mineralization of CO₂. Direct addition to a paint formulation was attempted. To deposit TiO₂ on the surface, commercial grout marker was exerted. To bind TiO₂ to the surface, white cement was used. A binder-TiO₂ formulation, which shows superhydrophilic properties and activity was applied on glass successfully. Raman characterization experiment was done for Ti-O-Si bonds at the interface of the glass and the coating. R² tests applied to linear regression lines, which is used for calculating rate constant of the reactions showed that, the inconsistencies are increasing when the activity is low (for 1% TiO₂) or in the dark experiments.

By using CO₂ and NO as probe molecules, 15 commercial TiO₂ surfaces were characterized. Adsorbed states and amounts were changed according to TiO₂ morphology or surface modifications. A similarity in adsorption behavior was observed for low and high surface area TiO₂ samples from interpretation of NO studies. The surface treatments of some commercial samples are justified such as S1 due to peaks on the region 2800-3000 cm⁻¹.

Coated samples, pure TiO₂, and grout samples with or without TiO₂ were compared for CO₂ adsorption on S8. For TiO₂ top coatings, extra bicarbonate peaks (1550, 1430 cm⁻¹) were observed probably due to preparation of the sample from water solution, which leads to hydroxylation of the surface and water adsorption. This shows that increased hydroxylation and adsorbed water is involved positively in the mechanism of bicarbonate formation.

CHAPTER 5

DISCUSSION

5.1 COMMENTS ON SELECTION OF TiO₂ POWDER and ACTIVITY MAXIMIZATION

Photocatalytic activity was brought into plaster and grout samples successfully. Since different activities were observed for TiO₂ samples in cement, a selection was done as S9 sample, which was best suited TiO₂ to use in cement based materials. The selection was based on the activity measurements.

The surface area increased the activity. However, S9 is not the highest surface area sample. The lowest surface area samples showed low activity. However, S12, which has the highest surface area showed lower activity than S9 sample.

Particle size also decreases with increasing surface area. However, particle size does not give enough information. Because the particles agglomerate with each other and form larger particulates. Larger particulates have bigger particle diameter than particle size. Larger agglomerates mean lower projected UV area.

Chemical modifications were observed on commercial TiO₂ samples. Larger and lower surface area samples showed similar peak formations. However, there are other peaks characteristic to the samples. For example, high negative intensity observed after NO adsorption for S1 and S15 in the region of 2800-3000 cm⁻¹ region shows the signs of organic compounds on the surface.

High surface area TiO₂ samples adsorbed high amount of benzene and water on the surface. However no direct relation was established between activity and adsorption amount of these species. Benzene and water adsorb on the same sites. It was also seen that CO₂ and water adsorb on the same sites, which lead to bicarbonate formations [302,303]. The number of active sites have not been determined in our study.

TiO₂ particles are found together with grout and plaster contents such as silica-calcium-water matrix and calcium hydroxide. These particles may have shadowing effect on TiO₂ particles on the surface.

Anatase and rutile content of the samples are also another matter of concern. In this study, samples with pure anatase and rutile content and their mixtures were used. Pure rutile content showed very low photocatalytic activity under UV irradiation. The activity is not highest for Degussa P25, which has both anatase and rutile content. The effect of crystal phase is not clear in this study.

Dispersion of the TiO₂ particles is different on glass surface, which can be observed easily. S13 samples show highest dispersion on glass. However, the activity is lower than S9, when used on the grout. High pH changes on grout samples may effect further agglomeration of the S13 particles.

In CO₂ adsorption studies, additional bicarbonate peaks (1550, 1430 cm⁻¹) are seen on top S8 coating. This seems to be a synergic effect on adsorption, however, bicarbonate species can be more stable on TiO₂ surface in increased hydroxylation case (due to coating deposition with water). This may lead to poisoning kind of behavior, which blocks the TiO₂ sites. After decomposition of benzene, formed CO₂ species can not be released, which explains the decreased rate on grout case compared to glass and independent behavior of specific rate wt. coated surface area.

Particle size, agglomerate size, surface area and dispersion of the particles on the surface effects the number of particles on the surface, which have UV accessibility. Therefore the main aim should be to maximize UV

accessible TiO₂ content at the surface as much as possible. Coating TiO₂ on the surface using an inorganic binder, deposition of TiO₂ on the surface by a spraying equipment separately during curing of grout and plaster or using TiO₂ in the formulation with appropriate surfactant to maximize TiO₂ content on the surface are different solution approaches to the problem.

Since this thesis was executed as part of a SAN TEZ project, there is a parallel project at KALEKIM ongoing with the thesis. A selection and order has been made from commercial TiO₂ powders and the increase in activity, when TiO₂ is used on the surface was shown. Different approaches have been recommended for application and maximization of TiO₂ on the surface. The company may optimize and select a final method and formulation considering economical aspect of the solutions. Besides that an alternative paint based approach was recommended for usage in ceramic surfaces, which is given in APPENDIX I.

5.2 COMMENTS ON OTHER PARTS OF THESIS

5.2.1 Visible Light Studies

The synthesis used in visible light studies was adapted from another procedure [137]. In this article the highest activity was achieved at 0.5at% of Fe doping. However in the procedure the pH was adjusted to 5. This adjustment was not applied since high pH values leads to Fe₂O₃ formation which shows no photocatalytic activity [136]. However, in these two articles the Fe sources were different (FeCl₂ and Fe(NO₃)₃) and the reactions may change in the solution. The activity increase was twofold [137] for 0.5 % Fe doping compared to Pure Degussa P25 nanotubes. The activity becomes similar with 0.1 % and 1% Fe doping. So inefficient doping may lead to decrease in Fe³⁺ concentration at the surface, which will decrease the activity. Besides that, the optimum activity was determined for TiO₂ nanotubes in this

article, whereas in our study, pure Degussa P25 was impregnated. However, there are other studies, where 0.5 at% Fe doping shows optimum charge trapping effect on the surface [136,128]. Optimum charge trapping is obtained for specific particle size. Choi et al obtained this optimum percent for 2.2 nm particle size. For bigger particles, optimum Fe % should increase. Using different TiO₂ powders with different particle sizes should change the optimum Fe concentration. Chemical modifications done on the surface of TiO₂ or trace elements left from TiO₂ production should also be considered.

5.2.2 Synergic Effect of TiO₂ and Cement Medium for the NO_x Removal

A particularly interesting subject of TiO₂/cement composites is that there is a clear synergy between the cement and TiO₂ that makes cement an ideal substrate for environmental catalysis. Many photo-oxidizing compounds, such as NO₂ and SO₂, are acidic. The basic nature of cement matrix is particularly suitable for fixing both the polluting reagent and photo-oxidation products at its surface. High surface area is important which increases the photo-activity of TiO₂/cement system [16]. When NO₂ is formed, part of the gas may escape from the photocatalytic surface, but in the presence of cement matrix, the gas may be effectively trapped, and nitrate salt formed [304].

Cement structure is very basic, since Ca(OH)₂ keeps the solution alkaline (pH 12.4-13.5). NO is a basic molecule, which is not stable on cement structure and can disproportionate on to NO₂⁻ or N₂O. However, TiO₂ surface is ideal for NO adsorption as also shown in NO adsorption studies in Chapter 4 due to its acidic nature. TiO₂ surface easily photo-oxidize NO to NO₂, which is a molecule with acidic nature. This molecule is much easily desorbed from TiO₂ surface as also shown in the experiments done in our laboratory. However, when TiO₂ is in the cement medium, NO₂ can make interaction with the basic surface, as seen in Figure 5.1, and can disproportionate to NO₂⁻ and NO₃⁻ which are thermodynamically most stable forms in the basic structure.

The decrease in NO_2 formation in the grout was also observed in our laboratory experiments. The total NO removal was the same for on glass and on grout experiments.

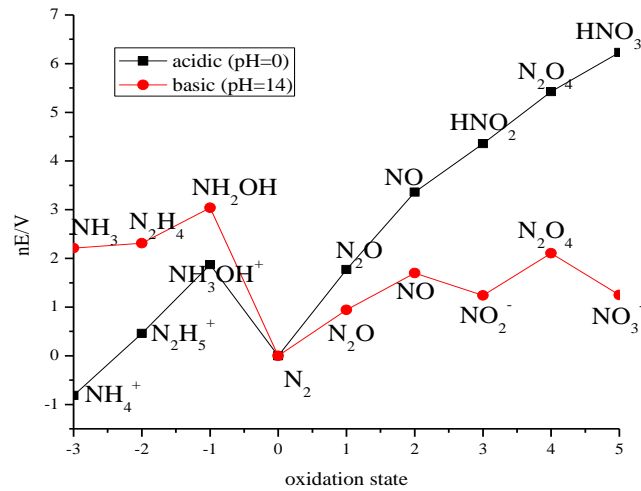


Figure 5.1 Frost Diagram formed for N atom.

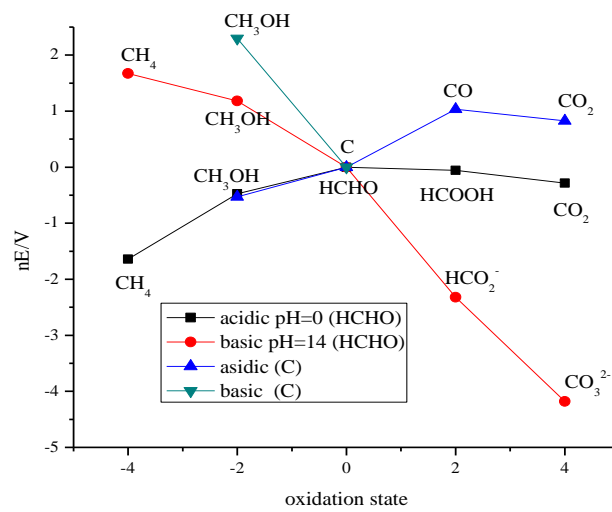


Figure 5.2 Frost Diagram formed for C atom.

When a similar Frost diagram was drawn for C or HCHO (formaldehyde) in the basic media, CO_2 can be stored as carbonate in high stability (Figure 5.2). After a reaction series between benzene and TiO_2 , when CO_2 forms, it can easily be desorbed from TiO_2 surface due to acidic character of both and CO_2 may be stored in the cement medium easily as carbonate.

5.2.3 Photocatalysis in Reduction Reactions

In photosynthetic reactions, reduction of CO_2 occurs by Calvin Cycle in the dark by using ATP and NADPH obtained from water splitting reactions under the sun. Our studies on photocatalytic CO_2 reduction to methane showed that the rate limiting step for CO_2 reduction to methane with water is the water splitting reactions. Methane formation occurs at higher rates with spilled over hydrogen on the surface. Besides that, methane formation rates are also observed in the dark in parallel to dark reactions of photosynthesis. In addition to that increasing surface area of the catalysts increased the methane formation activity [305].

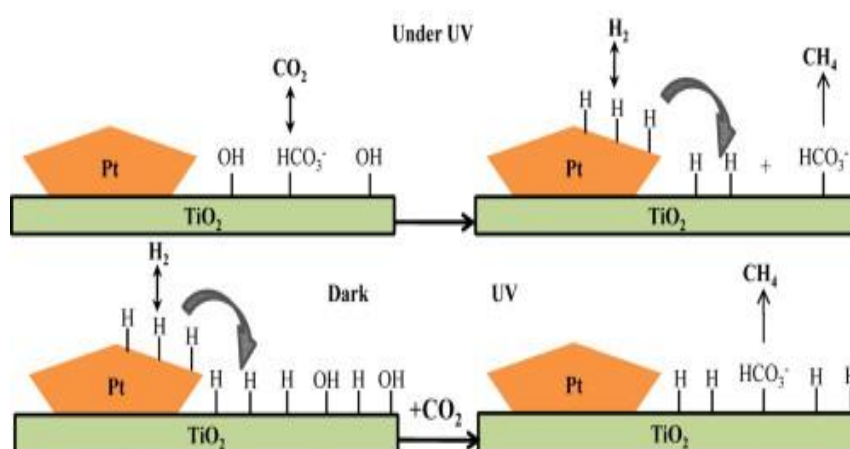


Figure 5.3 Schematic diagram of the formation of methane from spilled over hydrogen and carbon containing species on the surface under UV and dark conditions [305].

5.2.4 UV-VIS Diffuse Reflectance Studies

Increased TiO₂ loading increased the UV absorption properties of the surface and the activity of grout and plaster. UV-Vis with Diffuse Reflectance equipment was used to characterize the surface of S9-grout sample with absorption properties on UV region. UV-Vis data correlated with the activity ($R^2=0.84$). The aim was to measure the activity indirectly. However, due to equipment usage, the samples used in the measurement were scratched from surface of the samples and used in powder form. Since, this kind of sampling distorts the original sample properties, the results are not so reliable. The UV-Vis measurements have to be done by using original cured grout samples. The results were given in Appendix E.

CHAPTER 6

CONCLUSIONS

To be used in cement based materials specifically in grout and plaster, a commercial sample was selected for utilization in self cleaning applications, which is more effective if coated on the surface.

Photocatalytic gas phase benzene oxidation reaction was used as activity characterization method under UV, visible light and dark conditions. Besides selection of convenient TiO₂ powder, it was also seen that, surface area effect was not so prominent when compared with UV accessibility. Mass transfer limitations were observed.

15 TiO₂ powders, grout and plaster samples were characterized using different techniques such as XRD, BET, DRIFTS, UV-Vis with Diffuse Reflectance, SEM and Raman Spectroscopy. The morphology of the materials were characterized and related with the activity.

Experiments on gas phase CO₂ reduction to methane reaction using water and hydrogen showed that water splitting reactions are rate limiting and hydrogenation reactions can take place in the dark. In addition, increasing surface area of the catalysts increased the methane formation activity.

CHAPTER 7

RECOMMENDATIONS

Visible light catalysis is gaining importance and further improvement is needed on this area. Doping of titania is studied extensively, by different methods and materials and also other semiconductor materials are also in consideration.

FTIR studies were done in ambient conditions, since the samples will be used in ambient conditions. However, in ambient conditions, surface is mostly covered with water, hydroxyl groups and other impurities. Surface pre-treatments can be done to activate and clean the surface and determine the surface site characteristics much clearly.

This study has an industrial part conducted parallel to this thesis. A commercial product is aimed but due to economical reasons, it could not be achieved. However, a better optimization of activity and economic aspect of work can be done by considering the competitive nature of the sector.

There are cement modeling programs, which calculates the hydration reaction kinetics for different type of cement mixtures. TiO_2 may be incorporated to this kind of program and the results are further justified.

There are also modeling studies, which takes into account oxidation reactions of dissolved and adsorbed species, e^-h^+ recombination, adsorption and desorption and reduction of oxygen. This kind of model can be used to predict reactor geometry, TiO_2 amount, light intensity and mixing during photocatalytic oxidation, which can extend the applicability of the results [306].

REFERENCES

- [1] Diebold U., Surf. Sci. Reports 48 (2003) 53.
- [2] http://en.wikipedia.org/wiki/Titanium_dioxide 'Refractive Indices of TiO₂'
Last Access date: 09.07.2012.
- [3] Samsonov G.V., The Oxide Handbook, IFI/Plenum Press, New York, 1973.
- [4] Fujishima A., Zhang X., Tryk D.A., Surf. Sci. Reports 63 (2008) 515.
- [5] Hoffmann M.R., Martin S.T., Choi W., Bahnemann D.W., Chem. Rev., 95 (1995) 69.
- [6] Yamakata A., Ishibashi T., Onishi H., J. Phys. Chem. B 105 (2001) 7258.
- [7] Iwata K., Takaya T., Hamaguchi H., Yamakata A., Ishibashi T., Onishi H., Kuroda H., J. Phys. Chem. B 108 (2004) 20233.
- [8] Fujishima A, Rao T.N., Tryk D.A., J. Photochem. Photobiol. C, 1 (2000) 1.
- [9] Nosaka Y., Daimon T., Nosaka A.Y., Murakami Y., Phys. Chem. Chem. Phys. 6 (2004) 2917.
- [10] Heller A., Acc. Chem. Res. 28 (1995) 503.
- [11] Tamaki Y., Furube A., Murai M., Hara K., Katoh R., Tachiya M., J. Am. Chem. Soc. 128 (2006) 416.
- [12] Davit P., Martra G., Coluccia S., J. Japan Petroleum Institute 47 (2004) 359.
- [13] Ahmed A.Y., Kandiel T.A., Oekermann T., Bahnemann D., J. Phys. Chem. Lett. 2 (2011) 2461.
- [14] Wang S., Ang H.M., Tade M.O., Environ. Int. 33 (2007) 694.
- [15] Cassar L., Beeldens A., Pimpinelli N., Guerrini G.L., Photocatalysis of Cementitious Materials, in: RILEM Int. Symposium on Photocatalysis "Environment and Construction Materials", Florence, Italy, 2007, pp. 131.

- [16] Cheng M., Brown S.K., Proceedings of National Clean Air Conference, Newcastle, England, 2003, pp. 23.
- [17] Demeestere K., Dewulf J., Witte B.D., Beeldens A., Langenhove H.V., Building and Environ. 43 (2008) 406.
- [18] Day K.W., Concrete Mix Design, Quality Control and Specification, Taylor&Francis Group, New York, 2006, pp. 37.
- [19] Türkiye İnşaat Malzemeleri Sektör Görünüm Raporu, TOBB, 2011
- [20] Toto Today newsletter 2003/Dec Timely news letter No.36.
- [21] Maira A.J, Yeung K.L., Soria J., Coronado J.M., Belver C., Lee C.Y., Appl. Catal. B: Environ. 29 (2001) 327.
- [22] Zhang Z., Wang C.C., Zakaria R., Ying J.Y., J. Phys. Chem. B 102 (1998) 10871.
- [23] Grela M., Colussi A.J., J. Phys. Chem. 100 (1996) 18214.
- [24] Maira A.J., Yeung K.L., Lee C.Y., J. Catal. 192 (2000) 185.
- [25] Anpo M., Shima T., Kodama S., Kubokama Y., J. Phys. Chem. 91, (1987) 4305.
- [26] Lackhoff M., Prieto X., Nestle N., Dehn F., Niessner R., Appl. Catal. B: Environ. 43 (2003) 205.
- [27] Satoh N., Nakashima T., Kamikura K., Yamamoto K., Nature Nanotechnology 3 (2008) 106.
- [28] Kavan L., Stoto T., Gratzel M., Fitzmaurice D., Shklover V., J. Phys. Chem. 97 (1993) 9493.
- [29] Serpone N., Lawless D., Khairutdinov R., J. Phys. Chem. 99 (1995) 16646.
- [30] Kormann C., Bahnemann D.W., Hoffmann M.R., J. Phys. Chem. 92 (1988) 5196.
- [31] Monticone S., Tufeu R., Kanaev A.V., Scolan E., Sanchez C., Appl. Surf. Sci. 162 (2000) 565.

- [32] Bickley R.I., Gonzalescarreno T., Lees J.S., Palmisano L., Tilley R.J.D., *J. Solid State Chem.* 92 (1991) 178.
- [33] Hurum D.C., Agrios A.G., Gray K.A., Rajh T., Thurnauer M.C., *J. Phys. Chem. B* 107 (19) (2003) 4545.
- [34] Ohno T., Sarukawa K., Tokieda K., Matsumura M., *J. Catal.* 203 (2001) 82.
- [35] Li G., Gray K.A., *Chem. Phys.* 339 (2007) 173.
- [36] Ohno T., Sarukawa K., Matsumura M., *New J. Chem.* 26 (2002) 1167.
- [37] Taguchi T., Saito Y., Sarukawa K., Ohno T., Matsumura M., *New J. Chem.* 27 (2003) 1304.
- [38] Ollis D.F., *C. R. Acad. Sci. Paris, Serie IIC, Chim.* 3 (2000) 405.
- [39] Berger T., Sterrer M., Diwald O., Knözinger E., *Chem. Phys. Chem.* 6 (2005) 2104.
- [40] <http://www.ifqc.org/> 'IFQC Ranks Top 100 Countries by Gasoline Benzene Standards; U.S. Ranks 67th.' Last access date: 12.10.2011.
- [41] Galbraith D., Gross S.A., Paustenbach D., *Critical Rev. in Toxicology*, 40(S2) (2010) 1.
- [42] National Research Council, *Indoor Pollutants*, National Academy Press, Washington DC, 1981.
- [43] Williams P.R., Knutsen J.S., Atkinson C., Madl A.K., Paustenbach D.J., *J. Occup. Environ. Hyg.* 4 (2007) 547.
- [44] Zuo G-M., Cheng Z-X., Chen H., Li G-W., Miao T., *J. Hazard. Mater. B*, 128 (2006) 158.
- [45] Özbek S., *Studies on photocatalytic reactions: Heterogenous photocatalysis by titanium dioxide*, Master's thesis, Chemical Engineering Department, METU, Ankara, 2005.
- [46] Özbek S., Uner D., *Studies in Surf. Sci. and Catal.* 126 (1999) 411.
- [47] Bouazza N., Lillo-Rodenas M.A., Linares-Solano A., *Appl. Catal. B: Environ.* 84 (2008) 691.

- [48] Einega H., Ibusuki T., Futamura S., *J. Sol. Energy Eng.* 126 (2004) 789.
- [49] Einega H., Teraoka Y., *Res. Chem. Intermed.* 34 (2008) 617.
- [50] Einega H., Futamura S., Ibusuki T., *Phys.Chem.Chem.Phys.* 1 (1999) 4903.
- [51] Geng Q., Guo Q., Cao C., Wang H., *Chem. Eng. Technol.* 31 (2008) 1023.
- [52] Doucet N., Zahraa O., Bouchy M., *Catal Today* 122 (2007) 168.
- [53] Jo W-K., Park J-H., Chun H-D., *J. Photochem. Photobiol. A* 148 (2002) 109.
- [54] Larson S.A., Falconer J.L., *Catal. Lett.* 44 (1997) 57.
- [55] Lewandowski M., Ollis D.F., *Appl. Catal. B.* 43 (2003) 309.
- [56] Lewandowski M., Ollis D.F., *Appl. Catal. B.* 45 (2003) 223.
- [57] Ma C-M., Wang W., Ku Y., Jeng F.T., *Chem. Eng. Technol.* 30 (2007) 1083.
- [58] Tsoukleris D.S., Maggos T., Vassilakos C., Falaras P., *Catal. Today* 129 (2007) 96.
- [59] Vorontsov V.A., *Catal. Commun.* 8 (2007) 2100.
- [60] Wang W., Chiang L-W., Ku Y., *J. Hazard. Mater. B*101 (2003) 133.
- [61] Wang W., Ku Y., *J. Photochem. Photobiol. A* 159 (2003) 47.
- [62] Wu J-F., Hung C-H., Yuan C-S., *J. Photochem. Photobiol. A.* 170 (2005) 299.
- [63] Wu W-C., Liao L-F., Lien C-F., Lin J-L., *Phys. Chem. Chem. Phys.* 3 (2001) 4456.
- [64] Zhong J., Wang J., Tao L., Gong M., Zhimin L., Chen Y., *J. Hazard. Mater. B* 139 (2007) 323.
- [65] Hong W-J., Kang M., *Mater. Lett.* 60 (2006) 1296.

- [66] Lin T., Pi Z., Gong M.C., Zhong J.B., Wang J.L., Chen Y.Q., Chinese Chem. Lett. 18 (2007) 241.
- [67] Jacoby W.A., Blake D.M., Fennell J.A., Boulter J.E., Vargo L.M., George M.C., Dolberg S.K., J. Air&Waste Management Association 46 (1996) 891.
- [68] D'hennezel O., Pichat P., Ollis D.F., J. Photochem. and Photobiol. A: Chem. 118 (1998) 197.
- [69] Brown S.K., Sim M.R., Abramson M., Indoor air 4 (1994) 123.
- [70] D'Hennezel O., Ollis D.F., J. Catal. 167 (1997) 118.
- [71] Mendez-Roman R., Cardona-Martinez N., Catal. Today 40 (1998) 353.
- [72] Fu X., Zeltner W.A., Anderson M.A., Appl. Catal. B: Environ. 6 (1995) 209.
- [73] Strini A., Cassese S., Schiavi L., Appl. Catal. B: Environ. 61 (2005) 90.
- [74] Gaya U.I., Abdullah A.H., J. Photochem. and Photobiol. C: Photochem. Rev. 9 (2008) 1.
- [75] Liu H., Ye X., Lian Z., Wen Y., Shangguan W., Res. Chem. Intermed. 32 (2006) 9.
- [76] Cao L.X., Gao Z., Suib S.L., Obee T.N., Hay S.O., Freihaut J.D., J. Catal. 196 (2000) 253.
- [77] Pinna F., Trevisan V., Cassar L., Pepe C., Pernicone N., Photocatalytic and surface abatement of aromatic hydrocarbons by anatase, in: RILEM Int. Symposium on Photocatalysis "Environment and Construction Materials", Florence, Italy, 2007, pp.171.
- [78] Erdoğan T.Y., Construction Materials, METU Press Publishing Company, Ankara, 2005 pp. 193,250-251.
- [79] Reichel A., Hochberg A., Köpke C., Plaster, Render, Paint and Coatings, Architektur-Dokumentation GmbH&Co. KG, Munich, 2004, pp. 32,34-36,42,43,47,48,101.
- [80] Aligizaki K.K., Pore Structure of Cement-Based Materials, Bentur A., Mindess S. Eds.; Taylor & Francis Group, New York, 2006, pp. 4-11.

- [81] Hewlett P.C., Lea's Chemistry of Cement and Concrete, Third Edition, Elsevier Ltd., Oxford, 2004, pp. 21, 75, 295, 528.
- [82] Shepelev A., Plastering, MIR Publishers, Moscow, 1986, pp. 28-30, 43.
- [83] Wikipedia, <http://en.wikipedia.org/wiki/Grout> Access date: 17.08.2012.
- [84] Sevinç M., Seramik Yer ve Duvar Karosu Uygulama Teknikleri, Kaleseramik Eğitim Sağlık ve Sosyal Yardım Vakfı Yayınları, İstanbul, 2006, pp. 69.
- [85] The Council of the European Union, "Council Directive 1999/30/EC (1999) – relating to limit values for sulphur dioxide, nitrogen dioxide, and oxides of nitrogen particulate matter and lead in ambient air", 1999.
- [86] Hüsken G., Hunger M., Brouwers H.J.H., Comparative study on cementitious products containing titanium dioxide as photo-catalyst, in: RILEM Int. Symposium on Photocatalysis "Environment and Construction Materials", Florence, Italy, 2007, pp.147.
- [87] Kawakawi M., Furumura T., Tokushige H., NO_x removal effects and physical properties of cement mortar incorporating titanium dioxide powder, in: RILEM Int. Symposium on Photocatalysis "Environment and Construction Materials", Florence, Italy, 2007, pp. 163.
- [88] Guerrini G.L., Peccati E., Photocatalytic cementitious roads for depollution in: RILEM Int. Symposium on Photocatalysis "Environment and Construction Materials", Florence, Italy, 2007, pp. 179.
- [89] Beeldens A., Air purification by road materials: Results of the test project in Antwerp in: RILEM Int. Symposium on Photocatalysis "Environment and Construction Materials", Florence, Italy, 2007, pp. 187.
- [90] Crispino M., Lambrugo S., An experiment characterization of a photocatalytic mortar for road bituminous pavements, in: RILEM Int. Symposium on Photocatalysis "Environment and Construction Materials", Florence, Italy, 2007, pp. 211.
- [91] Dalton J.S., Janes P.A., Jones N.G., Nicholson J.A., Hallam K.R., Allen G.C., Environ. Pollution 120 (2002) 415.
- [92] Linkous C.A., Carter G.J., Locuson D.B., Ouellette A.J., Slattery D.K., Smitha L.A., Environ Sci Technol 34 (2000) 4754.

- [93] Giannantonio D.J., Kurth J.C., Kurtis K.E., Sobecky P.A., *Int. Biodeterioration & Biodegradation* 63 (2009) 252.
- [94] Rachel A., Subrahmanyam M., Boule P., *Appl. Catal. B: Env.* 37 (2002) 301.
- [95] Rao K. V. S., Rachel A., Subrahmanyam M., Boule P., *Appl. Catal. B: Env.* 46 (2003) 77.
- [96] Subrahmanyam M., Boule P., Durga Kumari V., Naveen Kumar D., Sancelme M., Rachel A., *Solar Energy* 82 (2008) 1099.
- [97] Ruot B., Plassais A., Olive F., Guillot L., Bonafous L., *Solar Energy* 83 (2009) 1794.
- [98] Karatasios I., Katsiotis M. S., Likodimos V., Kontos A. I., Papavassiliou G., Falaras P., Kilikoglou V., *Appl. Catal. B: Environ.* 95 (2010) 78.
- [99] Neppolian B., Kanel S.R., Choi H.C., Shankar M.V., Arabindoo B., Murugesan V., *Int J. Photoenergy* 5 (2003) 45.
- [100] Wang K.H., Hsieh Y., Chou M., Chang C., *Appl. Catal. B: Environ.* 21 (1999) 1.
- [101] Ramirez A.M., Demeestere K., Belie N., Mantyla T., Levanen E., *Building and Environ.* 45 (2010) 832.
- [102] Guerrini G.L., Plassais A., Pepe C., Cassar L., Use of photocatalytic cementitious materials for self-cleaning applications in: RILEM Int. Symposium on Photocatalysis "Environment and Construction Materials", Florence, Italy, 2007, pp. 219.
- [103] Watts M.J., Cooper A. T., *Solar Energy* 82 (2008) 206.
- [104] Rachel A., Lavedrine B., Subrahmanyam M., Boule P., *Catal. Commun.* 3 (2002) 165.
- [105] Wang R., Hashimoto K., Fujishima A., *Nature* 388 (1997) 431.
- [106] Machida M., Norimoto K., Watanabe T., *J. Mater. Sci.* 34 (1999) 2569.
- [107] Iler, R. K. *J. Colloid Interface Sci.* 1966, 21, 569.
- [108] Lee D., Rubner M.F., Cohen R.E., *Nano Lett.* 6 (2006) 2305.

- [109] Ren D., Cui X., Shen J., Zhang Q., Yang X., Zhang Z., *J. Sol-gel Sci. Tech.* 29 (2004) 131.
- [110] Guan K., *Surf. & Coatings Tech.* 191 (2005) 155.
- [111] Guan K., Lu B., Yin Y., *Surf. & Coatings Tech.* 173 (2003) 219.
- [112] Tanabe K., Sumiyoshi T., Shibata K., Kiyoura T., Kitagawa J., *Bull. Che. Soc. Japan* 47 (1974) 1064.
- [113] Lee H.J., Hahn S.H., Kim E.J., You Y.Z., *J. Mater. Sci.* 39 (2004) 3683.
- [114] Yu J.C., Yu J., Ho W., Zhao J., *J. Photochem. Photobiol. A: Chem* 148 (2002) 331.
- [115] Gu Z.Z., Fujishima A., Sato O., *Appl. Physics Lett.* 85 (2004) 5067.
- [116] Hou W., Wang Q., *Langmuir* 25 (2009) 6875.
- [117] Nakata K., Sakai M., Ochiai T., Murakami T., Takagi K., Fujishima A., *Langmuir*, 27 (2011) 3275.
- [118] Bico J., Thiele U., Quere D., *Colloids and Surf. A: Physicochemical and engineering aspects* 206 (2002) 41.
- [119] Drelich J., Chibowski E., *Langmuir* 26 (2010) 18621.
- [120] Xie X.N., Lim S.X., Wang Y.Z., Gao X.Y., Lee K.K., Sow C.H., Chen X.H., Loh K.P., Wee A.T.S., *Macromol Chem Phys*, 211 (2010) 2187.
- [121] Onda T., Shibuichi S., Satoh N., Tsujii K., *Langmuir* 12 (1996) 2125.
- [122] Shibuichi S., Onda T., Satoh N., Tsujii K., *J. Phys. Chem.* 100 (1996) 19512.
- [123] Callies M., Quere D., *Soft Matter*, 1 (2005) 55.
- [124] Gündüz G., “Boya Bilgisi,” TMMOB Kimya Mühendisliği Odası.
- [125] Mowrer N.R., http://ppgamercoatus.ppgpmc.com/psx/.../presentation_polysiloxanes.pdf Last Access date: 21.05.2010.

- [126] Andriot M., Chao S.H., Colas A., In: Silicon-Based Inorganic Polymers, Jaeger R.D., Gleria M., Ed., Nova Science Publishers, New York, 2008, Chapter 2.
- [127] Carp O., Huisman C.L., Reller A., Prog. in Solid Chem. 32 (2004) 33.
- [128] Choi W., Termin A., Hoffmann M.R., J. Phys. Chem. 98 (1994) 13669.
- [129] Al-Salim N.I., Bagshaw S.A., Bittar A., Kemmitt T., McQuillan A.J., Mills A.M., Ryan M.J., J. Mater. Chem. 10 (2000) 2358.
- [130] Kang, M., J. Mol. Catal. A-Chem. 197 (2003) 173.
- [131] Anpo M., Takeuchi M., J. Catal. 216 (2003) 505.
- [132] Xu, A.W., Gao, Y. and Liu, H.Q., J. Catal. 207 (2002) 151.
- [133] Anpo M., Takeuchi M., Ikeue K., Dohshi S., Current Opinion in Solid State & Mater. Sci. 6 (2002) 381.
- [134] Kwan C.Y., Chu W., Water Res 37 (2003) 4405.
- [135] Pal B, Hata T, Goto K, Nogami G., J Mol Catal A: Chem 169 (2001) 147.
- [136] Yu H., Irie H., Shimodaira Y., Hosogi Y., Kuroda Y., Miyauchi M., Hashimoto K., J. Phys. Chem. C 114 (2010) 16481.
- [137] Yu J., Xiang Q., Zhou M., Appl. Catal. B: Environ. 90 (2009) 595.
- [138] Asahi, R., Morikawa, T., Ohwaki, T., Aoki, K., Taga, Y., Sci. 293 (2001) 269.
- [139] Sakthivel S., Kisch H., Chemphyschem 4 (2003) 487.
- [140] Sakthivel S., Janczarek M., Kisch H., J. Phys. Chem. B 108 (2004) 19384.
- [141] Orlov A., Tikhov M.S., Lambert R.M., Comptes Rendus Chimie 9 (2006) 794.
- [142] Neumann B., Bogdanoff P., Tributsch H., Sakthivel S., Kisch H., J. Phys. Chem. B 109 (2005) 16579.

- [143] Ohno T., Akiyoshi M., Umebayashi T., Asai K., Mitsui T., Matsumura M., *Appl. Catal. A-Gen.* 265 (2004) 115.
- [144] Zhao W., Ma W.H., Chen C.C., Zhao J.C., Shuai Z.G., *J. Am. Chem. Soc.* 126 (2004) 4782.
- [145] Li D., Haneda H., Hishita S., Ohashi N., *Chem. Mater.* 17 (2005) 2588.
- [146] Livraghi S., Paganini M.C., Giamello E., Selloni A., Di Valentin C., Pacchioni G., *J. Am. Chem. Soc.* 128 (2006) 15666.
- [147] Lin Z.S., Orlov A., Lambert R.M. and Payne M.C., *J. Phys. Chem. B* 109 (2005) 20948.
- [148] Irie H., Watanabe Y., Hashimoto K., *J. Phys. Chem. B* 107 (2003) 5483.
- [149] Yates H.M., Nolan M.G., Sheel D.W., Pemble M.E., *J. Photochem. Photobiol. A: Chem.* 179 (2006) 213.
- [150] Nakamura I., Negishi N., Kutsuna S., Ihara T., Sugihara S., Takeuchi K., *J. Mol. Catal. A: Chem.* 162 (2000) 205.
- [151] Ihara T., Miyoshi M., Ando M., Sugihara S., Iriyama Y., *J. Mater. Sci.* 36 (2001) 4201.
- [152] Auroux A., Gervasini A., *J. Am. Chem. Soc.* 94 (1990) 6371.
- [153] Auroux A., *Mol. Sieves* 6 (2008) 45.
- [154] Kozlov D., Bavykin D., Savinov E., *Catal. Lett.* 86 (2003) 169.
- [155] Perruchot C., Chehimi M.M., Vaulay M.J., Benzarti K., *Cement and Concrete Research* 36 (2006) 305.
- [156] Tsyganenko A.A., Pozdnyakov D.V., Filimonov V.N., *J. Mol. structure* 29 (1975) 299.
- [157] Busca G., Lorenzelli V., *Mater. Chem.* 7 (1982) 89.
- [158] Busca G., Saussey H., Saur O., Lavalley J.C., Lorenzelli V., *Appl. Catal.* 14 (1985) 245.
- [159] Martra G., *Appl. Catal. A: Gen.* 200 (2000) 275.

- [160] Hadjiivanov K., Klissurski D., *J. Chem. Soc. Faraday Trans.* 87 (1991) 175.
- [161] Skoog D.A., Holler F.J., Nieman T.A., *Principles of Instrumental Analysis*, Fifth Edition, Harcourt Brace & Company, Florida, 1998, pp. 410,418-419.
- [162] Robinson J.W., Frame E.M.S., Frame II G.M., *Undergraduate Instrumental Analysis*, Sixth Edition, Marcel Dekker, New York, 2005, pp. 252-253.
- [163] Primet M., Pichat P., Mathieu M-V., *J. Phys. Chem.* 75 (1971) 1221.
- [164] Yates D.J.C., *J. Phys. Chem.* 65 (1961) 746.
- [165] C. N. Rusu, J. T. Yates, Jr., *J. Phys. Chem. B* 104 (2000) 1729.
- [166] Hadjiivanov K.I., *Catal. Rev.* 42 (2000) 71-144.
- [167] Mikhaylov R.V., Lisachenko A.A., Shelimov B.N., Kazansky V.B., Martra G., Alberto G., Coluccia S., *J. Phys. Chem. C* 113 (2009) 20381.
- [168] Mguig B., Calatayud M., Minot C., *Surf. Rev. and Lett.* 10(2-3) (2003) 175.
- [169] Dines T.J., Rochester C.H., Ward A.M., *J. Chem. Soc. Faraday Trans.* 87(4) (1991) 643.
- [170] Hadjiivanov K., Bushev V., Kantcheva M., Klissurski D., *Langmuir* 10 (1994) 464.
- [171] Hadjiivanov K., Knözingerb H., *Phys. Chem. Chem. Phys.* 2 (2000) 2803.
- [172] Wu J.C.S., Cheng Y.T., *J. Catal.* 237 (2006) 393.
- [173] Nagao M., Suda Y., *Langmuir* 5 (1989) 42.
- [174] Suda Y., *Langmuir* 4 (1988) 147.
- [175] Guglielminotti E., Boccuzzi F., *J. Catal.* 141 (1993) 486.
- [176] Nakamura I., Sugihara S., Takeuchi K., *Chem. Lett.* 11 (2000) 1276.

- [177] Pozdnyakov D.V., Fillmonov V.N., *Kinet. Catal.* 14 (1973) 655.
- [178] Belanger R., Moffat J. B., *Langmuir* 12 (1996) 2230.
- [179] McCormick R. L., Boonrueng S. K., Herring A.M., *Catal. Today* 42, 145 (1998).
- [180] Herring A. M., McCormick R. L., *J. Phys. Chem., Part B* 102, 3175 (1998).
- [181] Kantcheva M., *J. Cat.* 204 (2001) 479.
- [182] Papp J., Soled S., Dwight K., Wold A., *Chem. Mater.* 6 (1994) 496.
- [183] Tanabe M.W. *Discuss. Faraday. Soc.* 8 (1950) 270.
- [184] Auvinen J., Wirtanen L., *Atmospheric Environ.* 42 (2008) 4101.
- [185] Deniz U., Oymak M.M., Bahar I., *Int. J. Global Warming* 3 (2011) 142.
- [186] Chen C., Ma W., Zhao J., *Chem. Soc. Rev.* 39 (2010) 4206.
- [187] Mo J., Zhang Y., Xu Q., *Atmospheric Environ.* 43 (2009) 2229.
- [188] Han F., Kambala V., Subba R., Srinivasan M., *Appl. Catal. A-Gen.* 359 (2009) 25.
- [189] Chatterjee D., Dasgupta S., *J. Photochem. and Photobiol. C-Photochem. Rev.* 6 (2005) 186.
- [190] Ballari M.M., Yu Q.L., Brouwers H.J.H., *Catal. Today* 161 (2011) 175.
- [191] Allen N.S., Edge M., Verran J., *Polymer Degredation and Stability* 93 (2008) 1632.
- [192] Nonoyama, N., Koga, H. *Air Purification-functioning road and method for purifying polluted air over road.* US2003129412A1 (2003).
- [193] Nonoyama, N., Koguchi, T., Kadowaki, Y. *Construction method for pavement with atmospheric clarification function.* JP2009191509A (2009).
- [194] Tsukamoto, K. *Tile material for building.* JP2006248793 (A) (2006).

[195] Katayama, T. Concrete block manufacturing method and concrete block. JP2005053078 (A) (2005).

[196] Naoto, I. Roof material. JP2918884B1 (1999).

[197] Honda, T. Manufacture of concrete product having photocatalyst function. JP2000038706A (2000).

[198] Sugiyama, Y. Concrete product having photocatalytic titanium oxide coating and method of fixing the coating. JP2001151581A (2001).

[199] Kubota, N., Ayabe, T. Antifouling surface layer of water immersion structure and antifouling method. JP2000017202A (2000).

[200] Hisashi, F. Cement-base surface-colored board and its manufacturing method. JP2006089292A (2006).

[201] Bai, F., Gould, R.A.T., Anderson, M.T. Photocatalytic coating. WO2008079756 (2008).

[202] Barucco E. Antibacterial potassium-silicate-based paint containing titanium dioxide in anatase form. EP1559753A3 (2005).

[203] Park, J.M., Park, K.S. Inorganic ceramic paint comprising potassium silicate in controlled molar ratio and functional powder. KR1020050092827A (2005).

[204] Murasawa, S., Murakami, H., Fukui, Y., Watanabe, M., Fujishima, A., Hashimoto, K. Photocatalyst composite and process for producing the same. US5547823A (1996).

[205] Murasawa, S., Murakami, H., Fukui, Y., Watanabe, M., Fujishima, A., Hashimoto, K. Photocatalytic body and set of paint composition for forming the same. JP2007289955A (2007).

[206] Yoshioka, K., Okuda, T., Fujii, H., Kamimoto, Y., Fukazawa, Y., Ohyama, R., Tamaoka, M., Cho, T. Uniformly dispersed photocatalyst coating liquid, method for producing same, and photocatalytically active composite material obtained by using same. EP1997860A1 (2008).

[207] Hong, K.C., Shiao, M.L., Jacobs, G.F., Photocatalytic colored roofing granules. WO2008124344 (2008).

- [208] Stavrakev, N.A., Astashkin, S.N. Inorganic disinfection additive to construction mixtures and solutions, methods for its obtaining and usage. WO2006050588 (2006).
- [209] Linkous, C.A. Photocatalytic nuisance organism inhibitor agents. US2002010097A1 (2002).
- [210] Linkous, C.A. Photocatalytic nuisance organism inhibitor agents. US6472346B1 (2002).
- [211] Linkous, C.A. Photocatalytic nuisance organism inhibitor agents. US5518992A (1996).
- [212] Jacobs, J.L. Photocatalytic composition and method for preventing algae growth on building materials. US6881701B2 (2005).
- [213] Yu, S.J. Functional mortar using colored quartz for preventing sick house syndrome and using as finishing material. KR1020050037540A (2005).
- [214] Kiriakidis, G., Binas, V., Tudose, V. Method of production of photocatalytic powder comprising titanium dioxide and manganese dioxide active under ultraviolet and visible light. WO2011080304 (2011).
- [215] Ishibai, Y., Nishikawa, T., Sato, J. Visible light-responsive photocatalyst, method for producing same, photocatalyst coating agent using same, and photocatalyst dispersion. EP2025404A4 (2009).
- [216] Kuroiwa, Y., Fukushima, Y., Murata, Y. Pavement block. JP2007332700A (2007).
- [217] Oh, I.H., Hong, C.H. Concrete pavement block using waste stone and a manufacturing method thereof for reducing the cost by substituting waste stone and stone dust sludge for the existing aggregate. KR100754910B1 (2007).
- [218] Dae M., Method for preparing mortar for molding concrete structure using recycled functional porous particles and the structure. KR100942990B1 (2010).
- [219] Steketee, J., Air purifying panel. EP1847647A1 (2007).
- [220] Yamamoto, M. Process for producing novel material with high functional capability from waste diatomaceous earth, and novel material with high functional capability from waste diatomaceous earth, and diatomaceous earth

composition for building material utilizing such diatomaceous earth. WO2005123614 (2005).

[221] Goodwin, G., Stratton, J.L., McIntyre, R. Composition for use as NO_x removing translucent coating. WO2011034880 (2011).

[222] Stratton, J., Composition useful for providing nox removing coating on material surface. WO2006030250 (2006).

[223] Menini, C., Sergi, M. Use of photocatalytically coated particles for decomposition of air pollutants. WO2009121396 (2009).

[224] Madec, Y., Verdebout, R. A depolluting facing. WO2009056492 (2009).

[225] Hong, C.H., Kim, M.H. Ceramic composition using scoria aggregate, which removes various exhaust gases as air pollutants and has self-cleaning property. KR100483475B1 (2005).

[226] Murata, Y., Kuroiwa, Y., Nishida, R., Kuroki, Y. NO_x cleaning sound absorbing body and its production method. JP2002001064A (2002).

[227] Itakura, S., Yamamoto, Y., Incidental facility to road having atmosphere purifying function. JP2001122678A (2001).

[228] Harada, K., Tanaka, J., Goto, T. Cement composition for shotcrete. JP11263660A (1999).

[229] Gannon, P., O'Keeffe, C. A doped material. WO2012007534 (2012).

[230] Kanamori, T., Yoshimura, N., Nishikawa, A. Coating composition. EP1535975A4 (2005).

[231] Fu, G., Monk, B.M., McIntyre, R. Transparent, stable titanium dioxide sols. WO2009029856 (2009).

[232] Fu, G., Monk, B.J.M. Colloidal titanium dioxide sols. WO2010110763 (2010).

[233] Gueneau, L., Rondet, M., Besson, S., Boilot, J.P., Gacoïn, T., Durand, C. Substrate with a self-cleaning coating. US2006014050A1 (2006).

[234] Miura, M. Building indoor surface finishing material and finishing method using the same. JP2002327523A (2002).

- [235] Miura, M. Finishing material and method for finishing building surface shape by utilizing it. JP2002155612A (2002).
- [236] Miura, M. Finishing material and method for finishing surface section of building by utilizing this finishing material. JP2002154861A (2002).
- [237] Seki, M., Kurahashi, H. Composition of raw material for coating material. JP2002167524A (2002).
- [238] Tawara, S. Joint body having dirt preventing function. JP2001026992A (2001).
- [239] Tawara, S., Kobayashi, H., Photocatalyst joint material and joint structure. JP2001179093A (2001).
- [240] Tahara, S., Akimoto, J., Kobayashi, H., Fujii, H. Cement-based joint body and joint material therefor. WO0046165A1 (2000).
- [241] Fujimori, K., Haino, T., Ogawa, H. Dry construction method of tile, and photocatalyst dry joint filler for tile. JP2007170144A (2007).
- [242] Reinders, J.A.M. Evaporative cooler with antimicrobial provisions. WO2004065857 (2004).
- [243] Nonami, T., Kakuta, M., Someya, M., Ogasawara, M., Ishibashi, T., Ishibashi, K. Tooth bleaching agents and method of bleaching teeth. EP1356804B1 (2003).
- [244] Deblauwe, V., Saenen, W., Air-purifying fiber reinforced cementitious building material. WO2011006709 (2011).
- [245] Anderson, M.T., Gould, R.A.T., Jacobs, J.L. - Monolithic building element with photocatalytic material. EP1993725A1 (2008).
- [246] Gronet, C.M., Truman, J.K., Self-cleaning coatings. WO2007012026 (2007).
- [247] Kim, J.P. Method for manufacturing an extruded cement panel coated with a photocatalyst and the extruded cement panel coated with a photocatalyst for easily removing pollutants by applying the photocatalyst with photolytic effect and super-hydrophilicity on the cement panel. KR1020060097971A (2006).
- [248] Leong, M.L. Composite photocatalytic coating. WO2005044446 (2005).

- [249] Yoshimura, K., Suyama, H., Fukushima, T., Morita, H. Production of filter unit. JP2000153113A (2000).
- [250] Nakayama, J., Nishimura, T., Wada, R., Yasunaga, T. Disposal container, disposal facility and disposal method for radioactive waste. JP2003107196A (2003).
- [251] Toulan, E., Maze, M., Rousseau, P. Depolluting device for confined spaces. EP1652827A1 (2006).
- [252] Toulan, E., Maze, M., Raffegeau, H. Coating composition for sound-absorbing and pollution-abating facings. EP1642643B1 (2006).
- [253] Terruzzi, C. Bituminous road surface with a photocatalytic effect and procedure for the preparation of said road surface. US2007017417A1 (2007).
- [254] Hamamura, T. Photocatalyst-deposited granular substance, and package for air clarification and grass-proofing using the same. JP2007275767A (2007).
- [255] Ogawa, S. Atmosphere purification material, atmosphere purification panel, and external panel. JP2005168784A (2005).
- [256] Oikawa, K., Asada, E. Composite wooden cement board having adsorption and decomposition layer of chemical material. JP2003026485A (2003).
- [257] Cassar, L., Pepe, C. - Use of organic additives for the preparation of cementitious compositions with improved properties of constancy of colour. EP0885857B1 (1998).
- [258] Cassar, L., Pepe, C. Hydraulic binder and cement compositions containing photocatalyst particles. WO1998005601 (1998).
- [259] Cassar, L., Pepe, C. Hydraulic lime for cement compositions containing photocatalyst particles. EP1564194B9 (2005).
- [260] Cassar, L., Pepe, C. Architectural concrete comprising photocatalyst particles. EP1535886B1 (2005).
- [261] Alfani, R. Coatings based on hydraulic binders with an optimal rheology and a high photocatalytic activity. EP2181077A2 (2010).
- [262] Guerrini G.L., Grelaud, J.P. A paving with a pollution-abating activity and a photocatalytic mixture for its preparation. WO2009133094 (2009).

- [263] Cucitore, R., Cangiano, S., Cassar, L. High durability photocatalytic paving for reducing urban polluting agents. EP1778919A1 (2007).
- [264] Borzetti, F., Guerrini, G.L., Cassar, L., Campanella, L., Visco, G. Method of measuring the photocatalytic activity of cementitious materials. EP2282203B1 (2011).
- [265] Amadelli, R., Cassar, L., Pepe, C. Use of photocatalytic preparations of colloidal titanium dioxide for preserving the original appearance of cementitious, stone, or marble products. WO2001000541 (2001).
- [266] Guerrini, G.L. Cementitious products and articles of manufacture containing carbon-doped titanium dioxide. WO2011045038 (2011).
- [267] Ancora, R., Borsa, M., Cassar, L. Titanium dioxide based photocatalytic composites and derived products on a metakaolin support. WO2009080647 (2009).
- [268] Ancora, R., Borsa, M., Iler Marchi, M. Photocatalytic composites containing titanium and limestone. WO2010012488 (2010).
- [269] Anora, R., Borsa, M., Iler Marchi, M. Photocatalytic composites containing titanium and limestone free from titanium dioxide. WO2010012489 (2010).
- [270] Shimobukikoshi, M., Iso, S., Watabe, T. Hayakawa, M., Kitamura, A., Chikuni, M. Method for water film formation with design material having ultrahigh hydrophilicity. JP3704806B2 (2005).
- [271] Watabe, T., Hayakawa, M., Chikuni, M., Kitamura, A. Lighting Apparatus For Tunnel Or Road. JP4120943B2 (2008).
- [272] Soma T., Fujishima A., Hashimoto K., Hayakawa M., Watabe T. Antifouling tunnel interior wall and antifouling method and washing method thereof. JP3115534B2 (2000).
- [273] Watabe T., Hayakawa M., Kojima E., Chikuni M., Kitamura A. Reflector for road marker with self-purifying surface. JP3596834B2 (2004).
- [274] Watabe T., Hayakawa M. Visible road surface marking, its construction method and self-cleaning method. JP3648848B2 (2005).
- [275] Watabe T., Chikuni M., Kitamura A., Hayakawa M. Water permeable paving materials. JP3744061B2 (2006).

- [276] Hayakawa M., Kojima E., Watabe T, Chikuni M., Kitamura A. Cold reserving show case JP3707130B2 (2005).
- [277] Hayakawa M., Kitamura A., Kojima E. Bathroom member JP3534072B2 (2004).
- [278] Hayakawa M., Chikuni M., Watabe T., Kojima E., Kitamura A. Washstand bowl and method for cleaning it. JP3695552B2 (2005).
- [279] Watabe T. Photocatalyst mechanism. JP3063685B2 (2000).
- [280] Watanabe T., Kitamura A., Kojima E., Hashimoto K., Fujishima A. Air treating method using photocatalyst under interior illumination. EP0630679B1 (1999).
- [281] Ogawa T., Saito T., Unno K., Hasegawa K., Yoshioka Y., Tsubouchi N., Hosoiri S., Katayama T., Watabe T., Murasawa S., Fujishima A., Hashimoto K., Tsubochi N., Katayama T., Watabe T. Nosokomial infection preventing method. JP2790596B2 (1998).
- [282] Watabe T., Kitamura A., Kojima E., Saeki Y. Ceramics having bacteriocidal action. JP3063735B2 (2000).
- [283] Watabe T., Kitamura A., Kojima E., Saeki Y. Photocatalytically functional material for sticking. JP3075261B2 (2000).
- [284] Miyauchi M., Tokutome H., Shimai A., Mitsui T. Photocatalyst used for cleaning water quality. JP4438087B2 (2010).
- [285] Kanehira K., Sonezaki S., Ogami Y., Banzai T., Kameshima J. Method for killing cells using photocatalytic titanium dioxide particles US2011060269 A1 (2011).
- [286] Sonezaki S., Kanehira K., Ogami Y., Banzai T., Kubota Y. Therapeutic method of administering pharmaceutical titanium dioxide composite and light irradiation. US2011014245A1 (2011).
- [287] Miyauchi M., Tokudome H., Sonezaki S., Ishikawa H., Bekki M., Kanehira K., Oohara H., Yamada Y., Ogami Y. Method of specifically detecting test substance by using photocurrent and electrodes, measurement cell, measurement device and buffer solution to be used therefor. WO2005093418A1 (2005).

- [288] Norimoto K., Kojima E., Watabe T. Activity measuring method for photocatalyst thin film, and activity measuring film. JP355540B2 (2004).
- [289] Kobayashi H., Saeki Y., Tanaka S., Nakashima Y., Mayumi Y. Method for producing high-performance material having photocatalytic function and device therefor. WO0006300A1 (2000).
- [290] Chee Y.H., Cooney R.P., Howe R.F., Van Der Heide P.A.W., J. Raman Spectrosc 23 (1992) 161.
- [291] Ohsaka T., Izumi F., Fujiki Y., J Raman Spectrosc 7 (1978) 321.
- [292] Best M.F., Condrate R.A., J. Mater. Sci. Lett. 4 (1985) 994.
- [293] Chmel A., Eranosyan G.M., Kharshak A.A., J. Noncryst. Solids 146 (1992) 213.
- [294] Schraml-Marth M., Walther K.L., Wokaun A., Handy B.E., Baiker A.J., J. Noncryst. Solids 143 (1992) 93.
- [295] Deo G., Turek A.M., Wachs I.E., Huybrechts D.R.C., Jacobs P.A., Zeolites 13 (1993) 365.
- [296] Srinivasan S., Datye A.K., Hampden-Smith M., Wachs I.E., Deo G., Jehng J.M., Turek A.M., Peden H.F., J. Catal. 131 (1991) 260.
- [297] Deschamps T., Martinet C., Bruneel J.L., Champagnon B., J. Phys.:Condens. Matter 23 (2011) 035402 (7pp).
- [298] Courtesy of İstem Özen and Sabancı University FENS MCL.
- [299] Lachheb H., Puzenat E., Houas A., Ksibi M., Elaoui E., Guillard G., Hermann J.M., Appl. Catal. B: Environ. 39 (2002) 75.
- [300] Stylidi M., Kondarides D.I., Verykios X.E., Appl. Catal. B: Environ. 40 (2003) 271.
- [301] Aissa AH, Puzenat E, Plassais A., Appl. Catal. B-Environ. 107 (2011) 1.
- [302] K. Tanaka and J.M. White, J. Phys. Chem., 86 (1982) 4708.
- [303] M.A. Henderson, Surf. Sci., 400 (1998) 203.

[304] Cassar L., 2nd Int. symposium on Nanotechnology in construction, Bilbao, Spain, 2005.

[305] Uner D., Oymak M.M., Catal. Today 181 (2012) 82.

[306] Stafford U., Gray K.A., Kamat P.V., Res. Chem. Intermed. 23 (1997) 355.

APPENDIX A

HYDRATION AND PRE-PRODUCTION REACTIONS FOR IMPORTANT BINDERS IN CONSTRUCTION INDUSTRY AND ADDITIVES USED

Table A.1. Important inorganic binding agents used in construction industry

	Lime Binders	Calcium Silicate Binder	Calcium Sulphate Binder
	Quick lime CaO	3CaO.SiO ₂ (C ₃ S)	Gypsum CaSO ₄ .2H ₂ O
	slaked lime Ca(OH) ₂		Plaster of Paris Ca.SO ₄ .1/2H ₂ O
	Lime CaCO ₃	2CaO.SiO ₂ (C ₂ S)	Anhydrite CaSO ₄
Production Reactions	<p>Firing CaCO₃+heat → CaO+CO₂</p> <p>Slaking CaO+H₂O → Ca(OH)₂ + heat</p>	Figure A.1	<p>CaSO₄.2H₂O + heat (below 300°C) → CaSO₄.1/2H₂O + 3/2 H₂O</p> <p>CaSO₄.2H₂O + heat (over 300°C) → CaSO₄ + 2H₂O</p>
Hardening reactions	Ca(OH) ₂ + CO ₂ → CaCO ₃ + H ₂ O	3CaO.SiO ₂ + (3-x+y)H ₂ O → xCaO.SiO ₂ .yH ₂ O + (3-x)Ca(OH) ₂	CaSO ₄ .1/2H ₂ O + 3/2 H ₂ O → CaSO ₄ + 2H ₂ O → CaSO ₄ .2H ₂ O
Hardening Time	Months to years for non-hydraulic Months hydraulic	App. 28 days	1-20 hours

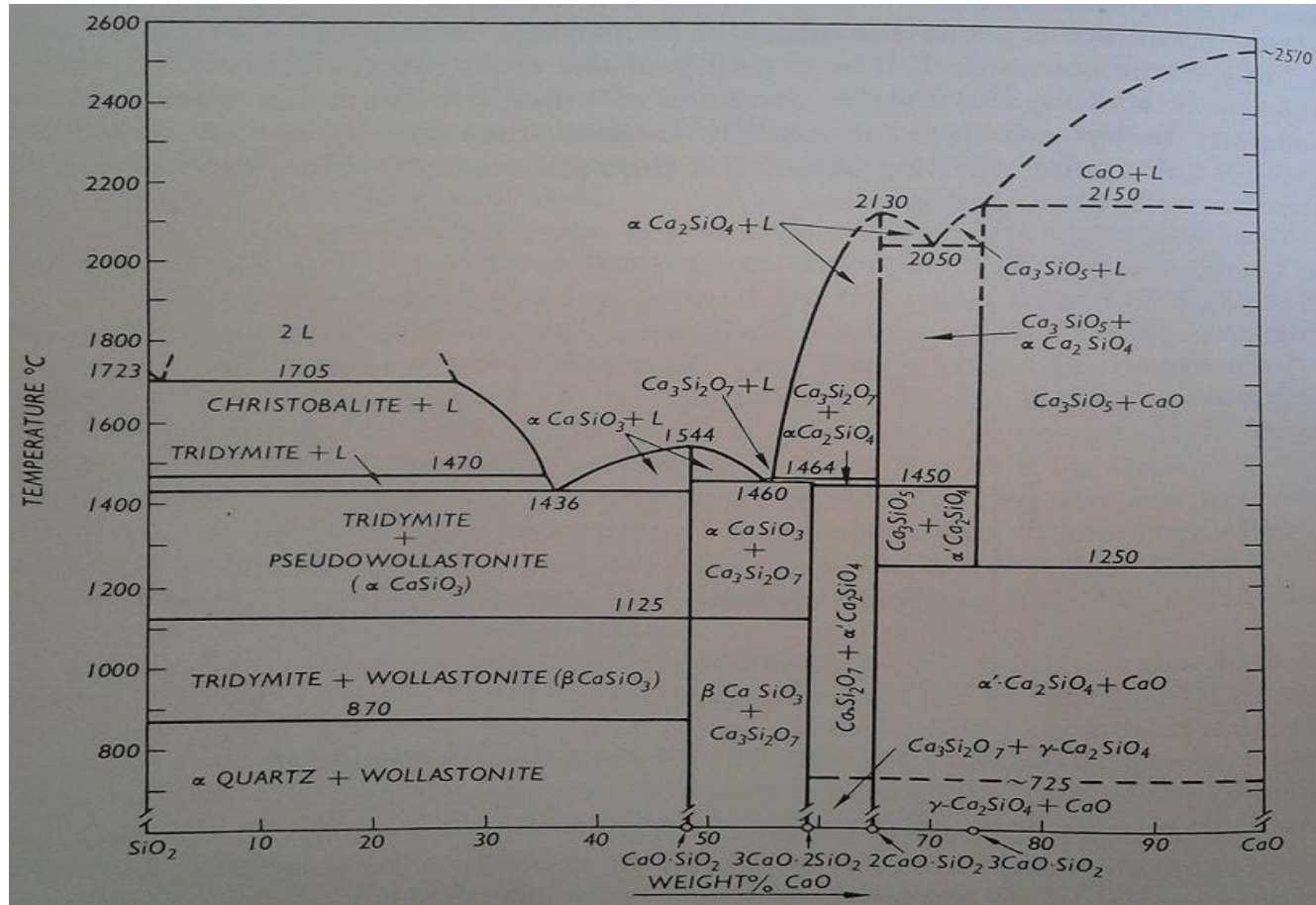


Figure A.1 Phase Diagram of CaO-SiO₂ System [81]

Table A.2 Examples of plaster admixtures [79]

Influenced Properties	Purpose	Mode of Action	Historical Admixture	Synthetic admixture	Effect of overdosing
Porosity	-Improve the workability -Reduce the settled apparent density -Increase the frost resistance -Increase the vapor permeability -Deposition of salts	Changes the surface tension of the mixing water, causing formation of small, stable pores	Blood	Tensides	- Increase the stickiness - Poor workability
Water retaining potential	-Prevent firing on by early release of water to the background -Improve the workability characteristics	Physical binding of mixing water in admixture capable of swelling	Wood fibres	Cellulose	- Increase the stickiness - Poor workability -Disturbance of the setting time and hardening
Strength	-Prevent slipping from rendering base	Physical binding of mixing water in admixture capable of swelling	Betonite, starch	Starch ether	-Increase the stickiness - Poor workability
Elasticity	Prevent crack formation	Composite, formation of a “reinforcing skeleton”	Animal hairs, straw, wood fibres	Glass fibres, polymer fibres, cellulose fibres	-Poor workability
Bond Strength	-Improve bonding with background	Adhesion	Curd cheese, casein, blood	Polymer Dispersion	-Increase the stickiness

Table A.2 (Continued)

					-Poor workability
Water-repelling capability	-Reduce the capillary adsorption	Increase the surface tension in the capillaries and therefore reduce the capillary adsorption	Animal and vegetable fibres, oils, soaps	Stearates, oleates, palmitates, silicone resins	-Reduce the final strength
Setting time (Retardation)	-Increase the setting time and the pot life	Slow down the binder reaction	Gypsum, sugar, wine, lime water, borax, okra roots	Fruit acids, phosphates, silicone fluorides, sucroses, lignosulphonates, hydrogen carboxylic acids	-Accelerate the setting time -Blooming -Signs of expansion
Setting Time (Acceleration)	-Shorten the setting time	Accelerate the binder reaction and solidification	Gypsum	Chloride, aluminate, hydrogen carbonate	- Final strength too low -Blooming -Signs of expansion
Color	-Adjust the color	Distribution of the pigment in the binder matrix	Charcoal, minerals, brick meal, stone meal	Anorganic/mineral and organic pigments	-Bleeding -Mottling

APPENDIX B

PICTURES FROM THE EXPERIMENTAL SET UP AND SAMPLES USED IN THIS THESIS



(a)

(b)

Figure B.1 a) Cured grout sample b) Pure Coated Glass Slides used in the experiments.



(a)

(b)

Figure B.2 Experimental set up used in a) Photocatalytic Benzene Oxidation Experiments b) CO₂ hydrogenation to methane experiments.

APPENDIX C

DRIFTS SPECTRA of GROUT, POWDER, and COATING APPLICATIONS of S8 in the REGION 4000-1200 cm^{-1}

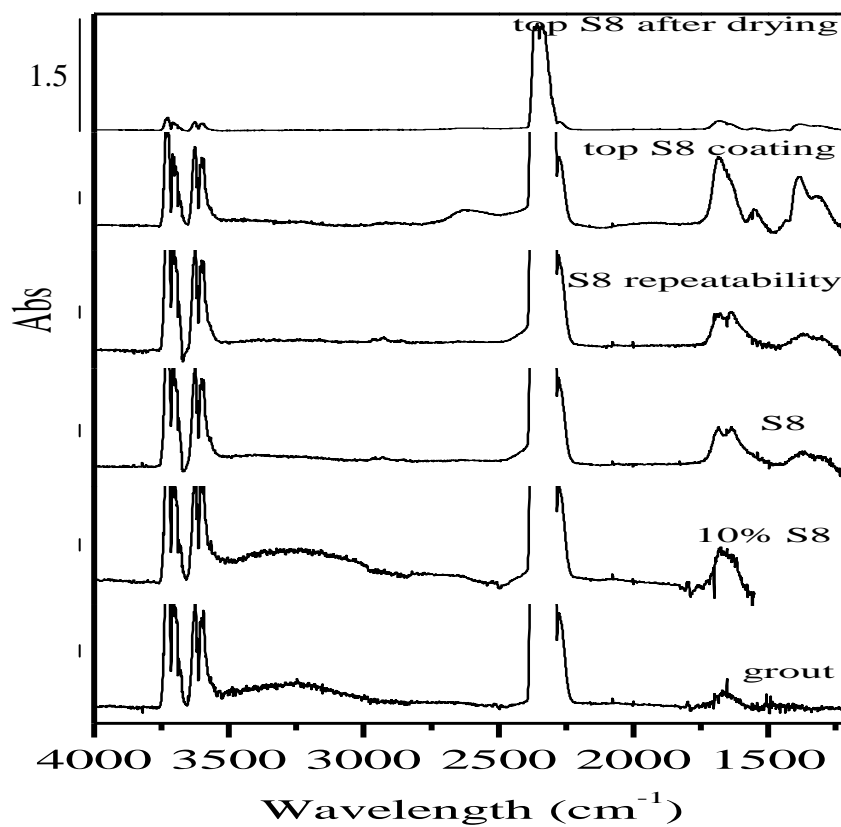


Figure C.1 DRIFTS Spectra Comparison of pure powder, coating and grout applications using S8 powder.

APPENDIX D

PEAK ASSIGNMENTS OF NO ADSORPTION ON 15 TiO₂ POWDERS

Table D.1. Peak assignments in 1750 – 1150 cm^{-1} region for NO Adsorption on 15 Commercial TiO_2 Powders *.

	NO_3^- (free like)	NO_3^- (monodentate)	NO_3^- (chelating)	NO_3^- (bridged)	N_2O	NO_2^- (nitro-nitrito)	NO_2^- (nitro)	NO_2^- (bidentate-nitrito)	NO_2^- (monodentate-nitrito)
S1	[1760, hp, sh, as1, as2], [1725, hp, as2, as9], [S(1668 to 1673), g+, v---, un], [1630, g+, v---, as3, as4], [1570, ihp, v-, as5, as6, as8]	[1480, g+, sh, v-, un], [S(1440 to 1423), g+, v-, as8], [S(1355 to 1345), g+, v-, as2, as11]	[1260, ihp, sh, as5], [1225, sp, as4, as5], [1150, usp, as10], [1105, usp, un]						
S2	[1760, hp, v0, as1, as2], [1715, hp, v0, as2, as9], [S(1650 to 1640), np, as4], [1625, g+, v---, as3, as4], [1605, hp, v-, as4, as5], [1580, lhp, v-, as5, as6]	[S(1420 to 1430), g+, v-, un], [S(1350 to 1340), g+, v-, as2, as4, as11]	[1100, un]						
S3 (no vac)	[1760, hp, as1, as2], [1635, lp, shp, as3, as4], [1605, g+, as4], [S(1580 to 1583), as5, as6], [1565, sh, as5, as6, as8]	[1550, sp, as6, as8], [1510, sh, as6], [1475, g+, as5], [1380, sh, as2]	[S(1340 to 1335), as4, as11], [1318, g+, as4, as11], [1295, g+, as6], [1280, lp-shp, as6], [1250, g+, ihp, as5], [1235, Lp-hp0, as5], [1195, Lp-hp0, as4, as6, as7]						

Table D.1 (Continued)

S4	[1760,hp,as1,as2],[1635,lp,shp,as3,as4] [S(1603to1607),g+,as4,as5],[S(1580to1584)g+, as5,as6]	[1550,sp,as6,as8],[1510,sh,as6],[S(1475to1480 ,g+,as5],[1380,sh,as2]	[1335,g+,as4, as11],[1320,lp,shp,as4,as6, as11] ,[S(1285to1292), as6],[1260,sp,shp] [1250,g+,ihp,as5][1205,Lp-hp0,as4,as6,as7]
S5	[1760,hp,as1],[1633,sh,as3,as4],[1603,g+,as4,as5 ,[1582,g+,as5,as6][1573,hp,sh,as5,as6]	[1550,sp,hp,as6,as8],[1510,sh,as6] [1475,g+,v-,as5]	[1335,g+,sp, as4, as11],[1295,sp, as6][1250,g+, hp,as5],[1205,lp-hp0,as4,as6,as7]
S6	[1765,hp,v-,as1],[1655,Np0,v-,as4][1625,g+ ,v- ,shp,as3, as4],[1605,hp,v-,as4,as5], [1580,hp,v-,as5,as6]	[1490,g+,sh,as6],[S(1430to1420),g+,v- ,as8],[1355,g+,v-,as2]	[1250,lp-hp0,as5], [1190,np,hp,v0,as4,as6,as7]
S7 (no vac)	[1765,hp,as1],[1633,g+,sh,as3,as4],[1607,g+ ,as4,as5],[1580,hp,as5,as6],[1573,g+,sh,as5,as6], [1553,g+,sh,as6,as8]	[1526,lp,sh-hp0,as6,as8],[1482,g+,un] [1470,g+,as5,as8]	[1330,sh, as4, as11],[1295,g+, as6],[1270,sp,un] [1250,hp,as5],[1195,lp-hp0,as4,as6,as7]
S8	[1765,hp,v-,as1,as2],[1710,hp,v-,as2,as9] [1655,Np0,v-,as4],[1630,g+,v-,shp,as3, as4] [1605,hp,v-,as4,as5],[1580,hp,v0,as5,as6]	[1490,g+,sh,as6],[S(1440to1420),g+,v- as5,as8],[1355,g+,v-,as2]	[1195,np,hp,v0,as4,as6,as7]
S9	[1760,hp,v-,as1,as2],[1697,np0,v-,un], [1689,g+,un],[1670,g+,un],[1652,g+,sh,as4], [1642g+,sh,as4],[1615g+,sh,as3,as4,as5],	[1487,g+,v-,un],[1482to1475,g+,v-,un] [1526,lp,sh-hp0,as6,as8],[1375g+,v-,as2]	[1340,g+,v+, as4, as11],[1326,sh, as4, as11] [S(1310to 1318),Np,as4,as6, as11],[1292,g+,as6],[1282,g+,sh,

Table D.1 (Continued)

	[1605g+,v+,as4,as5],[S(1585to1582),g+,v0,as5,as6]		as6],[1270,sp,un], [1255,g+,v0,as5] [1248,g+,v0,as5],[1238,g+,ihp,v0,as5], [1200,lp-hp0,as4, as6,as7]
S10	[1760,hp,as1,as2],[1652,sp,lp,hp0,as4] [1642,sp,lp,hp0,as4],[1605,g+,as4,as5] [1582,g+,as5,as6]	[1526,lp,sh-hp0,as6,as8],[1485,g+,un] [1375,sp,as2]	[1340,g+,as4, as11],[1324,sp,as4, as11],[1310, Np,as4,as6],[1292,g+,as6],[1282,g+,sh,as6],[127 0,sp,un],[1255,g+,as5][1200,Lp-hp0,as4,as6,as7
S11	[1765,hp,as1],[1642,sp,lp,hp0,as4],[1633,sp,lp,h p0,as3,as4],[1615,sp,lp,hp0,as3,as4,as5], [1605,g+,as4,as5],[1580,g+,as5,as6]	[1553,g+,hp,as6,as8],[1526,lp,sh-hp0,as6 ,as8],[1476,g+,as5]	[1292,g+,as6],[1250,g+,hp,as5] [1200,Lp-hp0,as4,as6,as7]
S12	[1689,g+,un],[1663,g+,un],[1603,g+,v- ,as4,as5],[1582,g+,v0,as5,as6],[1563,g+,sh,as5,as 6][1550,g+,as6,as8]	[1484,g+,un],[1350,g+,v-, as11]	[1326,np,as4, as11],[1314,g+,as4,as6] [1294,g+,hp,as6],[1255,g+,sh,as5]
S13	[1760,hp,as1,as2],[1689,g+,un],[1670,g+,un] [1642,g+,sh ,as4],[1605,g+,as4,as5],[1582,g+,as 5,as6]	[1526,lp,sh-hp0,as6,as8],[1487,g+,un] [1375,g+,as2]	[1292,g+,as6],[1282,g+,sh,hp0,as6] [1255,g+,as5],[1200,Lp-hp0,as4,as6,as7]
S14	[1760,hp,as1,as2],[1672,sp,hp,v--,un] [1625,g+,sh,as3,as4][1603,g+,hp,v-,as4,as 5] [1582,g+,v0,as5,as6]	[1430,g+,hp,un],[1375,g+,hp,sh,as2]	

Table D.1 (Continued)

S15	[1675,g+,v--,un],[1652,g+,hp0,as4], [1633,g+,sh,as3,as4],[1608,g+,v-,as4,as5], [1582,g+,v0,as5,as6]	[1526,g+,sh,as6,as8],[1430,g+,hp,as8]	[1340,g+,hp,as4,as11]
-----	---	---------------------------------------	-----------------------

* For table abbreviations and assignments see Table D.3

Table D.2. Peak Assignments in 4000 – 1800 cm^{-1} region for NO Adsorption on 15 Commercial TiO_2 Powders *.

	Region between 4000 cm^{-1} - 3000 cm^{-1}	Region between 3000 cm^{-1} - 2000 cm^{-1}	Region between 2000 cm^{-1} - 1800 cm^{-1}
S1	[S(3700to3695),g-,v-,as7],[3672,g-,v-,as7],[3000-3500,g+,as4,as5]	[2800-3000,h,as3],[2100-2550,(2360pt),g+,v-,as2]	[1846,1905,as1] [2000,sp,un]
S2	[3730g-,v-,as8], [S(3700to3695),g-,v-,as7], [3672g-,v0,as7],[3000-3500,g+,as4,as5]	[2800-3000,l,as3],[2100-2550,(2360pt),g+,v-,as2]	[1846,1905,as1] [2000,sp,un]
S3	[3695,g-,as7], [3672,usp,as7],[3660,g-,as7],[3630,g-,as7], [3200-3600,g+,as4,as5,as6]	[3000-2000,g-,broad],[2200-2600,(2330,p),g+,d,as2],[2575,hp,un],[2500,hp,un],[2255,sh,hp,as10]	broa [1846,1905,as1] [2000,hp,un]

Table D.2 (Continued)

S4	[3695,g-,v+,as7],[3669,usp,as7],[3660,g- -, v+,as7] [3630 ,g- ,v0,as7],[3600-3000,g+,(3530p,3400p,3180,shp),as4, as5,as6]	[2900-2000,g-,broad],[2600-2000,g+,v-,as2], [2580,hp,un],[2490,hp,un], [2255,sh,hp,as10]	[1846,1905,as1] [1935,v0, as9],[2000,hp,un]
S5	[3695,g-,v+,as7] ,[3675,sh,as7],[3660,g--, v+,as7], [3630 ,g-,v0,as7],[3600-3000,broad,g+,as4,as5,as6]	[2900-2000,g-,broad][2600-2200,broad,(2330p,hp), g- -, as2][2580,hp,un][2490,hp,un], [2255,sh,hp,as10]	[1846,1905,as1],[193 5,v0, as9],[2000,hp]
S6	[3730,sp,lp-hp0,v-,as8],[3672,g-,v-,as7],[3700,g-,v- ,as7,as8],[3250-3500,broad,g+,v-,as4,as5]	[2800-3000,l,as3],[2800-2100,broad,g+,v-,as2], [2400,hp,v-,un]	[1846,1905,as1]
S7	[3695,g-,as7], [3675,sh,as7], [3658,g--,as7],[3630,g-,as7], ,[3600-3100,broad,g+,as4, as5 ,as6]	[3000-2000,g-,broad],[2600-2200,broad,(2330p, hp),g-- ,as2][2580,hp,un],[2490,hp,un],[2255,sh,hp, as10]	[1846,1905,as1] [2000,hp,un]
S8	[S(3700to3695),g-,v-,as7], [3672,g-,v-,as7],[3640,sh,g-, as7],[3000-3550,broad,g+,v-,as4,as5]	[2800-3000,l,as3],[2800-2100,broad,g+,v-,as2] [2400,ihp,v-,un]	[1846,1905,as1]
S9	[3695,g-,v-,as7],[3650,g-,v+,as7],[3631,g-,v0,as7] [3610-2700,broad,g+,(3400p-3520sh),as4,as5,as6]	[2000-2250,broad,g-, as2], [2550-2200,broad,g+,as2] ,[2580,hp,un],[2450,sh,hp,un],[2360,np,un], [2255,sh,hp, as10],	[1846,1905,as1] [1935,v0, as9] [2000,hp,un]
S10	[3695,g-,as7],[3658,g-,as7],[3631,g-,as7], [3610-2700,broad,g+,(3400p-3520sh),as4,as5,as6]	[2800-2000,g-,broad,un],[2550-2200,(2340p),g+, broad,as2], [2580,hp,un] ,[2450,sh,hp,un] [2360,np,un],[2255,sh,hp, as10]	[1846,1905,as1] [1935,v0, as9] [2000,hp,un]

Table D.2 (Continued)

S11	[3695,g-,as7],[3660,g-,as7],[3630,g-,as7], [3610-3000,broad,g+,(3400p-3520sh),as4,as5,as6]	[3000-2550,g-,un],[3000-2000,broad,g-,un],[2200-2550,g+,hp,(2330p),as2],[2580,hp,un], [2450,sh,hp,un],[2255,sh,hp, as10]	[1846,1905,as1] [1935,v0,as9] [2000,hp,un]
S12	[3745,g-,v+,as8],[3735,g-,v+,as8],[3695,g-,v0,as7], ,v+,as7],[3660,g-,v+,as7],[3650,g-,v+,as7], [3610-3000,broad,g+,as4,as5,as6]	[3670,g- [3630,g-,v+,as7], [2200-2550,g+,(2360p), as2], [2000-2250,broad,g-, as2], [2580,hp,un]	[1846,1905,as1] [1935,v0, as9] [2000,hp,un]
S13	[3695,g-,v-,as7],[3681,g-,v-,as7],[3660,g-,v0,as7] ,v0,as7],[3600-2800,broad,g+,(3370p,3520sh),as4, as5,as6]	[3630, g- as2],[2580,hp,un]	[2200-2550,g+,(2380p, 2310p),as2],[2000-2200,g-, [1846,1905,as1] [1935,v0, as9] [2000,hp,un]
S14	[3730,g-as8], [3681,g-,v-,as7] [3600-3000,broad,g+,(3370p,3520sh),as 4,as5,as6]	[3000-2800,l,as3],[2700-2300,broad,(2425p), as2],[2760,hp,un], [2350,hp,un]	g+,v- [1846,1905,as1]
S15	[3670,g-,v-,as7],[3690,g+,v-,as7],[3735,g-,as8] [3600-2800,broad,g+,(3370p,3520sh), as 4,as5,as6]	[3000-2800,h,as3],[2800-2300,broad,g+,v-,as2], 2250,g-, as2],[2760,ihp,un],[2450,ihp,v-,un]	[1846,1905,as1] [2000,hp,un]

* For table abbreviations and assignments see Table D.3

Table D.3 Table abbreviations and literature assignments done for Table D.1 and Table D.2.

Assignments for Table D.1	Assignments for Table D.2	Table Abbreviations	
Un – unassigned	Un – unassigned	shp:	Shoulder formation at high NO pressures
As 1 – dinitrosyl species trans $-(NO)_2$ 1764 cm^{-1} [167].	As 1 – Characteristic NO gaseous peaks 1846, 1905 cm^{-1} [167].	lh:	Increased formation at high NO pressures
As 2 – $\nu_{as}(NO_2)=1758-1730$ cm^{-1} + shoulder 1710 cm^{-1} , $\nu_s(NO_2)=1368-1359$ cm^{-1} [167]	As 2 – NO^+ or NO_2^+ formation due to adsorption of NO_2^- and NO_3^- fragments 2100-2400 cm^{-1} [167], 2210-2150 cm^{-1} , 2210 cm^{-1} .	hp:	Formed at high NO pressures
As 3 – $\delta(H_2O) = 1620$ cm^{-1} adsorbed water [173]	As 3 – C-H stretching region 2800- 3000 cm^{-1} [164]	lp:	Formed at low NO pressures.
As 4 – Bridged nitrate 1610-1190 cm^{-1} , [170], 1622-1322 cm^{-1} [167], 1644-1628— 1220-1175 cm^{-1} , 1630-1625—1215 cm^{-1}	As 4 – Undissociated $\nu(H_2O)$ region 3000-3400 cm^{-1} [173]	hp0:	disappearance at high NO pressures
As 5 – Bidentate nitrate 1586-1240 cm^{-1} [170], 1612-1241 cm^{-1} [167], 1576 cm^{-1} , 1458 cm^{-1} [173], 1578, 1572 – 1250-1220 cm^{-1} , 1615, 1580, 1555-1215 cm^{-1}	As 5 – Isolated $\nu(H_2O)$ 3456 cm^{-1} [173]	S:	Shift
As 6 – Monodentate nitrate 1545-1190 cm^{-1} , 1582-1302 cm^{-1} [167], 1540 cm^{-1} , 1525 cm^{-1} , 1508 cm^{-1} [173], 1505-1286 cm^{-1}	As 6 – $\nu(OH)$ of NO-H 3565 cm^{-1} [173]	v:	Vacuum
As 7 – Bidentate nitrite, $\nu_s(NO_2)$, 1192 [179, 180, 173]	As 7 – H bonded OH groups 3700- 3550 cm^{-1} [173]	l:	Low
As 8 – Nitro-nitrito 1450-1550 cm^{-1} , 1542 cm^{-1} [167]	As 8 – Surface free OH groups 3750-3700 cm^{-1} [173]	h:	High
		p:	Peak
		sh:	Shoulder
		g	Gradual
		0:	No effect
		+, + +,	Peak increase from low to high
		+++	
		-, - -, - -	
		- :	Peak disappearance from low to high
		Sp:	Small peak
		Usp:	Unclear small peak
		Np:	Negative peak

Table D.3 (Continued)

As 9 – Ti ³⁺ -NO 1715 cm ⁻¹	As 9 – 1930 cm ⁻¹ N ₂ O ₃ (Possibly
As 10 NO ⁻ , Ti ⁴⁺ -NO ⁻ /NOH 1170 cm ⁻¹ , 1160 cm ⁻¹ .	NO), 1913-ON-Ti ⁴⁺ -ONO ₂
As 11 – Hyponitrites 1335 cm ⁻¹	As 10 – N ₂ O 2242, 2231 cm ⁻¹

APPENDIX E

UV-VIS DIFFUSE REFLECTANCE STUDIES

An increase in the absorbance was observed with increasing TiO₂ content around UVA region (Figure E.1). The area under reflectance curve was integrated between 250-400 nm (Equation E.1) and graphical representation of calculated area and change with respect to TiO₂% are shown in Figure E.2. The integrated area increased with increasing TiO₂% content. The integral area is also correlated with the activity and a linear increase was observed with increasing TiO₂ content for S9 sample (Figure E.3). Using this correlation, by only measuring the reflectance values of the S9 sample, the activity can be calculated. By using this correlation, the activity of other TiO₂ samples can not be determined for all TiO₂ powders since every TiO₂ has a different process history, morphology.

$$\text{Absorbed Area} = \int_{250}^{400} (R_{x\%TiO_2}) d\lambda \quad (\text{E.1})$$

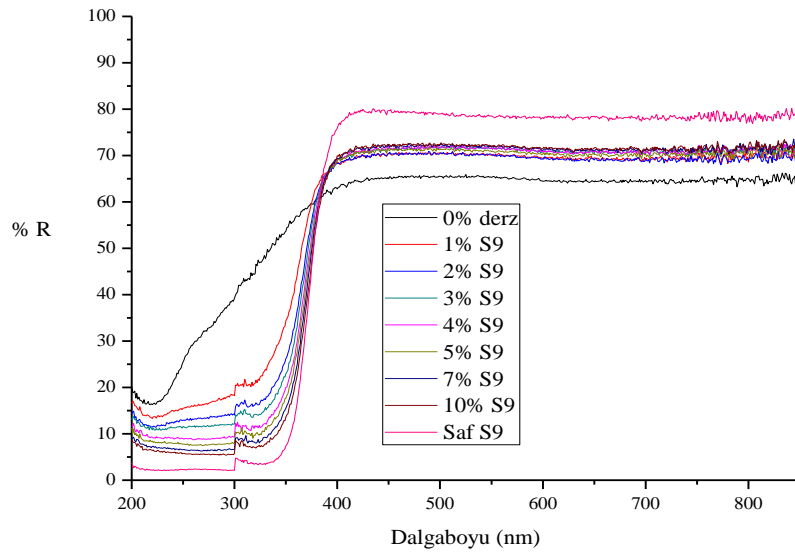


Figure E.1 Results of UV-Vis spectra for changing S9 wt%.

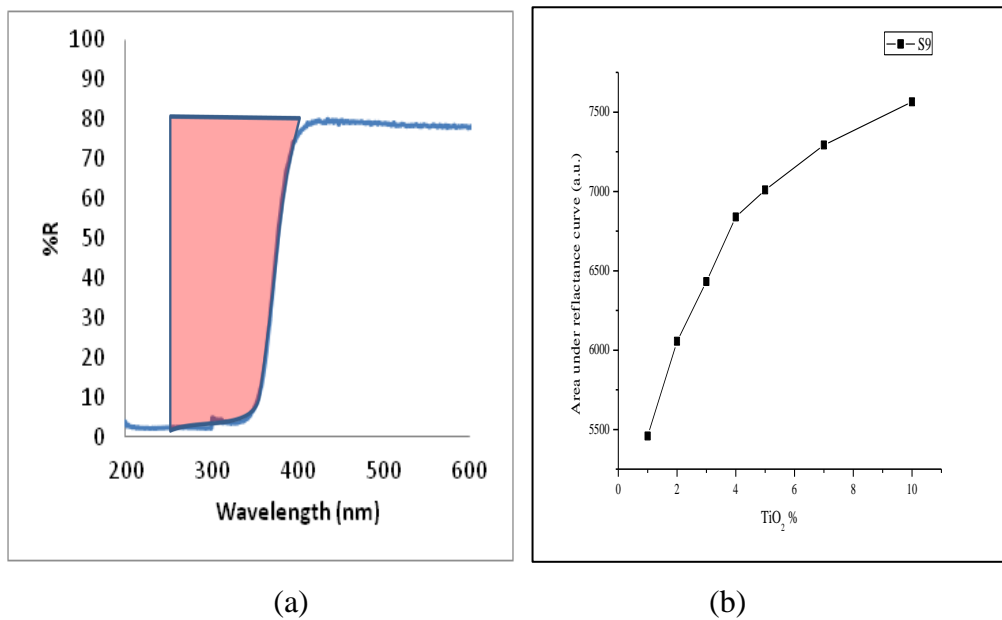


Figure E.2 a) Graphical representation of calculated area under UV absorption, b) the increase of the area intensity with TiO₂% content.

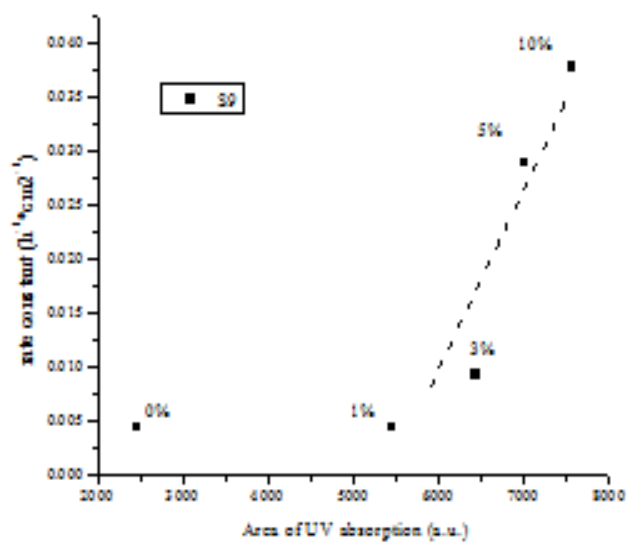


Figure E.3 Absorption area vs reaction rate correlation for S9 sample.

APPENDIX F

REPEATIBILITY EXPERIMENTS

Table F.1 Repeatability experiment results for UV illuminated area increase experiments of TiO₂ on glass

S13 on glass-0.004 g (under UV light)						
~2 cm ²		~5 cm ²		~10 cm ²		
k (1/h)	k (1/h×g _{cat})	k (1/h)	k (1/h×g _{cat})	k (1/h)	K (1/h×g _{cat})	
0.57	151	1.58	395	2.29	573	
0.63	158	2.10	525	2.61	653	
0.47	118	1.48	370	2.46	615	
0.60	150	1.44	360	2.58	645	
Average	0.57	144	1.65	413	2.49	622
S.D.	0.07	17.9	0.31	76.4	0.15	36.2

Table F.2 Repeatability experiment results for UV illuminated area increase experiments of TiO₂ on grout

S13 on grout-0.004 g (under UV light)						
~2 cm ²		~5 cm ²		~10 cm ²		
k (1/h)	k (1/h×g _{cat})	k (1/h)	k (1/h×g _{cat})	k (1/h)	K (1/h×g _{cat})	
0.20	50	0.26	65	0.34	85	
0.29	73	0.31	78	0.26	65	
0.18	45	0.35	88	0.28	70	
0.27	68	0.34	85	0.34	85	
Average	0.24	59	0.32	79	0.31	76
S.D.	0.05	13.6	0.04	10.2	0.04	10.3

Table F.3 Repeatability experiment results for 10% TiO₂ added grout experiments

Sample Code	1	2	3	Average		S.D.
	k (1/h)	k (1/h)	k (1/h)	k (1/h)	k (1/h×g _{cat})	
S1	0.601	0.618	0.449	0.556	0.589	0.093
S8	0.272	0.682	0.456	0.470	0.498	0.205
S9	0.676	0.880	0.713	0.756	0.801	0.109
S12	0.357	0.648	0.522	0.509	0.540	0.146
S13	0.506	0.412	0.323	0.414	0.439	0.092

Table F.4 Repeatability experiment results for TiO₂ on grout experiments

Sample Code	1	2	3	Average		S.D.
	k (1/h)	k (1/h)	k (1/h)	k (1/h)	k (1/h×g _{cat})	
S1	0.811	1.305	0.933	1.016	101.6	0.257
S8	0.559	0.410	0.730	0.566	56.6	0.160
S9	1.019	1.460	1.362	1.280	128	0.231
S12	0.654	0.744	1.021	0.806	80.6	0.191
S13	0.311	0.752	0.516	0.526	52.6	0.220

APPENDIX G

EXPERIMENTS CONDUCTED IN DARK CONDITIONS

The dark experiments done for similar amount and area were averaged for 10% TiO₂-grout samples and found as 0.06 1/h and this was assumed as average value for diffusive effects for 10%, 1% and TiO₂ coatings on grout. In these experiments, same coated area and amount was illuminated under UV light. This value was subtracted from UV irradiated results and then presented as benzene degradation results under UV illumination. In a typical calculation, For 10% S9-grout sample,

UV irradiated benzene decrease (1/h) – average dark benzene decrease (1/h) = benzene degradation under UV irradiation (1/h).

$$0.736 - 0.06 = 0.676 \text{ 1/h}$$

Averaged dark experiment results are given in Table G.1 and Table G.2.

Table G.1 Dark experiment results averaged and used for calculating 10%, 1%, TiO₂ on grout samples.

Sample Code	k (1/h)
10% S1	0.075
10% S8	0.058
10% S9	0.043
10% S12	0.089
10% S13	0.030
1% S8	0.065
average	0.06

*9.44 g grout are used in the experiments including TiO₂ mentioned as %. (20 cm²).

Table G.2 Dark experiment results averaged and used for calculating 2 cm² pure TiO₂ samples

Sample Code	Coating Amount (g)	k (1/h)
S1	0.0037	0.163
S8	0.0036	0.164
S9	0.0038	0.257
S12	0.0036	0.229
S13	0.0038	0.193
average		0.2

APPENDIX H

IR AND UV-VIS SPECTRA OF SOME MATERIALS USED IN THE STUDY

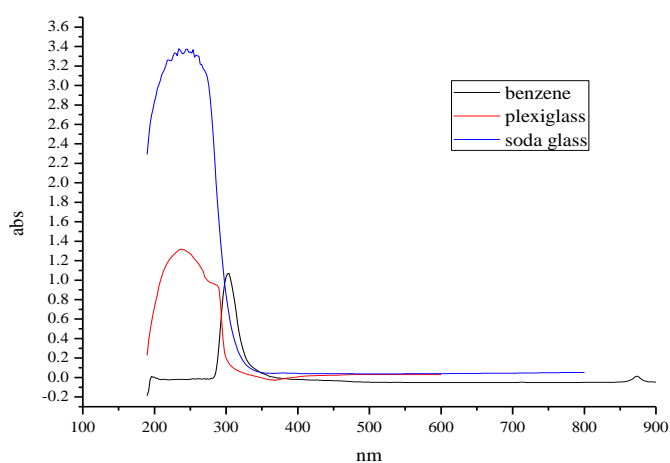


Figure H.1 UV-Vis Spectra of used materials in photocatalytic experiments.

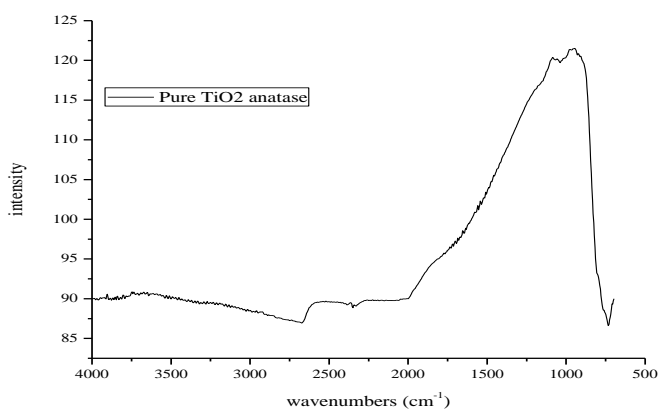


Figure H.2 Typical IR spectrum of anatase sample in ambient conditions.

APPENDIX I

COATING APPLICATION USING COMMERCIAL SILICONE BASED RESIN

I.1 HYDROPHILIC-HYDROPHOBIC STUDIES

A Resin-S13 formulation was formed and surface binding and superhydrophilic or superhydrophobic properties were observed and compared with empty resin and pure TiO_2 on glass. Both superhydrophobic and superhydrophilic properties were observed for different temperatures. TiO_2 was bound to the surface (Table I.1). The observations are based on eye. The finger test result was shown in Figure I.1.

I.2 EFFECT OF POST TREATMENT TO THE ACTIVITY

The activity of coatings was inspected parallel to superhydrophilic-superhydrophobic properties. The calcination temperature did not increase the activity. However, the coating gained superhydrophilic property and bound to the surface at 700°C . At this temperature, the coating was steeped to water treatment at RT and at 105°C . The post treatment resulted in increase in activity when boiling water was used.

Table I.1 Studies done for binding TiO₂ to the surface.

Empty binder on glass		S13-binder formulation on glass			S13 pure on glass	
	Super-hydrophilic or hydrophobic property (No UV inducing)	Binding to the surface	Super-hydrophilic or hydrophobic property (No UV inducing)	Binding to the surface and resin	Super-hydrophilic or hydrophobic property (No UV inducing)	Binding to the surface and resin
RT	Water in droplet form (No Rolling after 90° slope)	Yes	Water in droplet form	Yes	Yes	No
350°C	Water in droplet form (No Rolling after 90° slope)	Yes	Superhydrophobic (Rolling droplets with small slope)	Yes	Yes	No
500°C	-	-	Superhydrophobic effect was lost water in droplet form	Yes	-	-
650°C	-	-	Yes superhydrophilicity	Yes	-	-
700°C	Water in droplet form The droplet spreading angle increased. (No Rolling after 90° slope)	Yes	Superhydrophilic	Yes	Yes	Yes some improvement much better

Table I.2 Results of photocatalytic benzene oxidation activity test

	S13-binder formulation on glass k (1/h)	S13 pure on glass k (1/h)
RT	-	5.25
350°C	0.42-Boiling water 0.26	5.31
700°C	2.85-Boiling water 2.07-Boiling water 0.26-water 0.24	0.86



Figure I.1 Finger testing of S13-binder formulation prepared at 700°C.

APPENDIX J

ON THE MECHANISM OF PHOTOCATALYTIC CO₂ REDUCTION WITH WATER IN THE GAS PHASE

I want to give my sincere regards to Elsevier Publishing Group, since they give permission to use the article “On the mechanism of Photocatalytic CO₂ Reduction in the Gas Phase” into my thesis. The article is put here in the manuscript form without any change from the original pressed version [305]. The figures, tables and reference numbers are left in their original form. The references are given following the article.

On the Mechanism of Photocatalytic CO₂ Reduction with Water in the Gas Phase

Deniz Uner,* Mert Mehmet Oymak

Middle East Technical University Chemical Engineering Department, Ankara,
06531, Turkey

*Corresponding author: Tel: +90 312 210 26 01 Fax: +90 312 210 2600, e-mail:
uner@metu.edu.tr

Abstract:

The mechanism of photocatalytic reduction of CO₂ with H₂O over Pt-TiO₂ films produced by the sol gel deposition over glass beads was investigated. The accumulation of significant amount of carbonaceous intermediate on the surface followed by deactivation indicated the rate limiting reaction is the water splitting reaction, similar to the natural photosynthetic systems. When gas phase hydrogen was allowed in the system, the carbonaceous intermediates were converted to methane at rates higher than the artificial photosynthesis conditions. In the presence of hydrogen, formation of methane reaction proceeded in the dark albeit at lower rates. The progress of the reaction is very similar to the natural photosynthetic reactions however the rates are seven orders of magnitude slower than the reactions in the natural photosynthetic processes. Furthermore, the role of spilled over hydrogen in the reaction was also demonstrated.

Keywords: Artificial Photosynthesis, TiO₂, Pt, hydrogen spillover

1. Introduction

CO₂ reduction to hydrocarbons by harvesting solar energy is a promising approach since it may be the candidate to the solution of two problems: High CO₂ levels in the atmosphere which could not be compensated by CO₂ fixation cycles and future world fuel crisis which is inevitable due to long formation times of coal, natural gas or oil. In this paper, we report a comparative study of photocatalytic reduction of CO₂ with water and H₂ over sol-gel coated TiO₂ films promoted with Pt.

One of the pioneering works on CO₂ hydrogenation to methane was reported by Sabatier and Serenders in 1902 [1 and references therein]. In

recent years, the need for CO₂ mitigation prompted new studies on catalyst and process development for CO₂ based products. Very high methanation activities are reported for Ru doped Ceria, reasonable levels of methane production can be observed at temperatures as low as 300 K [1]. Ru is reported to be a very active catalyst, highest activity of hydrogenation of CO₂ to formic acid in a solution of triethylamine and ethanol was achieved at 80 °C [2]. The mechanism of CO₂ hydrogenation is still being debated: some studies report that the CO₂ hydrogenation proceeded similar to CO hydrogenation with an initial oxygen elimination step from the molecule via a surface formate intermediate over Ni/ZrO₂ catalysts [3], while some other reports indicate that CO and CO₂ hydrogenation reactions take place via different paths [1]. Over Fe and Co based Fischer Tropsch catalysts, it was observed that when the CO amounts in the feed gas (composed of CO, CO₂ and H₂) decreased, the FT product-distribution shifted exclusively to methane [4]. Later studies on K promoted F catalysts, the same group reported that the reverse water-gas shift reaction imposed a thermodynamic limit to conversions and therefore selectivity, supporting their arguments with a mathematical model [5].

Not just the catalyst, but also the reactor type influences the product distribution and selectivity. Later studies on Group VIII catalysts indicated that the product distribution and site time yields are strong functions of the reactor type: among fixed bed, fluidized bed and slurry reactor types, fluidized bed and slurry type reactor performances better than the fixed bed reactor for CO₂ conversions and hydrocarbon selectivities [6]. These findings indicate that the micromixing conditions impose significant influence over the selectivities; a topic which is not as broadly covered by the catalysis community as it is needed. The catalyst structure examined along the length of a packed bed reactor revealed that the catalysts at the inlet of the reactor undergone phase transformations while at the exit the carbide formations deactivated the catalyst [7]. All of these indicate the complexity of the reaction scheme, and the need to understand not just the catalyst and its

microstructure, but also the need to tailor the operating conditions for higher selectivities towards the desired products.

Over Rh/SiO₂ catalysts, it was observed that the metal loading had a significant effect of the CO₂ hydrogenation selectivity: over 1% Rh/SiO₂ catalysts the selectivity of the CO₂ reaction was towards CO, resulting from the formation of Rh carbonyl clusters stabilized by OH groups on the surface of silica, while the large particles yielded mainly methane due to the low amount of silanol groups adjacent to Rh sites over large particles inhibited the formation of Rh carbonyls [8].

The adsorption of CO₂ over TiO₂ is also one of the challenges of the scientific community. The adsorption sites, the O-C-O bond angle upon adsorption, bending induced changes in the LUMO of the molecule and the resultant change in the electron transfer to the adsorbed molecule is very nicely reviewed in a recent article [9]. In summary, it was reported that CO₂ adsorption occurred at five coordinate Ti⁺⁴ sites and oxygen vacant sites created by vacuum annealing on TiO₂ (110) single crystals [10]. According to DFT studies on triplet defect-free clusters, CO₂ and stoichiometric TiO₂ anatase do not lead to charge transfer and form CO₂^{*-}, the transfer is possible for surface defects such as steps, kinks and vacancies [11]. Bicarbonate formation is also seen on anatase TiO₂ which is very labile [12, 13]. No dissociation of CO₂ occurs on anatase TiO₂ [12, 14, 15]. CO₂ dissociation is seen on Pt/TiO₂ by using FTIR at RT and XPS [16, 17]. It is also important to mention here that Pt brings in its own activity to the reaction by efficient adsorption and dissociation of O₂ in the dark than TiO₂, reverse spillover process for hydrogenation, enhancing the activity of OH sites which acts as hole traps [18]. Photocatalytic CO₂ reduction with H₂ [19] is studied on titania and CO and CH₄ evolution have been observed. In the same study, the enhancing effect on CH₄ production is shown when H₂O was added besides H₂ as reactant. Methanation of CO₂ with H₂ has been observed on Ru/TiO₂ at RT and atmospheric pressure which is greatly enhanced with photoirradiation [20].

Photoreduction of CO_2 by H_2 occurred on Rh/TiO_2 under low pressure and RT [21]. Product change has been observed from CO to CH_4 when oxidation state of Rh has changed to metallic state. This was explained by the suppression in the H_2 dissociation ability by Rh in an oxide state [21]. Hydrogen remaining adsorbed on the solid after reduction promotes the dissociation of CO_2 on Rh/TiO_2 [22-24]. On TiO_2 (110) surfaces, heating of the hydrogenated sample did not lead to recombinative desorption of H_2 (or H_2O) molecules, contrary to the observation over hydroxylated oxide surfaces, but to migration of H atoms into the bulk [25]. Hydrogen molecule spills over on $\text{Pt}-\text{TiO}_2$ systems at low temperatures [26]. Hydrogen spillover effect was studied with conductivity measurements [26, 27], NMR [28], ESR [29] studies.

Table 1. Water Splitting Reaction Rates on TiO₂ Photocatalysts

Photocatalyst	H ₂ Production rate (μmol/g _{cat} -h)	Initial production rate ^a (μmol/g _{cat} -h)	O ₂ production rate, (μmol/g _{cat} -h)	Conditions	References
1% Degussa P25 SCR ^b SO ₄	2.72	1.6	20.64	TiO ₂ initial concentration. 0,75 g/l, 2 mM Ce ₂ (SO ₄) ₃ pH = 1, T= 20 °C	[33]
Fe (1.2% wt.) doped TiO ₂	15.5	-	-	Distilled water	[34]
Rh/TiO ₂ (MCB [®])	1497	1497	748.5	10 % wt. NaOH soln.	[35]
Pt/TiO ₂ -A1 + TiO ₂ -R2 mix ^c	360	240	180	40 mmol NaI, pH = 11, 0.5% wt. Pt loading	[36]
Au/TiO ₂ - P25	7200	-	4200	1% vol. MeOH, 2% wt Au loading	[37]
Au/FP5 ^d	52.4	110	-	Distilled water, FP5 Xylene/Pyridine = 8/2	[38]
Au/FP5 ^d	7890	7890	-	6% vol MeOH, FP5 Xylene/Pyridine = 8/2	[38]
1 % Pt/TiO ₂	3000	3000	-	Pure ethanol, T = 71 °C	[39]

^aConverted from line graph using initial data. ^b Soft Chemical Reduction ^cA:Anatase,R:Rutile ^d Flame Spray Pyrolysis

Table 2. Photocatalytic CO₂ reduction rates

Photocatalyst	CH ₄ production rates (μmol/gTiO ₂ -h)	CH ₄ initial production rates ^a (μmol/gTiO ₂ -h)	CH ₃ OH production rates (μmol/gTiO ₂ -h)	Reductant	Light Source	References
1%Rh / TiO ₂	-	-	0.53	Water (l)	500W high Pressure Xe Lamp	[40]
1%Rh + TiO ₂ + 2%WO ₃	-	-	3.97	Water (l)	500W high Pressure Xe Lamp	[40]
TiO ₂ on glass (Vycor [®])	0.1 ^b	-	0.02	Water (g)	75W Hg lamp >280 nm	[41]
JRC-TiO-4 ^c	0.2	-	-	Water (g)	75W Hg lamp >280 nm	[42]
ex ^d -Ti-oxide/Y-zeolite	4.2 ^b	6.7	2.78	Water (g)	75W Hg lamp	[43]
Pt - ex ^d -Ti-oxide/Y-zeolite (1%)	7.3 ^b	-	0.53	Water (g)	75W Hg lamp	[43]
Ti-MCM-48	7.7 ^b	-	3.07	Water (g)	Hg lamp	[44]
Pt-Ti-MCM-48 (1%)	12.3 ^b	-	0.28	Water (g)	Hg lamp	[44]
Pt-Ti-MCM-48 (0.1%)	9.6 ^b	-	1.02	Water (g)	Hg lamp	[44]
Ti-MCM-41	1.8 ^b	-	0.8	Water (g)	100W Hg Lamp	[45]
Ti-PS (h,50) ^e	4.3 ^b	-	1.13	Water (g)	100W Hg Lamp	[45]
Ti-β(F) ^f	0.4 ^b	-	0.31	Water (g)	100W High pressure Hg lamp	[46], [47]
TS-1	0.8 ^b	-	0.25	Water (g)	100W High pressure Hg lamp	[46]
Ti-β(OH) ^g	3.5 ^b	-	0.43	Water (g)	100W High pressure Hg lamp	[46]
P25	0.2 ^b	-	-	Water (g)	100W High pressure Hg lamp	[46]
TiO ₂ on pyrex glass	1.4 ^a	1.8	-	H ₂	UV light 365 nm	[19]
TiO ₂ on pyrex glass	1.7 ^a	2.2	-	Water (g)	UV light 365 nm	[19]
TiO ₂ on pyrex glass	4.1 ^a	16.1	-	Water (g)	UV light 365 nm	[19]
Ti-SBA-15	63.9 ^b	-	16.6	Water (g) + H ₂	100W Hg lamp >250 nm	[48]
Cu-Fe(0.5wt%)-P25 on glass	0.06	-	-	Water (g)	150W Hg lamp	[49]
Cu-Fe(0.5wt%)-P25 on fiber optic cable	0.9	-	-	Water (g)	150W Hg lamp	[49]
Cu-Fe(0.5wt%)-P25 on fiber optic cable	0.3	-	-	Water (g)	Sun light	[49]
TiO ₂ (in pellet form) (Degussa P25)	0.0025 ^a	-	-	Water (g)	1.6W Germicidal lamp 253 nm	[50]
TiO ₂ coated beads	4.3 ^a	5.0	-	Water (g)	150W Hg lamp	[51]
Pt-TiO ₂ coated beads (0,25%)	11.5 ^a	17.2	-	Water (g)	150W Hg lamp	[51]

^a Converted from line graph using initial data. ^b Converted from bar graph ^c Reference standard catalyst from Catalysis Society of Japan ^d Prepared by ion exchange ^e PS: Pore structure, (h,50):hexagonal structure with a Si/Ti ratio of 50. ^f Ti- β zeolite synthesized under hydrothermal conditions using F⁻ ions as anions of structure directing agent. ^g Ti- β zeolite synthesized under hydrothermal conditions using OH⁻ ions as anions of structure directing agent.

Unfortunately, the engineering aspects, yields and selectivities of photocatalytic CO₂ reactions are not as extensively studied due to the slow rates of the reaction requiring primarily batch processes. Furthermore, the photocatalytic CO₂ reduction with H₂O, or artificial photosynthesis, reactions are further hampered by the additional resistances due to the water splitting kinetics. We have reviewed the literature for the photocatalytic water splitting rates as well as CO₂ reduction rates and presented a sample pool of the results in Tables 1 and 2. The immediate conclusion we can draw from the data presented in Tables 1 and 2 is that photocatalytic water splitting reactions have higher rates than CH₄ formation rates. However, this fact has to be taken with some caution: the highest rates observed in photocatalytic water splitting reactions have sacrificial reagents such as MeOH or NaOH in the system thus the true rates of water splitting are a little bit elusive under the reported conditions. Similar to the catalytic CO₂ reduction reaction with H₂ over unpromoted Fe catalysts [4], the primary product of photocatalytic CO₂ reduction reaction with water is methane. A recent report [30] challenges the low production rates of methane formation during artificial photosynthesis reactions. The authors studied the CO₂ reduction rates with ¹³C labeled CO₂ to observe that formed methane is mostly ¹²C indicating that the methane evolution was a result of the structural carbon remained in the catalyst from residual organic material of the starting precursor. Although this challenge is genuine, the vast amount of information pouring in the knowledgebase about

highly active catalysts operating at low temperatures without illumination cannot be disregarded [1,2].

In this study, we report the carbon deposition over Pt/TiO₂ structures, and the removal rates of the carbon with water and with H₂ under photo driven and thermally driven reaction conditions. Our results indicate that the photocatalytic activation is predominantly required for water splitting reaction and in the presence of gas phase H₂, the methane formation rates from the surface carbon layer are much higher than that observed during the photocatalytic reduction of CO₂ with water.

2. Experimental

2.1. Catalyst Preparation

The sol was prepared by mixing Ti(OC₃H₇)₄, C₂H₅OH, CH₃COOH, H₂O at the ratio [15:90:1:1] respectively [31]. The solution was mixed for 15h. The glass beads were dip-coated (dipping rate: 7.5 cm/min - 10 min holding in the solution) 1-3-5 times with the sol, dried at 120⁰C and calcined in the end at 450⁰C for 5 h. Several layers were coated as such. Pt incorporated into the structure by adding Pt precursor (Pt(NH₃)₄Cl₂.H₂O) into the solution in 0.1 mol %. These samples are indicated as (Pt(in)-TiO₂). In addition, for reaction tests in series, Pt was dip-coated on the surface of 5 times coated Pt(in)-TiO₂ glass beads by the same procedure using Pt precursor dissolved in water. These samples are indicated as (Pt(on)-Pt(in)-TiO₂). The samples were further calcined at 450⁰C for 5 h for Pt activation.

2.2. Catalyst characterization:

The XRD measurements of the catalysts were performed using Rigaku D/Max 2200 PC X-Ray Diffractometer using Cu-K α radiation. BET measurements were done with Micromeritics Gemini V Surface Area and Pore Size Analyzer. HR-TEM analysis was performed on a JEOL JEM 2100F field emission gun scanning transmission electron microscope operating at an accelerating voltage of 200 kV using a single tilt holder. Specimen was prepared after scraping the film by a scalpel from the glass substrate as powder, dispersing this powder in ethanol in an ultrasonic bath for 10 min. The solution was dropped on copper grids covered with lacey carbon films.

2.2 Reaction Tests

The reaction tests were carried out in a Pyrex manifold (79,7 cm³) connected to a high vacuum system (10⁻⁶ Pa range) under batch conditions. Prior to the reaction measurements, H₂ pretreatment was done over the catalyst for 2 h at 220°C around 250 torr gas pressure while replacing H₂ gas was replaced every hour. After the reduction the manifold was evacuated and the sample was cooled to room temperature under vacuum. After ensuring that all the gases were evacuated from the manifold, liquid water was injected in the manifold with a syringe through the sampling septum and allowed to evaporate to its vapor pressure ~20 Torr at room temperature. CO₂ gas was introduced into the manifold to bring the total pressure to around 680 Torr. The reaction was allowed to progress under UV light or in dark. The reaction products were collected using a syringe from the gas phase and were analyzed by Varian 3900 GC with FID detector and PoraPLOT Q capillary column at every 30 min. After 2h of reaction progress, the chamber was evacuated and fresh gases were introduced. The vacuuming time between runs was kept at 10-15 min. UV irradiation of the catalysts was carried out using a 100-W high pressure Hg lamp (average λ ~365 nm). Due to the heating of the reaction chamber by

irradiation, the chamber was at ~80-85°C. When the gas phase was pure H₂, the chamber pressure was kept at 680 Torr.

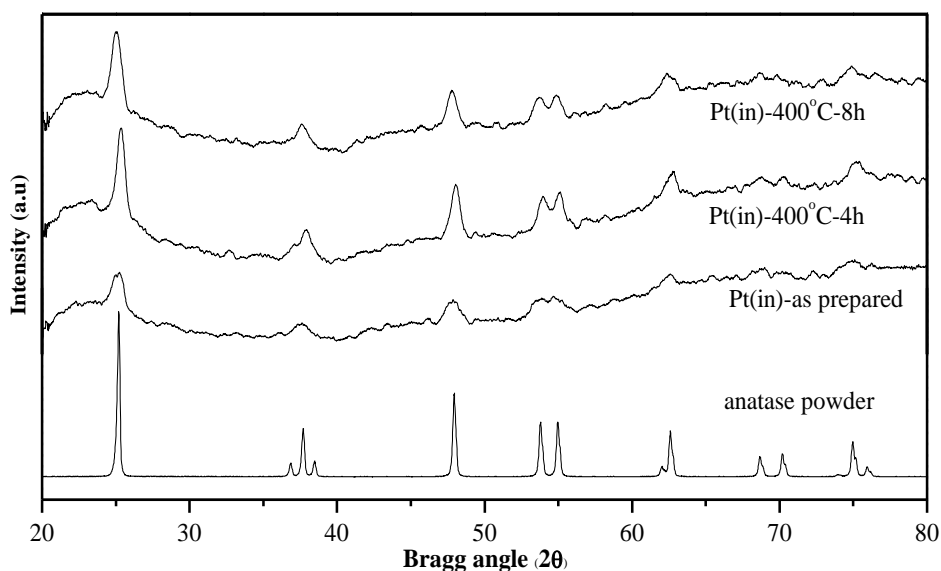
3. Results and Discussion

The objective of this work was to investigate the CO₂ reduction performance of sol gel coated TiO₂ films. The effect of Pt metal introduced into the sol-gel structure as well as added on the films by incipient wetness technique was also investigated. In this part, the results of this study and our interpretations for the future material design will be presented.

The crystal structures of the sol-gel coated films with Pt incorporated both in and on the structures monitored by XRD are given in Fig. 1. The XRD data of the films are compared to the XRD structures of pure anatase powder. In Fig. 1a TiO₂ films with Pt added in the sol are presented. The pretreatment procedure was definitely not sufficient to form crystalline phases as the increase in the calcination temperatures increased the crystallinity indicated by the increase in the Anatase related peaks with increasing duration of the calcination. On the other hand, not much variation in the peaks were observed for the samples when more Pt was added by incipient wetness technique, as seen in Fig. 1b. Due to the low amounts of the samples, the diffraction patterns exhibit very low signal to noise ratio. However, the data can be used to confirm the formation of the anatase phase based on the peaks at $2\theta = 25.28$ and 48.05 . The XRD patterns of the samples further calcined for 4 h and 8 h revealed a lack of change, indicating the completion of calcinations and the formation of long range order. Furthermore, the lack of change also confirms that the calcination of the samples was sufficient to remove all the organic phase [30] and the formation of TiO₂ phase would not be altered with further calcinations. The HR-TEM image shown in Fig. 1c confirms the crystallinity of the Pt. It is even possible to observe Moire fringes on some of

the particles. Furthermore, the crystal planes of TiO_2 are also clearly visible in the image indicating the formation of long range order.

The effect of the film thickness on the activity was tested for pure and Pt containing sol-gel films of TiO_2 . The motivation for this part of the study was to investigate the effect of Pt “doped” in the structure on the CO_2 reduction activity of TiO_2 films. In Fig. 2, the results of film thickness on the catalytic activity under photocatalytic water reduction of CO_2 were presented. The reaction rates were presented normalized to the amount of the catalyst presented. It was observed that the methane evolution rates did not change much when the film thicknesses were increased. The results are interpreted as the formation of a tortuous TiO_2 structure such that the lower layers were accessible to illumination and also to chemical conversion.



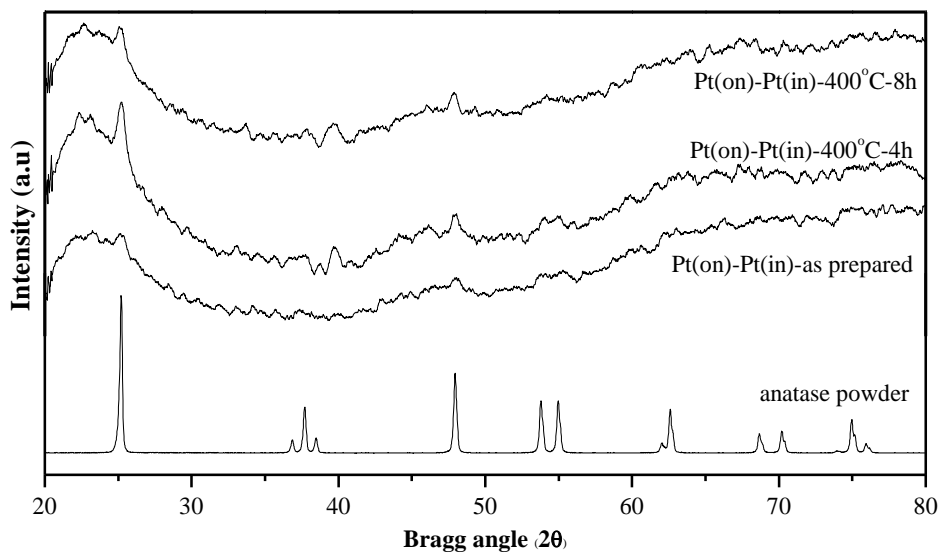


Fig. 1. XRD patterns of the TiO₂ films coated on the glass beads (a)TiO₂ films with Pt incorporated in the sol prior to calcinations, calcined at three stages; (b) The films are further coated with Pt via the incipient wetness technique and (c) the corresponding HR-TEM image containing Pt incorporated via incipient wetness technique.

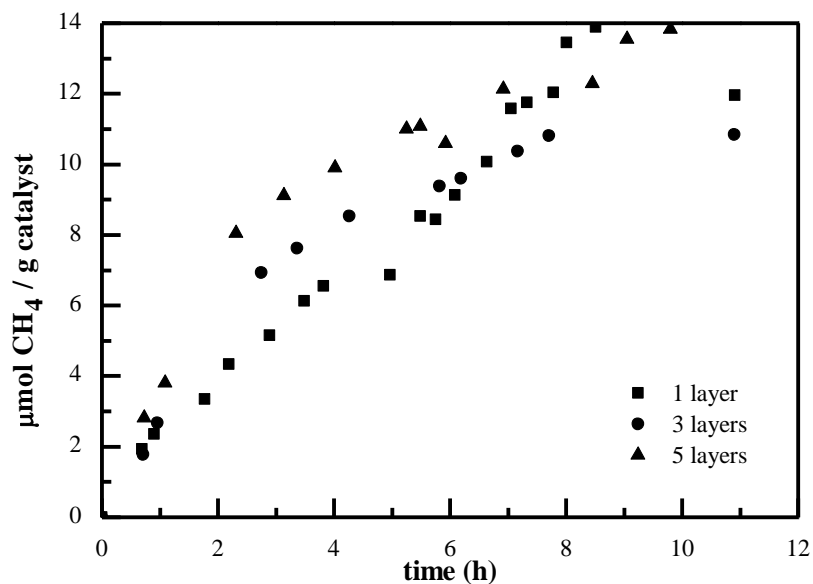


Fig. 2. The photocatalytic methane formation rates from CO₂ and H₂O over pure TiO₂ films. The activities are reported normalized to the amount of the catalyst.

When Pt(in) samples were tested for photocatalytic CO₂ reduction reaction with H₂O, it was observed that the activity of the films with one layer of coating was greater than the other samples (Fig. 3). In fact, a systematic decrease of the methane formation rates was observed with increasing film thickness. This was interpreted as Pt catalyzed crystallization of the TiO₂ structures. The tortuous framework observed in the pure films was no longer present. The BET analysis of the films revealed that the Pt containing films indeed had lower surface areas.

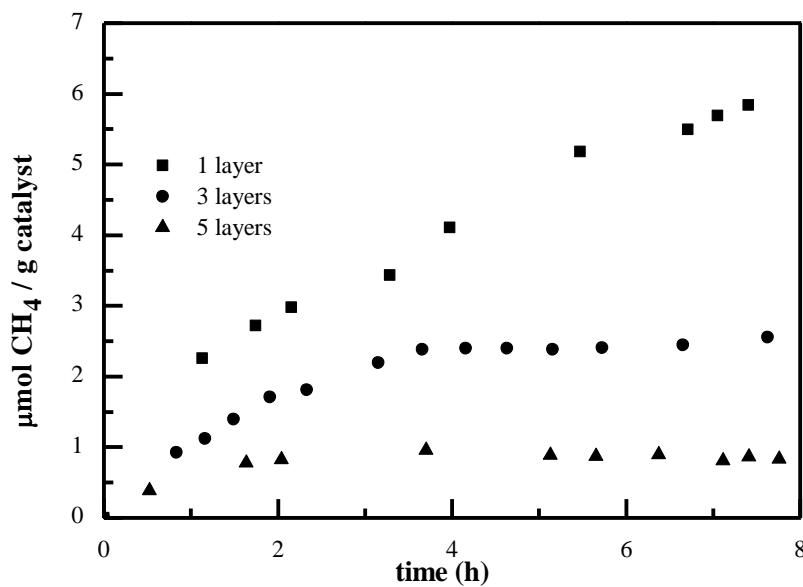


Fig. 3. The photocatalytic methane formation rates from CO₂ and H₂O over TiO₂ films containing Pt in the structure. The activities are reported normalized to the amount of the catalyst.

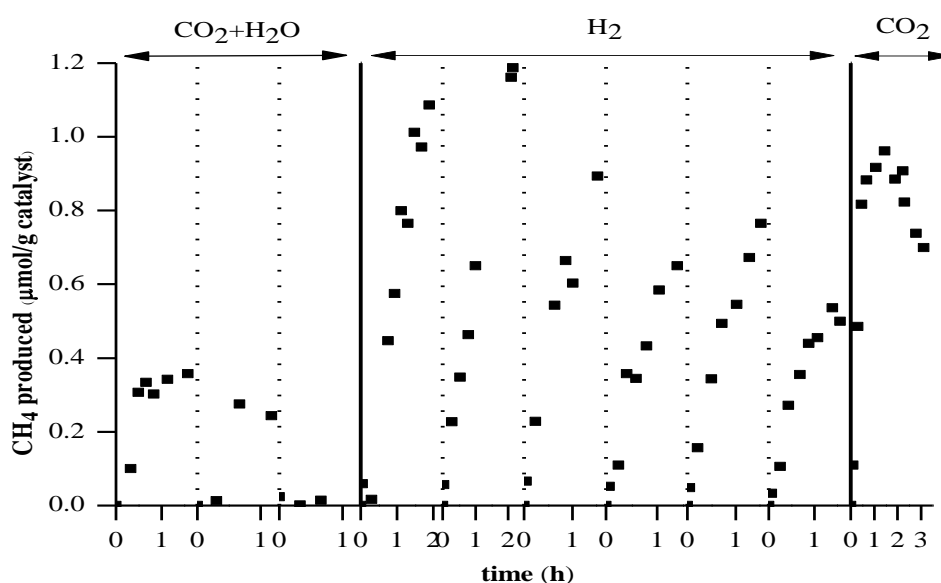
Table 3. Photocatalytic CO₂ reduction rates obtained in this study along with the specific surface areas of the samples

Catalyst	BET surface Area (m ² /g)	Rate (μmol/g cat.h)
TiO ₂ -1 layer	-	2.05
TiO ₂ -3 layer	49	2.55
TiO ₂ -5 layer	63	3.50
Pt-TiO ₂ -1 layer	-	1.53
Pt-TiO ₂ -3 layer	43	0.94
Pt-TiO ₂ -5 layer	29	0.44

After this point, it was decided to look for the methane formation mechanisms over the samples which had the most dense structure. The sample with Pt incorporated in the TiO₂ sol with further Pt added via incipient wetness technique was chosen for further study. The sample was exposed to different gas atmospheres and the results of the photocatalytic methane production reaction are presented in Fig. 4. There are three different reaction zones, and the vertical dotted lines indicate evacuating the system and replenishing the gas phase atmosphere. In the first reaction zone, CO₂ reduction with water vapor was followed. The deactivation of the catalyst could be followed by the activity loss with each subsequent gas replenishment. In the second reaction zone, only gas phase H₂ was provided and the reaction products with respect to time was followed. In this zone, no carbon source was available except the carbon deposited on the surface most probably in the form of a surface carbonate. It is clear that the rate of methane formation was much faster, and a significant amount of methane was formed during this reaction zone. After the methane formation rates decreased to that of the fresh catalyst, the system was evacuated and pure CO₂ was delivered in the reaction chamber with no source of hydrogen (Third reaction zone). In this zone significant formation of methane was still observed, due to the presence of spilled over hydrogen over TiO₂ surface.

In order to demonstrate that the hydrogen spilled over from the metal to TiO₂, the fresh catalyst was reduced with hydrogen followed by a brief evacuation period ensuring that spilled over hydrogen is not removed from the catalyst (10 min, in this system) [28]. Subsequently, CO₂ was sent to the chamber, and the kinetics of the methane formation was monitored. The results are presented in Fig. 5. The follow up figures indicate the presence of only one reactant, (CO₂ or H₂) and the other reactant is present in the system as a surface intermediate. In the first step, the spilled over hydrogen over the support is used to reduce CO₂. In the second step, we observe a very high rate of methane formation. Methane forms from the carbon containing

intermediate over the surface via the hydrogen adsorbed on the surface from the gas phase. After 1 h of monitoring the kinetics, the system was evacuated and fresh hydrogen was fed to the system. The decrease in the methane formation rates upon each hydrogen dose was due to the depletion of the carbon intermediate over TiO_2 surface. In the last frame, the system was dosed with pure CO_2 and methane formation kinetics from spilled over hydrogen was monitored. It is important to note that the methane formation rates in the first and the last steps are similar indicating that the activity of the catalyst was not altered during the tests.



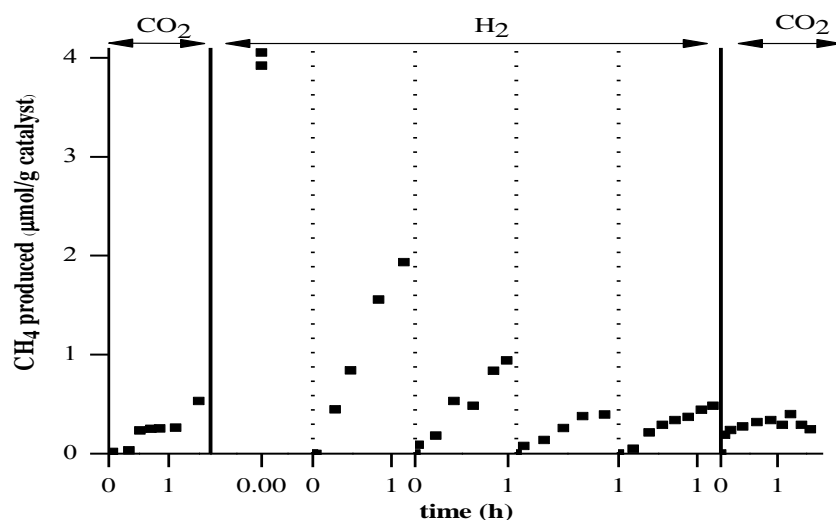


Fig. 5. Methane formation rates under different reaction conditions: first frame; methane formation from residual hydrogen on the surface from reduction and gas phase CO₂; next five frames; methane production from surface carbon intermediate and gas phase hydrogen; last frame; methane formation from surface hydrogen and gas phase CO₂.

Finally, the dark reaction kinetics of CO₂ reduction with hydrogen was followed. For this purpose, the surface of the catalyst was populated with the carbon containing intermediate by exposing CO₂+H₂O mixture twice and irradiated under UV for 1 h each and methane formation kinetics were monitored (Fig. 6). After establishing that the surface is coated with carbon containing intermediate, the dark reaction kinetics upon hydrogen exposure was followed. Methane formation was observed, but the rates were lower than that observed under UV irradiation (Fig. 5) and the activity was lost immediately. The effect of temperature was also monitored by setting the temperature to 85°C and higher rates of methane formation was observed in the dark. It should be noted that the methane formation rates exhibited a peak

during these tests which needs further exploration of the surface reaction mechanism. In the last step of the measurements, the methane formation rates were monitored in the presence of hydrogen gas only and under UV irradiation. The rates under UV irradiation are much higher than the dark reaction kinetics indicating a thermal and a photocatalytic component of the surface carbon containing intermediate hydrogenation.

All of these experiments indicated that during the photocatalytic reduction of CO_2 with water, a significant carbon containing intermediate deposition took place. The carbon containing intermediate deposition started as surface HCO_3^- formed from CO_2 and surface OH groups [13]. Once dissociated hydrogen is available, the surface intermediate was immediately converted to methane. Hydrogen is present over the surface as spilled over form, and it can resist evacuation due to the surface diffusion resistance [28]. These results present a different perspective and can be used to design photocatalytic CO_2 reduction systems.

The results presented in this study reveal striking similarities between natural and artificial photosynthesis systems. The experiments intended to elucidate the mechanism of reduction of CO_2 with H_2O over TiO_2 surfaces revealed that it was very easy to accommodate CO_2 on basic TiO_2 structures. CO_2 was essentially titrating the OH groups present over TiO_2 and forming HCO_3^- structures similar to the accommodation of the CO_2 via the CAM (Crassulacean Acid Metabolism) in Cacti and succulent plants.

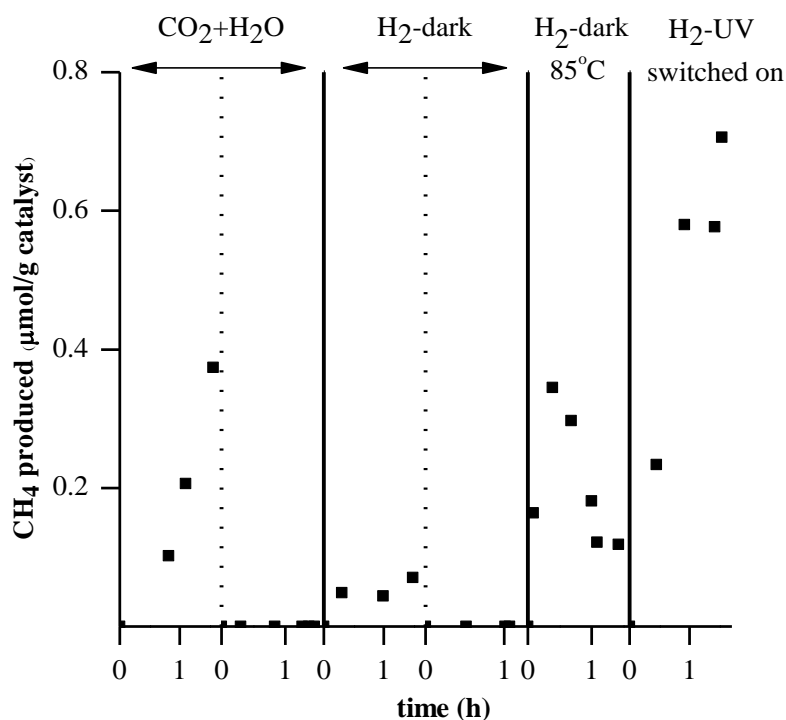


Fig. 6. Dark kinetics of methane formation after artificial photosynthesis conditions; first two frames; UV irradiated CO₂+H₂O reactants; next two frames; methane production in dark from surface carbon intermediate and gas phase hydrogen; 5th frame; methane production in dark at 85°C from surface carbon intermediate and gas phase hydrogen; last frame; methane production from surface carbon intermediate and gas phase hydrogen under UV illumination.

There are two important steps in the artificial (and natural) photosynthesis systems. One is the activation of CO₂ and the other one is the activation of H₂O. The data presented above clearly indicated that the adsorption and accommodation of CO₂ is not limiting the rate of methane formation. On the other hand, production of protons and electrons, or hydrogen atoms, is the rate limiting step in the overall process. As can be seen from the data compiled from the literature, the rates of methane formation are

close to the rates of photocatalytic water splitting in neutral conditions when no sacrificial agents (such as methanol) are present. It is also important to note that the photocatalytic water splitting rates are still 6-7 orders of magnitude behind the rates of water splitting in the photosynthetic cells [32]. Thus, while there is a huge room for improvement of the artificial photosynthesis mechanisms, the role of the surface and interface transport mechanisms in enhancing the rates and selectivities towards glucose in the photosynthesis is still waiting to be explored for designing efficient artificial photosynthesis systems.

4. Conclusions

Photocatalytic reduction of CO₂ with H₂O was limited by the rates of water splitting reaction, similar to the natural photosynthesis. Carbon deposition over the photocatalyst surface was identified, which could be removed by a hydrogen dose, indicating that the carbon was in partially hydrogenated form. Spilled over hydrogen was responsible for the final hydrogenation step. Furthermore, in the presence of gas phase hydrogen, significant dark activity was also present.

Acknowledgements

This work was supported by TUBITAK under research grant nos: 106Y075 and 107M447. Scholarship for MMO from SANTEZ program in collaboration with Kalekim and Turkish Ministry of Industry and Trade under grant no 00336.STZ.2008-2 is kindly appreciated. The authors are grateful to METU Central Laboratory and Prof. H.J.Kleebe, Mathis M.Muller, Margarete Schlosser for TEM analysis.

6. References

- [1] S. Sharma, Z.P. Hu, P. Zhang, E.W. McFarland, H. Metiu, *J. Catal.*, 278 (2011) 297.
- [2] C.Y. Hao, S.P. Wang, M.S. Li, L.Q. Kang, X.B. Ma, *Catal. Today*, 160 (2011) 184.
- [3] C. Schild, A. Wokaun, R. A. Koepfel, A. Baiker, *J. Phys. Chem.*, 95 (1991) 6341.
- [4] T. Riedel, M. Claeys, H. Schulz, G. Schaub, S.S. Nam, K.W. Jun, M.J. Choi, G. Kishan, K.W. Lee, *Appl. Catal. A-Gen.*, 186 (1999) 201.
- [5] T. Riedel, G. Schaub, K.W. Jun and K.W. Lee, *Ind. Eng. Chem. Res.*, 40 (2001) 1355.
- [6] J.S. Kim, S. Lee, L. S.B., M.J. Choi and K.W. Lee, *Catal. Today*, 115 (2006) 228.
- [7] S.C. Lee, J.S. Kim, W.C. Shin, M.J. Choi and S.J. Choung, *J. Mol. Catal. A- Chem.* 301 (2009) 98.
- [8] H. Kusama, K.K. Bando, K. Okabe and H. Arakawa, *Appl. Catal. A-Gen.*, 197 (2000) 255.
- [9] V.P. Indrakanti, J.D. Kubicki, H.H. Schobert, *Energ. Environ. Sci.*, 2 (2009) 745.
- [10] M.A. Henderson, *Surf. Sci.*, 400 (1998) 203.
- [11] V.P. Indrakanti, H.H. Schobert and J.D. Kubicki, *Energ. Fuel.*, 23 (2009) 5247.
- [12] G. Ramis, G. Busca and V. Lorenzelli, *Mater. Chem. Phys.*, 29 (1991) 425.
- [13] K. Tanaka and J.M. White, *J. Phys. Chem.*, 86 (1982) 4708.
- [14] J. Rasko and F. Solymosi, *J. Phys. Chem.*, 98 (1994) 7147.
- [15] J. Rasko, *Catal. Lett.*, 56 (1998) 11.
- [16] K. Tanaka and J.M. White, *J. Phys. Chem.*, 86 (1982) 3977.

- [17] K. Tanaka, K. Miyahara and I. Toyoshima, *J. Phys. Chem.*, 88 (1984) 3504.
- [18] D. Uner, The effect of addition of Pt on the gas phase photocatalysis over TiO₂, in: M. Anpo, P.V. Kamat (Eds.), *Environmentally benign photocatalysts: Application of Titanium oxide based materials*, Springer, New York, 2010, pp. 479-502.
- [19] C.C. Lo, C.H. Hung, C.S. Yuan and J.F. Wu, *Sol. Energ. Mat. Sol. C.*, 91 (2007) 1765.
- [20] K.R. Thampi, J. Kiwi and M. Gratzel, *Nature*, 327 (1987) 506.
- [21] Y. Kohno, H. Hayashi, S. Takenaka, T. Tanaka, T. Funabiki, S. Yoshida, *J. Photoch. Photobio. A*, 126 (1999) 117.
- [22] F. Solymosi, A. Erdohelyi and T. Bansagi, *J. Chem. Soc. Faraday T. I*, 77 (1981) 2645. [23] M.A. Henderson and S.D. Worley, *J. Phys. Chem.*, 89 (1985) 1417.
- [24] M.L. McKee, C.H. Dai and S.D. Worley, *J. Phys. Chem.*, 92 (1988) 1056.
- [25] X.L. Yin, M. Calatayud, H. Qiu, Y. Wang, A. Birkner, C. Minot and C. Woll, *Chemphyschem*, 9 (2008) 253.
- [26] U. Roland, R. Salzer, T. Braunschweig, F. Roessner and H. Winkler, *J. Chem. Soc. Faraday T.*, 91 (1995) 1091.
- [27] U. Roland, T. Braunschweig and F. Roessner, *J. Mol. Catal. A-Chem.*, 127 (1997) 61.
- [28] D.O. Uner, M. Pruski and T.S. King, *J. Catal.*, 156 (1995) 60.
- [29] T.M. Salama, H.K. Ebitani, H. Hattori and H. Kita, *Chem. Mater.*, 6 (1994) 21.
- [30] C.C. Yang, Y.H. Yu, B. vander Linden, J.C.S. Wu and G. Mul, *J. Am. Chem. Soc.*, 132 (2010) 8398.
- [31] K. Hayek, R. Kramer and Z. Paal, *Appl. Catal. A-Gen.*, 162 (1997) 1.
- [32] D. Uner, M.M. Oymak, B. Ipek, *Int. J. Global Warming* 3 (2011) 142.
- [33] E.A. Kozlova, T.P. Korobkina, A.V. Vorontsov and V.N. Parmon, *Appl. Catal. A-Gen.*, 367 (2009) 130.

- [34] R. Dholam, N. Patel, M. Adami and A. Miotello, *Int. J. Hydrogen Energ.*, 34 (2009) 5337.
- [35] K. Yamaguti and S. Sato, *J. Chem. Soc. Faraday T. I*, 81 (1985) 1237.
- [36] R. Abe, K. Sayama, K. Domen and H. Arakawa, *Chem. Phys. Lett.*, 344 (2001) 339.
- [37] O. Rosseler, M.V. Shankar, M.K.L. Du, L. Schmidlin, N. Keller and V. Keller, *J. Catal.*, 269 (2010) 179.
- [38] G.L. Chiarello, E. Selli and L. Forni, *Appl. Catal. B-Environ.*, 84 (2008) 332.
- [39] Y.Z. Yang, C.H. Chang and H. Idriss, *Appl. Catal. B-Environ.*, 67 (2006) 217.
- [40] F. Solymosi, I. Tombacz, *Catal. Lett.*, 27 (1994) 61.
- [41] M. Anpo and K. Chiba, *J. Mol. Catal.*, 74 (1992) 207.
- [42] M. Anpo, H. Yamashita, Y. Ichihashi and S. Ehara, *J. Electroanal. Chem.*, 396 (1995) 21.
- [43] M. Anpo, H. Yamashita, Y. Ichihashi, Y. Fujii and M. Honda, *J. Phys. Chem. B*, 101 (1997) 2632.
- [44] M. Anpo, H. Yamashita, K. Ikeue, Y. Fujii, S.G. Zhang, Y. Ichihashi, D.R. Park, Y. Suzuki, K. Koyano and T. Tatsumi, *Catal. Today*, 44 (1998) 327.
- [45] I. Keita, S. Nozaki, M. Ogawa and M. Anpo, *Catal. Today*, 74 (2002) 241.
- [46] M. Kitano, M. Matsuoka, M. Ueshima and M. Anpo, *Appl. Catal. A-Gen.*, 325 (2007) 1.
- [47] K. Ikeue, H. Yamashita, M. Anpo and T. Takewaki, *J. Phys. Chem. B*, 105 (2001) 8350.
- [48] J.S. Hwang, J.S. Chang, S.E. Park, K. Ikeue and M. Anpo, *Top. Catal.*, 35 (2005) 311.
- [49] T.V. Nguyen, J.C.S. Wu and C.H. Chiou, *Catal. Commun.*, 9 (2008) 2073.
- [50] S.S. Tan, L. Zou and E. Hu, *Science and Technology of Advanced Materials*, 8 (2007) 89.
- [51] O. Ozcan, F. Yukruk, E.U. Akkaya and D. Uner, *Appl. Catal. B-Environ.*, 71 (2007) 291.

CURRICULUM VITAE

MERT MEHMET OYMAK, Ph.D.

CURRENT ADDRESS

1509 Cad. İşçi Blokları Mah.
Merkez Sitesi No:15
Çankaya 06520
Ankara, Turkey

PERSONAL

Date and place of birth: 17.05.1979 - Edirne
Marital Status: Single
e-mail: mertoymak@yahoo.com

EDUCATION

2006 - 2012	PhD in Chemical Engineering Middle East Technical University, Ankara / Turkey
2008 – 2011	B.S. in Business Administration (distance education) Anadolu University, Eskişehir / Turkey
2003 – 2006	M.S. in Chemical Engineering Middle East Technical University, Ankara / Turkey
1997 – 2003	B.S. in Chemical Engineering Middle East Technical University, Ankara / Turkey

MAJOR SUBJECTS OF INTEREST

- Surface Science and Heterogeneous Catalysis
- Reaction Engineering

RESEARCH

2006 – 2012	Ph.D. Thesis: Photocatalytic Activity in Nano Sized Titanium Dioxide Structures
-------------	--

Supervisor: Prof. Dr. Deniz Üner, Co-supervisor: Dr. İstem Özen

Studied under 2 different projects during Ph.D. Thesis:

2009 - 2012

SANTEZ 00336.STZ.2008-2 (Under supervision of Science, Industry and Technology of Ministry): Photocatalytic Activity in Cement Based Materials (Collaboration Project between Middle East Technical University and Kalekim, company working on constructional chemicals)

Project Coordinator: Prof. Dr. Deniz Üner

Position: Project Assistant

- Integration of photocatalytic activity to the grout and plaster. Coating studies on grout, plaster and glass by using commercial TiO₂ powders.
- Characterization of photocatalytic by gas phase benzene oxidation reaction.
- Purchasing of FTIR-ATR, ESEM-EDX and NO_x Analyzer
- Used equipment in the project: GC, FTIR-DRIFTS, UV-Vis (Transmission, diffuse reflectance mode), ESEM-EDX, FTIR-ATR, Raman, XRD, BET Analysis, TGA, NO_x Analyzer.

2007 - 2009

CAYDAG 106Y075 (Under the supervision of Scientific and Technological Research Council of Turkey): Conversion of Carbon Dioxide Resulting from Combustion into Valuable Chemicals via Artificial Photosynthesis.

Project Coordinator: Prof. Dr. Deniz Üner

Position: Project Assistant

- Synthesis of TiO₂ and Pt-TiO₂ films by using sol-gel technique. Doped TiO₂ material synthesis by using incipient wetness impregnation techniques.
- Photocatalytic CO₂ reduction to CH₄ (Artificial photosynthesis).
- Used Equipment in project: GC, Vacuum Equipment (around 10⁻⁶ torr), BET, TEM.

2003 – 2006

M.S. Thesis: Drying and Stabilization of Wheat Germ in a Spouted Bed

Supervisor: Prof. Dr. Suzan Kınca Co-Supervisor: Dr. Cevdet Öztin

- Pilot scale spout bed unit construction, along with a pipe heater and air fan.
- Optimization of process parameters such as temperature and air flow speed of spouted bed
- Lengthening of expiration period of the wheat germ.
- Extraction of wheat germ oil and application of rancidity tests.

ACADEMIC PUBLICATIONS

- On the Mechanism of Photocatalytic CO₂ Reduction with Water in the Gas Phase Uner D.; Oymak M. M., Catalysis Today 181 (2012) 82.
- CO₂ Utilization by Photocatalytic Conversion to Methane and Methanol Uner Deniz; Oymak M. Mert; Ipek Bahar, Int. J. of Global Warming 3 (2011) 142.

JOURNAL ARTICLES IN PREPARATION

- Patents on TiO₂ Mediated Self Cleaning Cement Based Materials and Companies on the Field.
- Photocatalytic Oxidation of Benzene and Integration of Photocatalytic Activity to Cement based Materials.

ACADEMIC ACTIVITIES

September 2006	First Anatolian School on Catalysis (ASC-I) , (Workshop 1&2), Middle East Technical University, Ankara / Turkey. Key Lecturers: Prof. Dr. Rutger A. Van Santen, Prof. Dr. J.W. Hans Niemantsverdriet, ...
May 2007	Somer Symposium Series Middle East Technical University Ankara / Turkey
May 2007	Workshop on NO_x Reduction , Middle East Technical University Ankara / Turkey
July 2007	Nano-Tr III : Nanoscience and Technology 2007 ,

- September 2007 Bilkent University, Ankara / Turkey
IDECAT Summer school On Computational Methods For Catalysis and Material Science, Porquerolles, France.
- October 2007 **Seminars on EPR**, Hacettepe University, Ankara / Turkey
- November 2007 **NMR Workshop**, Middle East Technical University, Ankara Turkey
- June 2008 **Second National Catalysis Conference (NCC-2)**
 Erzurum / Turkey
Poster Presentation: Photocatalytic Reactivity of Crystalline and Fractal TiO₂ films.
- June 2009 **Global Conference on Global Warming 2009** İstanbul / Turkey
Oral Presentation: CO₂ Utilization by Photocatalytic Conversion to Lower Hydrocarbons and Alcohols
- September 2009 **EuropaCat 2009** Salamanca/Spain
Poster Presentation: CO₂ Reduction to Methane Using Titania Coated Glass Beads.
- May 2010 **Second Central and South European Drymix Mortar Conference** İstanbul/Turkey. **Oral Presentation:** Degredation of Surface and Air-borne Pollutants by Photo-catalytically Active Cementitious Mortars.
- July 2010 **Tocat 6 /Apcat 5 The Sixth Tokyo Conference on Advanced Catalytic Science and Technology & Fifth Asia Pacific Congress on Catalysis**, Tokyo, Japan,
Poster Presentation-1: Photocatalytic NO Oxidation with TiO₂ and Storage in Cement Based Materials.
Poster Presentation-2: On the Mechanism of Photocatalytic CO₂ Reduction with water in the Gas Phase.
- September 2010 **6th EFCATS Summer School Catalysis and Surface Sciences for Renewables & Energy**, İzmir, Turkey,
Poster Presentation: Photocatalytic Benzene Oxidation in Cement Based Materials. Key Lecturers: **Prof. Dr. Rutger A. Van Santen, Prof. Dr. J.W. Hans Niemantsverdriet, Prof. Dr. Terry S. King, Prof. Dr. Deniz Uner, Prof. Dr. Norbert Kruse, Prof. Lars G.M. Pettersson, Prof Dr. Karine Philippot...**
- May 2011 **TEM Workshop**, Middle East Technical University, Ankara, Turkey,
 Key Lecturer: **Prof. Dr. Hans-Joachim Kleebe**
- May 2011 **Ecamp (Energy Challenges for Advanced Materials and Processes: Harvesting, Storage, and Efficient**

Utilization), Cappadocia, Turkey. **Poster Presentation:** “Effect of Exposed Surface On Photocatalytic Activity”.
 Key Lecturers: **Prof. Dr. Frigyes Solymosi, Jens Rostrup Nielsen, Prof. Dr. Martin Mühler, Prof. Dr. Klaus Hermann, Prof. Dr. Jeffrey Reimer...**
 March 2012 **NCM-4 (4th National Catalysis Conference)**, Kocaeli, Turkey
Oral Presentation: “Creating Self Cleaning Surfaces for Construction Materials Using TiO₂” Key Lecturer: **Prof. Dr. Enrique Iglesia**

CERTIFICATES

- IDECAT Summer School on Computational Methods for Catalysis and Materials Science, 15-21 September 2007, Porquerolles, France.
- First Anatolian School on Catalysis (ASC-I), (Workshop 1 &2), 25 August – 06 September 2006, Middle East Technical University, Ankara / Turkey.

AFFILIATIONS

- Turkish Catalysis Society
- Metu Alumni Association

INDUSTRIAL EXPERIENCE

Trakya Glass Plant – Kirklareli / Turkey (2000).

Flat glass, car glass (laminated, tempered), mirror production.

Zentiva Health Products Company Kirklareli / Turkey (2001).

Pomad ,Liquid ,Pill production and Packaging Departments.

REFERENCES

Prof. Dr. Deniz Üner, Middle East Technical University, Chemical Engineering Department,

contact: uner@metu.edu.tr

Prof. Dr. Deniz Üner is my Ph.D. advisor

Dr. İstem Özen, Istituto Officina dei Materiali – CNR and International Centre for Theoretical Physics, Trieste, Italy.

contact: istem@sabanciuniv.edu

Prof. Dr. Suzan Kıncal, Retired from Middle East Technical University, Chemical Engineering

contact: nskincal@metu.edu.tr

Prof. Dr. Suzan Kıncal was my advisor in M.S. Studies.

Dr. Cevdet Öztin, Middle East Technical University, Chemical Engineering Department,

contact: oztin@metu.edu.tr

Dr. Cevdet Öztin was my co-advisor in M.S. Studies.